THE STRUCTURAL FEASIBILITY OF TIMBER WIND TURBINE TOWERS IN THE NETHERLANDS

C. G. van Weelden

The structural feasibility of timber wind turbine towers in the Netherlands

MASTER OF SCIENCE THESIS

For the degree of Master of Science in Civil Engineering at Delft University of Technology

C.G. van Weelden

April 13, 2015

Faculty of Civil Engineering & Geosciences (CiTG) · Delft University of Technology

Abstract

The Dutch government has indicated it wants to double the amount of wind turbines in the country by 2020. In 2012 the TimberTower, the world's first multi-megawatt turbine with a tower made of timber, was built on an inland location in Germany. The goal of this research was to determine the structural feasibility of these timber turbine towers in the Netherlands, where wind conditions are higher and different soil conditions are present.

The main advantage of timber over conventional materials such as steel is that it is considered less harmful for the environment, adding to the sustainable image of wind energy. On a structural level it is considered to behave better under high cycle fatigue loading and exhibit better structural damping, both considered beneficial in the application in turbine towers.

To determine the feasibility of timber towers the requirements from design codes were first treated. The IEC-61400 design code, specific for wind turbine towers, defines several turbine classes on the basis of mean wind speed and turbulence intensity. Based on the wind conditions as described in the Eurocodes, it was found that the Dutch onshore wind conditions correspond with either turbine class IC, IIA and IIIA, depending on the location.

The main material and connections of a turbine towers should exhibit sufficient strength under extreme loads and sufficient fatigue strength. Furthermore, its natural frequencies should not coincide with the rotor frequency and blade-passing frequency to prevent resonance. Tower deflections should be limited so that blades and tower do not collide.

After a theoretical review of several structural systems, it was determined that the closed hollow section of the original TimberTower is favoured over spaceframe-like structures due to the uncertainty in frequency behaviour the many connections of the latter introduce. The design consists of a polygonal closed tower made from Cross Laminated Timber (CLT) panels glued together using a large amount of perforated steel plates.

The IEC-61400 prescribes almost two dozen load cases and corresponding detailed stochastic simulations, which were beyond the time available. Instead, designs were checked for frequency and ultimate strength of the material by constructing load cases that are considered to represent the governing cases for the tower. Fatigue and connection design were left out of the scope for the same argument of limited time. Fatigue is not considered to be governing for timber towers and the connections from the original TimberTower have been assumed to be applicable to all designs.

A 3 MW turbine was placed on top of 100 and 125 m tall towers, while a 5 MW turbine was only placed at a hub height of 125 m. Both turbines were subjected to operational loads

calculated using the Blade Element Momentum method and the turbines were subjected to extreme wind speeds during standstill using a simplified quasi-static method, that took into account turbulence and dynamic amplification. The governing loads turned out to be on the conservative side after a comparison was made with known loads from real-life turbines across the country.

A study into frequency behaviour showed that only the first natural frequency of the tower would potentially lie within the range of rotor resonance. It was further found that the influence of pile foundation stiffness and connection stiffness were small enough to ignore for the global design calculations made in this research.

For towers made solely of CLT, the natural frequency determined the amount of material needed. Because of the resulting low stresses, the use of higher strength classes was not found to be necessary. A hardwood CLT class constructed for this research therefore showed little promise, since it has the same Young's modulus as its softwood counterpart, resulting in the same thicknesses to reach suitable frequencies and no improvement in material use could be made. For the same reason, softwood-hardwood CLT hybrid towers were not considered to be an improvement to the original design. The unprotected application of durable hardwood on the outside of the towers was not considered desirable because the variations in moisture content of the timber would bring the tower frequency close to its limit values.

Towers made of Laminated Veneer Lumber (LVL) could become narrower than those made of CLT thanks to the higher strength and stiffness of LVL, but would require elements with a thickness beyond current production limitations and standards. Wind loading directly on the tower was hereby reduced and stress levels were low for these cases, which is considered to ease connection design.

When it was attempted to respect the production standards, towers had to become significantly wider than in the first case to meet frequency demands. Aside from the negative effect this has on the visibility and related acceptance of turbine towers, local buckling often became a problem. Furthermore, the higher resulting stress levels could pose problems in designing suitable connections. It is expected that the optimum LVL tower from a structural point of view will lie somewhere in-between these two extremes.

Using LVL as longitudinal layers in a CLT element, effectively making a CLT-LVL hybrid cross section, did not turn out to improve material use compared to the LVL designs. It showed the same advantages over CLT designs of reduced width or thickness as the all-LVL designs did, but to a lesser extent. They however used the same amount of LVL materials as comparable all-LVL towers, so no improvement in the total amount of material used was found.

In the end it is considered structurally feasible to construct timber wind turbines in the Netherlands, although it is recommended that these designs are subjected to the full load spectrum for turbines before final conclusions are drawn. The original CLT design of the TimberTower is already adequate, but a cross section of LVL shows promise in reducing the width of the tower cross section.

Preface

This report was written as part of my final graduation thesis for the MSc program of Structural Engineering at Delft University of Technology. It contains work done from February 2013 to April 2015, which has been combined with part-time work as a structural engineer in practice during that time.

The report is mainly aimed at those with a background in Civil Engineering. It assumes some prior knowledge on timber structures and to a certain extent also on wind turbines. For those unfamiliar with these subjects, the last part of the appendices provides additional reading, focussed mainly on wind turbine tower design. Most of the important subjects and reasoning, however, are also featured in the main report.

It has been over two years since I first saw pictures of the TimberTower in Hannover. It is the world's first multi-megawatt turbine with a tower made of timber, which impressed me right away. I knew then I wanted to incorporate this impressive feat in my thesis work in some way. Without a clearly defined assignment on the subject at the start, it took some time before it became clear what exactly I was going to do during this research. This may have resulted in some unnecessary work done, but together with my graduation committee we were able to steer the process in the right direction at the right times.

On a personal note, keeping the balance between this thesis and already working part-time turned out to be harder than I thought at first. Working on this thesis for only three days a week and finishing in little over a year was possible, in theory. But the many interruptions of the thinking process in the form of 'regular' work days kept me from really ever getting on a roll. Almost every week turned out to be a new start of this thinking process and it wasn't until very late in the process that I finally found that balance - and the peace of mind - to do both of my 'jobs' well. Looking back, I do not know if I would have liked it to be different, both of them have provided me with a lot of useful experience.

I would like to thank the members of my graduation committee for their advice, for answering my questions and for being patient and understanding during this long period. Additional thanks go to the people I met during the CLT Training Course in Trento, Italy, for providing me with a second motivational impulse after which I got things back on track again. The contacts gained there turned out to be more than helpful after getting back to Delft and I could not have finished this report without the documentation provided during the course. Finally, I would like to thank my colleagues at Pieters Bouwtechniek for giving me advice on

a wide range of subjects, letting me study there on my days off and respecting the fact that I was 'present, but absent' during these days.

This thesis was made out of pure academical interest and no commercial intentions were present.

Colin van Weelden
Delft, April 2015

Table of Contents

Results

Appendices

Additional and detailed results

Underlying formulas and software codes

Background information and further reading

List of Figures

List of Tables

Introduction

At the end of 2012 the first multi-megawatt wind turbine with a timber tower started producing electricity in Hannover, Germany. Defying what people thought was possible with the material, the 100 m high turbine showed that sustainable energy could become more sustainable by lowering the use of more environment-unfriendly materials such as steel and concrete. This thesis hopes to add more knowledge to the field by investigating the possibility of applying similar structures in the Netherlands, hopefully aiding in the further application of timber in the energy market.

1-1 Sustainable energy and wind energy in the Netherlands

The European energy supply depends for 50% on the import of fossil fuels, which are running out at an increasing rate [15]. The negative environmental effects and dependence on oil-exporting countries has made a lot of countries look for alternative energy sources. Among these sources is wind, a clean and inexhaustible source of energy. It is available in large amounts in the Netherlands, a country that has a rich history of using wind power for its own benefit. Wind energy has certain advantages and disadvantages. The most important advantages are:

– No use of fossil fuels, wind energy limits the emission of CO2;

– Wind is a sustainable energy source which is available in practically unlimited amounts;

– Increasing the contribution of wind energy lowers the dependence on oil producing countries and fluctuating oil prices.

However, various disadvantages are named by those opposed to wind power, the main ones being:

– The costs of wind power are generally higher than of power gained from the combustion of fossil fuels, although this depends on the (varying) price of fossil fuels;
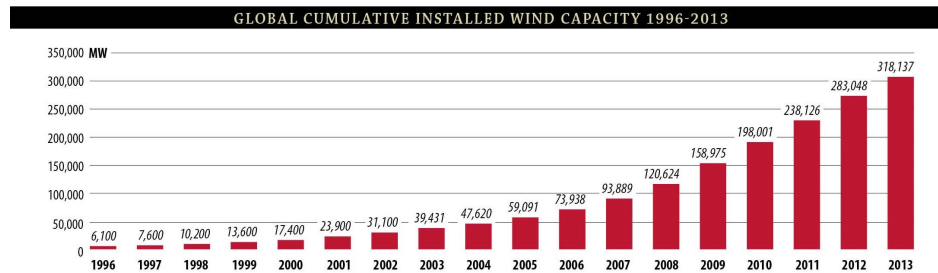
Figure 1-1: Globally installed wind turbine capacity
Source: Global Wind Energy Council [16]

— Dependence on the occurrence of sufficient wind, which fluctuates over time and space;

— Aesthetics. Wind turbines on land are clearly visible and considered a visible nuisance by some, though this is a subjective matter.

It should be noted that if one includes the so called 'hidden costs' such as pollution, global warming and health issues, the price for fossil fuels increases beyond that of most renewable energy sources. When compared to other forms of sustainable energy, wind energy is one of the cheapest forms available in the Netherlands.

Of the before-mentioned reasons, it is mostly the low carbon-dioxide emissions associated with wind power that causes the widespread application of wind turbines. The large growth of the wind turbine industry over the last years can be seen in Figure 1-1, the biggest relative growth occurring offshore.

The Dutch government has indicated that it wants to possess one of the most sustainable and efficient energy supply systems in Europe, which is why they are investing a lot of resources in the expansion of sustainable energy production [17]. Most of this will be done with the construction of wind turbines. The government has set a goal to install 6000 MW of wind power on land by 2020, including the turbines that have already been placed.

Not every location can be assigned to become a wind farm, because the turbines not only need a large free area around them for the wind to flow properly, there are also issues regarding safety and visibility. Assigning agricultural areas, areas along infrastructure and industrial sites to house wind turbines, even though they may not be built immediately, will help secure the goal and ease the process. Because of the scarcity of areas available for wind farms, the government decided to implement their plans early and plan ahead. Various locations throughout the country have been marked as potential wind park locations.

In 2011 a total of over 1,800 turbines - both on land and at sea - produced 4.3 TW of electricity in the country. Even though this is equal to the electrical needs of 1,5 million Dutch households, it only contributed 4% to the entire Dutch electricity use [15]. The turbines make up a total of 2100 MW, and combining this with the projects that are already being executed or have passed procedures - the so called 'pipeline projects' - only leads to a total of around 3000 MW. To reach the goal of 6000 MW in 2020, a lot more wind farms have to be created or expanded. This is technologically feasible, but it has to be supported up by the government and other parties in the market as well.

1-2   Turbine towers and the TimberTower

Since the introduction of wind turbines of reasonable height, the structure of the tower has almost always been made of steel. Lately also concrete, polymer and hybrid towers (steel and concrete) have been constructed. The use of steel and concrete in general has a negative impact on the environment during production, transportation and erection. The production and processing of the materials requires a lot of energy, produces a substantial amount of CO_2 and depletes finite natural resources [18]. A search for lighter and more sustainable materials (and methods) could result in an even smaller environmental impact of the production of wind energy.

In October of 2012 a timber turbine tower was erected in Germany using Cross Laminated Timber, the so called TimberTower [18]. Since December of the same year, the tower is supplying electricity to 1000 households in the Hannover area. The team behind the tower provides several advantages of their design over the more conventional materials and systems such as welded steel towers in various sources such as [18], [19], [20], [21] and [22]. These are discussed below:

– Environmental advantages

   As stated above, the use of timber is considered less harmful for the environment than other potential tower materials, when taken from sustainable sources. Production, processing and handling require less energy and produce less CO_2 (it is even stored in the timber during its lifetime), while the material itself is renewable. These environmental advantages are considered the main benefit of using timber as a tower material by many [18, 21, 22].

– Structural advantages

   Timber is considered to perform better in terms of structural damping [20], is deemed to exhibit better fatigue behaviour than steel [23] up to a point where the extreme loads are often found governing over fatigue loads [3]. The relatively large wall thickness of this timber design also prevents buckling from being the governing criterion most of the time as well. The damping behaviour and fire resistance of CLT are, when compared to steel, also more favourable [24].

– Advantages concerning transportation and dimensions

   The large dimensions of the prefabricated components of conventional welded steel towers require expensive special transport, while the maximum clearances on roads limit the width of the tower and thus its structural capacity. Concrete is mostly cast in-situ, requiring a lot of equipment and materials to be transported to site, which is not considered to be economically beneficial. The timber design of the original tower consists of panel elements which are small enough to fit in a standard truck and large enough to be quickly assembled on site. This eliminates the transport challenges and no longer limits the diameter of the tower.

   Although both points made above are valid, they are not specific advantages of the use of timber. Towers with shell components in both steel and concrete have been constructed, which offer both advantages named here as well [25]. Furthermore, they

are advantages of this specific design, which may not be the only suitable option for turbine towers made of timber.

– Economic advantages

The team also names the more stable prices - compared to steel - as an advantage of timber, while both the team and other sources [3] state that timber towers are overall cheaper as well. This might be the case when the design becomes more widespread, but the current economic risk and lack of experience with these types of towers will most likely cause this not to be the case yet. The trouble the team had finding investors for the first tower seems to confirm this.

In short, the use of timber as a turbine tower material is considered much less detrimental to the environment and might prove to be a economically suitable competitor for conventional systems, in time. It is considered to have several structural benefits over steel as well. The specific design made for the TimberTower has some additional benefits compared to conventional towers, in terms of a lack of restrictions on transportation and dimensions. Although another tower with the same system is in development, its structural and material choices may not be the only options for constructing timber turbine towers, since other systems have been used to create tall timber structures in the past.

1-3   Research goals and methods

The potential in the application of timber in wind turbine tower design is clearly present and the prototype built in Hannover shows the technological feasibility. With the desire of the Dutch government to increase the amount of electricity generated by wind energy, there might be an opportunity for timber turbine towers to be applied in the Netherlands.

The main goal of this thesis is to **determine the structural feasibility of constructing wind turbine towers out of timber in the Netherlands**, taking into account the specific conditions set by the locations. To do this, several subgoals are defined:

1. First, the demands set by design codes, physics and the Dutch wind conditions will have to be defined.

2. Secondly, an evaluation of several structural designs will then have to indicate what (type of) structural system or which design choices are most suited for constructing a timber turbine tower under these conditions.

3. Lastly, by using the available knowledge on other timber products than the Cross Laminated Timber panels used in the original TimberTower, it will finally be investigated if existing and potentially new designs can be improved further by applying these products.

The focus will lie on the technological and structural side of the turbine, not on the economic aspects. This thesis will further limit itself to wind turbines constructed on shore. The presence of salt water and waves near offshore turbines will increase the complexity to such

a degree that it will prevent the research from reaching any depth within the time available for it.

To reach the aforementioned research goals, several design situations will be defined. These will vary in location within the country, together with turbine size and height, thus varying in wind conditions and loads. Next a global structural system will be chosen that will be subjected to these conditions, optimizing the geometry for each case. For each case multiple materials will be investigated to be able to judge the performance of each material under the various conditions.

Because of the large number of design situations that are defined by varying the aforementioned parameters, calculations will be kept relatively simple and will be made using computer software.

1-4   Structure of the report

The structure of the main report is as follows:

Part 1: Basis for design
This part explains the scope and design principles of the research, used to define various design cases.

– Chapter 2 defines the design situations that are investigated in this thesis in the form of turbine types, hub heights and materials. It further describes which structural verifications one should perform when designing a turbine tower according to the design codes. Together with the more detailed information on wind turbines and wind turbine design in Part III of the appendices, it explains the demands set by design codes, thus answering the first of the subquestions mentioned in section 1-3.

– Chapter 3 relates the wind conditions in the Netherlands to those described in the codes dealt with in 2, further narrowing the design cases to be investigated.

– Chapter 4 describes the reasoning behind the choice of the structural design used in this thesis, answering the second of the subquestions.

Part 2: Methods
This part contains a description of the methods used throughout the design calculations.

– Chapter 5 explains the various methods used to calculate the natural frequency of the tower, which is one of the most important properties of a turbine tower. It also contains the conclusions drawn after parameter study into the frequency behaviour and an investigation into the possible influences on the frequency by foundation and connection stiffnesses.

– Chapter 6 contains the load cases used in this research, together with the various methods used to calculate the corresponding loads.

– Chapter 7 explains the calculation of stresses in the different materials, which differ from regular isotropic materials.

Part 3: Results

This part contains the observations made from all design calculations, along with theoretical considerations of new possibilities using other timber products.

– Chapter 8 discusses the results of various tower designs using only a single material per tower. A distinction is made between CLT and Laminated Veneer Lumber (LVL), both additionally divided into a softwood and a hardwood option.

– Chapter 9 contains additional designs, using potential combinations of the individual materials discussed in Chapter 8, while also discussing their technological feasibility and overall potential for improving the original design.

– Chapter 10 summarizes the findings once more and draws conclusions from these. It further contains a discussion of the limitations of the research and recommendations for the future.

The appendices supplement the main report and are divided into three parts as well, included in order of importance.

Appendices part I: Additional and detailed results

This part contains the detailed results of the various calculations and studies from the main report. Appendix A supplements Chapter 5, Appendix B supplements Chapter 6 and Appendix C supplements Chapters 8 and 9.

Appendices part II: Underlying formulas and software codes

Not all formulas and properties used in the calculations are fully explained in the main report, but are featured in this part of the appendices. Appendices D and E contain the properties of the materials and geometrical shapes used, respectively. Appendix F explains one of two methods used to calculate the natural frequencies of the tower, the other is described in Appendix H. The first part of the calculation model built within this research is described in Appendix G, followed by the second part in Appendix H which deals with the Finite Element Modelling part of the calculation model.

Appendices part III: Background information and further reading

The appendices in this part are mostly written as stand-alone pieces, to provide the reader with additional information on subjects featured in the main report. The terms related to wind turbines used frequently throughout the report are described in Appendix I, along with a short overview on the operation of a wind turbine. Appendix J contains information about conventional, non-timber turbine towers, along with their pros en cons. The original TimberTower is described in more detail in Appendix K, as an addition to the part about the design in Chapter 4. The last two appendices, L and M, contain a summary of how wind loading is modelled according to the codes, part of which is used in the first two parts of the main report.

Basis for design

Design principles and scope of research

The main goal of this chapter is to delimit the scope of the research and make a start with the distinction of the various design cases dealt with in the calculations further on in this research.

It first explains which design codes are to be used, which turbines will be applied and on which hub heights these will be placed. Together with the wind conditions that will be explained in Chapter 3, this will determine the design cases that will be investigated in this research. After this, the required structural checks to be performed during turbine design are shortly explained and an introduction of the materials used in this research is provided. Finally, the scope of the research is further determined by addressing some other aspects relevant to design.

2-1 Codes and regulations

The parameters used throughout this research are based on the combination of two codes:

The IEC-61400-1 [2]
  The international standard regarding wind turbines, written by the International Electrotechnical Commission. It is accepted in the Netherlands under the code NEN-EN-IEC 614100-1.

The Eurocodes
  The European codes for construction works within the European Union, developed by the European Committee for Standardisation. Within this research those parts related to basic structural design (1990-1 [26]), wind loading (1991-1-4 [13]) and timber structures (1995-1 [14]) will be used in particular. Since this research only deals with wind turbines in the Netherlands, all Dutch National Annexes are included.

Where both sets of codes overlap or contradict, the IEC code is considered governing. Not all sections of the Eurocodes may be suited for turbines, since the Eurocodes' focus lies mainly on buildings and bridges, whereas the IEC-61400 is developed specifically for wind turbines.

Wind turbine class		I	II	III
V_{ref}	(m/s)	50	42.5	37.5
A	$I_{ref}(-)$		0.16	
B	$I_{ref}(-)$		0.14	
C	$I_{ref}(-)$		0.12	

Table 2-1: Standard wind turbine classes according to the IEC 61400-1 [2].

Where:
V_{ref} is the reference wind speed, average over 10 mins;
I_{ref} is the expected value of the turbulence intensity at 15 m/s (mean value);
A   is the category for higher turbulence characteristics;
B   is the category for medium turbulence characteristics;
C   is the category for higher turbulence characteristics.

2-1-1   Turbine classes

One of the key parts in understanding the design process incorporated in this research is the use of turbine classes, as defined in the IEC-61400. Instead of designing turbines and their components for each specific location, one compares the site conditions to those defined in one of the nine standard turbine classes of the IEC. Manufacturers certify their products according to these classes, which makes the (re)design of the entire turbine not necessary for each new application of the design, only a comparison of wind conditions is needed. Foundations, however, do have to be designed for each specific case.

When site conditions are more severe than the class for which the turbine and its components are designed, one is allowed to still apply the turbine, when it can be proven that the turbine is still able to withstand these more severe conditions.

Depending on the reference wind speed at hub height (V_{ref}, comparable to the average 10-minute wind speed with a 50-year return period), locations are categorized in class I, II or III, from high to low. The turbulence intensity I_{ref} divides each of these classes further into subclasses A, B and C. The turbulence intensity in Section L-1-2 is defined as the standard variation of the wind speed variations divided by the mean wind speed. This means that when the turbulence intensity is higher, the chances of larger deviations from the mean wind speed are higher.

These nine classes are defined in such a way that they cover most (onshore) locations, but for other and special cases a tenth class is defined. This S-class allows the designer to tailor the design to the specific conditions and is used for most offshore turbines. More information about wind turbine classes and the IEC-61400 can be found in Appendix M.

The next chapter will link the wind conditions in the Netherlands to the turbine classes of the IEC.
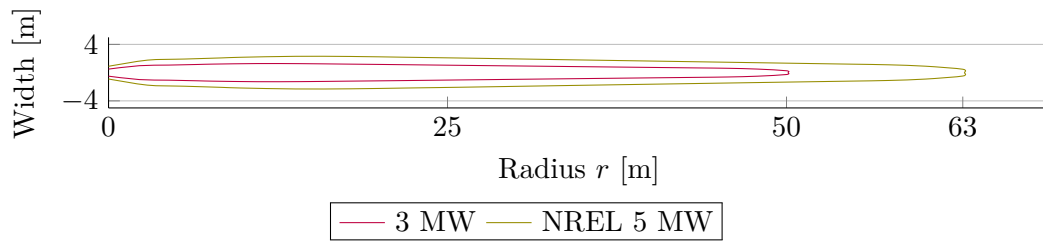
Figure 2-1: Blade profiles used in this research, based on Jonkman et al. [1]

2-2 Turbine types

Two different turbines will be investigated, with a rated power of 3 and 5 MW respectively. Both are larger than the 1.5 MW, 77 m diameter Vensys turbine on top of the original TimberTower, but comparable to the size of turbines applied in new projects in the Netherlands. Especially turbines with a rated power between 2.5 and 3.5 MW have been built in large numbers in the Netherlands over the last couple of years [27]. The 5 MW is included because of the relatively large availability of data and because it is comparable to the larger turbines built in the country [28].

For the 5 MW turbine the NREL 5 MW Baseline Turbine will be used, well-documented by Jonkman et al. [1]. Even though it is a fictional turbine, it is used extensively in research and represents actual turbines well. Lyrner et al. [3] have used a scaled down version of this turbine in their cost comparison of tower materials, which will be used in this research as well. Not all parameters are provided by Lyrner and some have been scaled to appropriate values in this research. An overview of the adjustments from the NREL 5 MW to the 3 MW turbine is given below.

Rated Power
   The rated power has obviously been scaled down from 5 to 3 MW.

Blade shape
   Because the 3 MW turbine rotor has a smaller diameter, the blades are assumed to be scaled down versions of the 5 MW blades. The diameter is reduced from $D_{5MW} = 126$ m to $D_{3MW} = 100$ m. Chord lengths of the cross sections are first scaled down by a factor $D_{3MW}/D_{5MW} \approx 0.80$.

   Chord lengths are further reduced by another 30% to take into account that the resulting root forces on a smaller blade are also smaller and thus require less overall material. Assuming that most of the mass is located on the surface of the hollow blades and the wall thickness remains the same, the 50% blade mass reduction as suggested by Lyrner would also lead to an approximate 50% reduction of outer dimensions. This justifies the total reduction of 44% used in this research.

   Later calculations will show that the loads on the 3 MW blades will still be conservative compared to examples from practice. A graphical representation of the final blade shapes is shown in Figure 2-1, where the part around $r = 0$ should not be regarded in much detail because of the presence of the hub. The blade twist is kept the same as for the 5 MW turbine, with the relative positions scaled to the smaller diameter. Lift and drag coefficients are, for lack of sufficient data, kept the same as well.

Mass

Rotor mass has been reduced from 110,000 kg to 56,500 kg and the mass of the nacelle has been reduced from 240,000 kg to 120,000 kg, corresponding with Lyrner.

Eccentricities The eccentricities of the centres of mass of the rotor and nacelle, have been scaled by a factor 0.8, similar to the blade length. These eccentricities will be defined later, when the load calculation methods are explained in detail in Chapter 6.

Rotor frequencies

The rotor frequencies are taken directly from Lyrner and can be found in Table 2-2.

Operating wind speeds

The turbines are both assumed to operate within the same wind speed domain, with a cut-in wind speed of 3 m/s and a cut-out wind speed of 25 m/s. The rated wind speed for the 3 MW has been set at 12 m/s, comparable to other 3 MW turbines on the market today. The definition of the operating wind speeds can be found in Appendix I.

Rotor speeds

The rated rotor speed has been taken directly from Lyrner, whereas the cut-in rotor speed of the 3 MW has been calculated by multiplying that of the 5 MW with the same ratio of the rated rotor speeds.

The properties for both turbines can be found in Table 2-2, resulting aerodynamic power curves in Figure 2-2. Both turbines are considered to be suited for turbine classes up to class IB. Restrictions on the top diameter of the tower are given by the size of the turbines. The 3 MW turbine requires a 3.0 m top diameter, while the 5 MW requires a 3.8 m top diameter [3].

2-3   Hub heights

The general rule of thumb is to place a tower with a height of 2 to 3 times the rotor radius under the turbine. That would mean hub heights between 100 and 150 m for the 3 MW turbine and between 125 and 188 m for 5 MW. For this research, hub heights of 100 and 125 m are used, comparable with other modern-day turbines made with various tower materials, especially those found in the Netherlands, as was found after investigating the turbines built in the last few years [27]. These hub heights will be used later on in Chapter 3 to calculate the relevant turbine classes corresponding with locations in the Netherlands.

2-4   Structural verification of turbine towers

When designing a turbine tower, many aspects are to be considered. The most important structural checks on the tower to be performed are listed in the sections below.

– Frequency considerations

– Strength considerations

Turbine type			NREL 5 MW	Scaled 3 MW
Rotor orientation			Upwind	
Rated power	P_{rated}	MW	5	3
Number of blades	n_{blades}	[-]	3	3
Control			Variable speed, collective pitch	
Rotor diameter	D	m	126	100
Cut-in speed	V_{in}	m/s	3	3
Rated speed	V_{rated}	m/s	11.4	14
Cut-out speed	V_{out}	m/s	25	25
Cut-in rotor speed		rpm	6.9	8
Rated rotor speed		rpm	12.1	14
Cut-in rotor frequency		Hz	0.115	0.133
Rated rotor frequency		Hz	0.202	0.233
Rotor mass	m_{rotor}	kg	110,000	56,500
Nacelle mass	$m_{nacelle}$	kg	240,000	120,000
Tip speed		m/s	80	73

Table 2-2: Properties for the NREL 5 MW Baseline Turbine as defined by Jonkman et al. [1] and the derived 3 MW turbine as found in Lyrner et al. [3]
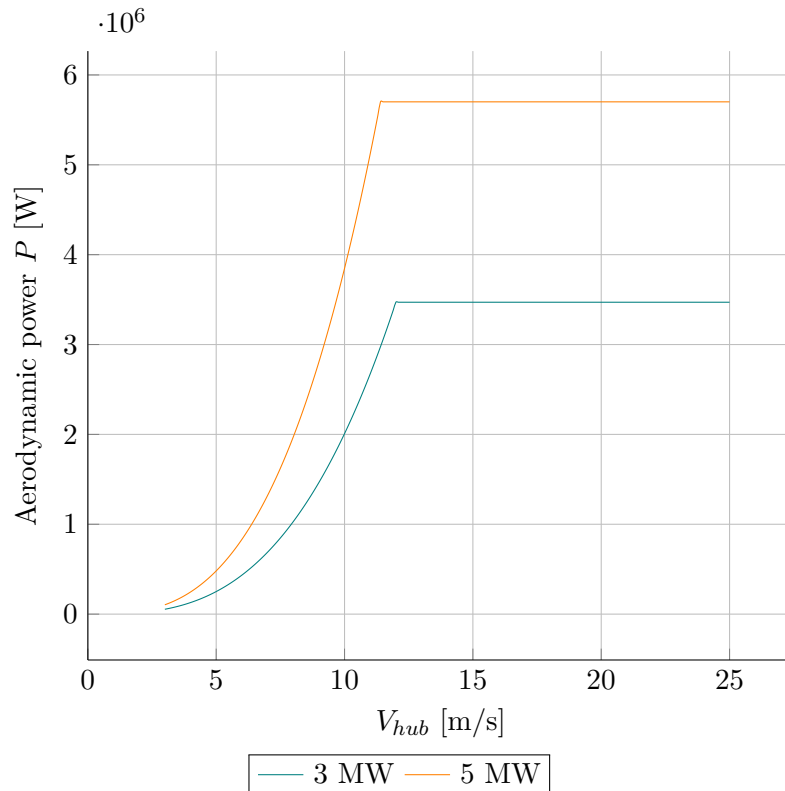
Figure 2-2: Resulting aerodynamic power curves for both turbines

– Deformation considerations

The reader is expected to be familiar with the terms concerning the operation of wind turbines used within this section. They are shortly explained in Appendix I.

2-4-1   Frequency considerations

One of the main design considerations lies in the natural frequency of the tower [5, 29]. Damping in turbine towers is usually small, so stress amplification by resonance between the tower and blades could lead to stresses that are unacceptably high. The main cause for this possible resonance would be fluctuations in rotor thrust at rotor frequency (called the '1P' frequency) or blade-passing frequency ('3P'). The first natural frequency of the tower should therefore not coincide with these rotor and the blade-passing frequencies.

Normally, no problems of load amplification occur when the first natural frequency of the tower is kept out of the ranges of 1P ±10% and 3P ±10%, according to DNV Risø [5]. For the variable-speed turbines used in this thesis, this means that the natural frequency of the tower cannot coincide with all rotor and blade passing frequencies between cut-in and cut-out. The frequencies remain the same from rated speed to cut-out, so essentially all frequencies between cut-in and rated power production are off-limits.

The NREL 3 MW Turbine, which can have a 1P frequency anywhere between 0.133 Hz

(cut-in) and 0.233 Hz (rated), the following boundaries can be determined:

$$1\text{P - Lower boundary - } 0.9 \cdot 0.133 = 0.120 \text{ Hz}$$
$$1\text{P - Upper boundary - } 1.1 \cdot 0.233 = 0.256 \text{ Hz}$$
$$3\text{P - Lower boundary - } 0.9 \cdot 0.400 = 0.360 \text{ Hz}$$
$$3\text{P - Upper boundary - } 1.1 \cdot 0.700 = 0.770 \text{ Hz}$$

And for the NREL 5 MW Turbine, which can have a 1P frequency anywhere between 0.115 Hz (cut-in) and 0.202 Hz (rated) this means:

$$1\text{P - Lower boundary - } 0.9 \cdot 0.115 = 0.104 \text{ Hz}$$
$$1\text{P - Upper boundary - } 1.1 \cdot 0.202 = 0.222 \text{ Hz}$$
$$3\text{P - Lower boundary - } 0.9 \cdot 0.345 = 0.311 \text{ Hz}$$
$$3\text{P - Upper boundary - } 1.1 \cdot 0.605 = 0.666 \text{ Hz}$$

For the 5 MW turbine, these values are displayed in Figure 2-3. In this figure, three categories of towers are shown as well, based on the value of the tower's first natural frequency compared to 1P and 3P. When the natural frequency is higher than 3P, the tower is classified as 'stiff', lower than 1P is called 'soft-soft' and in-between 1P and 3P is classified as a 'soft' tower.

Soft-soft towers are often not strong enough for high hub heights and both the 1P and 3P frequency pass the natural frequency of the tower during every startup. Stiff towers use a lot of material not required for strength, but have the slight advantage that the blade frequencies do not pass that the natural tower frequency during start-up. The aim in this research is to design a tower with a natural frequency between 1P and 3P, a 'soft' tower, which is the preferred and most often occurring case [29].

Often, when a tower is designed for extreme loads, its natural frequency will lie in the range of 3P. A balance has to be found between sufficient strength on one hand and a suitable natural frequency on the other. Since the magnitude of the load fluctuations affects the fatigue loads and life, it is best to keep the tower frequency as far from the 1P and 3P frequencies as possible, though according to Burton [29] the rotor frequency is of lesser importance than the blade-passing frequency. Cyclic loading at the 1P frequency will only occur when the blades are geometrically different from each other.

For conventional tower concepts, only the first natural frequency lies in the range of the 1P and 3P frequencies. For the timber design(s) used in this research, it will be investigated if this holds as well for timber towers. In this thesis, two methods for determining the natural frequency are used, the Rayleigh-Ritz method and a more accurate way using finite element modelling. Both are described in more detail in Chapter 5.

2-4-2 Strength considerations

It is obvious the tower needs to withstand all the loads it experiences throughout its entire lifetime. Firstly, its components may not fail under the maximum occurring load, so sufficient material strength needs to be present for these extreme loads. Secondly, two different aspects related to strength should also be verified:
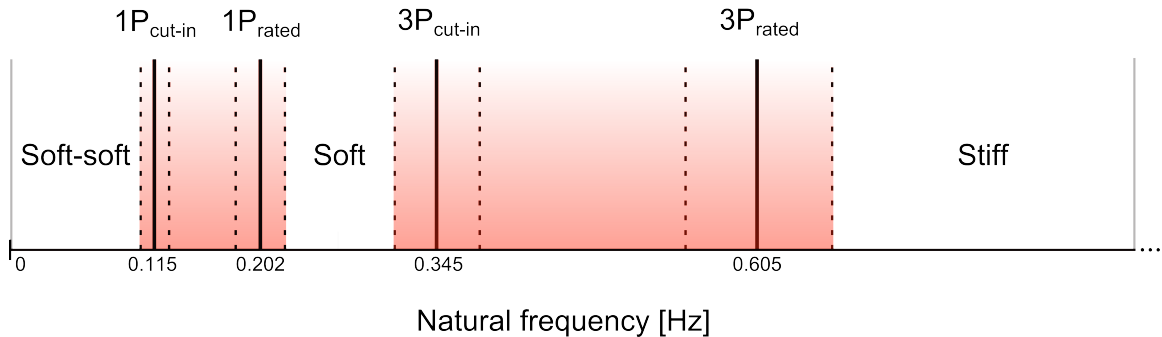
Figure 2-3: Restrictions on the first natural frequency of the tower for a NREL 5 MW turbine

Fatigue

Wind turbines are subjected to high-cycle fatigues, the blades experience around 10^9 cycles during a 30 year lifetime [30]. This means they can experience more than 1000 times as many load cycles than some other fatigue-prone structures, such as air plane wings and bridges. This makes fatigue strength an essential component of wind turbine design. Not all load cycles on the blades find their way to the tower, so the number of cycles for tower fatigue design could be slightly lower. Nevertheless, fatigue should be well investigated for the tower.

Unfortunately, fatigue is not included in this thesis because of limited time and tools available. It should be noted that this makes later conclusions on feasibility incomplete, because the important aspect of fatigue is not dealt with. However, it is the opinion of both the author and others, such as Lyrner [3], that fatigue will be of lesser significance for timber than it is for steel. A few extra remarks on how fatigue is checked and which conditions affect the fatigue strength can be found in Appendix M, to provide some basic background information.

Connections

The design of connections for timber structures is essential to their function and is thus of concern for timber turbine towers as well. Connections between tower sections and components influence both strength and natural frequency and should be well-designed. Although originally included in the scope of this research, it has been decided to leave the connections out of it for the same reason as fatigue analysis, time.

Instead, the connections from the original TimberTower will be used, as they are assumed to be applicable to the designed structures as well, in their original form. This does however not mean that these connections are the only ones suited for applications in timber wind turbine towers, but so far it is the only type that has been tested, approved and applied for these kinds of structures.

An explanation of the connections used in the TimberTower will be provided in Chapter 4. The connections are reasonably simple to execute, but large in number, making them

quite labor-intensive. Only specialized workers were allowed to execute the connections, to ensure satisfactory quality. Long-term behaviour of the connection is not yet known and the approval is still on a case-to-case basis.

2-4-3 Deformation considerations

When it comes to stiffness of the structure, not only the frequency has to be checked. The blades and the tower may - especially during operation - obviously not collide. In contrast to buildings, where deformations usually fall under serviceability limit states, load and material factors are taken into account when calculating the maximum deflection for wind turbines. The IEC prescribes the following formula for critical deflection analysis:

$$d_0 - \gamma u_{max} > F \tag{2-1}$$

Where:

d_0	is the distance between tower and blade, both in undeflected state;
u_{max}	is the maximum relative deflection of the blade and tower under characteristic loading; and with mean material properties;
γ	is the total partial safety factor, $\gamma = \gamma_f \gamma_m$;
γ_f	is the partial safety factor for loads;
γ_m	is the partial safety factor for materials, 1.1;
F	the minimum required distance between blade and tower (often just 0).

In short, this means the blade and tower deflections have to be checked under design load values (through the use of γ), instead of characteristic values, which are used on most other structures when looking at deformations. Excessive blade deflections will cause turbine failure and adequate safety is therefore required.

Since both the tower and the blade will deform under loading, the exact deformation behaviour over space and time of both the blades and tower is required to determine the smallest blade-to-tower distance. The tower and blades can be out of phase, making a single static deflection analysis insufficient. The highest loads do therefore not necessarily lead to the most critical deflection.

As the above suggests, detailed information on both the blade deflections and time-dependent behaviour of the entire system is needed to correctly use the formula above. Looking at both the available time and tools within this research, it is not feasible to conduct such a detailed simulation. With the tools available, a quasi-static deflection analysis of the tower deflection can be made, provided in Chapters 6 and 7. When looking at the eccentricities and the fact that it is possible to design blades for the NREL 5 MW with a relative small tip deflection [31], it is assumed that a quasi-static tower deflection $\gamma u_{max,tow} \leq 2.5$ m for the 5 MW turbine and $\gamma u_{max,tow} \leq 2.0$ m for the 3 MW turbine during operation will suffice.

There is no knowledge found in literature of tower deformations being the governing factor. Some turbines have a shaft that is tilted slightly upward to increase the clearance when needed, which can be applied for the designs within this research as well.

Figure 2-4: Example of the build-up of Cross Laminated Timber
Source: Wood Skyscrapers, http://www.woodskyscrapers.com/cross-laminated-timber.html, accessed
March 2015

2-4-4   Concluding remarks

Strength calculations will be limited to normal and shear stresses under extreme loading only. It is expected that fatigue will not be governing for timber turbine towers and it is assumed that the original connection type will be sufficient in the treated structures as well. Deflections will be dealt with in a limited fashion, because they are not considered as the governing design aspect, as explained above. The exact load cases and methods used in this research for ultimate strength design will be explained later in Chapter 6.

2-5   Materials used

The original TimberTower made use of standard (i.e. softwood) Cross Laminated Timber (CLT). As will be explained in Chapter 4, this will also be the main focus in this thesis, to subject this material to the loads caused by the Dutch wind conditions. Additional research will be done into the use of other timber panel products such as hardwood CLT and Laminated Veneer Lumber (LVL), as well as possible advantages of using hybrid systems.

Detailed information and calculation methods for the material properties can be found in Appendix D, while stress calculation methods (which differ slightly compared to regular sawn or laminated timber) are found in Chapter 7 for both CLT and LVL. A short introduction for those unfamiliar with the materials is provided below.

2-5-1   Cross Laminated Timber

CLT is an engineered wood product consisting of multiple longitudinal and transverse layers of solid wood glued together, to form in panels with large dimensions. For those unfamiliar with the appearance of the material, a picture is shown in Figure 2-4. It is well suited for structures with structural wall and floor elements, because of its high dimensional stability and rigidity, among others.

	Strength Class		CL24h	CL28h	CL30h	CL34h	CL40h
Bending strength	$f_{m,CLT,k}$	N/mm^2	24	28	30	34	40
Tensile strength	$f_{t,0,CLT,net,k}$	N/mm^2	16.8	18.9	21.6	24.3	28.8
Compression strength	$f_{c,0,CLT,net,k}$	N/mm^2	24	28	30	34	40
Shear strength (in plane)	$f_{v,CLT,IP,k}$	N/mm^2	5.0				
	$f_{T,CLT,k}$	N/mm^2	2.5				
Shear strength (out of plane)	$f_{v,CLT,OP,k}$	N/mm^2	4.0				
	$f_{r,CLT,k}$	N/mm^2	1.25				
Young's Modulus	$E_{0,mean}$	N/mm^2	11000		12000		11000
Density	ρ_{mean}	kg/m^3	420		460		650

Table 2-3: Characteristic material strength values for the various CLT strength classes

Table 2-3 shows the strength classes used within this research. The first four entries in the table are the standard strength classes as defined by Schickhofer [6], the lower strength classes being more commonly used. The fifth entry, CL40h, is a class constructed within this research. It is based around hardwood boards of class D40, glued together to form CLT panels. Design material properties for this hardwood CLT are calculated in the same way as the other classes, described in Appendix D, along with the reasoning behind the creation of this class.

Shear strength values (f_v, f_r, f_T) in Table 2-3 are the same for all regular CLT classes and without additional test results to suggest otherwise, have been used for the hardwood class as well. The different shear mechanisms in CLT corresponding with these values will be explained later in Section 7-3.

2-5-2   Laminated Veneer Lumber

Straight, defect-free wood, so-called clearwood, has strength values often more than twice has high as sawn structural timber, because the latter can contain all sorts of defects. LVL is made by peeling thin veneers from logs and gluing these together into structural beam and panel elements. In this way, large defects are spread out and this redistribution leads to higher strength properties.

Two kinds of LVL are considered in this research: Kerto LVL produced by Metsä Wood [11] and Baubuche LVL made by Pollmeier [12]. The first is made from softwood, while the latter is made from European beechwood, resulting in higher strength properties, especially in tension. Both come in two varieties, a cross-bonded version denoted by the letter Q and a

Figure 2-5: Example of the build-up of Laminated Veneer Lumber
Source: External Works,
http://www.externalworksindex.co.uk/entry/42457/Mets-Wood-UK/KertoQ-laminated-veneer-lumber,
accessed March 2015

version with all fibres oriented in one direction, denoted by the letter S.

The parallel bonded S option is mostly suited for beams, lintels and other bar-like products loaded mainly in one direction. The cross bonded Q-variant has 20 % of its veneers glued in the crosswise direction, improving "the lateral bending strength and stiffness of the panel, thus increasing the shear strength" [11] and is suited for surface structures, such as load-bearing walls. Characteristic strength values for the LVL types is found in Table 2-4.

LVL is available in smaller dimensions than CLT, especially regarding the thickness of the panels. Current production limitations are described in Appendix D, as well as formulas for the design material properties and partial factors to be used for calculations on LVL.

2-5-3   Hybrid panels

To a certain extent, it is possible to replace layers of the CLT by other timber materials. For instance, Metsä Wood has a product line where their standard Kerto-LVL is included as a layer in regular CLT panels [32]. Additional research in the combination of different wood species into one panel is also being conducted [33]. Researchers have successfully constructed hybrid panels of different species. Examples are:

– Panels made up of eucalyptus and pine;

– Ash and spruce;

– Birch and poplar.

Especially the last combination, birch and poplar, is considered promising [33].

These examples show that it is possible to improve or alter the properties of CLT by replacing a single layer by another timber product. For structures where the natural frequency is vital,

		Material	Kerto S	Kerto Q	Baubuche S	Baubuche Q
Bending strength (in plane)	$f_{m,0,LVL,IP,k}$	N/mm^2	44	32	70	60
Bending strength (out of plane)	$f_{m,0,LVL,OP,k}$	N/mm^2	50	36	65	45
Tensile strength	$f_{t,0,LVL,k}$	N/mm^2	35	26	60	40
Compression strength	$f_{c,0,LVL,k}$	N/mm^2	35	26	41.6	24.2
Shear strength (in plane)	$f_{v,LVL,IP,k}$	N/mm^2	4.1	4.5	8	9
Shear strength (out of plane)	$f_{v,LVL,OP,k}$	N/mm^2	2.3	1.3	8	3.3
Rolling shear strength	$f_{r,LVL,k}$	N/mm^2	0.3	0.6	1.65	3.3
Young's Modulus	$E_{0,mean}$	N/mm^2	13,800	10,500	16,800	11,800
Density	ρ_{mean}	kg/m^3	480		760	

Table 2-4: Characteristic material properties for LVL according used in this thesis

such as wind turbine towers, this could be a feasible solution for when (part of) the material has insufficient strength, but not much mass can be added because of frequency considerations. Chapter 9 will deal with the application and possibilities of these hybrid panels in more detail.

2-6   Other aspects relevant to design

The following lists provides additional subjects related to wind turbine design, which will or will not be taken into account during this research.

Secondary installations
> The weight and operational loads of the inner parts of the turbine tower (such as elevators, installations and scaffolding described in Appendix K) are expected to be negligible compared to the other loads and not taken into account.

Other environmental conditions
> Ice, temperature, lightning and other conditions as described in Appendix L are not considered.

Foundation
> The only aspect of the foundation that is included in this design is its influence on the natural frequency of the tower, in Chapter 5. The actual design of a foundation for each possible scenario is not necessary to answer the research questions and is left beyond the scope of this research. The large number of turbines erected in various regions of the country already prove that it is possible to design and construct suitable foundations for wind turbines under the Dutch wind and soil conditions.
>
> The bottom 5 m of the tower are assumed to be made of concrete, as is the case with the original TimberTower, see Chapter 4. Stresses in the bottom 5 m of the designed tower will therefore not be checked against timber strength parameters. For frequency considerations, however, this part is assumed to have the same stiffness and mass as the timber section.

Transfer structure
> At the top of the tower a steel (or polymer) transfer structure will allow the polygonal tower to be equipped with contemporary turbines, which require a circular cross section. More about this will follow in Chapter 4. The structural design of this transfer structure is not included either, so stresses in the top 5 m of the towers will not be checked against timber strengths. For frequency considerations, this part is also assumed to have the same stiffness and mass as the timber section, as is done at the bottom.

Doorway
> Any doorway or access point for personnel is assumed to be included in the concrete foundation, not in the timber part itself.

Production limitations
> Individual size limitations for elements are respected as much as possible and will prove to provide adequate design possibilities in many situations. Slight exceedances of the production limitations are accepted as well, within reasonable limits. The thought

behind this is that for a (somewhat prestigious) project as timber turbine towers, with a possibility of repetition or large demand, producers will arrange their production to suit the needs.

Furthermore, glued Laminated Timber (glulam) elements have already been successfully joined together to overcome limitations in member width caused by production [34]. The same is assumed to be possible for CLT and LVL elements. It is however considered to be cheaper and quicker to be able to use readily available standard elements. Volume effects on the material parameters are assumed to follow the same trend for these possible larger dimensions as they do for regular dimensions. Production limitations of the various materials are dealt with in Appendix D.

Wind conditions in the Netherlands

This chapter will delimit the geographical scope of this research and determine the associated IEC wind turbine classes for Dutch wind conditions. As stated before, this chapter will also relate the wind turbine classes found in the IEC to the wind conditions throughout the entire country. For additional information, the definition of the different wind speeds, turbulence parameters and wind models used in wind turbine calculations, reference is made to Appendix L.

3-1 Wind areas

The National Annex of Eurocode 1-1-4 [13] divides the country into three wind areas, as shown in Figure 3-1. It also defines three terrain categories:

- Terrain category 0 for locations at sea or in coastal areas;

- Terrain category II for remote areas, with little development and buildings;

- Terrain category III for areas with buildings.

This research will include all wind areas, but exclude terrain category III, since it was already addressed in the introduction in Chapter 1 that large multi-megawatt turbines are not built in densely built areas. Furthermore, terrain category 0 does not exist in wind area III.

3-2 Turbine classes

The IEC defines three turbine classes, as shown in Table 2-1 and described in section 2-1-1. These are internationally accepted and allow turbines that are designed for these classes to be applied in all locations where the wind conditions are equal or less severe than defined by the turbine class.
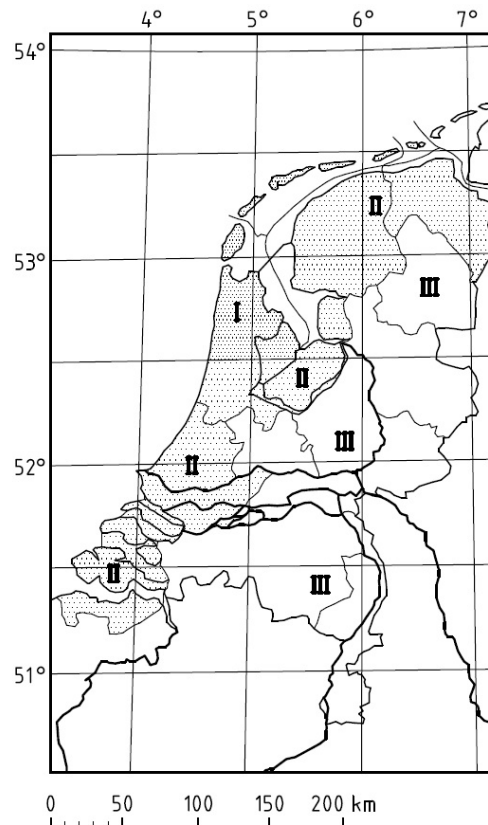
Figure 3-1: The three different wind areas in the Netherlands
Source: Eurocode 1-1-4 [13]

The boundary conditions as described in the previous section lead to various wind conditions and resulting turbine classes, considering the Eurocode [13]. These can be found in Table 3-1 for hub heights of both 100 and 125 meters. Examples of the parameters used in the calculation of the values from Table 3-1 can be found in Tables B-1 and B-2, while the corresponding formulas can be found in section L-2-2.

To be able to determine the feasibility of timber turbine towers in the Netherlands, it is decided to investigate all aforementioned calculated turbine classes, namely IC, IIA and IIIA. Class IC is only required for turbines places in locations of terrain category 0, which is a small part of wind areas I and II (Figure NB.4 from Eurocode 1-1-4 [13]) along the coast. When looking at the locations of the current Dutch turbines in Figure 3-2, the great majority of these turbines lie outside of these areas. Terrain category 0 also requires the turbine to placed in or in close proximity of salt water. Since the effects of possible degradation and precautionary measures are not known, it is not expected that timber turbine towers will be placed in these locations in the first stages of their possible implementation. Nevertheless, strength calculations for class IC will be made, to be able to judge the feasibility for the entire country.

For comparison, the original TimberTower carried a Vensys 77 turbine, suited for wind speeds up to class IIIA [35].

Height	Terrain category	Wind area		
		I	II	III
100 m	0	$V_m = 47.3$ m/s $I_v = 0.101$ Turbine class IC	$V_m = 43.2$ m/s $I_v = 0.101$ Turbine class IC	N/A
	II	$V_m = 38.4$ m/s $I_v = 0.161$ Turbine class IIA	$V_m = 35.1$ m/s $I_v = 0.161$ Turbine class IIIA	$V_m = 31.9$ m/s $I_v = 0.161$ Turbine class IIIA
125 m	0	$V_m = 48.3$ m/s $I_v = 0.099$ Turbine class IC	$V_m = 44.2$ m/s $I_v = 0.099$ Turbine class IC	N/A
	II	$V_m = 39.8$ m/s $I_v = 0.155$ Turbine class IIA	$V_m = 36.4$ m/s $I_v = 0.155$ Turbine class IIIA	$V_m = 33.0$ m/s $I_v = 0.155$ Turbine class IIIA

Table 3-1: Determination of the IEC turbine classes for different locations in the Netherlands

As can be found in section L-2-1, IEC-61400 section 11.9 [2] requires the wind characteristics on site to be equal or less severe than those defined by the turbine class. The conditions described below should be met. Wind area I, terrain category II, resulting in class IIA, is used as an example:

$V_{m,50} < V_{ref}$

Using $p = 0.02$ in the calculation of c_{prob} from the Eurocode, $V_{m,50} = V_m = 39.8$ m/s. With $V_{ref} = 42.5$ m/s, this condition is met.

$V_{50yrs}^{3secs} < V_{e,50}$

Where $V_{e,50} = 1.4V_{ref} = 59.5$ m/s. The extreme 3-second average wind speed $V_{m,50yrs}^{3secs}$ cannot be defined using the Eurocode directly. Lungu et al.. [36] have defined a relation between wind speeds of different standards, among which the early draft of the Eurocode. $V_{m,50yrs}^{3secs} = 1.5V_{m,50} = 1.5 \cdot 39.8 = 59.7$ m/s. This condition does not meet the turbine class completely, but is accepted.

$p(V_{hub})$ on site $< p(V_{hub})$ in design   for $0.2V_{ref} < V_{hub} < 0.4V_{ref}$.

p is the probability density function of the wind speed. Again, it is not possible to determine this completely for the Dutch conditions, but the Rayleigh distribution of wind speeds adopted by the IEC is applicable to many areas. It is therefore assumed that the site value of the probability density function of V_{hub} is less than the design probability density function at all values of V_{hub} between $0.2V_{ref}$ and $0.4V_{ref}$ and the condition is met for all locations in the Netherlands.

$\sigma_1 \geq \hat{\sigma} + 1.28\sigma_\sigma$ for $0.2V_{ref} < V_{hub} < 0.4V_{ref}$.

This condition says that the representative turbulence standard deviation σ_1 should be greater or equal to the site value of the estimated 90% quantile, given by the right side of the equation. The Eurocode does not give a clear distribution of the turbulence standard deviation so, it is not possible to directly derive the 90% quantile for all wind speeds at hub height. It is therefore again assumed that all locations in the Netherlands also fulfil this criteria.

So, for ease of design, the final locations of the turbine in this design are assumed to fulfil all the conditions set by the IEC-61400, in order to design for the turbine classes specified there. Since the many turbines already built in the country have also been designed for these classes, this assumption is justified.

3-3   Wind turbine locations in the Netherlands

3-3-1   Current turbines

Figure 3-3 and Table 3-2 show the number of turbines and their capacity for different parts of the country at the end of 2013. It can be seen that more than 93% of the turbines are located in wind areas I and II. This does however not change the number of turbine classes to include in this study. Most of the turbines that have been build in the past years have a rated power of around 3 MW and a hub height of around 100 m [27].

An example of one the latest wind parks to be realized is wind park 'de Zuidlob', in the southern part of the province of Flevoland. It was completed in 2013 and contains 36 turbines with an individual capacity of 3.4 MW and a hub height of 100 m. Based on their location and turbine types [37], these appear to have been designed for class IIA and IIIA. They are one of the few multi-megawatt turbines in the country for which load data is available publicly [37], which will be used as a verification throughout this thesis.
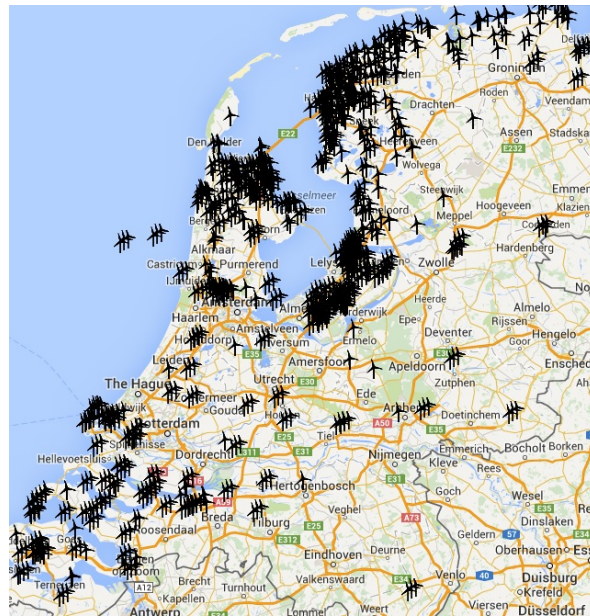
Figure 3-2: Location of all constructed turbines in the Netherlands in 2014
Source: Bosch & Van Rijn, http://windstats.boschenvanrijn.nl/, accessed January 2015

3-3-2   Future plans

The aim of the Dutch government is to obtain at least 14% of our energy needs from renewable sources by 2020 [38] . A large contribution will be made by increasing the total wind turbine capacity on land from 2500 MW (Table 3-2) to 6000 MW, as is desired. To facilitate this, the government has designated 11 areas for the development of large-scale wind parks, shown in Figure 3-4. It can be seen that no large-scale development is planned in wind area III. The feasibility of timber turbines in wind area III will be judges nonetheless, to be able to provide a concluding answer for the entire country.
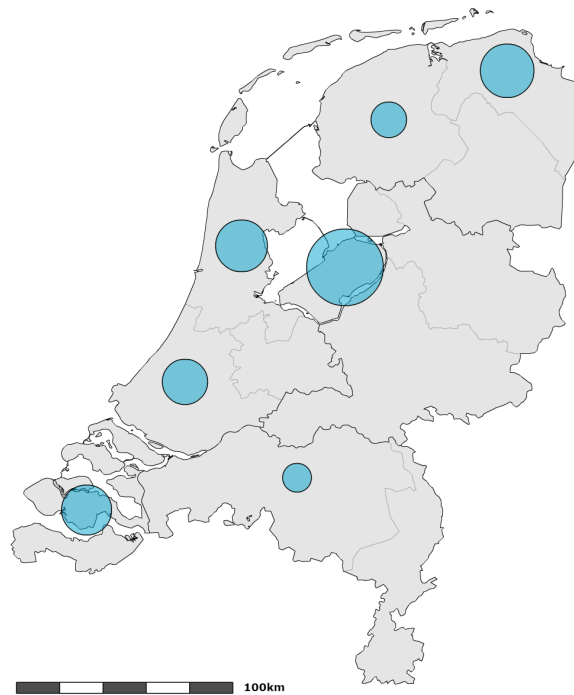
Figure 3-3: Wind energy production and capacity for the Netherlands at the end of 2013
Source: CBS, 'Windenergie op land - productie en capaciteit per provincie', accessed February 2015

Region	Production	Capacity	
	Electricity production [10^6 kWh]	Power [MW]	Number of turbines
Groningen	842	376	207
Friesland	368	165	325
Flevoland	1322	772	626
Noord-Holland	767	353	328
Zuid-Holland	501	269	150
Zeeland	636	330	210
Noord-Brabant	200	108	76
Other provinces	195	106	53
Netherlands - Total	4832	2479	1975

Table 3-2: Wind energy production and capacity for the Netherlands at the end of 2013, as provided by the Centraal Bureau voor de Statistiek [4]
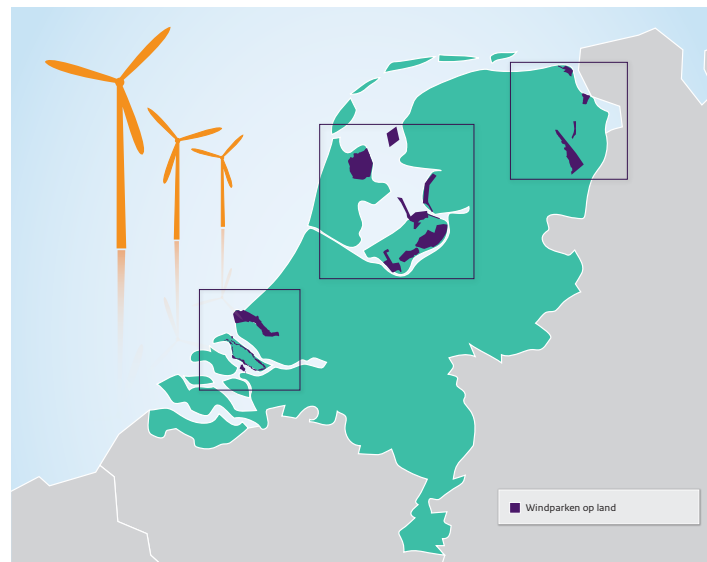
Figure 3-4: The 11 locations on land designated by the Dutch government for new large-scale
wind parks
Source: Rijksoverheid [39]

Global structural design

This chapter gives a short introduction on the general structural systems of wind turbine towers, both in general and the one(s) used in this thesis. It starts with a short overview of non-timber turbine towers, about which more information can be found in Appendix J, followed by a list of other tall timber structures that could serve as inspiration for alternate designs than the one used in the TimberTower. After a choice is made for the most suitable design, this design is further explained in the last part of this chapter.

4-1 Overview of structural systems

4-1-1 Conventional towers

The tower usually makes up for a large part of the costs, but is a relative low-tech part of the entire system [5]. This makes it an ideal component for optimization to achieve cost reduction and the availability of many alternatives will aid in this goal.

Most turbine towers are made of tubular steel sections, welded together into large sections in the factory and further bolted together on location. This design is preferred because of its predictable dynamic and fatigue properties and the large amount of experience with it. The closed shape also allows personnel to ascend safer and more comfortable, although this is not specific to the use of steel. The largest downside of this design is the need to transport the large sections to the wind site, restricting the maximum diameter of the structure. This usually leads to uneconomical designs for larger hub heights, because the required stiffness is then reached by applying larger wall thicknesses instead of a larger base diameter. This is usually the case for towers with a hub height above 85 to 90 m [19].

Another design system in steel is the lattice tower, which reduces cost and wind shade by using less material, but these towers are considered less aesthetically pleasing and are therefore seldom applied for large-scale turbines nowadays. New designs that apply an outer shell to the space frame [40] take away this aesthetic argument, while maintaining the ease of transportation and reduction of materials.
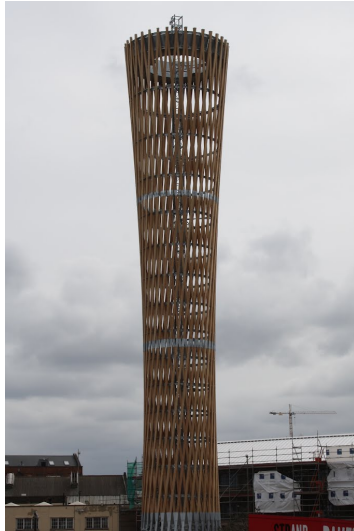
(a) The Strand East Tower in London
Source: Tripomatic, http://www.tripomatic.com/United-
Kingdom/Greater-London/London/Strand-East-Tower,
accessed February 2015

(b) The Jüberg Observation Tower
Source: Arch Daily, http://www.archdaily.com/72575/
jubergtower-hemer-birk-und-heilmeyer-architekten,
accessed February 2015

Figure 4-1: Examples of medium-high hyperboloid structures in timber

Concrete cast in-situ towers are also a viable option, but require the transportation of a lot of work on site, usually not proving to be economical [29]. Turbine towers made of other materials, such as composites, or steel-concrete hybrid structures, have also been applied. Bolted steel or prefab concrete shell elements are being developed and applied as well, eliminating the diameter limitations set by transportation. The application of these designs is on the rise, but not widespread yet.

4-1-2   Tall timber structures

Timber is one of the oldest building materials and many structures have been made using it, even the first (smaller) turbine towers and turbine blades. When looking at tall structures made of timber, the following division can be made, according to the overall structural system:

Lattice towers
Timber lattice (or truss) towers towers have been used to reach substantial heights, by combining a large number of axially loaded members. Especially in-between the two World Wars a large number of tall timber lattice towers have been built, the highest ever being a 190 m high transmission tower in Germany.

Hyperboloid structures
Essentially a kind of lattice tower, hyperboloid structures are mentioned separately because of their slightly different structural behaviour. The hyperboloid geometry of the tower is one of the main load-bearing characteristics. Some medium-height towers have been built in timber, shown in Figure 4-1.

(a)
Source: KLH, http://www.klhuk.com/portfolio/residential/
stadthaus,-murray-grove.aspx, accessed December 2014

(b)
Source: Techniker, [41]

Figure 4-2: The Stadthaus, in London

Solid wall structures

It is becoming more and more common to build mid-rise apartment buildings out of timber. The Stadthaus in London of Figure 4-2 is a well-known example, but is certainly not the only one. Floors and walls made of large CLT elements form the load-bearing structure and stabilizing elements of the buildings, where the most height-limiting factor often are the fire regulations, not the capacity of the material. The original TimberTower in Hannover also uses large CLT elements and can be placed in this category as well.

4-1-3   Choice of design

Systems using a large number of smaller size elements, such as the afore-mentioned trusses and hyperboloid structures, contain a lot of connections. These connections all introduce some slip and thus a certain amount of uncertainty in the dynamic behaviour of the structure. This uncertainty will carry through into the natural frequencies of the tower and make them hard(er) to predict. Furthermore, the large number of individual elements, in for example a lattice tower, all need protection from the elements, which is costly and likely to be labor-intensive. This leads to believe that the solid-walled timber tube design of the original TimberTower is the one most suited for the application as wind turbine tower.

In the end, it is decided that the existing structural design of the TimberTower will be used to determine the feasibility of timber towers in the Netherlands. It will be subjected to the Dutch wind conditions, which are often higher than those in Hannover, for heights classes and turbines mentioned in Chapter 2. Further investigation into alternative material use might prove to optimize this design further or, at least, offer alternatives. The next paragraphs will shortly explain the design of this tower. More detailed information about the TimberTower, including its history, can be found in Appendix K.

4-2   Overview of the chosen design

The TimberTower company, formed in 2008, was the first to use a timber tower to erect a multi-megawatt turbine. Its global design will be used within this thesis as well, for reasons discussed a moment ago. This section will deal with the overall structure of the tower design,

(a) The overall exterior structure of the tower

(b) Part of the interior scaffolding

(c) The transfer structure which is placed at the top of the tower

(d) The base of the tower

(e) The connection between concrete and timber
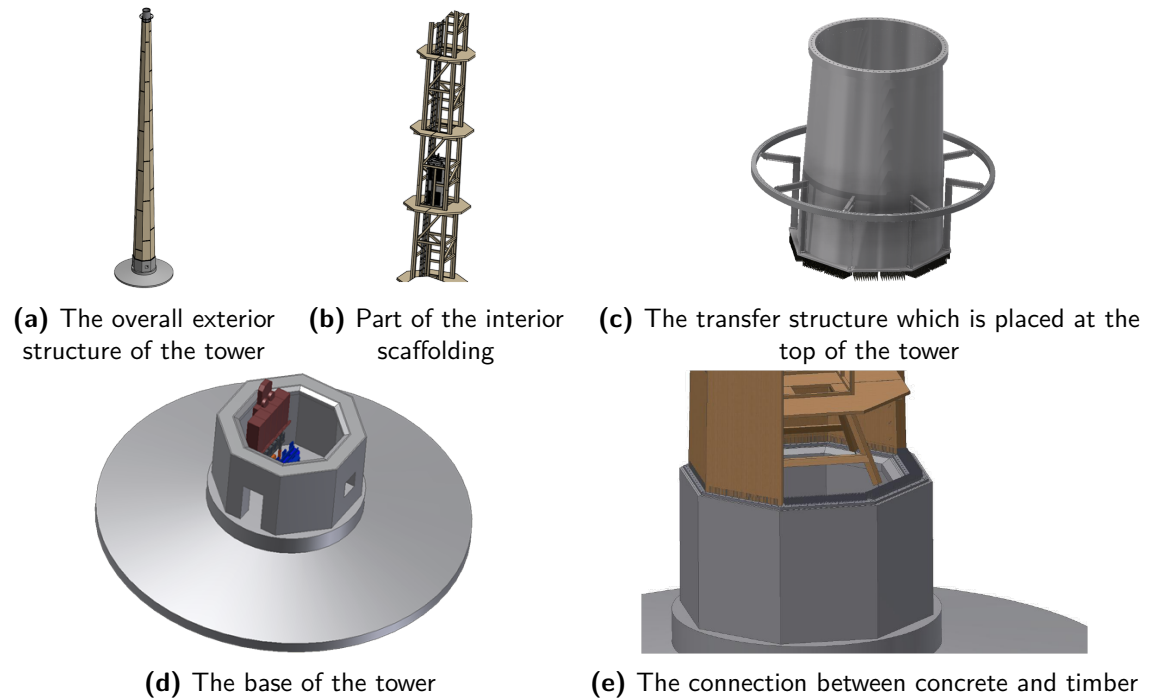
Figure 4-3: Several components of the original TimberTower, whose design is applied in this thesis as wel
Source: TimberTower GmbH [42]

without stating specific values for the dimensions and other parameters of the original tower. Since this section is a summary of part of Appendix K, those specifics on the TimberTower can be found there, along with other subjects regarding the project.

4-2-1 Overall structure

The tower stands on a concrete foundation, either a shallow or pile foundation, depending on the soil conditions. The original tower was founded on a shallow slab foundation, made possible by the soil conditions in Hannover. The concrete base extends several meters above the surface, to accommodate the access door, installations, and prevent vandalism (Figure 4-3d). On top of this concrete pedestal a polygonal hollow body is formed by combining long CLT panels, which are glued together (Figure 4-3a). More about the connections used will follow later.

The tower is tapered, reducing material use and allowing the top diameter to reach a size compatible with the turbine on top. Because of the tapered shape, the individual elements are trapezoidal. A steel transfer structure makes up the top 5 meters of the tower, to change the tower shape from polygonal to circular (Figure 4-3c). In this way, the tower is compatible with contemporary turbine systems.

For protection against the elements, the timber part of the tower is wrapped in PVC lining. Installations within the base of the tower control the moisture content of the air within the tower, keeping it around 12 to 13% [22].

(a)   (b)

Figure 4-4: Horizontal connections are made by steel plates inserted into slots in the bottom
and top edge of the panels
Source: TimberTower GmbH[24] [42]

4-2-2 Connections

Vertical slits are cut into the horizontal edges of the panels (Figure 4-4a) and square perforated
metal plates with a thickness of 2.5 mm are inserted (Figure 4-4b). By filling the slits with two-
component polyurethane adhesive, the load is transferred between the panels by adhesion and
dowel-type action through the perforations. Specific strengths and stiffness of this connection
will be provided in section 5-7.

The great advantage of this connection is its strength and stiffness, allowing for very little slip
when loaded. Experiments and tests performed at MPA Wiesbaden have allowed designers
to optimize this connection, making it strong enough to withstand the extreme and fatigue
loads that a tower will experience, while maintaining its ductility through the use of the steel
plates.

The shear forces in the vertical seems of the original tower were low enough to allow for
adhesive bonding without adding additional steel elements. A perforated wooden strip is
placed in the gap between two panels and injected with the adhesive. The same is assumed
to be possible for the designs within this research.

4-2-3 Erection

The erection sequence of the original tower is more elaborately explained in Appendix K,
including pictures.

First, a timber scaffolding is partly erected out of prefabricated sections (Figure 4-3b). The
CLT panels are then assembled in a spiral-like fashion, using the scaffolding for temporary
support. This process is then repeated until the top height is reached. The helix-pattern of
the panels prevents horizontal seems that go all around the tower at a specific height. This
reduces material use, because the weak spots are smeared out over the height of the tower,
contrary to what is the case in traditional steel towers.

When finished, the scaffolding will have no structural function, but will allow personnel easy
access to different parts of the turbine. The horizontal and vertical seems are glued together

during erection using the connections described above. Once erected, the transfer structure and the rest of the turbine are added to complete the turbine.

Methods

CHAPTER 5

Frequency calculations

Sources agree [5, 29] that one of the most important characteristics to design for in a turbine tower is its natural frequency. To determine this frequency, the tower will be simplified and modelled as a tapered beam with a point mass on top. The beam cantilevers from the bottom, while the end with the point mass is able to move freely. The beam itself has mass as well, described by its density.

While analytic solutions for this model exist [43, 44], solving differential equations for each design is hard to do in a time-efficient manner. This is why numerical calculations have been used, with which the author is more familiar.

Two methods have been used:

Rayleigh-Ritz method - natural frequency estimation
Considering simplicity and computation speed, the preferred method was introduced by an MS Excel worksheet [45] developed by the Offshore Engineering Department of the faculty of Civil Engineering at Delft University of Technology, based on the Rayleigh-Ritz method. It is shortly explained in Appendix F. The author has adapted this sheet into Matlab code, which is found in Appendix G.The use of this method would be preferable over other options because it is fast and easy to incorporate with other simple calculations using spreadsheets or Matlab.

Finite Element Method (FEM) for determining the natural frequency
The tower is also modelled using ANSYS, commercial finite element software, under an educational/research license. These calculations take more time, but provide more accurate results, when used correctly.

Both methods will be explained in more detail first, where the description of the FEM-model will also focus on element type, size and convergence of the model. A parameter study is then performed and described in section 5-5, followed by investigations into the influence of both foundation and connections stiffness on the frequency.

The main goal behind the frequency investigation is to determine the validity of both methods, draw conclusions about the influence of several important parameters on the natural frequency

Geometrical parameters			
Thickness	t	0.45	m
Outer side width top	$a_{out,T}$	1.35	m
Outer side width bottom	$a_{out,B}$	4.00	m

Material parameters			
Density timber	ρ_{timb}	420	kg/m^3
Effective Young's modulus	$E_{eff,mean}$	8.80E+09	N/m^2

Other parameters			
Top mass	M_{top}	350000	kg

Table 5-1: Input parameters for the base model for the frequency analysis. Geometric parameters are defined in Figure 5-1.

and to determine possible differences between circular and octagonal towers. To be able to make valid statements about the influence of certain parameters, a base model was constructed first to serve as reference throughout the frequency study.

5-1 Base model

The base model for both tools has the properties displayed in Table 5-1, which also leads to the geometrical properties found in Table 5-2. The mean Young's modulus $E_{eff,mean}$ is the Young's modulus of the longitudinal layers averaged over the entire thickness of the cross section. For a Young's modulus of 11,000 N/mm^2, with 80% of the fibre orientation along the tower, this leads to the value found in the table. The chosen values are based on a combination of simple calculations and literature, and limited to an octagonal tower of 125 m. Definitions of the geometrical parameters can be found in Figure 5-1, the corresponding formulas in the appendix on the geometrical properties of polygons, Appendix E.

In the base model it is assumed for now that the top mass has no rotational inertia, leaving just a dimensionless mass. Material values for Cross Laminated Timber strength class CL24h are used, based on the ones provided by Schickhofer [6] and described in Appendix D

5-2 Rayleigh-Ritz method - natural frequency estimation

Originally designed for circular tubular (steel) towers, the equations behind the aforementioned worksheet have been adjusted to also be applicable on polygonal towers. For this purpose, the input has been adjusted to incorporate the taper, and the second moment of area has been updated, among others. The precise adjustments are found in Appendix F.

The Rayleigh-Ritz method is described in many pieces of literature, such as Ilanko [46]. It estimates the natural frequencies of multi-degree of freedom systems by assuming a certain

Inner side width top	$a_{in,T}$	0.98	m
Inner side width bottom	$a_{in,B}$	3.63	m

Outer radius top	R_T	1.76	m
Inner radius top	r_T	1.63	m
Outer radius bottom	R_B	5.56	m
Inner radius bottom	r_B	4.84	m

Width circumference top	b_T	3.53	m
Width circumference bottom	b_B	10.45	m
Width top	d_T	3.26	m
Width bottom	d_B	9.66	m

Area top	A_T	4.19	m^2
Area bottom	A_B	13.73	m^2

Moment of inertia top	I_T	4.48	m^4
Moment of inertia bottom	I_B	154.13	m^4

Table 5-2: Calculated geometrical properties from the base model, using Appendix E. The parameters are defined in Figure 5-1.
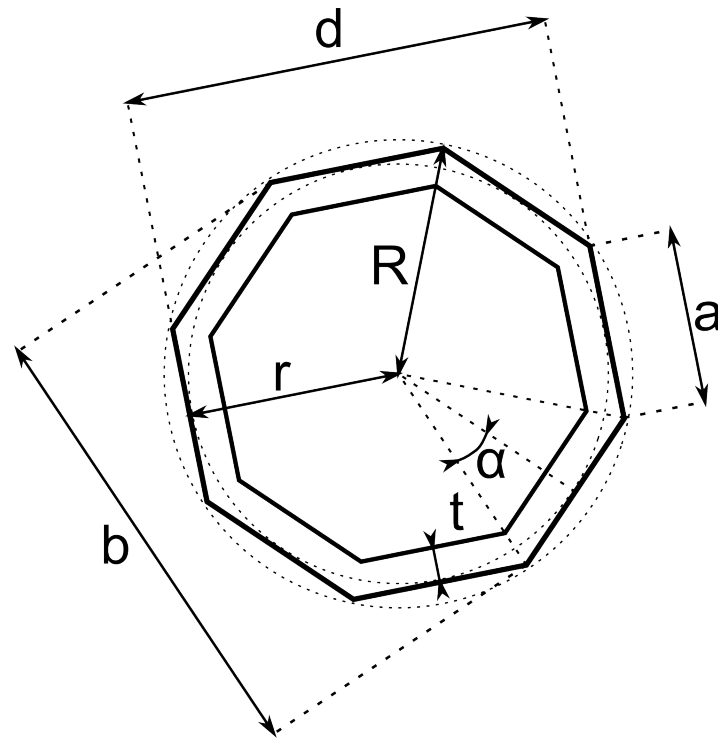
Figure 5-1: Geometric definition of a regular hollow octagon

mode shape. Unless the exact mode shape of the system is used, the method will always overestimate frequencies.

A main underlying assumption for the use of this tool within this thesis is similarity between mode shapes for circular hollow towers and polygonal hollow towers. The mode shape used for circular towers will also be used for polygonal ones. This assumption is verified later on in this chapter.

5-2-1   Convergence

A quick check of convergence was made using different element sizes in the original worksheet, for the base model described above. The results are found in Table 5-3. It can be concluded that this specific model already reaches its final value for an element size of $l = 5.44$ m, based on 4 significant figures. Since the computational load caused by the worksheet is very low, the element size will be kept at its default value of $l = 1.0$ m. This element size is also used in the Matlab code based on this method, found in Appendix G.

5-3   Finite Element Analysis - ANSYS

5-3-1   Model

This section requires some affinity with FEM modelling from the reader. The script used to create the models analysed in this section can be found in Appendix H, where the build-up

Element size		
Number of elements n	Length per element l	Frequency f
1	125	0.1961
5	25	0.2630
10	12.5	0.2642
50	2.5	0.2646
100	1.25	0.2646
125	1	0.2646
23	5.44	0.2646

Table 5-3: Convergence checks for the Rayleigh-Ritz base model

is explained in more detail.

5-3-2 Convergence and element type

A simple check of convergence of the frequency results was also made here, using the base model. Element size was halved in every subsequent run to determine the ideal mesh size. The underlying goal was to reach sufficient accuracy in the results, keeping future stress calculations in mind as well, while still keeping computation time to a minimum. The investigation also served as a way of determining the proper element type. An accuracy of three significant numbers was decided as amply sufficient for design purposes.

The first check was made with a model containing 8-node solid elements (SOLID185), a simple solid element. Computations were fast, but convergence was only reached for a very fine mesh in the case of the second natural frequency. This turned out be to be of lesser importance, since this second natural frequency did not lie within the vicinity of the rotor frequencies, as can be seen in Table 5-4.

20-node solid elements (SOLID186) converged much faster, showing no substantial difference between the coarse and finer meshes. The presence of a mid-node along the thickness of the wall and the higher number of nodes increased precision. When using solid elements, the mesh should be fine enough to prevent shear locking of the elements, which will affect the precision of results in a negative way. Whether shear locking is adequately prevented can be confirmed by comparing the results of the solid element model to those of a shell element model. Shell elements are two dimensional, with the thickness being a element property, instead of being physically present. Shells are naturally suited for thin structures, whereas solid elements are better suited for bulkier models. Two types of elements were therefore tested as well, 4-noded SHELL181 elements and 8-noded SHELL281 elements.

As with the solids, the 8-noded elements already showed no sign of converging further from the coarse mesh, while the 4-noded elements might not yet have converged at the finest mesh investigated, see Table 5-4.

In the end, a relatively fine mesh was chosen with a low computational time. This mesh is also shown in Figure 5-2b, where essentially 1 m high elements are applied. Solid elements were chosen over shell elements, even though the results ended up not differing substantially. The potentially small ratio of top diameter over wall thickness might result in a thick-walled structure and thus potential errors when using shell elements.Furthermore, to be able to judge the shear stresses over the cross section, solid elements are required, with adequate accuracy. Concerning the type of solids, the 20-node solid elements containing mid-nodes were chosen over 8-noded elements for accuracy reasons.

(a) Relative division parameter = 1   **(b)** Relative division parameter = 4
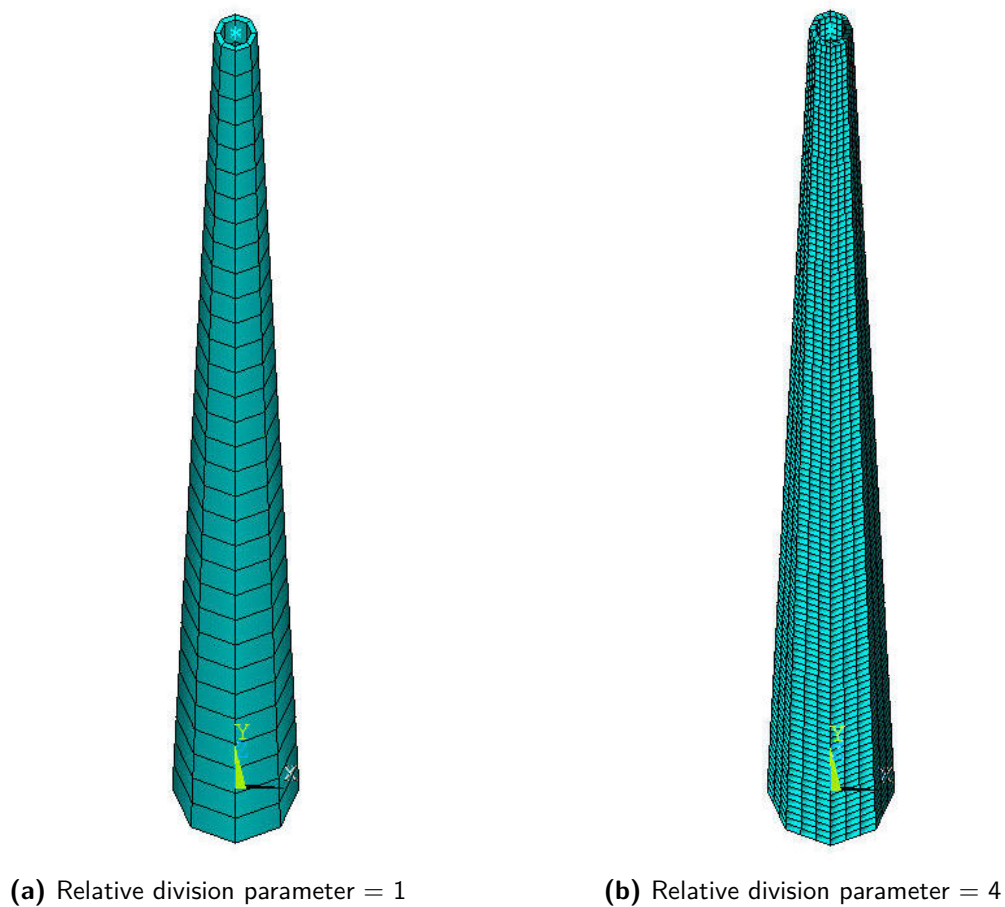
Figure 5-2: Examples of mesh sizes used in ANSYS

5-4 Mode shapes

The Rayleigh-Ritz worksheet adaptation was limited to the first natural frequency, while the first three unique mode shapes of the tower were investigated with ANSYS. Because the tower is symmetrical, some of the modes come in pairs, where two modes are identical but

Convergence - 8-node solid elements				
Relative division parameter	f_1	f_2	f_3	Computation time
1	0.2511	1.830	5.131	< 5 sec
2	0.2438	1.754	4.880	< 5 sec
4	0.2418	1.732	4.810	ca. 5 sec
8	0.2413	1.726	4.787	ca. 10 sec
16	0.2412	1.725	4.780	ca. 2 min

Convergence - 20-node solid elements				
Relative division parameter	f_1	f_2	f_3	Computation time
1	0.2412	1.725	4.781	< 5 sec
2	0.2412	1.725	4.779	ca. 5 sec
4	0.2412	1.725	4.780	ca. 10 sec
8	0.2412	1.725	4.779	ca. 3 min
16	Not feasible, computation time too high for design purposes			Runout

Convergence - 8-node shell elements				
Relative division parameter	f_1	f_2	f_3	Computation time
1	0.2411	1.721	4.763	< 5 sec
2	0.2411	1.720	4.762	< 5 sec
4	0.2411	1.720	4.763	ca. 15 sec
8	0.2411	1.720	4.762	ca. 30 sec
16	0.2411	1.720	4.762	ca. 20 min

Convergence - 4-node shell elements				
Relative division parameter	f_1	f_2	f_3	Computation time
1	0.2348	1.682	4.693	< 5 sec
2	0.2358	1.688	4.680	< 5 sec
4	0.2401	1.713	4.743	< 5 sec
8	0.2408	1.718	4.757	ca. 10 sec
16	0.2410	1.719	4.760	ca. 20 sec

Table 5-4: Convergence checks for the ANSYS base model on the first three eigenfrequencies f_i

perpendicular to each other. By setting the number to six, the first three unique mode shapes were found in all cases.

Although in most cases the first six modes consist of three pairs, and one could argue that the value could thus also be set at five, results showed that for certain sets of parameters a non-bending mode would become more dominant and end up within the first three unique modes. A minimum of six modes was therefore still investigated per model, to be able to determine when these non-bending modes occurred as one of the first three unique modes.

Higher modes than the first three are assumed not to play a significant role and are not incorporated here. Based on frequencies found, it is even concluded that only the first natural frequency will lie within range of the rotor frequencies for timber towers, just as they do for conventional towers. This conclusion is used in the final calculation model, to save computation time. It also strengthens the validity of the Rayleigh-Ritz tool, which was programmed to be limited to the first natural frequency as well.

For the base model from section 5-1, the first three unique modes were all bending modes, displayed in figure 5-3.

(a) First mode   **(b)** Second mode   **(c)** Third mode
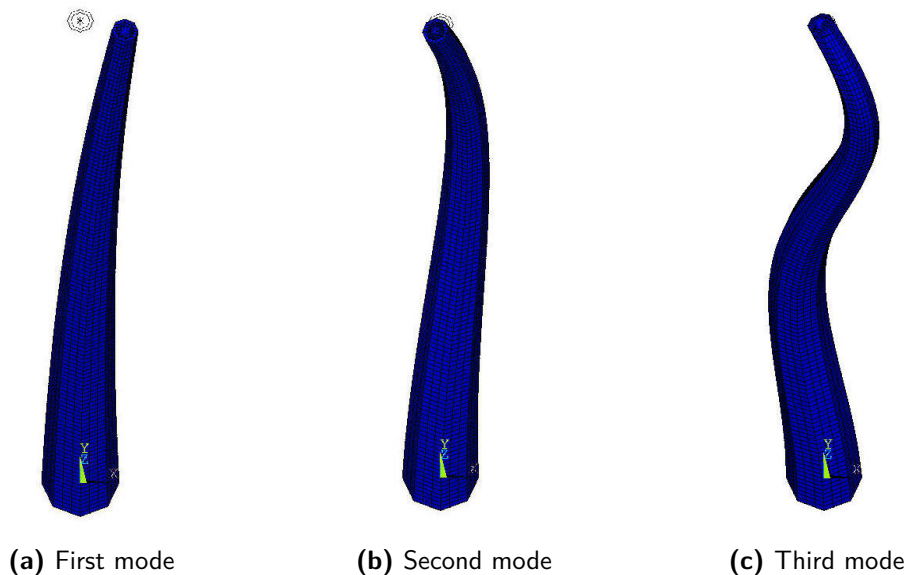
Figure 5-3: The first three bending modes of the base model, exported from ANSYS

5-5   Parametric investigation into frequency behaviour

To determine the influence of the different parameters in the model on the natural frequencies of the tower, each parameter is varied in the base model in turn, ceteris paribus. A number of different values for each parameter are run through the ANSYS script and the Rayleigh-Ritz worksheet, keeping the parameters within realistic limits. A description of the results can be found below, tables and graphs containing the data can be found in Appendix A. This part is limited to octagonal towers with a height of 125 m. Lower hub heights and decagonal tower shapes are expected display the same behaviour.

5-5-1 Geometry-related parameters

Comparison with circular towers

Since circular towers are the norm in today's wind turbine practice, it is important to know if the frequency behaviour of polygonal towers is similar. If this is the case, many assumptions, rules of thumb, tools and software can be used without having to radically adjust them. Defining the outer diameter of the circle as $D_{circle} = 2\frac{R_{\text{octagon}} + r_{\text{octagon}}}{2}$, the size - and consequently also the stiffness - of the cross sections was kept practically the same. R and r are defined in Appendix E.

Both frequency calculation methods were used:

– **Rayleigh-Ritz method**
   For the Rayleigh-Ritz method the octagonal and circular cross sections had a similar equivalent beam stiffness for the entire structure, which is the expected result from a nearly identical stiffness for each cross section along the tower, resulting from the close correspondence of cross sectional dimensions. The results were not surprising: differences between the circular and octagonal tower were less than 1%, see also Table 5-5.

– **ANSYS FEM-calculations**
   For the finite element model, differences remained within a 2.5% margin and are therefore not considered substantial. Results tended to become more similar as the width of the tower increased, see also Table 5-5.

Thickness

Increasing the wall thickness will lead to an increase of the first natural frequency. Within the investigated range of thickness between 0.25 and 0.85 m, differences with the base model went op to 20%. Increasing the thickness caused a decrease of the second natural frequency. The third natural frequency decreased for wall thicknesses greater than the base model. Both higher frequencies however remained out of range of the rotor frequencies. Small wall thickness resulted in a third mode shape where the structure shortened and stretched along the z-axis, without translation in the other directions. The results are shown in Table A-1 and Figure A-1

Taper

Results suggest that a larger taper (i.e. smaller top dimensions for the same base dimensions) lowers the natural frequency of the tower, as can be seen in Table A-2 and Figure A-2. Interesting to see is that for a non-tapered tower, the third unique natural frequency is not symmetrical. A torsional mode occurs for $a_{out,T} = a_{out,B}$. Again, higher frequencies did not come close to the rotor frequencies.

Results from the Rayleigh-Ritz and FEM-methods showed different severity in the influence of the taper, but the decrease in frequency with increasing taper was evident in both methods.

General geometry size

The influence of the general geometry size was investigated in two ways, while keeping the height constant at 125 m.

Circle vs Octagon - Rayleigh-Ritz method						
Width octagon		Diameter circle		Frequencies		Relative
d_T	d_B	$D_{out,B}$	$D_{out,T}$	Octagon	Circle	
7.24	2.50	7.53	2.61	0.1710	0.1727	+0.98%
9.66	3.26	10.04	3.39	0.2646	0.2661	+0.56%
12.07	4.10	12.55	4.27	0.3678	0.3697	+0.51%

Circle vs Octagon - ANSYS						
Width octagon		Diameter circle		Frequencies		Relative
d_T	d_B	$D_{out,B}$	$D_{out,T}$	Octagon	Circle	
7.24	2.50	7.40	2.50	0.15546	0.15207	-2.23%
9.66	3.26	9.88	3.33	0.24123	0.23748	-1.58%
12.07	4.10	12.53	4.24	0.33764	0.33936	+0.51%

Table 5-5: Differences between circular and octagonal cross sections, keeping all non-mentioned parameters equal

First, the cross section of the tower was scaled, adjusting both width and thickness. Height and taper were kept constant by multiplying $a_{out,T}$, $a_{out,B}$ and t all by the same factor. The results suggest a linear correlation between the scaling factor and the natural frequency. Increasing the overall size of the cross section, increases all natural frequencies.

Secondly, the thickness was kept constant while varying the width of the cross section. The same effect could be seen, although less severe. Interesting to see was that for a scaling factor of 2 times the base model, the third natural frequency was a local buckling mode. For scaling factors between 1.5 and 2, the third unique mode was a shortening mode.

Top mass

The top mass was ranged from 0 kg to 700,000 kg, a value twice that of the base model and the associated 5 MW turbine. Adding more mass on top of the tower proved to lower the natural frequencies significantly, as could be expected. The influence appears to be asymptotic, the relative decrease in frequency becoming smaller for higher masses.

Interesting to see is that the third natural frequency drops when the top mass starts to exceed the tower mass (which lies around $4.7 \cdot 10^5$ for this particular model). A new mode appears at this point, one where the tower is only vibrating along the height (i.e. shortening and stretching) and not transversely. This became more apparent as the mass was increased even further, using models whose results are not shown here. Still, these higher frequencies did come near the 1P and 3P frequencies.

Rotational inertia of the top mass

Although not modelled in many simple analysis models, in reality the nacelle and rotor will have a certain rotational inertia. Determining whether or not this affects the natural frequency was done by assigning a rotational inertia to the point mass, defined as a certain scaling factor times the top mass.

Results show that, when varying the rotational inertia between $0 \cdot M_{top}$ and $10 \cdot M_{top}$, the first natural frequency of the tower is not influenced. Even for a value of $100 \cdot M_{top}$ the difference with the base model is only around 1%. The assumption in many other frequency models that take I_M as 0, is justified.

The higher natural frequencies experience a greater influence of the rotational inertia, which can be explained by the torsional modes becoming more dominant. Because of the inertia, torsional natural frequencies become lower, up until a point where they are lower than most of the bending natural frequencies. Hence, this mode appears in the top three unique mode shapes shown in the results.

5-5-2   Material-related parameters

Modulus of elasticity

Increasing the Young's modulus increases the stiffness of the tower and thus the natural frequency, as is to be expected. When applied to the base model, the ratio between the different aspects of the geometry causes the first three unique natural frequencies to be associated with pure bending modes, for all investigated values.

Density

Lowering the density decreases the natural frequencies slightly, as can be seen in Figure A-8. For low densities the shortening mode became the third unique mode, because the top mass exceeded the mass of the tower.

Isothropy vs Orthotropy

Unlike materials such as steel, wood is not an isotropic material. For the models used in the frequency calculations thus far, the timber has been modelled as an isotropic material. Here it will now be discussed whether the material should be modelled as orthotropic or can just be modelled as an isotropic material. The latter is easier to model for the different materials applied throughout this research.

For isotropic materials, ANSYS calculates the shear modulus based on the relation $G = \frac{E}{2(1+\nu)}$. For a Young's Modulus of 8800 N/mm^2, which corresponds to a cross section with 80% of its fibres oriented along the tower ($k_{net} = 0.8$, see Figure 5-10) and a Poisson's ratio of 0.3 this equals to G=3380 N/mm^2, which is not in the correct order of magnitude for timber materials. Suggested values given by Schickhofer [6] for CLT are much lower at G_{mean}=650 N/mm^2.

Therefore, it is has been investigated if modelling the correct shear modulus influences the natural frequency results significantly. Only the value of G_{mean}=650 N/mm^2 as suggested by Schickhofer is investigated. Applying three different geometries will cancel out any coincidental influence of the geometry. Those geometries are shown in Table A-9 in the appendices.

First, the shear modulus was altered between the correct value of 650 N/mm^2 and the default value of 3380 N/mm^2, while keeping the Young's modulus isotropic. It did not influence the first natural frequency significantly, lowering it by 4% at most. Results of this can be found in Table A-10. The higher modes would change up to 30% because other mechanisms, like torsion, became more dominant. They did however not come near 1P and 3P and will therefore not jeopardize any conclusions drawn from later models and designs, which will focus on the first natural frequency only.

Secondly, the Young's modulus in longitudinal direction was kept at $0.8 \cdot 11000 = 8800$ N/mm^2, resembling a cross section of which 80% of the fibres are along the axis of the tower. The Young's modulus in the other in-plane direction was set at $0.2 \cdot 11000 = 3380$ N/mm^2, accounting for the other 20% of the fibres. The out-of-plane stiffness, which is the one perpendicular to the fibre, was set at 450 N/mm^2, corresponding to suggested values for CLT [6].

Changes in the first natural frequencies of these models were found to be neglectable and isotropic modelling is concluded to be applicable for all frequency calculations in this research, saving time. Additional checks of stresses within the tower showed that no significant change occurred here either.

5-5-3   Conclusion and discussion

A short summary of the results found during this parameter study is provided below.

Rayleigh-Ritz versus Finite Element method

Unless the exact mode shape is substituted in the Rayleigh-Ritz method, the natural

Increase of parameter	Influence
t	increase
E	increase
width/size	increase
ρ	neglectible
I_M	neglectible
M_{top}	decrease
taper	decrease

Table 5-6: Influence of the investigated parameters on the first natural frequency

frequency that is found will always be too high [46]. The difference between this method and the exact answer from finite element analysis lies around 10%, confirming this overestimation. Because of the low computational time, final verification of the natural frequency will be made using ANSYS, but designs are first made using the Rayleigh-Ritz method.

Circular versus octagonal

When it comes to frequency analysis, it can be concluded that the differences between a circular and an octagonal tower can be neglected, especially in this stage of design. This conclusion could potentially make it possible to use existing software designed for circular cross sections without having to alter its source code, but inputting circular towers to represent octagonal ones.

Number of natural frequencies

Although interesting things happen with the higher modes, only the first natural frequency lies in the same range as those of the rotor. Critical frequency calculations can therefore limit themselves to just the first natural frequency.

Isotropic versus orthotropic

Accounting for the lower shear modulus and orthotropy of the timber material did not lead to significant changes in the first natural frequency. For frequency analysis, isotropic models will give accurate enough results, saving time.

Parameters

Table 5-6 gives an overview of the influence of the investigated parameters. This can be used to quickly assess and alter the behaviour of the tower when designing.

5-6   Influence of foundation on the tower frequency

Characteristic for the Netherlands is its soil, with load bearing layers often found deep below the surface. The capacity of the top soil layers is seldom sufficient for shallow foundations, requiring pile foundations for various types of structures, from simple houses to multi-megawatt wind turbines.

Many sources give an overview of the different foundation types of turbines, such as Burton [29]. Governing is the overturning moment caused by extreme wind conditions. Slab or raft foundations resist the overturning moment by activating the load-carrying capacity of the soil underneath a large concrete slab. They can not be applied on weaker soils, where pile foundations make for a more efficient solution. Multi-pile foundations transfer the loads to deeper load-bearing soil layers, while mono-pile foundations (i.e. a single, large diameter pile underneath the turbine) resists the overturning moment by mobilizing soil lateral loads.

It is important to know the feasibility of foundations for large turbines under the Dutch soil conditions, in order to judge the overall feasibility. The first timber turbine tower in Germany has been placed on soil that did allow for a raft foundation, but for multi-MW turbines in the Netherlands, this is not considered feasible. In Vlissingen, however, two turbines with a capacity of 6.2 MW have been build on multi-pile foundations [28], proving that it is possible to build foundations in Dutch soil suited for these massive turbines.

While the load bearing capacity of the foundation is not considered to be an issue for the NREL 5 MW, as proven by the larger turbines in Vlissingen, it can still influence the natural frequency of the tower. In design calculations the foundation is modelled as completely rigid, while in reality it will have a finite stiffness. This part will investigate whether foundations suited for Dutch soil conditions will influence the natural frequency significantly. This is done by comparing the stiffness of existing foundations with frequency results from FEM-calculations.

Stiffness under dynamic loads may differ from the static foundation stiffness, especially for high-frequency vibrations. For wind loading, the static foundation stiffness is representative for the dynamic stiffness [5]. This can not be assumed the same for earthquake loading, but large enough earthquake are assumed not to occur in the Netherlands.

5-6-1   Rotational stiffness of a pile foundation

The total rotational stiffness of a pile foundation k_ϕ [Nm/rad] is calculated using a formula widely found in literature [47, 48]:

$$k_\phi = \sum k_{v,i} R_i^2 \tag{5-1}$$

Where:

$k_{v,i}$ is the vertical translational stiffness of pile i [N/m];
R_i is the lever arm of pile i in the direction of bending [m].

Which is shown in Figure 5-4. It is assumed that the concrete slab that transfers the loads from the turbine to the piles is completely rigid. In reality redistribution of the pile loads will take place, lowering the extreme pile loads and dividing the total load more evenly.
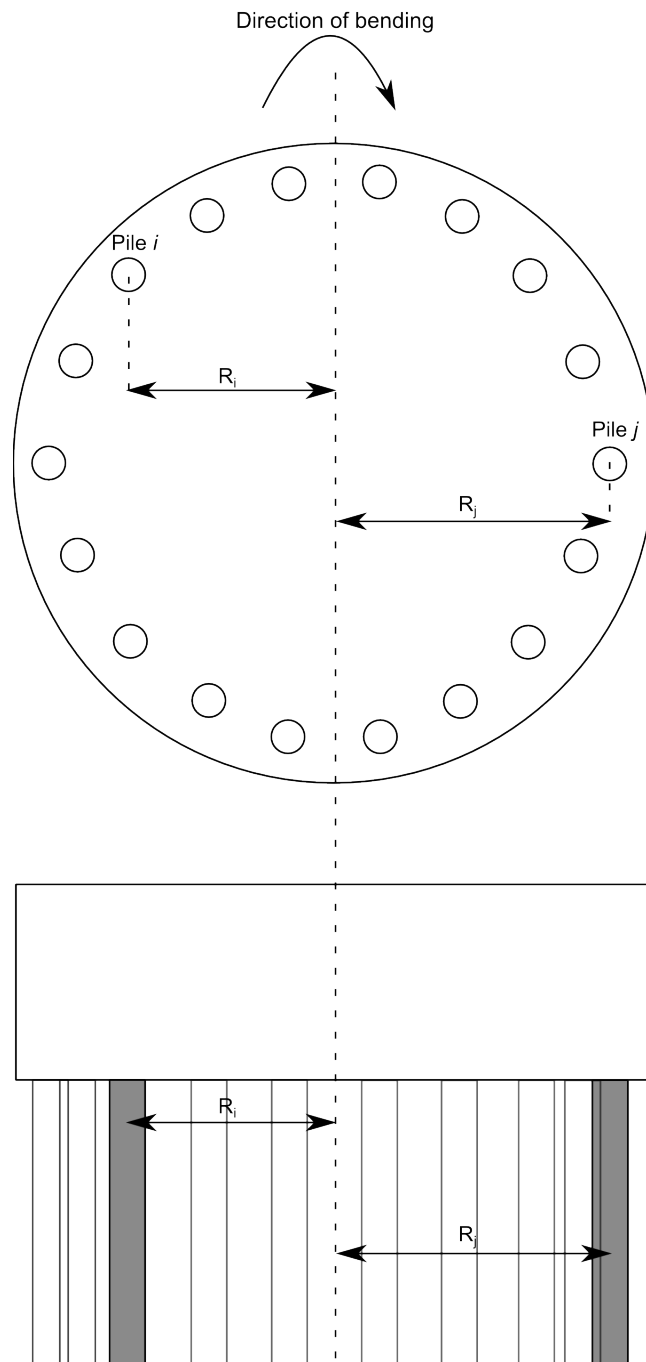
Figure 5-4: Definition of the individual lever arms described in Equation 5-1

5-6-2   Influence of foundation stiffness on frequency

To determine the influence of the foundation on the first natural frequency, a spring foundation was added to both the base model described previously and a second model (referred to from hereon as 'Model A' and 'Model B', respectively) created in ANSYS. The base model is described in Section 5-1. Model B is the same as the base model, but with $a_{out,B} = 4.65$ m and $a_{out,T} = 1.80$ m, resulting in a higher natural frequency

All nodes on the bottom surface of the FE-model have been copied with a vertical offset and connected to their mother nodes by a spring element. This way, the springs will be perfectly vertical at the start of the analysis.

The total rotational stiffness of the foundation is calculated with Equation 5-1. Since the placement of the nodes is not perfectly symmetric, the exact node coordinates were used for R_i, after being extracted from ANSYS. Differences between the total rotational stiffness in x and y-direction were 1% at most, suggesting a near-symmetric rotational stiffness. Even assuming an evenly distributed set of springs around the perimeter at $r_{out,B}$ resulted in a 2% higher stiffness than what was found using the exact coordinates. Because of these small differences, the stiffness as calculated in x-direction was taken as reference.

By adjusting the spring stiffness of these individual springs and calculating the first natural frequency, the curves in Figure 5-5 was made. It can be seen that for values of $k_\phi = 10^{11}$ Nm/rad the first natural frequency only differs 1% with the frequency of a completely rigid foundation. For values of $k_\phi = 10^{13}$ Nm/rad and up, this drops to less than 1‰.

5-6-3   Reference foundations

To be able to judge whether foundations in the Netherlands will influence the natural frequency of the tower, the rotational stiffness of existing foundations is calculated and compared in Figure 5-5. A foundation for the base model, used in the previous frequency study in 5-1, is also designed.

Two references were found containing foundations of turbines in the Netherlands. The first one is for two 6.2 MW turbines in Vlissingen, Zeeland [28], which are about the same size (rotor diameter of 130 m) and height (hub height 120 m) as the NREL 5 MW turbine considered in this research. The second foundation is for wind park 'De Zuidlob' near Zeewolde, Flevoland [37]. These are lower in height (90 m) and, with 3 MW, also lower in power. This results in a smaller foundations being applied there.

The individual pile stiffness is set at $1 \cdot 10^5$ kN/m, based on experience from practice. In reality this stiffness can reach values two or three times as high, especially in compression, but this lower stiffness is considered adequate for both tension and compression and on the conservative side. Similar values are found in Chapter 5 of Svensson [49] for relatively small pile diameters, confirming its conservative nature. Fugro [50] has found stiffness values ranging from $2.2 \cdot 10^5$ to $5.6 \cdot 10^5$ kN/m for piles underneath 1.5 MW turbines in the Noordoostpolder in compression, further confirming this.

Usual requirements set by manufacturers for the rotational stiffness of foundations lie between 30 and $100 \cdot 10^9$ Nm/rad[51, 37, 52, 53]. Codes to calculate the foundation stiffnesses in Figure 5-5.
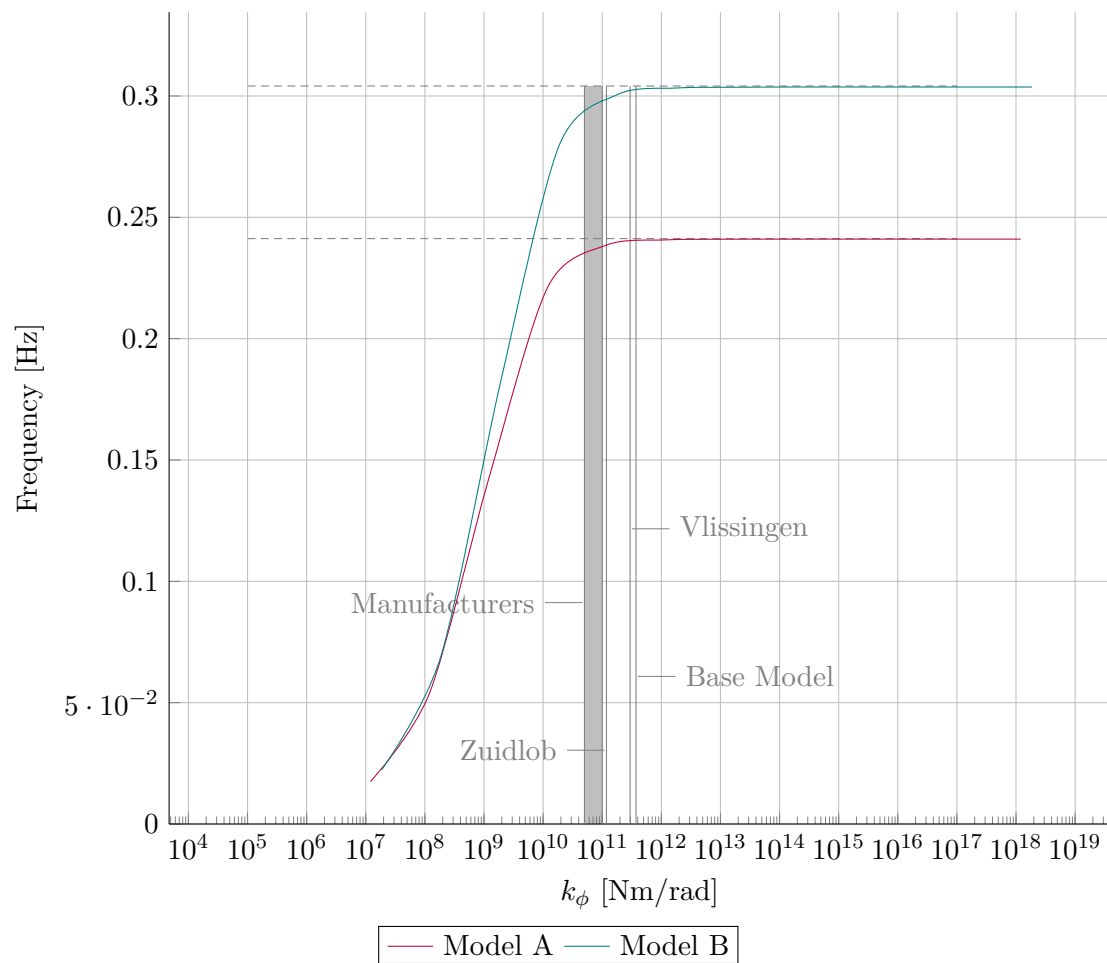
Figure 5-5: The influence of the foundation rotational stiffness on the first natural frequency, using ANSYS
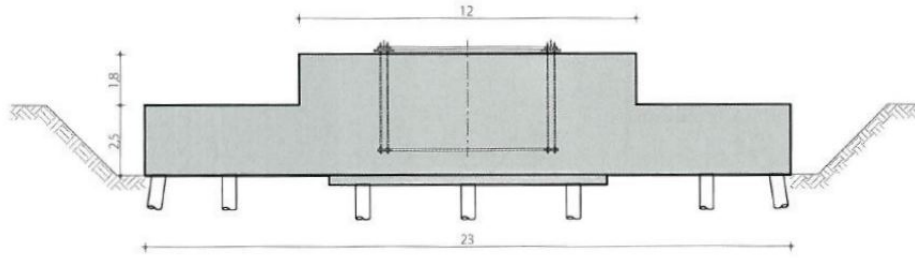
Figure 5-6: Side view of the foundation underneath the turbines in Vlissingen
Source: Koch [28]

Vlissingen

For the aforementioned 6.2 MW turbines in Vlissingen, Zeeland, pile foundations using 63 piles were built [28]. The circular foundation slabs have a diameter of 23 m and their thickness ranges from 2.5 to 4.5 meter along that diameter. Based on the overview of the structure, the foundation piles are assumed to be in three concentric circles. 36 piles are at 11 m from the centre, 20 piles at 8.5 m and 7 piles at 3.7 m, shown in Figure 5-6. Summing these in equation 5-1, with $k_v = 1 \cdot 10^5$ kN/m, results in $k_\phi = 2.96 \cdot 10^{11}$ Nm/rad.

Based on their location and turbine type, the turbines are designed for turbine class IIA.

Zuidlob

Wind park 'De Zuidlob' [37] is located in the province of Flevoland, home to almost 600 turbines, with many more already planned. The 36 Vestas turbines of 'De Zuidlob' can produce 3 MW each, using a 112 m rotor with a hub height of 94 m. They are suited for turbine classes IIA and IIIA.

The foundation consists of 3 m thick octagonal slab, supported on 32 piles in radial formation. It is shown in Figure 5-7. Using equation 5-1, with $R = 8.6$ m and $k_v = 1 \cdot 10^5$ kN/m, leads to $k_\phi = 1.18 \cdot 10^{11}$ Nm/rad.

Foundation designed for base model, Class IC

Model A together with the 5 MW turbine and a tower width at the bottom of 9.64 m is used to calculate the foundation stiffness, resulting in the following loads:

$$M_{x0} = 370,000 \text{ kNm}$$

$$F_{z0} = 8000 \text{ kN}$$

Horizontal loads are assumed to be carried by the piles, possibly placed under a slight angle. This will be assessed at the end of the calculation. A circular or polygonal slab with an average thickness of 3.5 m and a radius of 13 m is assumed to be completely rigid and has a total weight of:

$$F_{slab} = 25 \cdot \pi \cdot 13^2 \cdot 3.5 = 46,500 \text{ kN}$$

In reality this slab will more resemble the stepped shape of Figure 5-6. The piles are located in two concentric circular rows underneath. Based on experience from practice
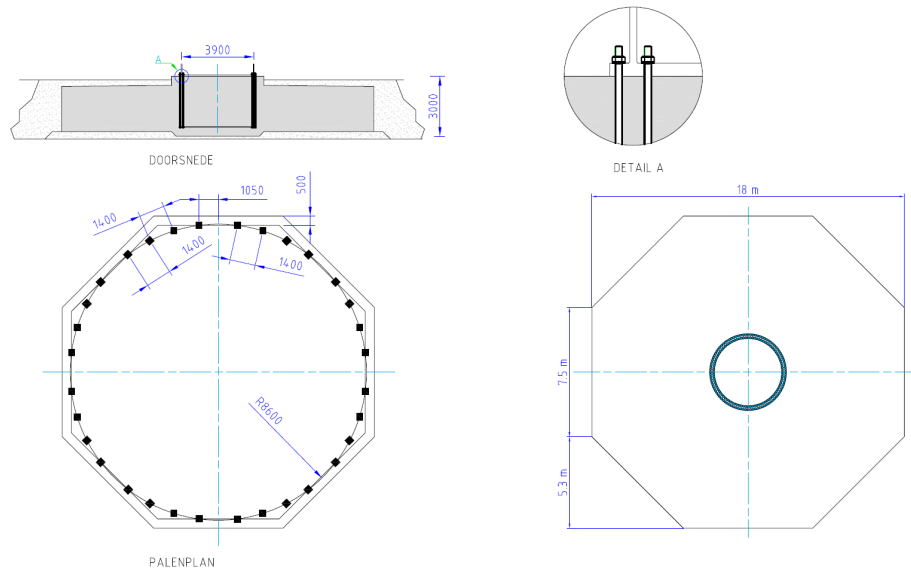
Figure 5-7: Basic overview of the foundation underneath the turbines in wind park Zuidlob
Source: De Gooijer [37]

and the foundation in Vlissingen, compression capacity of the piles is taken as 3000 kN in compression and 700 kN in tension.

The considered tower has a width of 9.64 m at the bottom, so the total load on one half of the foundation piles, due to M_{x0}, is:

$$F_{tot;m} = \frac{370000}{9.64} = \pm 38,000 \text{ kN}$$

Since the tension capacity is smallest, this side will be governing when determining the number of piles.

Modelling the slab as completely rigid, F_{z0} and F_{slab} will be divided evenly among the piles. The characteristic pile loads are calculated using:

$$F_{pile;slab} = \frac{F_{slab}}{n} \tag{5-2}$$

$$F_{pile;F_z} = \frac{F_{z0}}{n} \tag{5-3}$$

The individual pile loads due to the bending moment are calculated as:

$$F_{pile;m;i} = \frac{M_{x0}R_i}{I} \tag{5-4}$$

$$I = \sum R_i^2 \tag{5-5}$$

So the first indication of the number of piles will be:

$$2\frac{1.35F_{tot;m} - 0.9\left(\frac{1}{2}F_{z0}\right) - 0.9\left(\frac{1}{2}F_{slab}\right)}{700} = 78 \text{ piles}$$

Where a factor of 0.9 is used on favourable loads. Considering the probable redistribution of loads in the foundation slab, a total number of 64 piles is chosen, similar to the foundation in Vlissingen. 40 piles are placed at the outer perimeter of $R = 11.5$ m and 24 piles are placed at $R = 9.5$ m. The pile loads are calculated using Equations 5-6-3 to 5-6-3:

$$F_{pile;slab} = \frac{-46500}{64} = -726 \text{ kN}$$

$$F_{pile;F_z} = \frac{-8000}{64} = -125 \text{ kN}$$

The design compression loads in the piles will be:

$$F_{d;pile;comp;i} = -1.35F_{pile;m;i} - 1.35F_{pile;slab} - 1.35F_{pile;F_z}$$

The design tension loads in the piles will be:

$$F_{d;pile;tens;i} = 1.35F_{pile;m;i} - 0.9F_{pile;slab} - 0.9F_{pile;F_z}$$

The results can be found in Table 5-7, the calculation code used in Appendix G. As can be seen, a few piles exceed their assumed capacity. This is accepted, however, because redistribution through the concrete slab will most likely take place. Furthermore, the loads are calculated using the quasi-static method from the next chapter, which shown to be are conservatively high there.

Lateral loads will not be considered in-depth. The 3300 kN of lateral load will lead to around 52 kN of lateral load on each pile, assuming an even distribution. The piles are considered to be able to withstand these loads. If not, batter piles can also be applied to easily deal with this relatively small load.

Using Equation 5-1 and $k_{v,i} = 1 \cdot 10^5$ again, k_ϕ is found at $3.72 \cdot 10^{11}$ Nm/rad.

5-6-4   Conclusion and discussion

Looking at the results, shown in Figure 5-5, it can be concluded that it is possible to design pile foundations in the Netherlands that are stiff enough so that they do not influence the tower's natural frequency significantly. The large turbines in Vlissingen have already shown that it is possible to apply high-MW turbines in high-wind areas of the Netherlands and build a suitable foundation.

Stiffness as described here is based on a relatively low stiffness value per pile ($1 \cdot 10^5$ kN/m), but experience from practice learns that this value can be higher in the Dutch soil (up to $3 \cdot 10^5$ kN/m) for high capacity piles needed here. Demands made by producers are easily achievable with the pile foundations applied in the Netherlands.Pile loads in the foundation designed for the base model are high, but the quasi-static load method is a reasonably conservative method for determining the extreme loads, so it is expected that the actual loads will be lower.

Looking at the variance in the stiffness (i.e. Young's Modulus) of timber materials, it can be concluded that the foundation stiffness does not have to be included in this design stage yet. The small influence that the foundation stiffness might have on the frequency, is eliminated by the larger variance in Young's Modulus and its influence on the frequency. In the end, no problems are expected with making a pile foundation for the considered turbines and the assumption of a rigid foundation can be maintained throughout design calculations.

Compression		Tension	
Outer row	Inner row	Outer row	Inner row
-2690	-2422	775	507
-2671	-2378	756	464
-2614	-2251	700	337
-2522	-2049	607	134
-2395	-1785	481	-129
-2238	-1478	324	-436
-2054		140	
-1848		-66	
-1625		-290	
-1390		-525	

Table 5-7: The individual pile loads in tension and compression for model A, both for one quarter of the foundation

5-7   Influence of connections on frequency

This section determines the influence of possible stiffening effects of connections on the natural frequency of the tower. The original connection as used in the first TimberTower is used to calculate an equivalent stiffness and subsequent Young's Modulus for the combination of pure timber sections and connections. This is compared with the variance of the material's Young's Modulus to determine whether or not the influence of the connections has to be taken into account in this research.

5-7-1   Capacity and stiffness of the original connection

The main connection in the original tower, as described by Bathon [54] consists of a 2.5 mm thick perforated steel plate which is placed in a precut slit every 40 mm, perpendicular to the outer face of the walls. The plates are 300x300 mm and the slits are completely filled with polyurethane adhesive. Load bearing between adhesive and steel occurs mainly through the adhesive forming dowels through the perforations.

The connection was tested and displayed a tensile capacity of 125 kN before yielding occurred, at a strain of 0.4 mm [54]. It is stated by Bathon that the glue in the connection remained undisturbed, while the failure occurred due to yielding and subsequent fracture of the steel. Because the steel plate was the governing element, the capacity of the connection can be approximated based on the properties of the steel plate.

The elastic stiffness of this connection based on the results from Bathon is:

$$k_{con} = \frac{125,000}{0.4} = 3.13 \cdot 10^6 \text{ N/mm}$$

The metal plate of 2.5 mm thickness has a net cross section of $\eta_{steel} = 60\%$ of the total steel cross section. This is caused by 4 holes of 10 mm, every 100 mm of plate width. The net amount of steel in the yielding cross section is:

$$A_{steel,net} = \eta_{steel} t_{steel} t_{timber} \tag{5-6}$$

With a wall thickness of 300 mm, this leads to:

$$A_{steel,net} = 0.60 \cdot 2.5 \cdot 300 = 450 \text{ mm}^2$$

Looking at the deformed test specimen, it appears as if the yielding concentrated around the two rows of perforations on either side of the seam between the timber elements, as is also described by Bathon. The rows of 10 mm perforations are placed approximately 20 mm apart, resulting in a critical length of 30 mm, shown in Figure 5-8. Assuming the rest of the connection as perfectly rigid, the expected stiffness would become:

$$k_{con} = \frac{E_{steel} \cdot A_{steel,net}}{30} \tag{5-7}$$

$$k_{con} = \frac{2.1 \cdot 10^5 \cdot 450}{30} = 3.15 \cdot 10^6 \text{ N/mm}$$
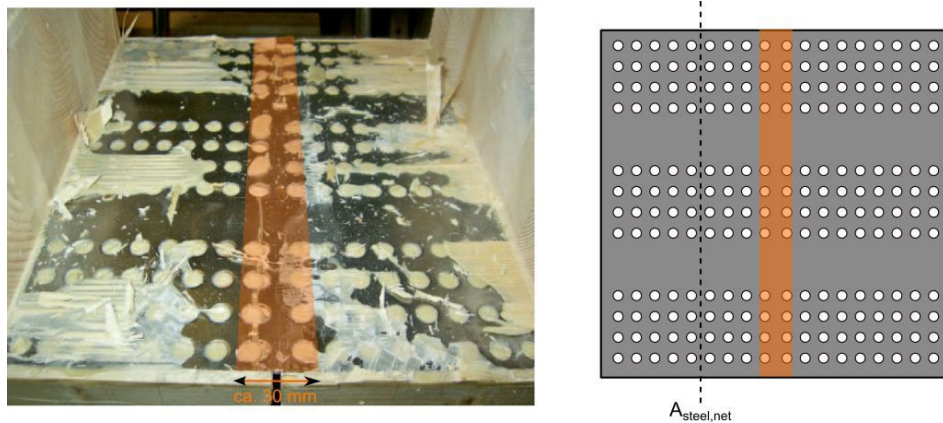
Figure 5-8: One of the test specimens from Bathon on the left (failed under fatigue loading)
and the definition of the yielding part of the plate on the right
Source: Bathon [54]

Which is remarkably close. No definite conclusions can be drawn from this, but the resemblance is however interesting.

It is assumed that for all proportions considered, the deformations will concentrate around the seam, around those first two rows of perforations mentioned earlier. As a result, the stiffness of the connection can be assumed to only depend on t_{timber}, which in that case is the only variable in the equation above.

Since the true behaviour of the connection is unknown, this remains an assumption. For this reason, several different values of the connection stiffness will be assessed.

5-7-2 Number of connectors required

To be able to determine the stiffness of the total connection, the amount of individual connections is required. The model from Figure 5-9 uses the centre-to-centre distance of the connectors b to describe this. This model assumes the walls are made up of elements with length l_{timber}, thickness t_{timber} and an effective area of $A_{timber} = b \cdot t_{timber}$ per connector. The connectors are square plates, meaning that $h_{steel} = t_{timber}$, which are placed at centre-to-centre distance b. Only the fibres in longitudinal direction are taken into account, by using k_{net} in the formulas below. k_{net} is defined in Figure 5-10.

$$A_{timber,net} = k_{net}t_{timber}b \tag{5-8}$$

$$E_{timber,net} = k_{net}E_{timber} \tag{5-9}$$

Although frequency considerations and requirements will be mostly considered under operational conditions, it is the extreme wind conditions that determine the required capacity of the connection. After all, the tower may not fail or permanently deform during extreme conditions, which would result in a unusable structure afterwards. Assuming the loads will dominate the design and will stress the timber to a stress level of $\sigma = 0.9f_{t,0,d}$, the required centre-to-centre distance of the plates b can be determined by:

$$b = \frac{F_{y,d}}{0.9f_{t,0,net,d}t_{timber}} \tag{5-10}$$
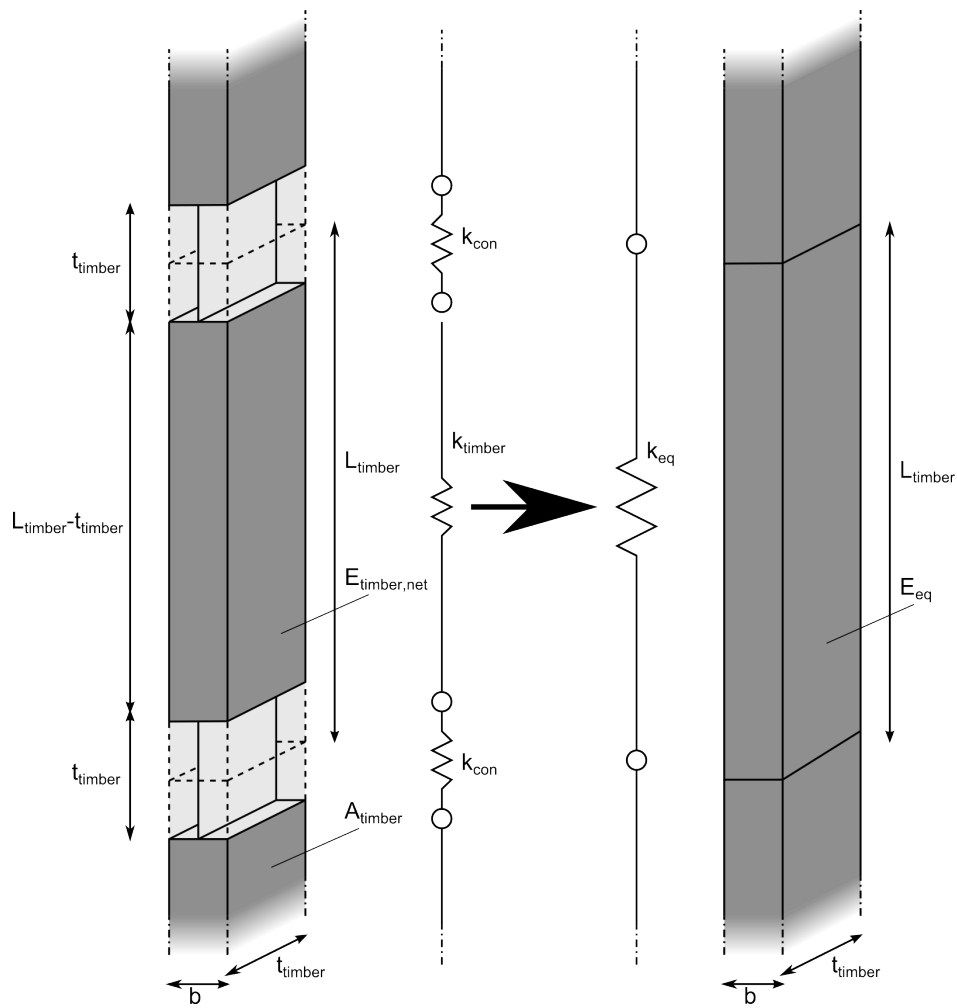
Figure 5-9: The spring model, based on a single connector and the relevant cross sectional area of the timber $A_{timber} = b \cdot t_{timber}$ for one connector
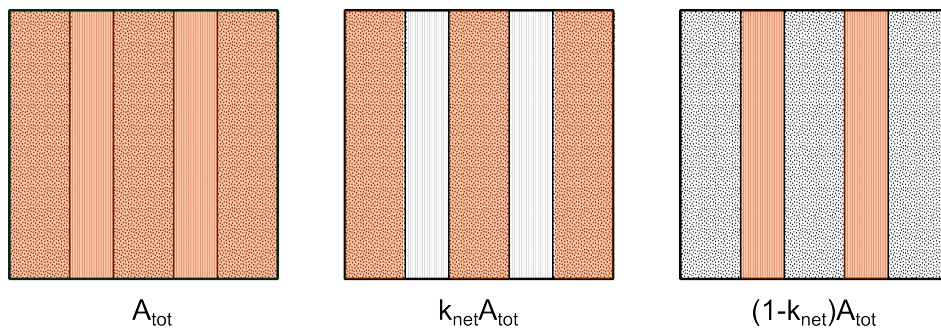
Figure 5-10: The definition of k_{net} on a horizontal cross section of a CLT element

Where:

F_y, d is the design yield force in the steel of one connector

$$F_y = A_{steel,net} f_{y,d,steel} = \eta_{steel} t_{steel} t_{timber} f_{y,d} \tag{5-11}$$

This results in:

$$b = k_{mod} \frac{F_{y,d}}{\gamma_M \cdot 0.9 f_{t,0,k} \cdot k_{net} t_{timber}} = k_{mod} \frac{\eta_{steel} t_{steel} f_{y,d}}{\gamma_M \cdot 0.9 f_{t,0,d} \cdot k_{net}} \tag{5-12}$$

In this formula, minimal spacing and execution considerations have not been taken into account. It can be seen that b does not depend on t_{timber}, but will become around 25 mm for representative values of the parameters (CL24h). In reality, the material will most likely not be stressed up to 90% of its capacity, since the frequency is expected to govern the design. This would result in a lower stiffness for the connection due to smaller centre-to-centre distances.

5-7-3   Equivalent springs stiffness and Young's Modulus

The total stiffness k_{eq} of an element with one connection as described above and shown in Figure 5-9, can be determined by the formula below. Both the pure timber section and the connection are modelled as springs, placed in series. The stiffness of each individual connector throughout the tower is assumed to be the same and no interaction between the individual connectors is modelled.

$$\frac{1}{k_{eq}} = \frac{1}{k_{timber}} + \frac{1}{k_{con}} = \frac{l_{timber} - t_{timber}}{E_{timber,net} A_{timber}} + \frac{1}{k_{con}} \tag{5-13}$$

Here the first term k_{timber} is considered as the part that consists purely of timber. Since the steel plates are square, a total length of t_{timber} per element contains the steel plate, and the total length of the pure timber part is $l_{timber} - t_{timber}$. This results in the first term coming from

$$k_{timber} = \frac{E_{timber,net} A_{timber}}{l_{timber} - t_{timber}} \tag{5-14}$$

From Equation 5-13 an equivalent Young's modulus for the entire system can be derived by

$$E_{eq} = k_{eq} \frac{l_{timber}}{A_{timber}} \tag{5-15}$$

The underlying assumption is that, due to the fact that the connections are placed at different heights for each side of the polygonal cross section, the overall influence on the stiffness can be smeared out over the entire height of the tower. This results in an equivalent spring stiffness and thus an equivalent Young's Modulus which could be used very easily in other calculations. It will be compared with the Young's modulus of the net timber cross section $E_{timber,net}$ below. l_{timber} is set at 15 m, based on the production limitations and experience from the first TimberTower.
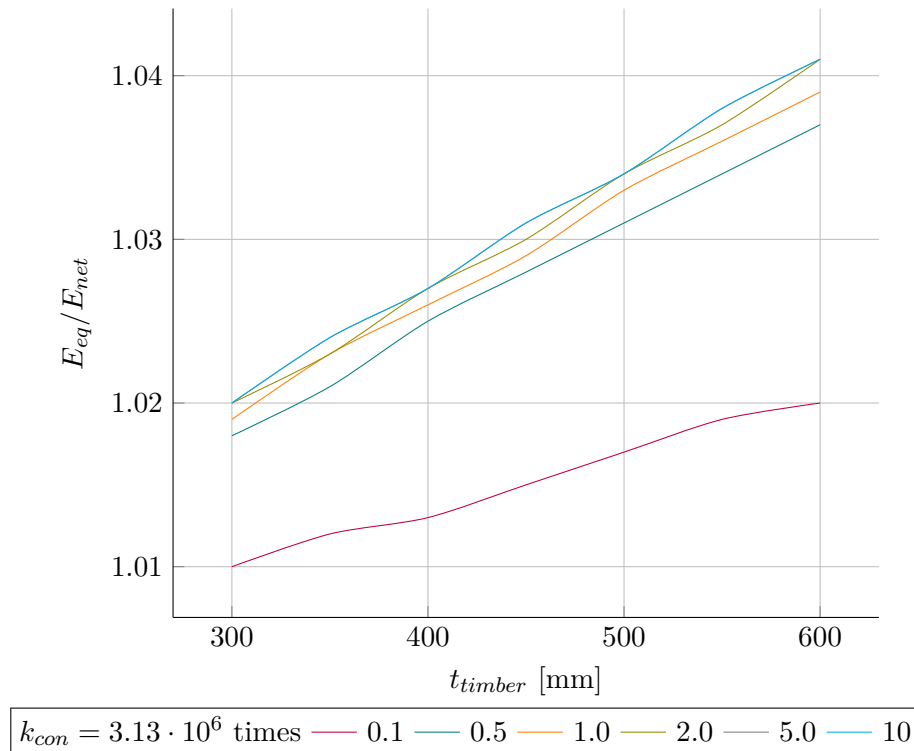
Figure 5-11: The influence of the connection stiffness on the equivalent Young's Modulus, shown for CL24h. The results are practically the same for all regular CLT strength classes

5-7-4 Influence on the frequency

The influence of the Young's Modulus on the natural frequencies has been determined during the initial frequency analysis, see Figure A-7 and the first part of this chapter. By varying the wall thickness, CLT strength class and individual connection stiffness , the relative increase in Young's Modulus was calculated. The calculation code used can be found in Appendix G and the results are displayed in Figure 5-11.

It turned out that the regular CLT strength classes displayed no difference in increase of this equivalent Young's modulus, so Figure 5-11 can be interpreted as being valid for all four regular softwood classes. For realistic wall thicknesses, ranging from 300 to 600 mm, the maximum increase turned out to be 4%.

5-7-5 Conclusion and discussion

As can be seen in Figure 5-11, the frequency increase due to the connections increases with thickness. The maximum increase found for realistic wall thicknesses lies at 4%. As with the foundation, this value is less than the variance in the mean Young's modulus of the material, so it can be concluded that the influence of the connections on the natural frequency can be ignored for this timber tower design, at least within this research. One might argue that the number of plates assumed here (spaced 25 mm) is high, but the effect of the connections on the frequency will only decrease for a smaller amount of fasteners, due to a lower relative connection stiffness.

$\text{C}\small{\text{HAPTER}}$ 6

Load calculation methods

This chapter describes the load calculations methods, corresponding wind models and load cases. Examples of calculated loads are provided in tabular form and compared with results from practice. They are also provided in graphical form in Appendix B. The examples in this chapter only serve as an indication. The exact loads for the tower design in Chapters 8 and 9 are recalculated for each of the designs made, due to the influence of various tower properties such as geometry and natural frequency on the loads.

6-1   Load calculations in practice

Wind is of a highly stochastic nature, with spatial variations and turbulence (variations of the mean wind speed over time) occurring in all directions, see Figure 6-1. The resulting three-dimensional flow on a rotor is highly complex, and load calculations are usually performed by computer software based on an aeroelastic calculation procedure. According to DNV Riso [5] " [t]he purpose of an aeroelastic wind turbine analysis is to solve the equations of motion for a given arbitrary set of forces acting on the structure and for forces generated by the structure itself. Often, such a code applies a geometrically non-linear finite element approach or a modified modal analysis approach." It is prescribed that at least 5 simulations of 10 minutes are made for each load case, and the results combined by using a statistical or semi-analytical model to determine both the fatigue load spectrum and the extreme load. This is further explained in Appendix M.

Since both the available computer software and time are limited here, it was decided to not make us of complete simulations, but use a quasi-static method to determine loads, to be able to use simple static calculations. Dynamic effects and turbulence are included by calculating appropriate factors and wind models are kept reasonably simple. More information about the nature of wind and all the different wind models prescribed by the IEC can be found in Appendix L.
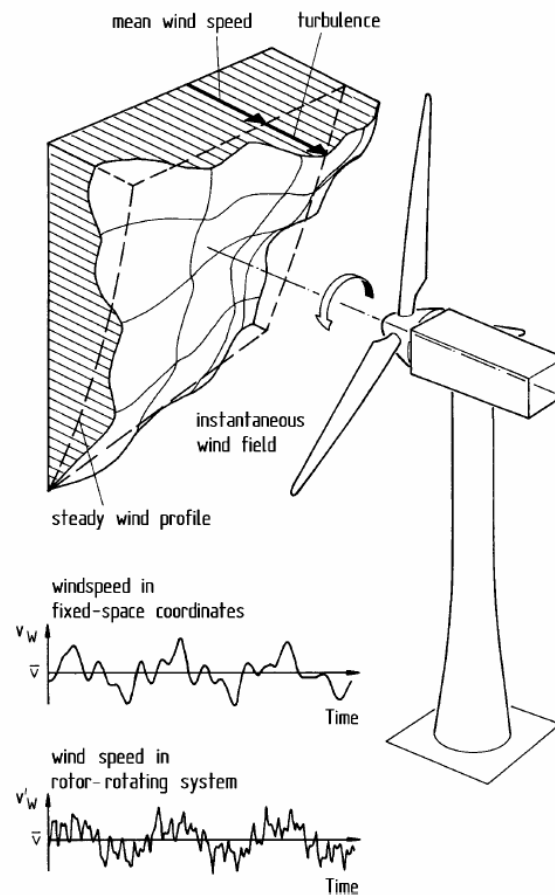
Figure 6-1: Turbulence can be seen as variations of the mean wind speed in all three directions, superimposed on a mean wind speed
Source: Matthiesen,
http://www.cfms-sols.org/sites/default/files/manifestations/091020/Schackines.pdf, accessed March 2015

6-2   Design load cases

For the complete design of a wind turbine and its components, the IEC [2] requires many different load cases, using various wind models, to be simulated and checked. These load cases can be found in Tables M-1 and M-2 in the appendices. Appendix M contains more information about the IEC load cases and calculations methods.

Most of these load cases are made by combining operational conditions of the turbine with several wind events and conditions, described in multiple wind models. Some load cases have a large effect on the mechanical components of the turbine, such as the generator or rotor shaft, but do not contribute significantly to the loads on the tower. Since this research involved a large number of designs and its main purpose is a global assessment instead of complete and detailed certification of the design, the time-consuming investigation of all loads cases is not necessary and simplifications in the design loads are made. Of all the design load cases (DLC) found in Tables M-1 and M-2, the following two aspects are not taken into account in this preliminary design stage:

– All load cases related to fatigue;

– All load cases related to transportation and erection.

Fatigue is too extensive to be covered during one single thesis and will be kept out of its scope. It is also expected that fatigue plays a less significant role for timber than for steel, as is also the case with concrete. This is an opinion shared by practice [3]. Loading from transportation and erection are not expected to play a significant role in designing the tower components. Furthermore, taking it into account requires detailed knowledge and design of these subjects, deemed not relevant for this research.

What remains are the loads during operation, start-ups, shut-downs and during standstill and idling. The start-ups and shut-downs are not expected to result in significantly different or higher tower loads than those during operation and standstill and will therefore not be included. The remaining two situations - power production and standstill during extreme wind conditions - will be investigated within this thesis by means of three separate load cases (1, 2a, 2b):

1. **Loads during power production**
   This load case simulates the loads on the tower caused by power production of the turbine. Although it will not cause the maximum loads, this load case is important for determining the maximum deflection of the tower during power production. The forces caused by the rotor are calculated for all wind speeds between cut-in (V_{in}) and cut-out (V_{out}). The maximum occurs for the rated wind speed (V_r) for the considered turbines.

   The occurrence of faults and possible dynamic load amplification during operation is harder to simulate using the tools available, and are accommodated here by adding an additional 10% and 25% respectively to the design loads. This is similar to what is used in the method described in section 4.5.2 of DNV Risø's wind turbine design guidelines [5].

2. **Loads during standstill**

   The IEC defines DLC's 6.1 to 6.4 and 7.1 for a idling or parked turbine (see Table M-1). According to Burton [29], the governing tower load for a pitch-regulated, three-bladed turbine would occur when the rotor is loaded sideways during standstill by the 50-year return storm (DLC 6.2). For this to occur, however, grid loss and resulting yaw misalignment should take place long enough for a wind direction change of 90° to arise. Since the electrical grid in the Netherlands is relatively dependable, this is not probable and DLC 6.2 will not be taken into account. Burton continues by stating that the governing load will then be caused by extreme yaw misalignment during the storm with a 1-year return period, described by DLC 6.3.

   Based on this information, two load cases are investigated during standstill. One load case deals with the extreme wind speed and the second with the largest yaw misalignment. The latter is included because it can possibly cause the largest torsional moment in the tower, which might be governing due to the relatively low (rolling) shear strength of the CLT material.

   (a) **Extreme wind speed**

   This load case coincides most with DLC 6.1. The turbine is subjected to wind speeds associated with a storm with a 50-year return period. If a steady wind model is used, the average 10-minute wind speed should be taken as $V_{10} = 1.4V_{ref}$, whereas a turbulent wind model, such as the method used, allows for $V_{10} = V_{ref}$, according to the IEC-61400.

   A yaw misalignment of 8°, as prescribed by the IEC, is also incorporated by multiplying the axial load from the rotor by the corresponding moment arm caused by this misalignment.

   The quasi-static method that is used, which will be described later, requires the drag and/or lift factor of the blades as one of the input parameters. For lack of more detailed data, the maximum value of 1.5 was conservatively taken for this load case, as is prescribed by DNV Risø [5], as if the blades were in their least favourable orientation to the wind. This introduces another fault - a lack of feathering of the blades - to this load case, causing it to be a mix between DLC's 6.1 and 7.1.

   (b) **Extreme yaw misalignment**

   This load case coincides most with DLC 6.3. The same approach as for the extreme wind speed case is used, but the wind speed used corresponds with a storm with a 1-year return period: $V_{10} = 0.8V_{ref}$.

   The extreme yaw misalignment of 15° is incorporated in the same way as in the previous load case.

Both of the situations described here (2a and 2b) will be calculated with the help of a quasi-static method, based on section 4.5.3 of DNV Risø citeDNVRiso2002, and described in more detail in both Appendix M and in Section 6-4-2. It takes into account turbulence and dynamic amplification by multiplying the steady wind load by a gust factor ψ. The exact formulas used will be provided in the corresponding section.

A few remarks concerning these load cases should be made. The load cases as described above will prove to be fairly conservative, mainly because of the conservative combination

of faults and wind speeds. Because of the complex and stochastic nature of wind loading, it is not certain that these load cases result in the highest ultimate load for all parts of the tower, although it is likely. Furthermore, the governing load case may also differ for different sections of the tower. However, it is assumed and considered likely that the load cases above will result in the highest stresses in the tower structure.

6-2-1   Partial factors

For design load cases 1 and 2b as described above, the partial load factor for all unfavourable loads should be taken as $\gamma_f = 1.35$, in accordance with what is defined by the IEC as normal design situations. When able to distinguish between loads caused by gravity and other sources, one is allowed to lower the total partial safety factor for unfavourable loads by applying:

$$\gamma_f = 1.1 + \phi\zeta^2 \tag{6-1}$$

Where:

$$\zeta = \begin{cases} 1 - |\frac{F_{\text{gravity}}}{F_k}| & \text{for } |F_{\text{gravity}}| \leq |F_k| \\ 1 & \text{for } |F_{\text{gravity}}| > |F_k| \end{cases}$$

$\phi = 0.25$ except for load case 1.1 of Table M-1, in which case it is 0.15

Since the contribution of gravity loads on the total stresses in the material was found to be only around 5% or less, the difference is very small. Therefore, γ_f is taken as 1.35 for all unfavourable loads. When the loads work in a favourable manner, such as gravity loads on the tensile stresses in the tower, γ_f is taken as 0.9.

For design load case 2a, the partial load factors for abnormal design situations ($\gamma_f = 1.1$) will be used. DLC 6.1 in IEC-61400 (normal standstill conditions with a once-in-50-year storm) prescribes normal partial factors, while DLC 6.2 (standstill with 50-year storm + fault) prescribes abnormal load factors. Load case 2a as described above combines the normal standstill with a non-feathered position of the blades, which is a fault and makes this load case closer to IEC DLC 6.2 than 6.1. Simply put, the chances of both the 50-year storm and the failure of blade feathering occurring simultaneously are so small, that the use of abnormal safety factors is justified.

In the rest of this chapter the load calculations will be explained in detail. The calculations have been made using Matlab, codes can be found in Appendix G.

Examples of calculated loads will be given to show the variation of the loads along the tower and show the difference between the different wind classes, supplemented by graphical representations in Appendix B. The example values will also be used to compare the calculated loads with those found for similar towers for real-life turbines in the Netherlands. Two situations will be investigated: the 3 MW turbine at a hub height of 100 m and the 5 MW at 125 m. The timber towers have been designed for a strength and stiffness comparable to several reference turbines (Table 6-10), to be able to make this comparison. These timber designs

Turbine		3 MW			5 MW		
Material		CL30h	CL30h	Steel	CL30h	CL30h	Steel
Shape		Octagon	Decagon	Cylinder	Octagon	Decagon	Cylinder
H	[m]	100			125		
$a_{out,T}$	[m]	1.15	0.93	-	1.45	1.17	-
$a_{out,B}$	[m]	3.40	2.74	-	4.30	3.46	-
$B_{out,T}$	[m]	3.00			3.80		
$B_{out,B}$	[m]	8.87	8.87	4.20	11.22	11.22	6.00
t	[m]	0.27	0.27	0.09	0.5	0.5	0.11
k_{net}		0.75	0.75	1.00	0.75	0.75	1.00
f (Rayleigh)	[Hz]	0.329	0.336	0.295	0.305	0.311	0.275

Table 6-1: The models used to display the forces in this chapter. The steel values are based on literature and frequency analysis.

are shown in Table 6-1. To be able to compare the results of the load calculation methods with loads found in practice, steel models have been designed as well.

Models used in this chapter might differ from the final design made in the next chapters, because only frequency and normal stresses were considered in determining their required dimensions. The final designs will also be checked for shear strength and judged on deflection, among others. Also, for each combination of turbine and hub height one model was used for all three considered classed (IC, IIA and IIIA), which may not be the optimal solution for each class.

The geometric parameters are defined in Figure 5-1, k_{net} in Figure 5-10.

6-3   Definition of loads and forces

For design purposes, the tower can be seen as a cantilevered beam. Loading occurs both on top of the tower and along the tower, caused by wind loading and gravity. Part of this can be seen in Figure 6-2, where the loads relevant for stress calculations are shown. The tower is assumed to end at hub height, so that loads on the hub also work directly on the top of the tower. In reality, the top of the timber section of the tower will be at a lower height and experience a bending moment, caused by the eccentricity of loads due to the height of the nacelle and transfer structure. The stresses in the top part of the tower - in what normally would be the transfer structure - are ignored. The same holds for the bottom 5 m of the tower.
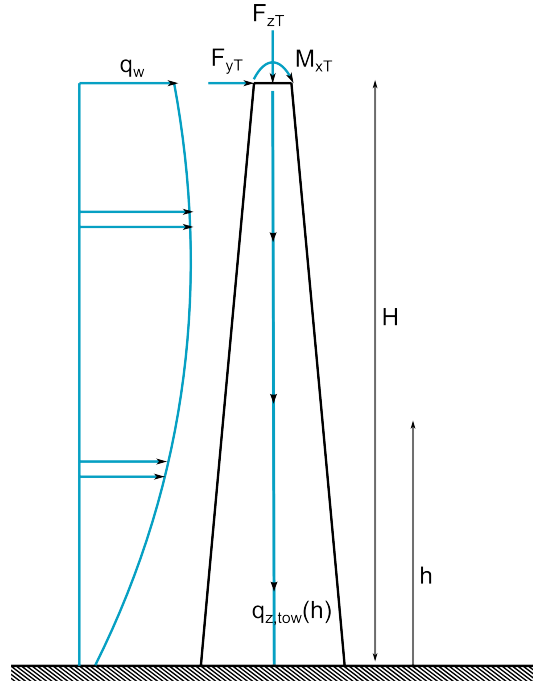
Figure 6-2: The loads used to calculate resulting stresses from bending and axial force along the tower

The rest of this chapter will define these loads and explain their general calculation.

6-3-1 Forces on top of the tower

The six forces working on top of the tower at hub height (denoted by subscript T) can be found in Figure 6-3. The resulting overturning moment $M_{x,T}$ is obtained by combining the rotor tilt moment and the proper eccentricities for loads not directly in the centre of the tower, such as the mass of the nacelle. This is shown in Figure 6-4 and Table 6-2. The eccentricities for the 5 MW turbine are defined by Jonkman [1] and are scaled down to 80% for the 3 MW turbine. The contribution of these eccentricities on the bending stresses in the tower is very small, small deviations from the actual values for a 3 MW turbine will not affect results significantly.

The six forces are at the top are:

- $F_{x,T}$ is the horizontal force in the rotor plane, taken as 0 here, as is usually done. If it were not taken as 0, its eccentricity should be taken into account, resulting in an increase in $M_{z,T}$.

- $M_{x,T}$ mainly consists of the tilt moment. The eccentricities of both hub and nacelle also contribute to moments in this direction:

$$M_{x,T} = M_{rot,x} + F_{nac,z}e_{nac,y} - F_{hub,z}e_{hub,y} \tag{6-2}$$

$M_{rot,x}$ is the moment around the x-axis caused purely by the rotor. To calculate the moment at the top of the timber part of the tower, $F_y\left(e_{hub,z} + h_{\text{transfer}}\right)$ should also
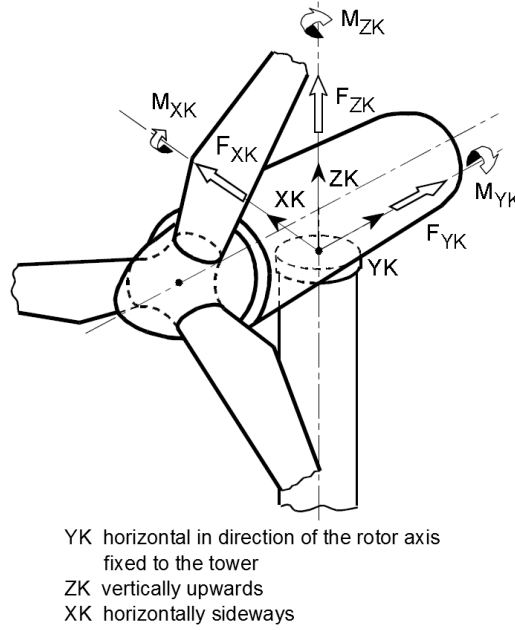
Figure 6-3: Coordinate system at the top of the tower
Source: Germanischer Lloyd [55]

be taken into account. However, instead of taking this contribution into account, the timber part of the tower is assumed to be present up to hub height, but stresses in the part from $z = H - (e_{hub,z} + h_{transfer})$ to $z = H$ are ignored. This is the part made up by the transfer structure and nacelle, as explained at the beginning of this section. $(e_{hub,z} + h_{transfer})$ will be taken as 5 m for both turbines, for simplicity.

– $F_{y,T}$ is the thrust force from the wind, working along the axis of the rotor.

– $M_{y,T}$ is the moment about the rotor axis, caused by the torque from the rotating blades.

– $F_{z,T}$ is the gravity force caused by the rotor, hub and nacelle.

$$F_{z,T} = F_{hub,z} + F_{nac,z} \tag{6-3}$$

– $M_{z,T}$ is the moment around the vertical axis, the torsion moment caused by e.g. yaw misalignment and skewness. In case of yaw misalignment of α degrees, the axial force is multiplied by the horizontal distance between the hub axis and the tower centre to obtain $M_{z,T}$:

$$M_{z,T} = F_{y,T} sin\left(\alpha\right) e_{hub,y} \tag{6-4}$$

6-3-2   Loads along the tower

Wind loads on the tower $q_w(h)$ are calculated for each cross section along the height, based on wind speed and the shape and size of the cross section. The exact calculation will follow in section 6-5, resulting in a varying line load on the tower.

	Symbol	5 MW	3 MW
Horizontal distance from hub centre to yaw axis	$e_{hub,y}$ [m]	5.01	4.01
Vertical distance from hub centre to yaw bearing	$e_{hub,z}$ [m]	1.96	1.57
Vertical distance from hub centre to tower top	h_{transfer} [m]	5.00	4.00
Vertical distance from hub centre to tower top	$e_{tot,z}$ [m]	5*	5*
Horizontal distance from nacelle centre of mass to yaw axis	$e_{nac,y}$ [m]	1.90	1.52
Vertical distance from nacelle centre of mass to yaw bearing	$e_{nac,z}$ [m]	1.75	1.4

Table 6-2: Eccentricities of the hub and nacelle for the NREL 5 MW turbine, as defined in Figure 6-4

*Taken as 5 m for both turbines, for simplicity
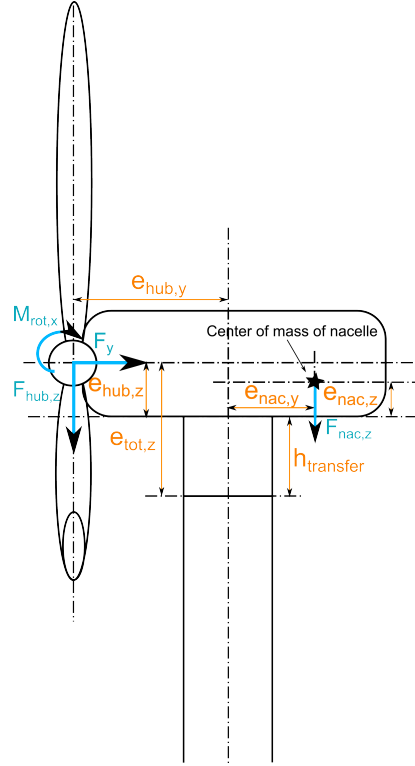
Figure 6-4: Definitions of the eccentricities and some of the loads at the top of the tower

By summing these wind forces along the height, the resulting shear force from wind loading (from hereon denoted by F_w) is found.

$$F_w(h) = \int_{H-h}^{H} q_w \tag{6-5}$$

When the wind loads are multiplied by the correct moment arm, the resulting bending moment due to wind force on the tower (M_w) is found.

The self-weight of the tower also contributes to the vertical force along the tower. In general, it is obtained by multiplying the cross-sectional area with its density. It is assumed that the transfer structure has the same self-weight as the timber part, for ease of calculation. Later on, it will become clear that the stresses due to vertical forces are small compared to those caused by bending and that this assumption has no influence on the results.

$$q_{z,tow}(h) = \rho_{tow}(h) A_{tow}(h) \tag{6-6}$$

6-3-3   Resulting forces

The resulting loads along the tower are obtained by using the following formulas:

$$F_x(h) = F_{x,T} \tag{6-7a}$$

$$M_x(h) = M_{x,T} + F_{y,T}(H - h) + \int_{h}^{H} q_w(z)(H - h - z)dz \tag{6-7b}$$

$$F_y(h) = F_{y,T} + \int_h^H q_w(z)dz \tag{6-7c}$$

$$M_y(h) = M_{y,T} \tag{6-7d}$$

$$F_z(h) = F_{z,T} + \int_h^H q_{z,tow}(z)dz \tag{6-7e}$$

$$M_z(h) = M_{z,T} \tag{6-7f}$$

Stresses due to bending and axial forces in the tower are the main interest in these initial calculations. The forces required to calculate these stresses are show in Figure 6-2. Of the forces perpendicular to this plane, only M_z is taken into account, according to the load cases described earlier. The other forces are assumed to play no part in the governing load case.

For some situations, such as the tension stresses at the bottom, favourable loads occur (self-weight) which are multiplied by $\gamma_f = 0.9$. It should be noted that the $F_{hub,z}e_{hub,y}$ part in Equation 6-7 should then also be multiplied by 0.9 instead of 1.35, but the difference is negligible. Additional moments that might occur because of tower deformation and the eccentricities it causes, are not taken into account. The calculations will be linear-elastic.

6-4 Loads at hub height

6-4-1 Loads during operation

This section deals with the calculation of the maximum loads during operation, using tools made available by the Delft University of Technology. It uses the Blade Element Momentum method (BEM) to calculate the thrust force, among others, for all wind speeds between V_{in} and V_{out}. BEM combines the blade element theory with the momentum theory and is described in detail by Burton in section 3.5.3. of his Wind Energy Handbook [29].

It requires some iterative calculations, making Matlab a useful tool. The equations and code needed to perform calculations using BEM, were readily provided during a course by Dr. ir. W.A.A.M. Bierbooms at TU Delft. The code was slightly adjusted to make it possible to incorporate this in a larger calculation model. Several changes were made to the original input file of the NREL 5 MW turbine to account for the timber design, a few of which are:

– Instead of 1%, 2% critical damping is assumed, since timber is considered to display better damping behaviour;

– The natural frequency of the tower is calculated using the Rayleigh-Ritz method for each design, instead of being set a constant value;

– The total mass of tower and nacelle was set to be recalculated for each design run, instead of being set to a constant value.

The same changes are made in a separate file that contains the data for the 3 MW turbine. Here, dimensional and inertia properties are scaled where needed, as described before in Chapter 2.

As stated before, the occurrence of faults during operation is harder to simulate using the tools available, and are accommodated here by adding an additional 10% to the design loads. To also include dynamic amplification, loads are increased by 25%, similar to section 4.5.2 of the method described in DNV Risø's guidelines [5].

Blade Element-Momentum method

The Blade Element Momentum method (BEM for short) is a combination of two theories, the momentum theory and the blade element theory. The method first divides the flow area into separate annular stream tubes and takes a angular momentum balance on these rotating stream tubes, assuming there is no dependency between them. This is combined with the blade element theory which provides formulas for the lift and drag forces on blade elements, again assuming they are independent of each other. Combining these provides a set of equations that can be solved iteratively to provide the blade forces.

Result examples

Using the Blade Element-Momentum method with a wind input from 3 m/s to 25 m/s - which is the relevant wind speed domain for both considered turbines - the maximum thrust force is found for $V = V_r$ m/s. This involves no turbulence, no gusts and no faults yet.

In the case of a 5 MW turbine at a hub height of 125 m the thrust is found at 882 kN, the rotor torque at 4316 kNm and the flap moment of one blade at 12846 kNm. In a three-bladed rotor under perfectly uniform wind, these flap moments keep each other in equilibrium and do not result in loading on the tower. However, this flap moment will be used as the rotor tilt moment $M_{rot,x}$, for lack of a better value and in correspondence with the quasi-static method that will be explained later on. When multiplied by the aforementioned factors for faults and dynamic amplification, $F_yT = 1213$ kN. These, and the other forces can be found in Table 6-3.

The turbine class does not influence these calculations, since the calculations are made at rated wind speed and not at V_{ref} and the turbulence intensity is not used. The classes do, however, result in different loads along the tower, as is shown in section 6-5.

6-4-2 Extreme loads during standstill

As stated before and explained in Appendix L in detail, the IEC requires many cases and models to be run, basically requiring computer simulation for all its load cases. Since this research requires a large number of models to be analysed, a less time-consuming alternative was sought. Several options were found in literature and have been recorded in Appendix M. The quasi-static method as described below was found in the Wind Turbine Design Guidelines report by DNV Risø [5]. It is the only simplified load calculation method that takes into account both turbulence and dynamic amplification due to resonance, while being simple enough to be quickly calculated for varying parameters.

Results from BEM				
As calculated from the BEM-method			*Including factors for faults and dynamic amplification*	
3 MW	$F_{rot,y}$	367 kN	$F_{y,T}$	**505** kN
	$M_{rot,x}$	4193 kNm	$M_{rot,x}$	5765 kNm
	Other loads at the top of the tower			
	$F_{z,T}$	**1731** kN	*No factors are applied to the self-weight*	
	Including eccentricities:		$M_{x,T}$	**5330** kNm
5 MW	$F_{rot,y}$	882 kN	$F_{y,T}$	**1213** kN
	$M_{rot,x}$	12847 kNm	$M_{rot,x}$	17664 kNm
	Other loads at the top of the tower			
	$F_{z,T}$	**3434** kN	*No factors are applied to the self-weight*	
	Including eccentricities:		$M_{x,T}$	**16731** kNm

Table 6-3: Calculation results for the maximum loads at the top of the tower during operation

Quasi-static method for load calculation

The quasi-static method as found in DNV Risø's report [5] is used throughout this thesis. It uses a simplified blade load to calculate various load magnitudes. This load per unit length of the blades is:

$$p(r) = \frac{1}{2}\psi\rho V_{10}^2 D(r)C \qquad (6\text{-}8)$$

Where:

$p(r)$ is the load per unit length of the blade;
ψ is the quasi-static gust factor, calculated using the formulas below;
ρ is the density of the air, 1.25 kg/m^3;
V_{10} is the extreme 10-minute mean wind speed with a recurrence period of 50 years at height h;
C is the maximum value of either the drag coefficient or the lift coefficient, ranging from 1.3-1.5;
$D(r)$ is the chord length of the blade at a distance r from the hub.

With the load per unit, the four design loads below can be calculated:

– The blade loads p are not of any interest for the tower loads directly, but are used to calculate the other forces. They are calculated as if one single blade was vertically above the hub. p can be found by summing $p(r)$ over this single blade.

– The design thrust force $F_{y,T}$ is obtained by summing the blade forces over all three blades. The orientation of the blades is arbitrary.

– The design tilt moment (part of $M_{x,T}$) is taken as the root moment of a single blade, as if it was pointed up vertically above the hub.

– The design yaw moment (leading to $M_{z,T}$) is calculated in a similar way, but with a single blade stretching horizontally from the hub.

Each of the loads described above uses different input parameters such as the threshold n^*, height h and corresponding eigenfrequency n_0 used in the formulas below. These can be found in Table 6-4. The gust factor ψ in the previous equation and other required parameters are calculated as follows:

Gust factor ψ

$$\psi = \begin{cases} \left(\frac{ln(\frac{z}{z_0})+3.1}{ln(\frac{z}{z_0})}\right)^2 & \text{for } \frac{n_0 L}{U_{10}} > n^* \\ 1 + 3.9\frac{2\sqrt{k_b+k_r}}{ln(\frac{z}{z+0})} & \text{for } \frac{n_0 L}{U_{10}} \le n^* \end{cases} \qquad (6\text{-}9)$$

Background turbulence effect k_b

$$k_b = \begin{cases} 0.9 - 2.5\frac{L}{l} & \text{for blade loads} \\ 0.75 - 3\frac{L}{l} & \text{for axial force} \end{cases} \qquad (6\text{-}10)$$

L is the length of a single blade

$$l = 6.8L_u \qquad (6\text{-}11)$$

Load	Eigenfrequency n_0 corresponding to	Threshold n^* [-]	Height h [m]
Blade load	Blade flapwise bending	1.7	$z + \frac{2}{3}L$
Axial force	Tower bending	0.45	z
Tilt moment	Blade flapwise bending	1.7	$z + \frac{2}{3}L$
Yaw moment	N/A	0	z

Table 6-4: The loads are calculated using different parameters, taken from table 4-6 of [5]

Integral length scale of the Kaimal spectrum L_u

$$L_u = 100Cz^m \tag{6-12}$$

C and m are taken from figure 3.4 from DNV Risø [5]

Resonance effect k_r

$$k_r = \frac{\frac{n_0 l}{V_{10}}}{\left(1 + 1.5\frac{n_0 l}{V_{10}}\right)^{5/3}} F(n_0)\frac{\pi^2}{2\delta} \tag{6-13}$$

Logarithmic increment of damping δ

$$\delta = 2\pi\left(\zeta_0 + \zeta_a\right) \tag{6-14}$$

ζ_0 and ζ_a are the structural and aerodynamic damping ratios

Aerodynamic admittance function $F(n)$

$$F(n) = \begin{cases} \frac{1}{1+3\frac{nL}{V_{10}}} & \text{for blade load} \\ \frac{1}{1+12\frac{nL}{V_{10}}} & \text{for axial force} \\ \frac{1}{1+4.4\frac{nL}{V_{10}}+21.8\left(\frac{nL}{V_{10}}\right)} & \text{for rotor moments} \end{cases} \tag{6-15}$$

Calculations using the quasti-static method were also made in Matlab, because of the high number of parameters and conditions, and to save time.

Result examples

Since the turbulence (in the form of roughness length z_0) has a large influence on the gust factor, examples for all three turbine class IC, IIA and IIIA have been calculated, load case 2a. Some of the input parameters can be found in Table 6-5. The intermediate and final results of the formulas for all classes can be found in Tables B-3 and 6-6 respectively. $F_{z,T}$ is the same as for the operational loads.

Class	IC	IIA	IIIA
V_{ref} [m/s]	50	42.5	37.5
I_{ref}	0.12	0.16	0.16
z_0 [m]	0.005	0.2	0.2
C	1.83	0.464	0.464
m	0.0885	0.366	0.336

Table 6-5: Parameters used in the calculation of loads according to the quasi-static method for the considered turbine classes

Class	Load	100 m - 3 MW			125 m - 5 MW		
		F_{blade} [kN]	F_y [kN]	M [kNm]	F_{blade} [kN]	F_y [kN]	M [kNm]
IC	Blade load	**383**	1150	8249	**844**	2532	22893
	Axial force	347	**1042**	7478	770	**2309**	20874
	Tilt moment	358	1075	**7713**	796	2388	**21592**
	Yaw moment	319	956	**6861**	713	2140	**19351**
IIA	Blade load	**352**	1057	7581	**762**	2286	20665
	Axial force	315	**945**	6782	667	**2001**	18090
	Tilt moment	325	975	**6996**	712	2136	**19309**
	Yaw moment	286	858	**6153**	633	1900	**17181**
IIIA	Blade load	**269**	807	5791	**583**	1750	15822
	Axial force	240	**720**	5170	519	**1558**	14084
	Tilt moment	251	752	**5396**	550	1649	**14913**
	Yaw moment	223	668	**4791**	493	1479	**13376**

Table 6-6: Example calculation results from the quasi-static method. Bold items are the relevant figures for each load

6-5 Wind loads along the tower

Using section 7.8 of Eurocode 1991-1-4 [13], the resulting force from wind directly on the tower is calculated. Based on the mean wind speed at hub height V_{hub}, the stationary wind speed along the tower is obtained by using

$$V(h) = V_{hub} \left(\frac{h}{H} \right)^{0.2} \tag{6-16}$$

for operational loads, using the Normal Wind Model of the IEC-61400 described in Appendix L, and

$$V(h) = V_{hub} \left(\frac{h}{H} \right)^{0.11} \tag{6-17}$$

for loads during standstill, using the Extreme Wind Model. These wind speeds are in turn used to calculate the wind force along the height in N/m:

$$q_w(h) = \frac{1}{2} \rho V(h)^2 B(h) c_f c_s c_d(h) \tag{6-18}$$

Where:
$q_w(h)$ is the resulting wind force per m' of height;
ρ is the density value of air;
$V(h)$ is the mean wind speed at height h;
$B(h)$ is the width of the cross section at height h;
c_f is the force coefficient for the cross section at height h;
$c_s c_d$ is the structural factor for the entire structure.

Factors c_f and $c_s c_d$ are calculated using the Eurocode.

Normally, $c_s c_d$ is only used in the Eurocode when determining the total force on a structure and takes "into account the effect on wind actions from the non-simultaneous occurrence of peak wind pressures on the surface (c_s) together with the effect of the vibrations of the structure due to turbulence (c_d)." One might not expect to see it in the formula for the calculation of the local pressure q_w, but q_w is not used to calculate local effects of the wind, but used to calculate the section forces along the tower. In short, q_w is summed up and used to calculate $F_y(h)$ and $M_x(h)$, in which the incorporation of non-simultaneous occurrence of peak pressures is justified.

The influence of the rotor on wind loading on the tower during operation is ignored, while in reality the tower behind the spinning rotor will experience lower wind speeds and higher turbulence because of the rotor wake. The Matlab code used to obtain $q_w(h)$ for the relevant turbine classes can be found in section G-1-10 of this report, while the formulas for the coefficients needed are provided below.

6-5-1 Force coefficient c_f

The force coefficient is calculated as

$$c_f = c_{f,0} \psi_\lambda \tag{6-19}$$

n_{sides}	Surface and corners	Reynold's number Re	$c_{f,0}$
8	Smooth surface	$Re \leq 2.4 \cdot 10^5$	1.45
	$\frac{r}{b} < 0.075$	$Re \geq 3 \cdot 10^5$	1.3
	Smooth surface	$Re \geq 2 \cdot 10^5$	1.3
	$\frac{r}{b} > 0.075$	$Re \geq 7 \cdot 10^5$	1.1
10	All	All	1.3

Table 6-7: Force coefficients for octagonal and decagonal cross sections

Where:

ψ_λ is the end-effect factor;

$c_{f,0}$ is the force coefficient of structural elements without free-end flow.

Circular towers

For circular towers the force coefficient is determined by:

$$c_{f,0} = \max \begin{cases} \frac{0.11}{\left(\frac{Re}{10^6}\right)^{0.14}} \\ 1.2 + \frac{0.18 \log\left(10\frac{k}{b}\right)}{1+0.4 \log\left(\frac{Re}{10^6}\right)} \\ 0.4 \end{cases} \leq 1.2 \tag{6-20}$$

Based on Figure 7.36 and Table 7.16 from Eurocode 1-4 [13], ψ_λ is taken as 0.78 for circular towers. This has been calculated for a tower with an (average) diameter of 3.6 m and a height of 100 m.

Polygonal towers

The force coefficient for polygonal towers depends on the Reynold's number and can be found in 6-7. Based on Figure 7.36 and Table 7.16 from Eurocode 1-4 [13], ψ_λ is taken as 0.90 for polygonal towers.

For the values of Reynold's number calculated in this research, $c_{f,0}$ was found to be 1.3 for both octagonal and decagonal shapes. Table 6-8 shows the wind loads for polygonal towers with the same diameter, which confirms that no difference was found between wind loads on octagonal and decagonal towers.

6-5-2   Structural factor $c_s c_d$

For some situations, determining the vale of $c_s c_d$ is straightforward. For instance, circular chimneys with a height less than 60 m or 6.5 times the diameter will have a structural factor equal to unity. In all cases, it may be determined by the formulas below, as long as $c_s c_d$ is larger than 0.85. According to the Dutch National Annex of Eurocode 1991-1-4, the structural factor may only be split into its two separate components if the structure height is less than 50

m and the ratio h/b is smaller than 5. This will not be the case for turbine towers considered in this research, so $c_s c_d$ will be calculated as one single factor.

Under the conditions that $0.6h \geq z_{min}$ and that only the along-wind vibration plays a significant part in the fundamental mode (which is the case for turbines towers), the following formula may be used to determine $c_s c_d$:

$$c_s c_d = \frac{1 + 2k_p I_v(z_s)\sqrt{B^2 + R^2}}{1 + 7I_v(z_s)} \tag{6-21}$$

Where:

z_s is the reference height, found in 6.3.1 of Eurocode 1991-1-4 or taken as h, the height of the structure;
k_p is the peak factor;
I_v is the turbulence intensity;
B^2 is the background factor;
R^2 is the resonance response factor.

These parameters will be explained further on.

The background factor B^2 is used to account for the lack of full correlation of the surface pressure. Using $B^2 = 1$ is considered safe [13], but otherwise:

$$B^2 = \frac{1}{1 + \frac{3}{2}\sqrt{\left(\frac{b}{L(z_s)}\right)^2 + \left(\frac{h}{L(z_s)}\right)^2 + \left(\frac{b}{L(z_s)}\frac{h}{L(z_s)}\right)^2}} \tag{6-22}$$

Where:

b, h are the width and height of the structure;
$L(z_s)$ is the turbulence length scale at reference height z_s.

The peak factor k_p is defined as the ratio of the maximum of the fluctuating part of the response to its standard deviation:

$$k_p = \sqrt{2\ln(vT)} + \frac{0.6}{\sqrt{2\ln(vT)}} \tag{6-23}$$

Where:

T is the averaging time, 600s;
v is the up-crossing frequency:

$$v = n_{1,x}\sqrt{\frac{R^2}{B^2 + R^2}} \geq 0.8\text{Hz} \tag{6-24}$$

Where:

$n_{1,x}$ is the first natural frequency of the stucture.

The resonance response factor R^2 accounts for turbulence resonating with the vibration mode of the tower:

$$R^2 = \frac{\pi^2}{2\delta}S_L(z_s, n_{1,x})K_s(n_{1,x}) \tag{6-25}$$

Where:

δ is the total logarithmic decrement of damping, explained in the next chapter;

S_L is the wind power spectral density function;

K_s is the size reduction function:

$$K_s(n) = \frac{1}{1 + \sqrt{(G_y\phi_y)^2 + (G_z\phi_z)^2 + \left(\frac{2}{\pi}G_y\phi_y G_z\phi_z\right)^2}} \tag{6-26}$$

With:

$$\phi_y = \frac{c_y b n}{v_m(z_s)} \qquad\qquad \phi_z = \frac{z h n}{v_m(z_s)} \tag{6-27}$$

Where:

$c_y = c_z$ is taken as 11.5. $G_y = 1/2$, $G_z = 5/18$
               for chimneys and towers.

6-5-3   Loads during operation

The procedure described above is used to calculate the wind loads along the tower. Examples of $V(h)$, q_w, F_w and M_w can be found in Figure B-1 for all turbine classes at $V_{hub} = V_{out}$, which will result in the highest loads on the tower during operation. As would be expected, the values are almost similar. The difference in turbulence conditions causes a slight difference between classes IIA and IIIA on one hand and IC on the other.

These forces will be recalculated for each final design separately, depending on the shape and size of the cross-section. The decrease in wind speed and increase in turbulence behind the spinning blades is conservatively ignored.

6-5-4   Loads during standstill

Again the procedure described at the beginning of section 6-5 is used to calculate the wind loads along the tower. One could argue that the gust factor ψ, as calculated for the loads at the top of the tower, has to be included, since it is a turbulent calculation model:

$$q_w(h) = \frac{1}{2}\rho V(h)^2 B(h)c_f c_s c_d(h)\psi$$

However, because a gust will not occur along the entire height of the tower at the same time and the calculation of the wind load on the tower already takes resonance into account ($c_s c_d$), this is not applied in this research. Examples of the wind loads and resulting forces for the towers during extreme wind conditions during standstill (load case 2a) are shown in Figure B-2 in Appendix B.

6-5-5   Remarks about cross sectional shapes

The influence of the cross sectional shape on the load magnitude has also been investigated. Base loads that represent the results for turbine class IIA are shown in Tables 6-8 and 6-9.

The other two classes are not shown, but show the same tendencies, where class IIA seems to represent the average of all classes well. A comparison with loads from practice will be made after the resulting loads are dealt with in the next section.

Both octagonal and decagonal timber towers have been investigated and show no significant difference in load magnitude when the same outer dimensions are applied. The polygonal towers in general show that wind base forces are 1.7 times as high as for steel towers with the same outer diameter (Steel-2). Both F_{w0} and M_{w0} show this behaviour. This value increases even more when the timber towers are compared to steel towers with dimensions as would be found in practice (Steel-2). These have smaller diameters, but a similar structural performance as their timber counterparts (CLT-1 and CLT-2). The loads on the timber variants then show to be between 2.3 and 2.6 times as high, depending on which of the two forces (F_{w0} and M_{w0}) one looks at.

Causes for the higher wind loads on the timber towers are both the larger diameter of the tower and the less aerodynamic shape of the cross section. In short, the polygonal shape of the cross section increases the wind loads on the tower by 70%, compared to a circular shape. The larger required outer dimensions of a timber tower increase this by another 35-50%, compared to a slimmer (steel) tower. This together results in an increase of 130 to 160% in tower wind loads when making a turbine tower out of timber instead of steel, using this specific design.

It can be seen in Tables 6-8 and 6-9, however, that the contribution of the tower wind loads on the total base overturning moment is very small. Since this moment is the governing load when it comes to the normal stresses, the negative effect of the larger and less aerodynamic timber cross section does not cause abnormally larger normal stresses.

It should be noted that only a few models have been investigated and that the values found may not represent all possible cases. Furthermore, only base loads have been investigated, mainly because this allows for a simple and clear representation and comparison. The tower dimensions may defer substantially from those used here, making the values provided only a rough indication, the 35-50% increase in particular.

Not only the dimensions, but also the tower frequency plays a role in the determination of the wind loads, making the judging more complex. In the end, the wind loads on timber towers will be substantially higher than those on their steel counterparts, but since the rotor loads are the main source of loading, the resulting total load increase is but small.

6-5-6   Vortex shedding

One aspects that can potentially play a significant role in the dynamic behaviour and resulting loads of tall structures has not been addressed yet. Vortex shedding is an alternating airflow behind a structure, which can lead to crosswind vibrations of the same structure. Vortex shedding is checked according to the critical wind speed(s) of a structure, the wind speed for which the frequency of the vortex shedding equals one of the natural frequencies of the structure, thus causing resonance. The Eurocode requires the structure to be checked for vortex shedding when the critical wind speed is 1.25 times the 10-minute average wind speed, or lower:

$$V_{cr} \leq 1.25 V_m \tag{6-28}$$

3 MW, 100 m

Material		Steel-1	Steel-2	CLT-1	CLT-2	CLT-1/Steel-1	CLT-1/Steel-2
Cross section		Circular	Circular	8 sides	10 sides		
B_{outB}	[m]	4.20	8.87	8.87	8.87	2.11	1.00
B_{outT}	[m]	3.00	3.00	3.00	3.00	1.00	1.00
F_{yT}	[kN]	965	934	945	942	0.98	1.01
$F_y(0)$	[kN]	1117	1171	1348	1344	1.21	1.15
$F_w(0)$	[kN]	152	237	403	402	2.65	1.70
$M_x(0)$	[kNm]	111031	111127	119996	119627	1.08	1.08
$M_w(0)$	[kNm]	7988	11176	18915	18903	2.37	1.69

	Steel-1	Steel-2	CLT-1	CLT-2
$F_w(0)/F_y(0)$	0.14	0.20	0.30	0.30
$M_w(0)/M_x(0)$	0.07	0.10	0.16	0.16

Table 6-8: Resulting wind loads of representative 100 m towers for the 3 MW turbine, with different cross sectional shapes, under extreme loading (LC 2a)

5 MW, 125 m

Material		Steel-1	Steel-2	CLT-1	CLT-2	CLT-1/Steel-1	CLT-1/Steel-2
Cross section		Circular	Circular	8 sides	10 sides		
B_{outB}	[m]	6.00	11.22	11.22	11.22	1.87	1.00
B_{outT}	[m]	3.80	3.80	3.80	3.80	1.00	1.00
F_{yT}	[kN]	2045	2001	2001	2001	0.98	1.00
$F_y(0)$	[kN]	2338	2367	2627	2625	1.12	1.11
$F_w(0)$	[kN]	250	366	626	625	2.50	1.71
$M_x(0)$	[kNm]	295548	290057	305223	305134	1.03	1.05
$M_w(0)$	[kNm]	16121	21573	36739	36651	2.28	1.70

	Steel-1	Steel-2	CLT-1	CLT-2
$F_w(0)/F_y(0)$	0.11	0.15	0.24	0.24
$M_w(0)/M_x(0)$	0.05	0.07	0.12	0.12

Table 6-9: Resulting wind loads of representative 125 m towers for the 5 MW turbine, with different cross sectional shapes, under extreme loading (LC 2a)

For structures such as towers, masts and chimneys, vortex shedding can cause significant loading. Especially when it occurs frequently, it can have a large influence on the fatigue life of the structure.

For turbines, this normally only causes issues during installation, according to DNV Risø [5]. As soon as the nacelle and rotor are placed, the critical wind speed is reduced to a value somewhere in-between V_{in} and V_{out}. For those wind speeds, the turbine is producing power and so the blades are spinning. The reduction in wind speeds and occurrence of turbulence caused by the rotation of the blades prevents the forming of vortices behind the tower.

It is assumed that the tower will be free-standing, i.e. not constructed in the vicinity of other tall structures, so that buffeting and other interactions will also not be an issue.

6-6   Resulting characteristic forces

This section displays examples of resulting forces on the tower, using the models and equations described before. These forces might differ slightly from those used in the final designs of Chapter 8, because the wind load on the tower depends on the shape and size of the cross section and the other loads depend on the natural frequency of the tower. Even though the loads will therefore be recalculated for each design, the global trend will be the same as displayed here.

By combining the different loads on top of and along the tower according to section 6-3-3, the resulting forces along the tower are obtained. Examples are shown in Figures B-3 and B-4 for load cases 1 and 2a, respectively. $F_x(h)$ and $M_y(h)$ are left out, because they are not calculated analytically and therefore can not be displayed in the same manner. Moreover, they are not relevant for the normal stress calculation and F_x and M_y are set at 0 for all classes. Load case 2b is not displayed here, because F_y and M_x will be larger for case 2a. M_z is constant along the height of the tower and therefore also not displayed.

During operation (LC 1)
    As can be seen in Figure B-3, loads between the different classes are virtually the same because the same wind speed is used.

During standstill (LC 2a)
    It can be seen in Figure B-4 that class IC provides the governing loads for the tower, which is to be expected because of the fact that $V_{hub} = V_{ref}$ is used, which is the highest for class IC.

Equation 6-7b show that $M_x(h)$ consists of three components: a constant part due to $M_{x,T}$, a linear part due to $F_{y,T}$ and a higher order component due to $q_w(h)$. The near straight lines depicting M_x confirm that the loads at hub height are a much larger contribution than the wind loads directly on the tower. $M_{x,T}$ is the reason the line does not start at 0 at hub height and is almost neglectable compared to $M_x(0)$.

Location			Noord-oost-polder	Windpark 'De Zuid-lob'	Vlissingen
Rated power	P	[MW]	1.5	3	6.2
Hub height	H	[m]	80	94	120
Rotor diameter	D	[m]	66	112	130
IEC Class			IIA/IIIA	IIA	IIA
Horizontal force at the bottom	$F_{y,k}(0)$	[kN]	765	868	2007
Vertical force at the bottom	$F_{z,k}(0)$	[kN]	2989	3669	9787
Bending moment at the bottom	$M_{x,k}(0)$	[kNm]	50330	70300	206910
Source			[50]	[37]	[28]

Table 6-10: The reference turbines from practice used to compare the calculated loads with

6-7   Reference turbines

The loads calculated in section 6-8 will be compared to those found in literature for steel towers in the Netherlands. Table 6-10 displays the forces at the base of the tower, along with the sources for these values. The loads from the 3 MW turbine in 'De Zuidlob' will be compared to the 3 MW model used in this research, while the 6.2 MW turbine near Vlissingen will be used to compare the load results from the 5 MW model to. Although the latter reference turbine has a larger rated power, its dimensions are comparable to the NREL 5 MW.

Differences are to be expected because of the slightly conservative methods used in this chapter, but most of all because of the larger width and aerodynamically disadvantageous shape of polygonal timber towers, compared to steel towers, as was explained above. All towers displayed in Table 6-10 are steel towers, designed for turbine class IIA. The loads displayed are characteristic loads.

6-8   Governing loads and verification

It can be concluded from the various calculations that the tower will experience the largest bending moment under conditions set by turbine class IC during standstill (LC 2a), which

was to be expected, because it represents the highest wind speeds. The calculation method does not result in significant differences between the different turbine classes during operation (LC 1). The BEM calculation for the rotor loads does not differentiate between the classes and although there is slight difference in the calculation of $c_s c_d$ for the wind loads on the tower, the contribution of this load to the total tower loads is very small.

When comparing the load results, several observations can be made from the results in Tables 6-11 and 6-12:

1. The loads at the base of the 3 MW turbine, as calculated by the quasi-static method are around between 1.55 ($F_y(0)$) and 1.7 ($M_x(0)$) times higher for the timber tower as for a reference steel tower. For the 5 MW turbine, these factors are only about 1.3 and 1.5, respectively.

2. It has been shown in section 6-5-5 that, on average, the base forces caused by pure wind loading on the tower are 2.3 to 2.6 times higher for timber towers than for steel ones. This increase was to be expected, because of two reasons mentioned before:

   – The polygonal shape of the timber tower is less streamlined than the cylindrical shape of the steel tower of the reference turbines, resulting in higher wind loads on the tower.
   – Since the steel towers underneath the reference turbines have a smaller base diameter, they will experience less wind load on the tower itself than a wider tower, even if it has the same strength capacity.

   The total increase in base load because of these reasons is fairly small, however. For the 3 MW the total base shear force $F_y(0)$ increased by 21% and the total base overturning moment $M_x(0)$ by only 8%. For the 5 MW model this came down to 12% and 3%.

Based on the values from points 1 and 2 above, one would for example expect the calculated $F_y(0)$ to be around 21% (3 MW) or 12% (5 MW) higher than the reference values, because of the cross sectional shape and dimensions (point 2). The final values under point 1, however, show that these are 55% and 30% respectively. This confirms the conservative nature of the methods used, since the values for $M_x(0)$ show the same trend.

Again, it should be noted that the values of the factors named here, are very specific, but only based on a very small amount of data. Even with this in mind, the difference is large enough to conclude the load calculation method is on the conservative side and is suited to be used in the preliminary designs intended to be made within this research.

6-9 Calculation models and software

Two software models were built during this research. The first consists of a large amount of Matlab code which incorporates everything that has been discussed in this chapter, as well as the normal stress calculations described in the next chapter. Furthermore, it also calculates geometric and material properties based on Appendices E and D, respectively, and the frequency according to Chapter 2.

Material		Reference	Steel-1	CLT-1	Steel-1/Reference	CLT-1/Reference
Cross section		Circular	Circular	8 sides		
B_{outB}	[m]	4.20	4.20	8.87	1.00	2.11
B_{outT}	[m]	3.00	3.00	3.00	1.00	1.00
$F_y(0)$	[kN]	868	1117	1348	1.29	1.55
$F_z(0)$	[kN]	3669	N/A*	3840	N/A*	1.05
$M_x(0)$	[kNm]	70300	111031	119996	1.58	1.71

Table 6-11: Comparison of calculated loads with values found for turbines in practice, for a 3 MW turbine

*The calculation model only allows for uniform wall thicknesses along the tower, so the weight of the steel tower is not valid

Material		Reference	Steel-1	CLT-1	Steel-1/Reference	CLT-1/Reference
Cross section		Circular	Circular	8 sides		
B_{outB}	[m]	6.00	6.00	11.22	1.00	1.87
B_{outT}	[m]	3.80	3.80	3.80	1.00	1.00
$F_y(0)$	[kN]	2007	2338	2627	1.17	1.31
$F_z(0)$	[kN]	9787	N/A*	9454	N/A*	0.97
$M_x(0)$	[kNm]	206910	295548	305223	1.43	1.48

Table 6-12: Comparison of calculated loads with values found for turbines in practice, for a 5 MW turbine

*The calculation model only allows for uniform wall thicknesses along the tower, so the weight of the steel tower is not valid

The entire code has been included in Appendix G. By adjusting just only ten parameters in the input file, the model displays the normal stresses along the tower, along with the frequency (based on Rayleigh-Ritz). These ten parameters are the turbine type and class, the material, the tower and cross section dimensions, and the load case, as shown in Figure 6-5. Unity checks for normal stresses are performed and displayed, as well as a message whether the natural frequency meets the demands set out in Chapter 5.

Furthermore, the Matlab model provides the user with a few lines of input code for ANSYS in APDL code. When combined with the rest of the APDL code, which uses these extra lines of codes to calculate additional parameters, it can be directly input into ANSYS, a finite element (FE) program. ANSYS then determines stresses, frequency and an buckling factor, although the latter is incorrect. The correct buckling factor requires additional calculation, but this incorrect buckling factor is a good indication of the order of magnitude of the actual factor. Appendix H explains this in detail and contains all the code used.

A lot of time was spent developing these models, doing parameter and sensitivity studies, together with "sanity checks", where basic engineering judgement was used to determine if the models worked as intended. The end result is a fast-working Matlab model, combined with an accurate FE model that determines quantities that are hard to calculate analytically, such as shear stresses. Apart from the buckling factor, it takes about a minute for one tower design to go through both models.

It was not deemed necessary to use Matlab to start ANSYS and make the calculations in the background, since the work required to write this code would be more than the time used to manually input the code in ANSYS. Moreover, only one tower design is calculated at a time, so ANSYS was not required to be used in batch mode, which would be a reason to couple both models. The decoupling further allows for a quick check of the ANSYS input, making mistakes in the original Matlab input less likely. Both models possess the possibility to calculate both octagonal towers as well as decagonal towers.
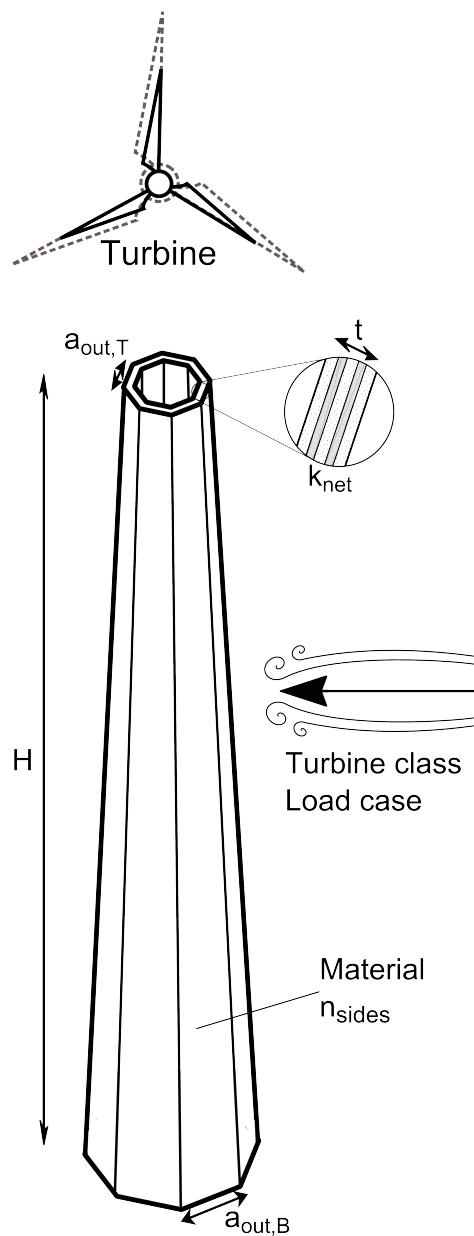
Figure 6-5: The adjustable parameters in the Matlab calculation model

Stress calculation methods

This chapter describes the various methods used to calculate stresses in the tower designs, since they differ from those used for isotropic materials such as steel. Furthermore, the strength of timber elements often depends on the size of the element, caused by volume effects and might thus not be the same for each design. The material properties will therefore be (re)calculated for each design, using the model found in Appendix G, which is in turn based on the material property formulas in Appendix D. A distinction is made between Cross Laminated Timber (CLT) and Laminated Veneer Lumber (LVL).

7-1 General remarks

The factors below are used in the calculation of stresses and material strengths. Some can be assigned values here, others will differ per design and will be calculated where needed.

Modification factor k_{mod}
  This takes into account the strength of the material relative to load duration. For both LVL and CLT it is taken as $k_{mod} = 1.1$, using the formula in sections D-1-4 and D-3-3. Gusts determine the extreme loads and thus the maximum stress. Since the extreme gusts only last a few seconds, the use of the modification factor for instantaneous actions is justified.

Net cross section factor k_{net}
  Factor k_{net} describes the amount of fibres in the main direction compared to the total cross section, by dividing the area of a cross section with its fibres in the longitudinal direction A_{net} by the total area of the cross section A_{tot} as defined in Figure 5-10.

$$k_{net} = \frac{A_{net}}{A_{tot}} \tag{7-1}$$

  For LVL the orientation of the layers has already been taken into account by the manufacturer when determining the material properties, so $k_{net} = 1.0$ for LVL.

Height factor k_h

> This takes into account various volume effects when dimensions other than the reference cross section from the codes have been used. k_h differs for the various materials and loading types and the formulas can be found in detail in Appendix D.

Material factor γ_m

> The partial safety factor for material strength γ_M also differs per material. For CLT it will be taken as 1.25, while the value of 1.2 is used for LVL, according to the Eurocodes.

Consequence of failure factors γ_n

> The IEC defines a factor γ_n to differentiate between the consequences of failure of components of the entire turbine. In short, replaceable components will have a γ_n slightly lower than 1.0 for ultimate strength calculations, while the turbine's protection system (part of the so-called "'non fail-safe mechanical components") can have a γ_n up to 1.3. The tower is considered a "non fail-safe structural component" and γ_n may therefore be taken as 1.0.

Strength classes and other relevant material properties, as well as the formulas required for the calculation of design material properties are provided in Appendix D.

The use of k_{net} leads to the definition of two different parameters for cross sectional strength:

- The strength of the net fibres $f_{i,net,d}$.

- The average strength of the entire cross section $f_{i,d} = k_{net} f_{i,net,d}$.

The need for this differentiation will become clear in the next section, but basically, the following holds:

$$A_{net} f_{i,net,d} = A_{tot} f_{i,d} \tag{7-2}$$

The analysis will be limited to static-linear. This means that the following is assumed:

- Material responses are linear;

- Deflections are small, making the original undeformed shape suited for stress analysis.

In reality, both these simplifications might prove to be insufficient to model the structural behaviour, but a non-linear analysis for each design case requires much more calculation time than a linear one, which is not available. The reasons not to apply elaborate dynamic and aerodynamic analyses have been discussed before.

7-2 Normal stresses

Stresses due to bending and normal force are of primary interest and are calculated by considering the tower as a cantilevering beam. Calculation equations for the loads used below have been provided in previous chapter. Normal stresses are not checked for elements at $h < 5$ and $h > (H - 5)$ because this is where transfer structures made from other materials are present.

The tensile and compression strength of CLT layers with a fibre orientation perpendicular to the loading direction is ignored in normal stress calculations, as can be found in the various design examples provided during the CLT Training Course in Trento in 2014 [56]. The strength analysis of the tower therefore has to take into account the orientation of the fibres in layered materials, which can be done in two ways. One could calculate the properties of the net cross section A_{net} and use this to calculate the actual occurring stresses $\sigma_{i,net,d}$. These would have to be compared with the design strengths of the material $f_{i,net,d}$. These are the actual occurring stresses and are calculated using the Matlab model described earlier, which can be found in Appendix G.

Alternatively, one could use the entire cross section A_{tot} to calculate the stresses $\sigma_{i,d}$ and account for the direction of the fibres by averaging the material strength over the entire section in $f_{i,d}$. This is what is done in the second part of the calculation model, in ANSYS. Both methods are described below in sections 7-2-3 and 7-2-4 respectively and because of certain simplifications, will yield the same results.

7-2-1 Cross sectional properties

The formulas to determine cross sectional properties of both hollow octagons and decagons can be found in Appendix E. Since the cross layers of the materials are ignored, the actual area A_{net}, moment of inertia I_{net} and section modulus W_{net} of the cross sections would have to be calculated for each longitudinal layer i and summed:

$$A_{net} = \sum_i A_i$$

$$I_{net} = \sum_i I_i$$

$$W_{net} = \sum_i W_i$$

To apply these formulas and calculate the actual stresses in a finite element model would result in unnecessary and time-consuming complications, such as the need to use of layered elements. However, since the distance between the individual layers is many times smaller than the width of the tower, one could also just multiply the total properties by k_{net} and get the same results (with a neglectable difference lower than 1%):

$$A_{net} = k_{net} A_{tot} \tag{7-3a}$$

$$I_{net} = k_{net} I_{tot} \tag{7-3b}$$

$$W_{net} = k_{net} W_{tot} \tag{7-3c}$$

7-2-2 Material strengths

Using the relationship described earlier on the compression strength f_c and tensile strength f_t:

$$f_{c,0,d} = k_{net} f_{c,0,net,d} \tag{7-4a}$$

$$f_{t,0,d} = k_{net} f_{t,0,net,d} \tag{7-4b}$$

7-2-3   Actual stresses $\sigma_{i,net,d}$

This is the method applied in the Matlab model of Appendix G. It calculates the actual stresses in the fibres of the longitudinal layers based on the simplified net cross sectional and material properties above.

Tower stresses due to bending $\sigma_{m,net,k}(h)$
These are calculated by dividing the bending moment by the section modulus of the net tower cross section.

$$\sigma_{m,net,k}(h) = \frac{M_{x,k}(h)}{W_{net}(h)} \tag{7-5}$$

Tower stresses due to axial force $\sigma_{ax,net,k}(h)$
Calculated by dividing the axial force in the tower over the net cross sectional area of the tower.

$$\sigma_{ax,net,k}(h) = \frac{-F_{z,k}(h)}{A_{net}(h)} \tag{7-6}$$

Load combination
Combining these using the appropriate load factors as found in Appendix M, leads to the maximum compression and maximum tensile stress in the net cross section:

$$\sigma_{c,net,d}(h) = -1.35\sigma_{m,net,k}(h) + 1.35\sigma_{ax,net,k}(h) \tag{7-7a}$$

$$\sigma_{t,net,d}(h) = 1.35\sigma_{m,net,k}(h) + 0.9\sigma_{ax,net,k}(h) \tag{7-7b}$$

For load calculations in load case 2a, the value of 1.35 is replaced by 1.1.

Unity checks
The results of these last two formulas will be compared with the material strengths of the longitudinal layers.

$$\frac{\sigma_{c,net,d}}{f_{c,0,net,d}} \leq 1 \tag{7-8a}$$

$$\frac{\sigma_{t,net,d}}{f_{t,0,net,d}} \leq 1 \tag{7-8b}$$

7-2-4   Equivalent stresses $\sigma_{i,d}$

This is the method applied in the ANSYS model in Appendix H. It calculates the stresses using the entire cross section.

Tower stresses due to bending $\sigma_{m,k}(h)$
These are calculated by dividing the bending moment by the section modulus of the total tower cross section.

$$\sigma_{m,k}(h) = \frac{M_{x,k}(h)}{W_{tot}(h)} \tag{7-9}$$

Tower stresses due to axial force $\sigma_{ax,k}(h)$

Calculated by dividing the axial force in the tower over the total cross sectional area of the tower.

$$\sigma_{ax,k}(h) = \frac{-F_{z,k}(h)}{A_{tot}(h)} \tag{7-10}$$

Load combination

Combining these using the appropriate load factors as found in Appendix M, leads to the maximum compression and maximum tension stress in the total cross section:

$$\sigma_{c,d}(h) = -1.35\sigma_{m,k}(h) + 1.35\sigma_{ax,k}(h) \tag{7-11a}$$

$$\sigma_{t,d}(h) = 1.35\sigma_{m,k}(h) + 0.9\sigma_{ax,k}(h) \tag{7-11b}$$

For load calculations in load case 2a, the value of 1.35 is replaced by 1.1.

Unity checks

The results of these last two formulas will be compared with the material strengths of the longitudinal layers.

$$\frac{\sigma_{c,d}}{f_{c,0,d}} \leq 1 \tag{7-12a}$$

$$\frac{\sigma_{t,d}}{f_{t,0,d}} \leq 1 \tag{7-12b}$$

7-2-5   Comparison

Because of the simplifications in section 7-2-1 the equations above should lead to:

$$k_{net}\sigma_{i,net,d} = \sigma_{i,d} \tag{7-13}$$

After thorough investigation of both methods, it can be concluded that the results from both Matlab and ANSYS agree. Matlab provides $\sigma_{i,net,d}$, while ANSYS provides $\sigma_{i,d}$ and the relation $k_{net}\sigma_{i,net,d} = \sigma_{i,d}$ holds.

7-3   Shear stresses

Shear stresses are determined using FE calculations ANSYS, which is why the coordinate system from the software is used within this chapter (see Figure 7-1), which might differ from the usual conventions. The z-axis is pointed upwards and the x-axis is perpendicular to the outer face of the tower.

It is not possible to use ANSYS to check the shear strength of each separate layer in the material without the time-consuming effort of modelling layered elements. Instead, a simplification is made where the maximum shear stress is assumed present in the entire cross section. If the cross section has sufficient strength to resist this, it will definitely be strong enough for the actual shear stress distribution. This leads to the following simplifications:

$$\int^A \tau_{yz} = A\tau_{yz,max} \tag{7-14a}$$
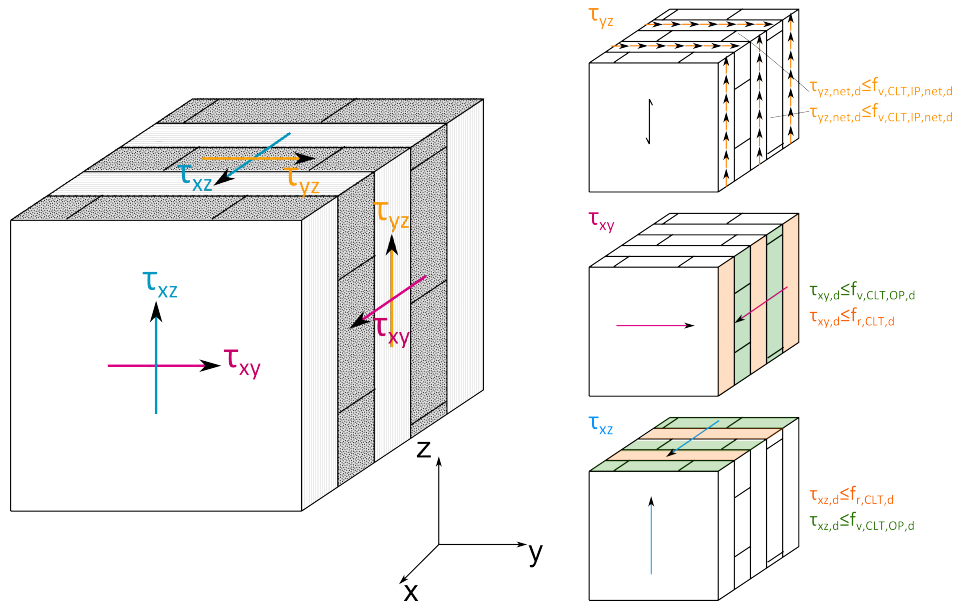
Figure 7-1: Definition of shear forces and the necessary strength of each layer

$$\int^A \tau_{xz} = A\tau_{xz,max} \tag{7-14b}$$

$$\int^A \tau_{xy} = A\tau_{xy,max} \tag{7-14c}$$

Shear is not checked for elements at $h < 5$ and $h > (H - 5)$, similar to the normal stresses. At these heights transfer structures are present.

The shear strength calculations differ for CLT and LVL, because the orientation of the layers of CLT has to be taken into account. The procedure for both materials is described below, where the CLT part is based on [57, 58, 59, 60, 56]

7-3-1   Shear calculations in CLT

Mechanisms

CLT knows four mechanisms that relate to shear, which can be divided into the ones occurring under loading in-plane and those occurring under loading out-of-plane:

1. **In-plane loading**
   Here, a combination of two mechanisms occurs and is best explained with the help of Figure 7-2, where a simplified element of two layers is shown. In-plane shear stresses are not divided evenly across all layers as is shown in the left side of the figure, and to calculate the actual shear stresses in the individual layers the internal structure of the CLT has to be considered. In-plane shear is resisted as a combination of in-plane shear of the individual layers (top right of the figure) and torsional shear in-between the layers (bottom right). This "internal torsional moment, acting on both sides of the gluing interface, vanishes all shear stresses, located at the narrow faces of the boards"

[57], which is why shear stresses are only present on the long edges of the boards and are higher than the average stress. This is shown in Figure 7-2, where the top right part shows the real shear stress distribution in a two-layer CLT element. This distribution is also extrapolated to a five-layered element in the top right of Figure 7-1.

The maximum occuring shear stress is assumed present on the entire cross section and is denoted here simply as τ_{yz}, according to Equation 7-14.

(a) **In-plane shear**

First, the shear stresses and shear strengths will be discussed for the two-layered element of Figure 7-2, after which it will be extrapolated to the element in Figure 7-1.

The average (nominal) shear stress is simply denoted by τ_{yz} in the left part of Figure 7-2. As stated before, the actual shear stresses are not transmitted on the narrow sides of the individual boards. Referring to Figure 7-2, this means there are no shear stresses present on the top and bottom sides for layer i and the left and right side for layer j. The actual shear stresses will therefore only work on a width of t_i on the top side of the element in Figure 7-2 and on a width of t_j on the right side and thus be higher than the nominal stress τ_{yz}:

$$\tau_{yz,net,i} = \frac{t}{t_i}\tau_{yz}$$

$$\tau_{yz,net,j} = \frac{t}{t_j}\tau_{yz}$$

When applied to Figure 7-1, maintaining the same subscripts i for the cross layers and j for the longitudinal layers :

$$\tau_{yz,net,i} = \frac{t}{\sum t_i}\tau_{yz} \tag{7-16a}$$

$$\tau_{yz,net,j} = \frac{t}{\sum t_j}\tau_{yz} \tag{7-16b}$$

These actual stresses should be lower than the shear strength of the CLT:

$$\tau_{yz,net,d} \leq f_{v,CLT,IP,d} \tag{7-17}$$

The contribution of the nominal layers to the entire cross section has been defined as k_{net} in Equation 7-1, which says:

$$\frac{\sum t_i}{t} = k_{net}$$

$$\frac{\sum t_j}{t} = 1 - k_{net}$$

Combining all the above leads to the following checks that have to performed:

$$\tau_{yz,i,net} = \frac{t}{\sum t_j}\tau_{yz} = \frac{\tau_{yz}}{k_{net}} \leq f_{v,CLT,IP,d} \tag{7-19a}$$
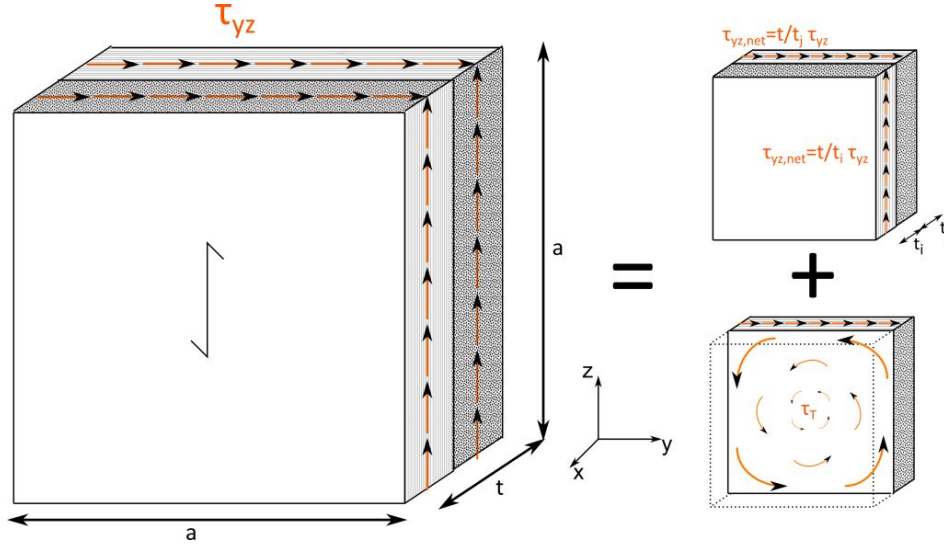
Figure 7-2: In-plane shear of a simplified CLT element

$$\tau_{yz,j,net} = \frac{t}{\sum t_i}\tau_{yz} = \frac{\tau_{yz}}{1-k_{net}} \leq f_{v,CLT,IP,d} \tag{7-19b}$$

For easier use in the ANSYS calculation model, these checks are rewritten, using the assumptions of equation 7-14, so that $\tau_{yz} = \tau_{yz,max,d}$:

$$|\tau_{yz,max,d}| \leq k_{net}f_{v,CLT,IP,d} \tag{7-20a}$$

$$|\tau_{yz,max,d}| \leq (1-k_{net})f_{v,CLT,IP,d} \tag{7-20b}$$

for the side face and top face of Figure 7-1, respectively. This allows the results from the ANSYS model to be directly checked against the lowest value of the right hand sides of these equations, without having to calculate the actual stresses using Equation 7-19.

(b) **Torsional shear**

Referring to the simple two-layered element in Figure 7-2, the in-plane shear mechanism of the top right (mechanism 1a) will occur simultaneously with a torsional moment on the crossing interface between the layers. The resulting stress can be calculated using formulas provided by Bogensperger in [57] and Thiel in [58]:

$$M_T = \tau_{yz}ta^2$$

$$W_p = \frac{1}{3}a^3$$

$$\tau_{T,d} = \frac{M_{T,d}}{W_p} = 3\tau_{yz}\frac{t}{a}$$

The resulting stress should be smaller than the torsional shear strength $f_{T,d}$ of the material:

$$\tau_{T,d} \leq f_{T,d}$$

When applied to elements with more than 2 layers, such as the one in Figure 7-1, each crossing surface has to be checked separately. This is done by modelling each crossing surface as a Representative Volume Sub-element (RVSE). This RVSE will consist of two layers, similar to Figure 7-2, and have a total thickness t_i^*, which is the smallest value of the thicknesses of the adjacent layers. For example, when checking the crossing surface between a layer of 40 mm and one of 30 mm, the RVSE will have a thickness t_i^* of 30 mm, as is explained in [57].

The shear stress is assumed to be divided across all the RVSE's in the total cross section, with a combined thickness $t^* = \sum t_i^*$:

$$\tau_{yz}^* = \frac{\tau_{yz} t}{t^*} \tag{7-21}$$

This is in turn used to calculate the torsional moment in a single RSVE as before:

$$M_{T,i} = \tau_{yz}^* t_i^* a^2 \tag{7-22a}$$

$$W_p = \frac{1}{3} a^3 \tag{7-22b}$$

$$\tau_{T,i,d} = \frac{M_{T,i,d}}{W_p} = 3\tau_{yz}^* \frac{t_i^*}{a} = 3\tau_{yz} \frac{t}{t^*} \frac{t_i^*}{a} \leq f_{T,d} \tag{7-22c}$$

For easier use in the ANSYS calculation model, these checks are again rewritten, using the assumptions of equation 7-14, so that $\tau_{yz} = \tau_{yz,max,d}$:

$$|\tau_{yz,max,d}| \leq \frac{f_{T,d}}{3} \frac{t^*}{t} \frac{a}{t_i^*} \tag{7-23}$$

According to Andreolli [60], another method found in many European Technical Approvals allows for the simple division of the torsional moment evenly over all the adhesive layers ($n_{layers} - 1$):

$$M_T = \frac{\tau_{i,net,d} a^2 \sum t_i}{n_{layers} - 1} = \frac{\tau_{j,net,d} a^2 \sum t_j}{n_{layers} - 1} \tag{7-24}$$

The resulting stress should again be smaller than the torsional shear strength $f_{T,d}$ of the material:

$$\tau_{T,d} = \frac{M_{T,d}}{W_p} = \frac{t}{a} \frac{3\tau_{yz,max}}{n_{layers} - 1} \leq f_{T,d} \leq f_{T,d} \tag{7-25}$$

In the European Technical Approval (ETA) for CLT it is stated that when edge bonding of the board within one layer is not applied, the shear stresses in the crossing surfaces have to be checked [56, 60]. For edge-bonded panels, mechanism one 1a will be the governing in-plane shear mechanism. This can be easily explained with Equation 7-23, where a becomes very large for edge-bonded layers working as one, resulting in a small $\tau_{T,d}$.

Comparing Equations 7-20 and 7-23, one is able to determine which of these two mechanisms will be governing for the designs used in this research for non-edge-bonded panels.

– Regarding Equation 7-20: $(1 - k_{net})$ will lie between 0.3 and 0.2 for k_{net} between 0.70 and 0.85, which are the values used throughout this research.

Therefore at most 30% of $k_{mod} \frac{f_{v,CLT,IP,k}}{\gamma_M}$ in Equation 7-20 can be utilized for resisting τ_{yz}. Taking $k_{mod} = 1.1$, $\gamma_M = 1.25$ and $f_{v,CLT,IP,k} = 5$ N/mm^2, leads to $\tau_{yz,max,d} \leq 1.2$ N/mm^2, at most.

– Regarding Equation 7-23:

  – $\frac{a}{t_i^*}$ is at least 5 for current production standards, where the maximum board thickness $t_i^* = 50$ mm and the standard board width $a = 150$ mm, but is even higher for thinner layers.

  – $\frac{t^*}{t}$ depends on the layer thickness of the cross section, but for walls of 300 mm and thicker, values of k_{net} ranging between 0.70 and 0.85, $\frac{t^*}{t}$ will lie somewhere between 0.4 and 0.9.

Therefore, at least $\frac{f_{T,d}}{3} \cdot 5 \cdot 0.4 = \frac{2}{3} f_{T,d}$ can be used to resist τ_{yz} Taking $k_{mod} = 1.1$, $\gamma_M = 1.25$ and $_{T,k} = 2.5$ N/mm^2, leads to $\tau_{yz,max,d} \leq 1.67$ N/mm^2, at least.

So, even when taking the most favourable values for mechanism 1a and the most unfavourable ones for mechanism 1b, mechanism 1a will be governing and therefore only Equation 7-20 has been included in the calculation model. This saves the effort of having to include the layer build-up in the calculations, which saves time and allows for faster comparison of designs.

Other calculation examples also show that the in-plane shear strength of mechanism 1a is most often governing over the torsional shear strength [56, 60] for other types of structures as well.

2. **Out-of-plane loading**
For out of plane loading, a certain shear stress distribution will occur in the cross section. Each layer will therefore be subjected to shear and should be able to resist the shear occurring in that layer. A distinction is made between longitudinal layers and cross layers, as shown in Figure 7-1.

(a) **Longitudinal layers: out-of-plane shear**
The out-of-plane shear strength of CLT is slightly lower than its in-plane shear strength. In the longitudinal layers of the top face in Figure 7-1, the out-of-plane shear stress may not be larger than this out-of-plane shear strength:

$$|\tau_{xz,d}| \leq f_{v,CLT,OP,d} \tag{7-26a}$$

The same holds for the side face, where the cross layers are the layers to consider:

$$|\tau_{xy,d}| \leq f_{v,CLT,OP,d} \tag{7-26b}$$

(b) **Cross layers: rolling shear**
Rolling shear occurs in the cross layers of the element, where, because of the shear in the longitudinal layers, the fibres will want to start 'rolling' over each other. It has to be ensured that the cross layers have sufficient rolling shear strength to prevent this from happening:

$$|\tau_{xz,d}| \leq f_{r,CLT,d} \tag{7-27a}$$

$$|\tau_{xy,d}| \leq f_{r,CLT,d} \tag{7-27b}$$

For ease of calculation, the weakest material property is assumed present in the entire cross section in this research. After all, if the shear stress at any point in the cross section remains lower than the lowest shear strength, the actual cross section, which even has some parts that are stronger, will suffice for sure. When this is not the case, a more detailed investigation will have to show if the shear strength of the material is sufficient.

Material strengths

The same shear strengths are used for all four regular CLT strength classes as well as for the hardwood CLT class constructed and can be found in Appendix D.

Unity checks

Combining the sections and formulas above, the governing unity checks to perform are:

$$\frac{|\tau_{yz,max,d}|}{\min\left[(1 - k_{net}) \, f_{v,CLT,IP,d}; \; k_{net} f_{v,CLT,IP,d}\right]} \leq 1 \tag{7-28a}$$

$$\frac{|\tau_{xz}|}{\min\left[f_{r,CLT,d}; \; f_{v,CLT,OP,d}\right]} \leq 1 \tag{7-28b}$$

$$\frac{|\tau_{xy}|}{\min\left[f_{r,CLT,d}; \; f_{v,CLT,OP,d}\right]} \leq 1 \tag{7-28c}$$

When these conditions are met, the shear strength of the design is deemed adequate. In cases where this is not the case, a detailed investigation will have to point out whether or not sufficient shear strength is present in the design.

7-3-2 Shear calculations in LVL

For LVL elements the orientation of the layers has already been taken into account when determining the material properties and Figure 7-1 becomes Figure 7-3. The governing unity checks become:

$$\frac{|\tau_{yz,max,d}|}{f_{v,LVL,IP,d}} \leq 1 \tag{7-29a}$$

$$\frac{|\tau_{xz,max,d}|}{f_{v,LVL,OP,d}} \leq 1 \tag{7-29b}$$

$$\frac{|\tau_{xy,max,d}|}{f_{r,LVL,d}} \leq 1 \tag{7-29c}$$

Aside from differences in bending and tensile strength between cross-bonded (Q) and parallel-orientated (S) varieties of LVL, there is a difference in shear strength. $f_{v,LVL,OP,d}$ is higher for the S-type, while $f_{v,LVL,IP,d}$ and $f_{r,LVL,d}$ are higher for the Q-type, as can be seen in Appendix D.
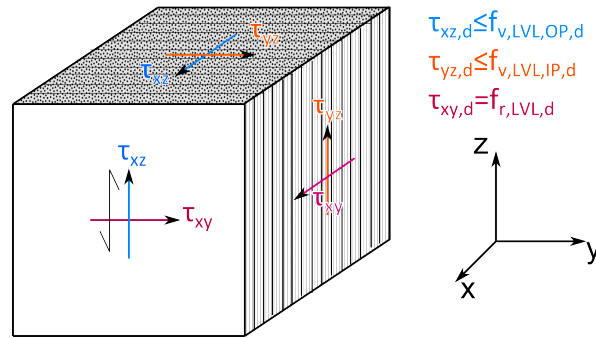
Figure 7-3: Definition of shear forces and the necessary strength for a S-LVL element

7-4   Local buckling

Stability calculations are limited to buckling analysis and buckling strength is considered to be sufficient when the buckling factor calculated for the structure is deemed sufficient. This buckling factor is defined as the ratio between the load at which buckling first occurs and the actual applied load:

$$\lambda_{buc} = \frac{F_{i,buc}}{F_{i,d}} \tag{7-30}$$

For such complex geometrical shapes as a tapered polygonal cylinder, buckling calculations are not feasible to do quickly by hand or analytically. Luckily, ANSYS has a separate analysis module for determining this factor. It steadily increases the loads applied in the model by a certain load magnification factor until buckling occurs. The first value of the load magnification factor for which buckling occurs, whether it is global or local, is displayed as the buckling factor. However all loads, including gravity loads, are multiplied by this factor, which is not correct, since only the wind loads are supposed to increase for this particular turbine tower model. Therefore, a trial-and error method is necessary, using a self-defined buckling factor (see the code in Appendix H). All wind loads are multiplied by this factor λ and applied to the model, while the gravity constant remains the same and the self-weight of the turbine and tower do not change. λ is varied until ANSYS displays a buckling factor of 1.0. The λ that has been input for that calculation will then be actual buckling factor.

For a perfect structure, a buckling factor of 1.0 would be sufficient to prevent buckling. In reality, however, the stiffness of the structure will be different due to the variance in Young's modulus and local and global imperfections, among others. It is found in literature that buckling factors for reinforced concrete cooling towers are required to be at least 5.0 [61]. Without valid reasons to lower such a value for timber turbine towers, and lack of information on this subject for large CLT panels, the same criterion is applied within this research. This means that buckling factors lower than 5.0 for a tower design will result in the buckling strength of the design being labelled as insufficient.

Because of the predominant bending of the tower, global buckling of the tower will not be the governing buckling mode. Instead, it was found that local buckling at the bottom of the compression side will occur first. Here, the part of the tower that is under the highest compression stress will become locally unstable and start to crease, similar to local buckling
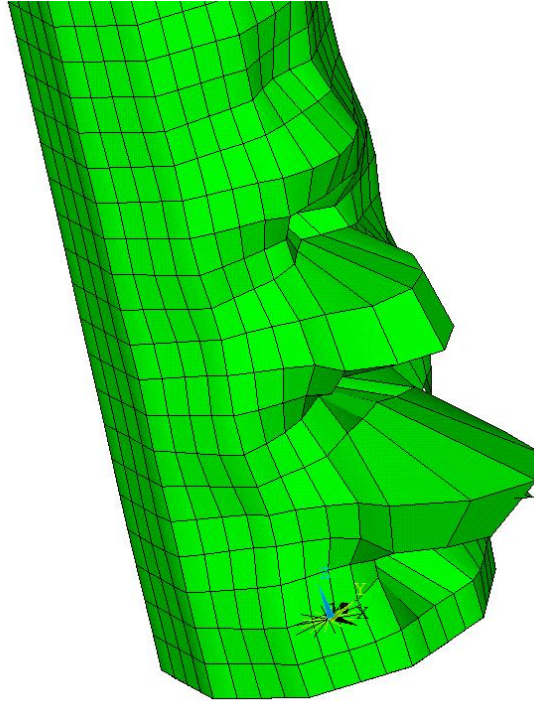
Figure 7-4: Example of a local buckling mode. The lower 20% of the tower is shown.

of a steel plate. Examples are shown in Figures 7-4 and 8-5. For most of the designs, failure in compression of the timber will occur before this buckling will.

7-5 Deflections

Normally deflection calculations for timber are different than those for steel, because of time-dependent deformations (creep) that can occur in timber. Instantaneous deformations u_{inst} are multiplied with a factor $(1 + k_{def})$ to take creep into account. The creep behaviour of timber depends on load duration, moisture content, temperature and stress level [62].

Wind loads in general are of a short nature and tend to change direction. In terms of load duration, the wind loads are far from what is considered long-term loading and k_{def} is not applied on them. Furthermore, results will later show that the contribution of permanent loading, which consists of the gravity loads from nacelle and tower, are much smaller than those caused by wind loads, so it can be concluded that applying $(1 + k_{def})$ in the deflection calculations in general will thus make little difference. Moisture content and temperature will be kept as constant as possible by installations at the base of the tower [22].

Mean stiffness values are to be used in the calculations, but should be divided by $\gamma_m = 1.1$, according to section 7.6.5 of the IEC-61400 [2], already explained in general in section 2-4-3. The same section of the IEC prescribes the use of the partial load factor γ_f on the characteristic loads, unlike most other structures where deformation analysis is carried out without load factors. γ_n may be taken as 1.0 and thus ignored. The governing tower deflection

can then be determined as:

$$u_{max,tow,d} = 1.1\gamma_f u_{inst,k} \tag{7-31}$$

Where:

$u_{inst,k}$ is the initial deformation under characteristic load values;
γ_f is the load factor, depending on the load case.

As explained in section 2-4-3, the maximum allowable tower deflection will be kept at 2.5 m and 2.0 m for the 5 MW and 3 MW turbines, respectively.

Results

CHAPTER 8

Mono-material calculation results and tower designs

This chapter contains observations made from the designs constructed for each design case that has been defined up to this point. Detailed input and calculation results from both the Matlab and ANSYS models can be found in Appendix C and will be frequently referenced to throughout this chapter.

The design cases from the previous chapter lead to twenty-seven different situations to be looked at for each material. First, a distinction is made between a 3 MW turbine with a hub height of 100 m, the same 3 MW turbine at 125 m and a 5 MW turbine at 125 m. As explained in the first part of this report, this is considered to represent the current and planned turbines in the Netherlands well. These three situations are split up into to the three wind turbine classes that represent the Dutch wind conditions, namely classes IC, IIA and IIIA. The three load cases (LC) defined in Chapter 6 - 1, 2a and 2b - further divide these nine cases into twenty-seven calculations models.

Four materials will be considered. First, there is softwood CLT, which has been used in the original TimberTower. Secondly, possible designs in hardwood CLT will also be investigated, as well as designs made in softwood LVL (Kerto). Lastly, possibilities for the use of hardwood LVL (BauBuche) will be explored. Only for the original softwood CLT design will all situations be considered. Some expectations exist on which turbine classes or load cases will govern the design. After the regular CLT designs have been made, it will be discussed which cases do not have to be taken into account in determining the feasibility of the other materials, in order to save time.

Strength and stiffness of the towers in this chapter will be altered by varying tower dimensions (thickness, overall width) and the number of fibres in the longitudinal directions for CLT (k_{net}). No combination of materials is used, nor is stiffening the tower in other ways than adding material, such as rings or ribs, performed. Those options are discussed in the next chapter.

Top diameters are fixed for each design at 3 m for the 3 MW turbine and 3.7 m for the 5 MW turbine.

8-1   Designs in softwood CLT

Part C-1 of Appendix C displays all designs made with the regular softwood CLT strength classes. Observations made from these results are discussed below.

8-1-1   Design process

The main design goal was to keep the tower frequency as far away from the 1P and 3P frequencies as possible, i.e. at a value right in-between. For the 3 MW turbine, this means the frequency has been kept around 0.30 Hz and for the 5 MW turbine around 0.26 HZ.

The reasoning behind this is that there is a certain variation present in the Young's modulus of the timber, so the actual stiffness of the material may differ from the mean value used in the calculations and using a bigger margin than the 10% suggested in Chapter 2 was considered wise. Although a short investigation in Chapter 5 showed that the influence of the foundation and connections can be ignored for these simple initial design calculations, keeping the tower frequency as far from 1P and 3P as possible will nonetheless make sure that their small influence does not bring the tower frequency into the domain of 1P or 3P.

The designs made are far from the only combinations of parameters that will yield a suitable tower. By altering the strength class and (slightly) adjusting the outer dimensions, the thickness of the tower walls and k_{net}, one is able to design a variety of towers that all meet strength and frequency requirements.

For load cases 1 and 2b only one model per case has been included here. To determine the influence of the cross sectional shape on maximum stresses and buckling strength, both octagonal and decagonal designs have been made for load case 2a. The differences will be explained shortly.

8-1-2   Material strength classes

The lowest possible material classes were used, with economics in mind. For the timber to be graded into the higher strength classes, it needs stronger base boards and stricter strength grading, which are assumed to be more expensive. If for some reason loads turn out to be higher than used here, the use of a higher strength class can already balance that without changing the dimensions of the design.

For models B and E shown in section C-1 the lowest strength class, Cl24h, already led to a design with an optimal frequency and sufficient strength for turbine class IIA. For this reason, calculations for class IIIA were not made, since the loads will only be lower here while there is no lower strength class available. This is not uncommon in practice, where many existing turbines are suited for the combination 'IIA/IIIA' as well.

8-1-3   Stresses

For all models considered, the normal stresses were highest at a position around $\frac{2}{3}$ to $\frac{3}{4}$ of the tower height, not at the base. A representative stress distribution has been shown in Figure
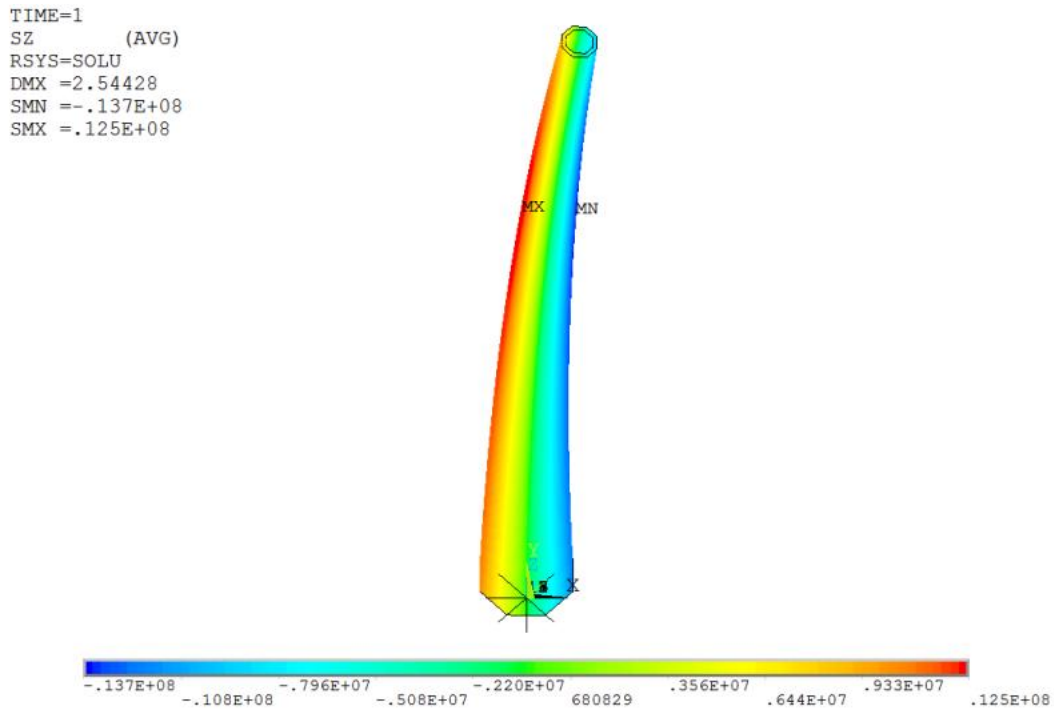
Figure 8-1: Normal stresses in z-direction for model G2

8-1. Results suggest that once the frequency has been optimized, the ultimate strength of the tower will be sufficient, at least for the load cases considered. Stresses in x and y direction are small enough to neglect and have not been included in the results. Shear stresses occur in all directions, as can be seen in Figures 8-2 through 8-4. The values of τ_{xy} are insignificantly small and can be ignored for CLT designs.

For some designs, the shear stresses do not comply with the simplified equations from section 7-3, such as model G, which is the one shown in Figure 8-3. A detailed investigation shows that this is only the case for the upper part of the tower, and only $\tau_{yz,max,d}$ exceeds $f_{v,CLT,d}$. These high stresses only occur very locally in the corners of the cross section. The exact cause for the occurrence of these high corner shear stresses is not entirely clear. They are most likely caused by the shape of the tower, where shear stresses are transferred from one face to the other at these locations.

Looking at the through-thickness average of the shear stresses, $\tau_{yz,ave,d}$ remains well under the shear strength of the material:

$$\frac{\tau_{yz,ave,d}}{\min\left[(1-k_{net})\,f_{v,CLT,IP,d};\ k_{net}f_{v,CLT,IP,d}\right]} \leq 1$$

The origin of this unity check has already been discussed in Chapter 7. In the other directions, the shear stresses are low enough to meet the simplified criteria from this chapter. For this reason the shear stresses are accepted for model G as well and all designs made are deemed feasible.

For now, no distinction is made between strength classes in CLT when it comes to shear strength, so the lowest values (those associated with class CL24h) have been used for all

classes. In reality, the shear strength will most likely be higher for the higher strength classes, reducing possible problems of insufficient shear strength even further, in cases where higher strength classes have been applied.

Governing shear stresses are highest under load case 2a, not under 2b, although the latter has a higher torsional moment. This means that for later designs LC 2b will not be taken into account anymore. LC 1 will be checked for deflection and overall stress level and LC 2a for ultimate strength and buckling, along with the natural frequency of the tower in general.

The overall stress levels under operating wind speeds might provide an indication for the fatigue strength of the material. If the stress level for operational wind speeds is already relatively high, fatigue might prove to be of concern, since the majority of the load cycles will take place at a relatively high stress level. Looking at the results, this is more of concern for class IIIA than for IC, caused by the fact that the operational and extreme wind speeds lie closer together for IIIA than they do for IC. Actual fatigue calculations will have to show if this is also the case.

8-1-4   Deflection

Deflections of the considered designs remain within the limits set out in section 7-5.

8-1-5   Buckling

It was expected that buckling would only have to be checked for load case 2a, since this case would result in higher compression stresses in the material than the other load cases. For the first few models though, the buckling factor was calculated for all load cases (especially 2b) and the buckling shape was determined for each model. After the first few models it was concluded that the buckling shape is the same for all load cases and buckling analysis was limited to load case 2a for later calculations. Buckling occurs locally on the compression side of the tower, at the bottom, and examples are shown in Figures 7-4 and 8-5.

After looking at the resulting buckling factors, it is concluded that this (local) buckling will not be an issue for CLT towers. The relatively large wall thicknesses of 270 mm and higher that have been used result in bulky sections. The timber will fail in compression before it will fail in buckling of the overall cross section. This does not, however, mean that later designs using other materials will exhibit the same behaviour, since their higher strengths may lead to more slender designs.

8-1-6   Cross sectional shape

It has already been concluded in Chapter 5 that a decagonal tower practically has the same frequency and will experience the same normal stresses as an octagonal tower of the same diameter and wall thickness. Results suggest that the cross sectional shape does not improve normal and shear stresses. It does however improve the buckling strength of the tower. This is to be expected, since the width of the individual faces becomes smaller for a decagonal tower.
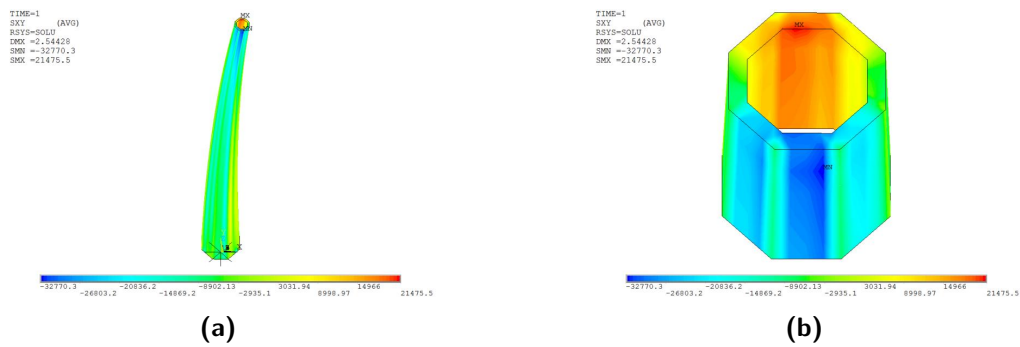
Figure 8-2: XY-shear stresses in for model G2, for 5<Z<(H-5) and for (H-10)<Z<(H-5)
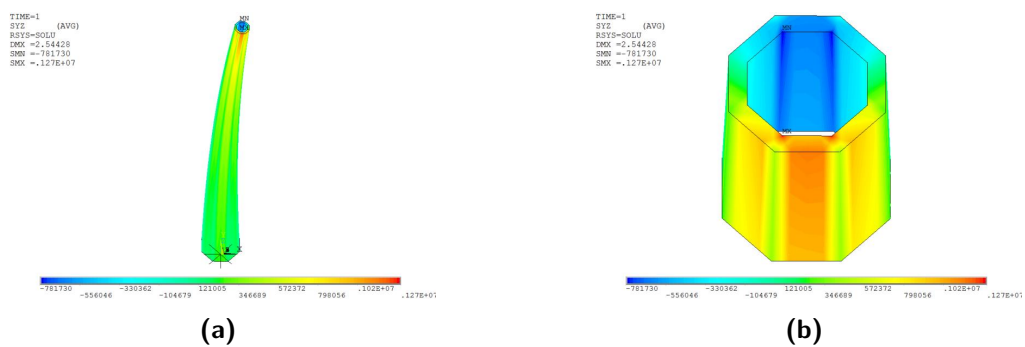
Figure 8-3: YZ-shear stresses in for model G2, for 5<Z<(H-5) and for (H-10)<Z<(H-5)
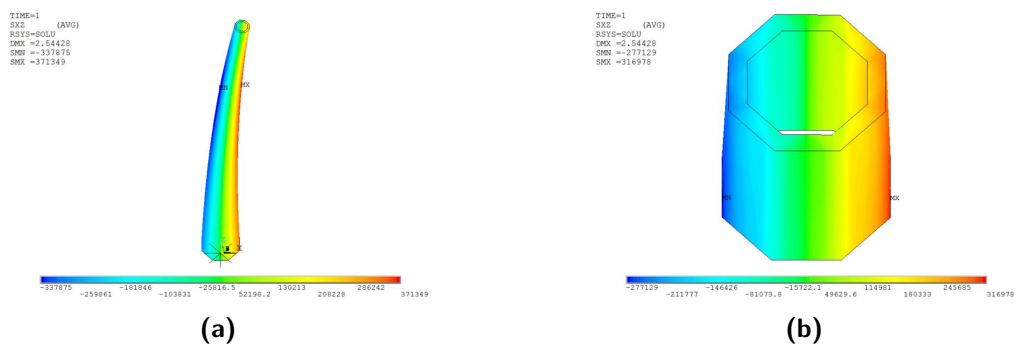
Figure 8-4: XZ-shear stresses in for model G2, for 5<Z<(H-5) and for (H-10)<Z<(H-5)
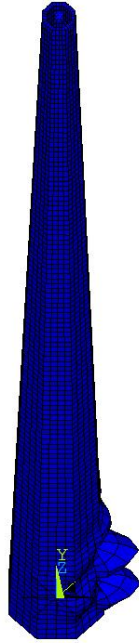
Figure 8-5: The governing buckling shape for all considered CLT towers

Deflections also seem to improve for the decagonal alternatives, based on the results in section C-1. The slightly higher frequency for the ten-sided towers suggest that they are slightly stiffer than their octagonal counterparts, which could explain the slightly lower deformation of the tower. For this reason, no improved deformation behaviour is attributed to the decagonal tower shape.

8-1-7   Feasibility

The results suggest that it is feasible to design towers for 3 MW turbines at 100 and 125 m and for a 5 MW turbine at 125 m for all three considered wind classes. These results have however been generated using simplified calculations that do not take into account the full set of structural checks that are prescribed by the IEC. This will be discussed in more detail at the end of this chapter.

8-1-8   Governing load cases

Several conclusions can be drawn from the results in section C-1 on which cases will govern the various aspects of the design checks. To make following calculations easier and faster, several adjustments to the process are made, described below.

Turbine classes

When looking at the loads at hub heights and the wind on the tower, turbine class IC produces the highest extreme loads of the three considered classes. When one is able

to design a tower for turbine class IC, the same model can thus be applied in IIA and IIIA. This does not mean that it is also the optimal design for IIA and IIIA, but since it is the overall feasibility that is of interest, being able to design a tower for class IC will be sufficient to assess the overall feasibility of the material.

If it is not possible to design a tower for class IC, only then class IIA is used to judge at least a partial feasibility. When the loads associated with class IIA are too high, only then will class IIIA be looked at, with the same reason.

Load cases

Load case 2b was included to determine if the higher torsional moment occurring under these circumstances would lead to higher shear stresses. Since this is not the case for all considered models and all other stresses are lower than for LC 2a, LC 2b is not considered from hereon.

Furthermore, since the buckling shape and behaviour was the same for all three load cases only the governing load case for extreme wind speeds (LC 2a) will include buckling calculations from heron. This will save a large amount of time, since it is the trial-and-error method of finding the correct buckling factor that takes up most of the calculation time.

Cross sectional shape

The timber towers have proven to be substantially wider than steel towers, which might become a problem with those opposed to the aesthetics of wind turbines in general. The biggest expected benefit of the stronger materials that will be considered next, is that they will lead to more slender designs than the CLT designs. These more slender towers might be more prone to buckling, e.g. because of smaller wall thicknesses. Therefore only decagons are considered from heron, since they exhibit better buckling behaviour than octagons.

8-2   Designs in hardwood CLT

The hardwood class CL40h defined in section D-2 has two main differences with the softwood classes. It has higher strengths in bending, compression and tension, and has a higher density because of the use of iroko (D40). It is expected that the hardwood strength class will have higher shear strength as well, but since strength values are not yet known for this type of CLT, the same values as for the other classes are used. The Young's modulus for iroko/D40 has been used, which is the same as for the lowest two softwood CLT classes.

8-2-1   Expectations

Designs in this section are limited to cross sections made entirely of hardwood CLT. Not a lot of benefit was expected over the other strength classes, since the properties essentially make it an even stronger CLT class than the ones treated in the previous section. For those cases the ultimate strength did not turn out to be the governing parameter, but the frequency was instead. Since the frequency parameter study already showed that higher density will lead to a slightly lower frequency, the combination of a higher density with a similar Young's

modulus is not considered beneficial overall. It should lead to around the same amount of material used, while the higher strength of the material would not be utilized.

8-2-2   Results

The input parameters and results from the calculation model can be found in section C-2 in Appendix C. Only three different cases have been investigated, because of the reasons explained in section 8-1-8. Buckling behaviour did not change significantly from the softwood designs, unity checks became lower while approximately the same tower dimensions were used to reach a suitable tower frequency, as was expected.

8-2-3   Feasibility

Designing a tower of pure hardwood is structurally feasible, as is shown by the designs in section C-2. However, hardwood CLT is considered to be more expensive overall. It is therefore considered economically less favourable to replace the entire softwood cross section with hardwood, since around the same amount of material would have to be used to reach suitable frequencies. Hardwood CLT was considered in the design process for the TimberTower as well, but was also considered economically less favourable there [22]. So even though the material is suited for turbine towers from a structural point of view, it is not expected to be applied in practice.

When the shear strength of the material does turn out to actually be higher, the width of the cross layers could be reduced. Referring to Equation 7-28a, the factor $(1 - k_{net})f_{v,IP,CLT,d}$ will be the governing value to check the shear stresses against. When $f_{v,IP,CLT,d}$ increases, $(1 - k_{net})$ is able to decrease. Since $(1 - k_{net})$ is the amount of fibres in cross-direction, this means the cross-layer thickness can be reduced.

The material stiffness has a much larger effect on tower frequency than the mass of the tower and the cross layers do not contribute to the longitudinal tower stiffness. The small decrease in tower mass caused by thinner cross-layers will only have a small effect on tower frequency. Still, using hardwood for the longitudinal layers seems a waste, since they are not necessary for strength purposes and softwood has the same stiffness. Furthermore, the expected decrease in cross layer width is very small, compared to the overall cross sections, so the gains seems trivial. Other options, such as using only a few layers made from hardwood, will be discussed in the next chapter in more detail, together with the possible benefits of the high natural durability of the hardwood.

8-3   Designs in softwood LVL

8-3-1   Expectations

The main difference in production sizes between LVL and CLT is in the thickness of the standards elements available. Standard available Kerto LVL elements are less than 7 cm thick, making them more prone to local buckling when applied with smaller thicknesses than the bulkier CLT elements used in section 8-1. This is why, as stated before, only decagonal
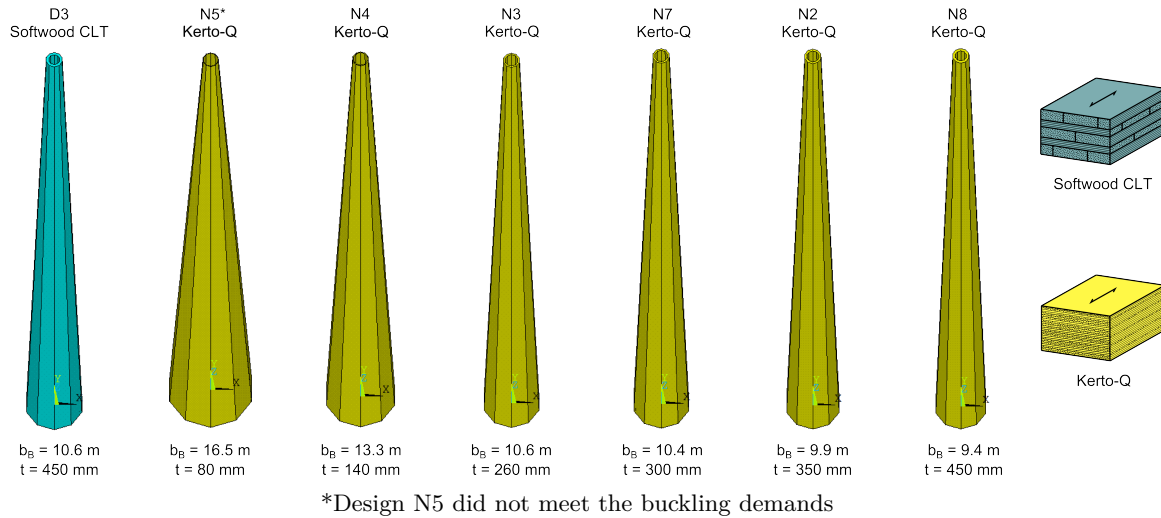
Figure 8-6: Several designs made in Kerto-Q for the 3 MW turbine at 125 m

towers in LVL are considered, to mitigate this. Keeping the wall thickness within the standard production limits is considered to be beneficial in terms of production speed and costs.

Stiffness and density values for cross-bonded Kerto-Q are similar to that of the net softwood CLT sections used in section 8-1, so one could expect the designs with the same tower dimensions to have somewhat thinner walls in general, since the Young's modulus has already been averaged over the entire cross section ($k_{net} = 1.0$).

Parallel-bonded Kerto-S has higher stiffness and strength than Kerto-Q, so it would be expected to allow for thinner or slimmer towers than with Kerto-Q, while still reaching a suitable frequency and having sufficient strength. However, the shear strength in the xy-plane ($f_{r,k}$) of Kerto-S is much lower than that of Kerto-Q, so before designs in Kerto-S are made, designs in Kerto-Q will have to show that these stresses are sufficiently low.

8-3-2   Results

Kerto-Q

Two main directions were chosen in determining the feasibility of softwood LVL towers. Firstly, towers with wall thicknesses within current production limitations were investigated, i.e. $t <\approx 70$ mm. Secondly, designs with diameters comparable to the CLT towers were made, resulting in relatively thick-walled towers. For the 3 MW turbine with a 125 m tall tower, a variety of designs is shown in Figure 8-6 that show these two directions in various degrees.

When trying to keep the designs within the standard production limits, much larger diameters for the tower were needed to satisfy frequency requirements. Aside from the fact that these wider towers have a larger (negative) visual impact, there are some structural disadvantages to them as well. Local buckling became an issue for most of these designs, where the towers did not meet the buckling requirements set out in Chapter 2. An example has been given in Figure 8-7 (design N5), where the large base dimensions of one of those designs can be seen, as well as the buckling shape.

Furthermore, the higher stress levels in the thinner-walled designs could also negatively affect fatigue strength and cause complications in finding suitable connections.

In the end, design N4 with a wall thickness of 140 mm was the thinnest design found for the 3 MW turbine at 125 m that more or less met all demands (it only came short on the buckling demand by a very small amount). Of the designs made with thinner walls than 140 mm, only design N5 has been included in Appendix C, to show the results associated with those designs that did not meet buckling demands.

Apart from global and local stiffness, the buckling factor as defined in Chapter 7 is affected by the magnitude of the loads applied. Designs will exhibit slightly higher buckling factors when a lower turbine class is considered, since the extreme loads are lower. The results presented in Appendix C are all made using class IC, but the same problems occurred for the lower classes as well and have therefore not been included.

The thicker-walled towers do not have this buckling problem, but make much less use of the higher strength of the Kerto-LVL. Stress levels are lower than for the thinner-walled towers, which might be beneficial in terms of fatigue strength, but also is considered a less efficient use of the high strength of the material. However, the tower width can become smaller than that of a comparable CLT tower, which is considered beneficial from non-structural points of view as well. This will be discussed later.

Kerto-S

The towers in Kerto-Q with smaller thicknesses make more use of the relatively high strength of the material in longitudinal direction, but also experience higher shear stresses. These shear stresses, however, remained well under the shear strength for the cross-bonded Kerto-Q. Because the (rolling) shear stresses τ_{xy} were very small, especially for the bulkier designs, the use of Kerto-S was also deemed feasible, despite the facts that its rolling shear strength is not provided by the manufacturer and is considered fairly low. To keep τ_{xy} within reasonable limits, these designs in Kerto-S could not contain very thin walls by default and suitable designs within standard production limits were not found. The smallest thickness

Still, it can indeed be observed from the limited amount of models (P, Q and R) provided in Appendix C that wall thicknesses can become slightly smaller for Kerto-S, compared to Kerto-Q. This is also shown graphically in Figure 8-8. Thin-walled designs were found with wall thicknesses from 120 mm to 190 mm, while τ_{xy} did not exceed 0.10 N/mm^2. Those values are considered well acceptable for the undeclared rolling shear strength.

In terms of thicker-walled towers, with thicknesses of up to 450 mm, designs in Kerto-S could also become substantially less wide than comparable designs in CLT and more slender than designs in Kerto-Q. This will be discussed below.

Comparison with CLT

A comparison with CLT is best made according to Figures 8-8 through 8-10, where either the tower width or the wall thickness has been kept constant. Wall thicknesses can be reduced compare to CLT towers, but especially the comparisons in Figures 8-9 and 8-10 show the
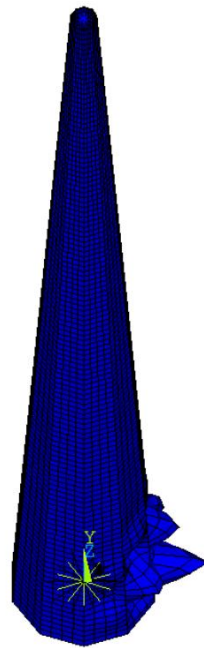
Figure 8-7: Example of the width and buckling of a relatively thin-walled Kerto design

potential in applying LVL. For the example towers shown, gains of 2 m in terms of base width could be achieved.

This results in lower wind loading on the tower and, although not a structural consideration, improved aesthetics. The structural improvement thus is only small, but in the end, the consideration in practice will be one based on economics.

8-3-3 Feasibility

It is possible to design towers in softwood LVL that meet frequency requirements, as well as strength and buckling requirements for the timber material. Especially the thicker-walled designs showed to have sufficient strength in all directions. The results and observations above are based on a small amount of data, but are considered to represent the various possibilities well. More calculations than displayed in Appendix C have been made and observations made support the conclusions drawn below.

Especially the results from designs P and R suggest that the high strength of the Kerto-S is exploited more in turbine towers than that of Kerto-Q. This is caused by the higher stiffness of Kerto-S, which allows for thinner walls to reach a suitable frequency, thus resulting in higher overall stresses. There are, however, many issues to be addressed with both the thin-walled and thicker ('bulky') designs.

One of the main issues with these LVL towers will be the connections. The number of connectors in the original CLT TimberTower was already quite high, where one connector was applied every 40 mm, while the wall thickness of the tower was 300 mm. The walls

with smaller thicknesses of the LVL designs made here, even those of the bulkier ones, would suggest that the number of connectors would have to increase to reach sufficient strength. This difficulty is increased even more by the overall higher stresses occurring in the thinner LVL designs, which will have to be carried by the connections as well. Towers with a thickness near the current standard production limits are therefore not considered feasible with the connections considered in this research. This does not mean that these kinds of designs will be put off completely, since the considered connection is most likely not the only suitable connection for this kind of structure.

The wall thicknesses used in designs are higher than the current standard maximum thickness available on the market. Higher thicknesses are applied to prevent local buckling in the tower and, to a lesser extent, improve the chance of finding a suitable connection. Further increasing the order of the polygon (i.e. applying a dodecagon) is expected to improve buckling behaviour, as it did from changing the shape from an octagon to a decagon. This might allow for designs closer to the current production limits. Moreover, there are other ways of improving local buckling behaviour apart from increasing the overall thickness of the cross sections. As stated at the beginning of this chapter, these are beyond the scope of the calculations made here. Aside from potential production limitations, it can not be said with certainty that the same material strengths may be used for the larger element sizes of the suggested bulky designs, because of possible volume effects present.

Where economics are concerned, designs in softwood CLT will most likely prove to be cheaper, since the base material is cheaper. They might also be more suited for this application than those in softwood LVL, because the benefits (higher strength) of the latter are not fully exploited due to frequency requirements.

An investigation into towers with a frequency lower than 1P ('soft' towers) showed that it is not possible to design a tower in softwood LVL with such a low frequency that still has sufficient strength. Because no suitable designs were found, results have not been included in Appendix C.

More potential is expected in the use of LVL as a single layer in CLT, which will be discussed in the next chapter.

8-4 Designs in beechwood LVL

8-4-1 Expectations

The higher strength and stiffness of BauBuche beechwood LVL should decrease the amount of material compared to the Kerto softwood LVL, because less material can be used to reach the same global stiffness while maintaining sufficient strength.

8-4-2 Results

The same tendencies can be observed for Baubuche as could for softwood LVL. Relatively small wall thicknesses are possible, which require larger tower diameters to satisfy frequency demands. Not all thinner walled designed are sufficient because of potential buckling issues,
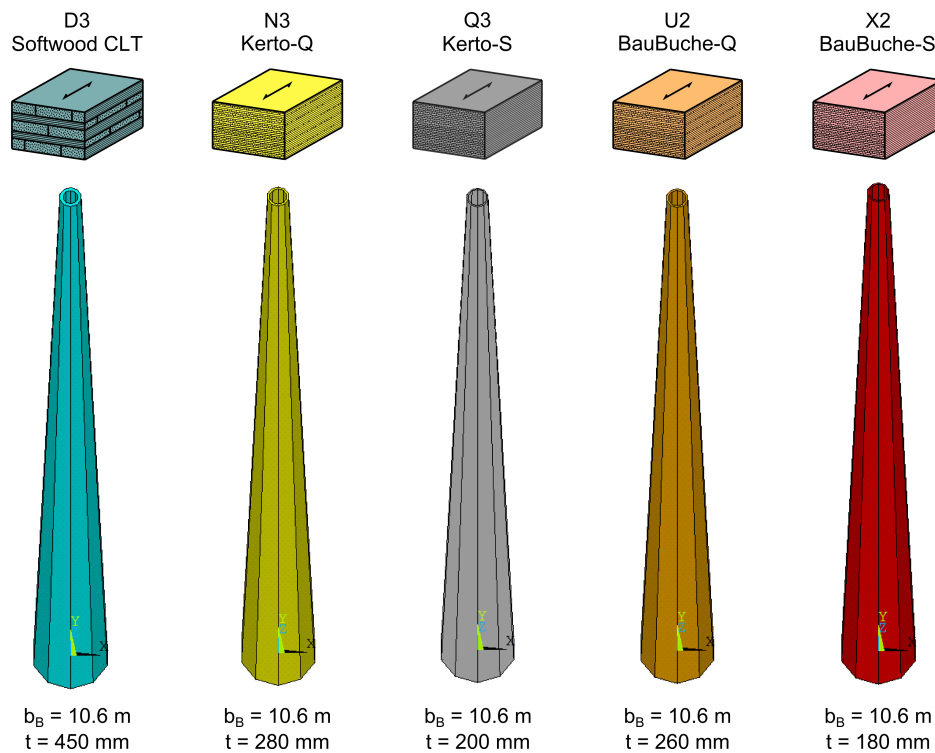
Figure 8-8: A comparison between towers with an equal tower width in different materials, for the 3 MW turbine at 125 m
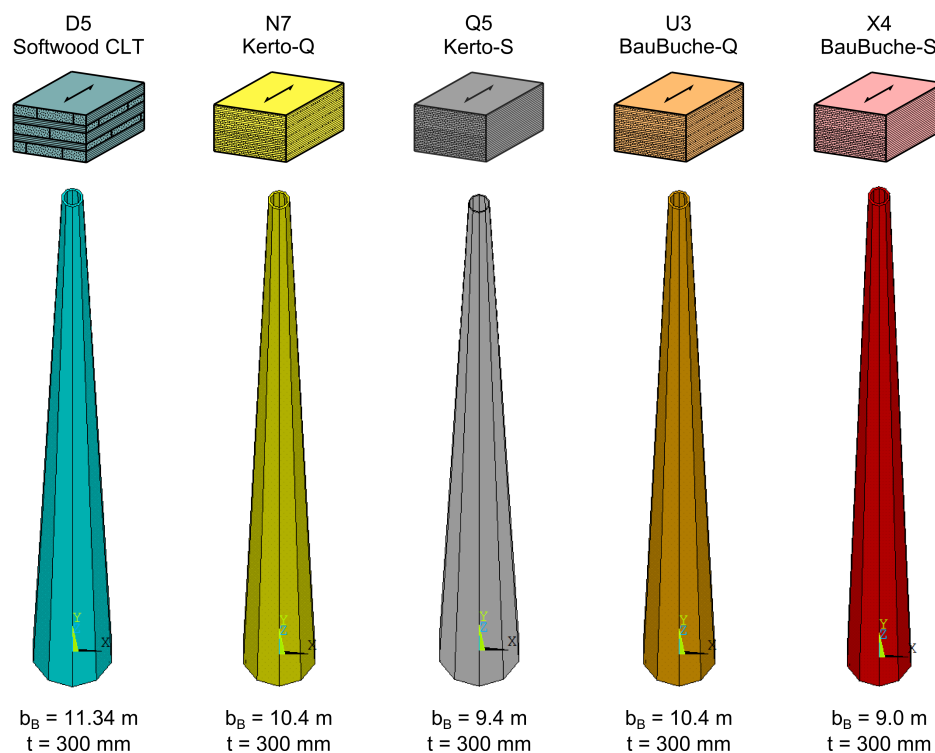
Figure 8-9: A comparison between towers with a wall thickness of 300 mm in different materials, for the 3 MW turbine at 125 m

| D3 | N8 | Q6 | U4 | X5 |
| Softwood CLT | Kerto-Q | Kerto-S | BauBuche-Q | BauBuche-S |

| b_B = 10.6 m | b_B = 9.4 m | b_B = 8.6 m | b_B = 9.4 m | b_B = 8.4 m |
| t = 450 mm | t = 450 mm | t = 450 mm | t = 450 mm | t = 450 mm |
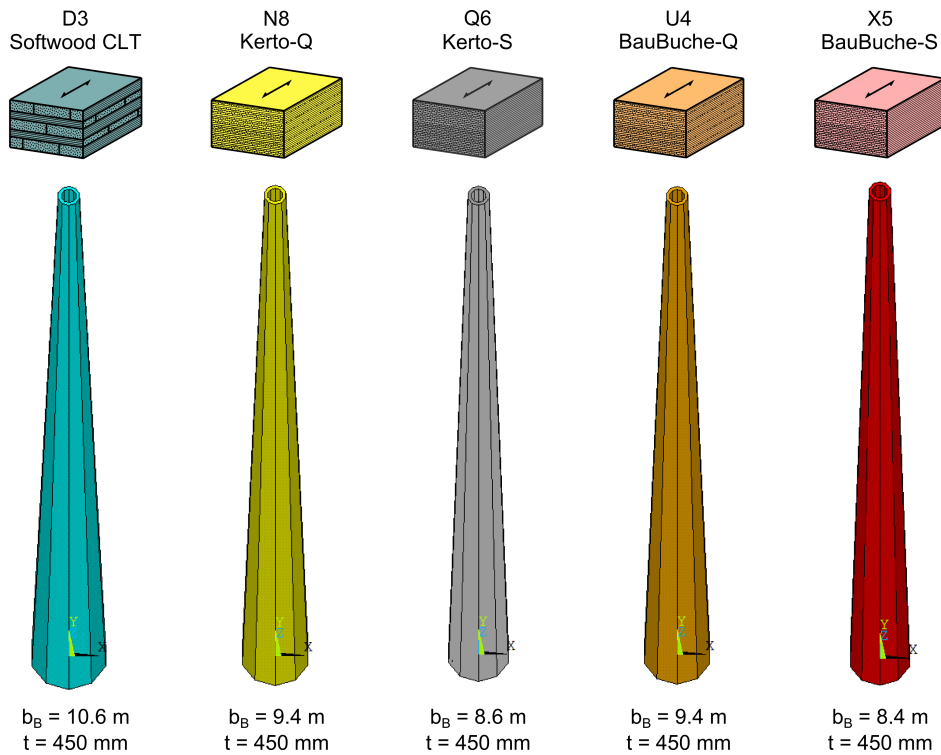
Figure 8-10: A comparison between towers with a wall thickness of 450 mm in different materials, for the 3 MW turbine at 125 m

which could be solved by increasing the wall thickness or using other methods beyond the scope of this research. Shear strength of the cross-bonded BauBuche Q is easily sufficient for all designs considered, but rolling shear stresses τ_{xy} for BauBuche S should be watched more closely as was the case with softwood LVL.

Comparing the hardwood LVL designs with their softwood counterparts in Figures 8-8 through 8-10, it can be observed that the towers can become even more slender.

8-4-3 Feasibility

Designs in BauBuche-S are able to make better use of the high base strength and stiffness of the material, allowing for fairly thin-walled towers, as low as 120 mm for the 3 MW tower at 100 m without buckling. Again, connections will be a sensitive issue for these towers and are expected to be the bottleneck that make all-LVL designs uneconomic, because they will require thicker sections to be able to reach sufficient connection strength. From a structural point of view, however, both hardwood and softwood LVL designs are feasible and allow for smaller wall thickness or more narrow towers than those in softwood LVL or CLT.

8-5 General remarks and discussion

The largest contribution to all stresses came from $F_{y,T}$ working at the top of the tower. The highest normal stresses occurred not at the base, but somewhere in the top half of the tower,

for most designs. Shear stresses were highest at the top of the tower, where the cross sectional area is smallest. A lot of emphasis was placed on whether or not the material could resist the rolling shear stress τ_{xy}, though only the peak value was considered. The overall values and the average stresses are much lower and are well within strength limits of the considered material for all designs. However, the material should be able to carry this peak stress nonetheless.

It should be noted that only a few load cases have been used that might not represent all governing cases for the tower, although this is expected to be the case. Even more important, fatigue has not been considered, which is normally one of the main concerns for wind turbine towers.

Local buckling was considered as the governing issue for some of the towers, though not all methods of preventing this have been investigated. Applying ribs, sandwich panels, all other options to increase (local) buckling strength are beyond the scope of this research and calculation model. They might influence the frequency through the increased stiffness, which should be investigated when applied.

The influence of connection and foundations stiffnesses on tower frequency has only been investigated for CLT, not for the other materials. It is however expected to have the same effect and be negligible in this stage of the design. The overall feasibility of connections for the thinner cross sections used for LVL is not known and will most likely be one of the main reasons while these kinds of towers will prove to be difficult to design, along with the negative visibility of large base diameters. Connections in the CLT designs are not expected to be a problem.

When designing towers in one single material, CLT seems the better choice, since it is a relatively cheap material with a fairly low strength-stiffness ratio, compared to the other materials investigated. This ratio leads to thicker-walled towers, which will have little problems reaching a sufficient natural frequency, (buckling) strength and connections strength. Designs in LVL are, however, structurally feasible as well.

However, from a structural point of view the use of LVL is considered superior. It will result in more narrow towers, reducing wind loads directly on the tower. Its higher strength and stiffness result in lower stress levels under both operational and extreme wind speeds, increasing fatigue behaviour and reducing the chances of failure under extreme loading.

8-6 Notes on the computation models

A few remarks are made on the agreement of results and suitability of the calculation models. Values for normal stresses coincide very well, as can be seen in the last rows of the tables in Appendix C.

The Matlab model distinguishes between favourable and unfavourable loads, where the ANSYS model does not. A slight difference in tension stresses is therefore to be expected, while the compression stresses found in both model should agree with each other. Neglectable differences in stresses also occur because of the difference in significant figures between the two models.

It can be observed that natural frequencies were overestimated around 10 % by the Matlab model, which uses the Rayleigh-Ritz estimation method.

The ANSYS model provides an incorrect buckling factor that is lower than the actual buckling factor. It does, however, provide a good indication of what the actual buckling factor will be. If it is too low (<5) the actual factor will be too low, and if it is sufficient (>5), the actual buckling factor will be sufficient as well. For the explanation of this buckling factor, reference is made to section H-2-2.

The total calculation time started at around one minutes per run, but became slightly higher for subsequent runs, as the calculations require a lot of computational memory. With sufficiently powerful hardware this is not a problem, but the element size might be reduced when using the models on less powerful hardware.

Hybrid materials and other considerations

This chapter deals with potential ways of improving the existing softwood CLT design by combining CLT with one of the materials investigated in the previous chapter. There it was found that towers made solely of hardwood CLT or LVL do not exploit the higher strengths and stiffnesses of those materials. More potential may lie in combining these materials with CLT to add strength and/or stiffness only at those places where it is needed.

The structural potential and feasibility will be discussed on the basis of several examples, but first the technological feasibility is discussed once more, as it already has been in short in Chapter 2. A few examples are used to show possible advantages of the hybrid cross sections discussed after that, instead of conducting many calculations for many different scenario's. The governing load case (2a) under the highest turbine class (IC) is used to judge the designs. Other considerations regarding the applied timber species, such as natural durability will be discussed in short at the end of this chapter.

9-1 Technical feasibility of hybrid cross sections

As was explained in section 2-5-3, replacement of one or more layers of a softwood CLT panel by either LVL or hardwood have both been successfully accomplished. The conditions under which are described below, together with a discussion of the potential for this research.

9-1-1 Hardwood CLT

Researchers have successfully replaced the outer layers of softwood CLT elements with a layer of hardwood and are conducting tests to determine the base material strengths [33]. Combinations of eucalyptus and pine, ash and spruce, and birch and poplar have been constructed so far. Material properties are not yet published, but it shows that it is possible to combine different species into one CLT panel.

Furthermore, the combination of beech and spruce has been successfully implemented in glued laminated timber. The Studiengemeinschaft Holzleimbau e.V. has received a technical approval for this combination [63], although it can only be used in Service Class 1 and does not cover chemically treated wood. No national or European standard exists for these combinations as of yet, so application will have to be based on individual approvals [64]. Nevertheless, both examples justify the use of a hardwood-softwood hybrid in this research.

No complications are expected from combining layers of hardwood and softwood, since the turbine design contains installations that keep the moisture level in the tower as constant as possible ($\approx 12\%$) and the tower is protected from outside moisture by a PVC lining. Shrinkage and swelling caused by moisture variations are effectively cancelled out by this, though problems might occur during production and transportation, both beyond the scope of this research.

9-1-2   Softwood LVL

Metsä Wood has a product line where their standard softwood Kerto-LVL is included as the center layer in regular softwood CLT panels [32]. No complications of increasing the amount of LVL layers is expected. Both CLT and LVL use the same base material, which avoids many incompatibility issues that otherwise might occur.

9-1-3   Hardwood LVL

As stated before, hybrid glulam elements made from beech and spruce are being investigated and show promise. For the same reason as mentioned for hardwood CLT above, complications from the application of hardwood LVL layers in a CLT panel are not expected.

The beechwood LVL used in the previous chapter might have to be joined by a cross-layer of beechwood CLT, because of potential problems caused by the differences in shrinkage and swelling with the softwood during production. But since suitable adhesives exist to construct beechwood CLT [33], no problems are expected in joining beechwood LVL with another layer of beechwood. Nevertheless, in the calculations below the material properties softwood CLT are used for the cross-layer, which at the very least will result in conservative strength values.

9-1-4   Potential

The highest potential is considered to be present in combining CLT with the BauBuche-S material, which has a substantially higher strength and stiffness than the other forms of LVL considered and resulted in a combination of relatively slender towers with low wall thicknesses in Chapter 8. The high stiffness should help reduce either wall thickness or overall cross sectional width compared to all-CLT designs.

9-2   Hardwood and softwood CLT hybrids

It is expected that, aside from having higher strength parallel to the grain, hardwood CLT layers will have a higher shear strength than the softwood kind as well, even though this has
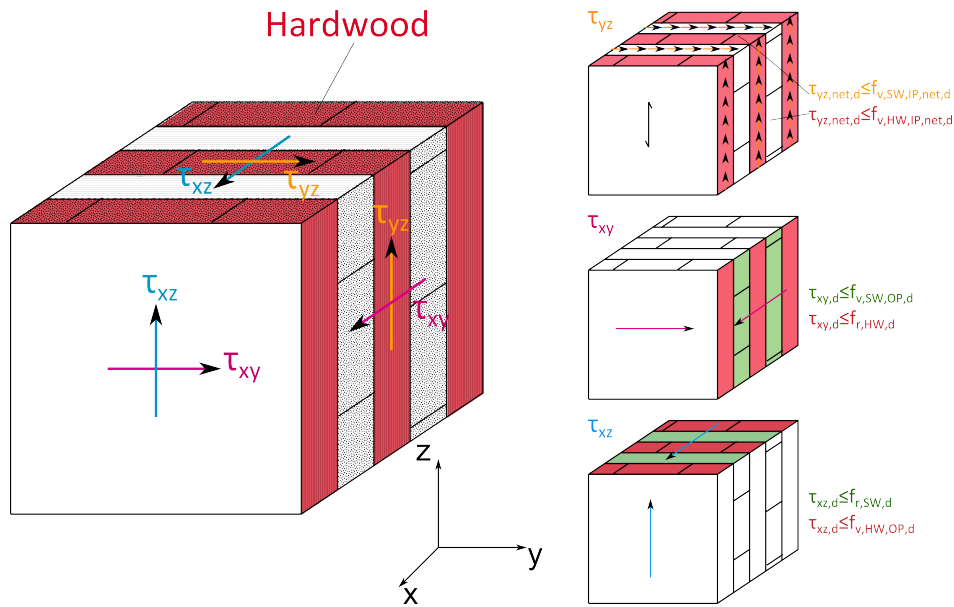
Figure 9-1: Shear mechanism in a hardwood-softwood CLT hybrid when the longitudinal layers are replaced

not been confirmed by research publications yet. This leads to two options regarding the fabrication of a hybrid panel of both materials. Firstly, one could replace the longitudinal layers by hardwood CLT, which would give the tower a higher longitudinal strength compared to a softwood CLT cross section. Secondly, one could replace the cross-layers with hardwood, making use of this potential higher shear strength. Because there is no conformation of this higher shear strength of hardwood CLT as of yet, no calculation examples are given, but the theoretical benefits are discussed. First, the stress calculations for both options are discussed.

9-2-1 Replacing longitudinal layers

Assuming all longitudinal layers are replaced by hardwood does not change the formulas for the unity checks for normal stresses compared those defined in Equation 7-28, other than that the strength values of the hardwood should be used. Adjusted shear checks from those in Equation 7-28 are provided for when sufficient data is collected that confirms a higher shear strength for hardwood CLT layers. A distinction is made between the strengths of the softwood cross-layers ($f_{i,SW,j,d}$) and the hardwood longitudinal layers ($f_{i,HW,j,d}$), as is also shown in Figure 9-1.

$$\frac{|\tau_{yz,max,d}|}{\min\left[(1-k_{net})\,f_{v,SW,IP,d};\ k_{net}f_{v,HW,IP,d}\right]} \leq 1 \tag{9-1a}$$

$$\frac{|\tau_{xz}|}{\min\left[f_{r,SW,d};\ f_{v,HW,OP,d}\right]} \leq 1 \tag{9-1b}$$

$$\frac{|\tau_{xy}|}{\min\left[f_{r,HW,d};\ f_{v,SW,OP,d}\right]} \leq 1 \tag{9-1c}$$
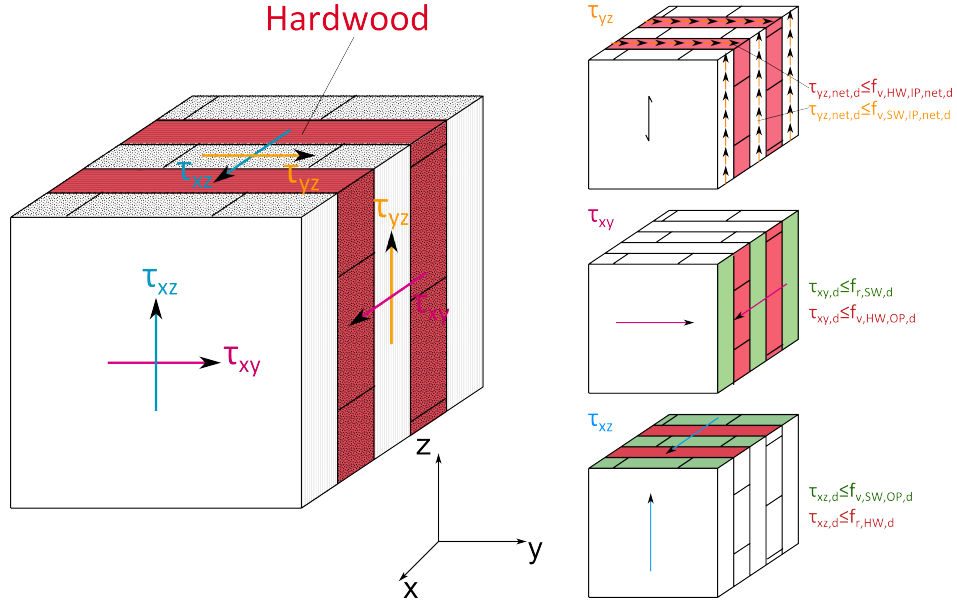
Figure 9-2: Shear mechanism in a hardwood-softwood CLT hybrid when the cross-layers are replaced

9-2-2 Replacing cross-layers

When replacing the cross-layers with hardwood, the unity checks for tensile and compression stresses do not change from those in Equation 7-28 either, where the softwood strengths should be applied. The shear checks are the opposite of those mentioned in 9-1, and also shown in Figure 9-2.

$$\frac{|\tau_{yz,max,d}|}{\min\left[(1-k_{net})\,f_{v,HW,IP,d};\;k_{net}f_{v,SW,IP,d}\right]} \leq 1 \tag{9-2a}$$

$$\frac{|\tau_{xz}|}{\min\left[f_{r,HW,d};\;f_{v,SW,OP,d}\right]} \leq 1 \tag{9-2b}$$

$$\frac{|\tau_{xy}|}{\min\left[f_{r,SW,d};\;f_{v,HW,OP,d}\right]} \leq 1 \tag{9-2c}$$

9-2-3 Potential

Based on the results of the all-softwood CLT designs in Chapter 8, only τ_{yz} - the in-plane shear - may prove to be a limiting parameter, when regarding the shear stresses. The peak values in the structure sometimes approached or exceeded the shear strength $(1-k_{net})f_{v,CLT,IP,d}$. This was governing over $k_{net}f_{v,CLT,IP,d}$ because k_{net} was always larger than 0.5. Out of plane shear stresses were less of a problem. τ_{xy} only became a potential issue for very thin cross sections in LVL. CLT does not possess sufficiently high stiffness to allow for designs within this thickness range. τ_{xz} did not pose any problems for any of the designs, regardless of the thickness.

Potential of replacing the longitudinal layers

Not much is expected to be gained from the first option of replacing the longitudinal layers by hardwood. Both the hardwood and softwood have Young's moduli of the same magnitude and the natural frequency turned out to be governing for the CLT designs. Replacing the longitudinal layers will provide the cross section with higher strength, but not with higher stiffness. Hence the same wall thickness is required to reach suitable frequencies, so no benefit in material reduction is expected. This point was already proven by the all-hardwood CLT designs in the previous chapter.

For a hybrid cross section to be a viable option, there should therefore be some gain in the shear strength of the material, so that the cross-layer thickness could be reduced. Looking at equation 9-1, one can observe that the shear strength properties of the softwood still dominate, since $(1 - k_{net}) < k_{net}$ in Equation 9-1a and $f_{r,SW,d} < f_{v,HW,OP,d}$ in Equation 9-1b. The denominator in the formula for τ_{xz} will become larger if $f_{r,HW,d}$ increases, but it was already determined that stresses in this direction do not pose a problem.

Replacing the longitudinal layers in softwood CLT by hardwood is therefore considered not to improve the structural performance of the tower.

Potential of replacing the cross-layers

There is a slight potential in the second option when the shear strength of the hardwood is confirmed to be higher than that of the softwood. Looking at equation 9-2, the governing in-plane shear strength increases slightly when the cross-layers are replaced by hardwood. One could use this to slightly reduce the total width of the cross-layers, while maintaining the same overall shear strength. Another option is to apply the same thickness as one would for softwood, but use the higher shear strength to make wider designs. Since the issue of increased visibility emerges for those designs, this is not considered beneficial.

Although the hardwood has a higher density, the effects of the added mass will have little effect on the natural frequency, as was found Chapter 5. For example, the difference in frequency between a 320 mm thick CLT section with $k_{net} = 0.75$ and one of 300 mm with $k_{net} = 0.8$ is only 0.002 Hz (same amount of material in longitudinal direction, less in the cross layers). The cross-layer width is small and since it is able to be reduced compared to softwood while maintaining equal shear strength, the total weight will not change substantially anyway.

Overall

The only structural advantage of these kind of hybrids would be a slightly higher shear strength when the hardwood considered turns out to have a higher base shear strength than the softwood CLT. Even then, the slight reduction in cross-layer thickness is not considered to compensate the higher cost that both the base material and production entail. It is therefore concluded that the use of the hardwood species considered within this thesis will be of no significant improvement to the structural performance of the original design.

The natural durability of the iroko hardwood considered has not been discussed here, but will be reviewed at the end of the chapter.

9-3   LVL and CLT hybrids

9-3-1   Expectations

As stated in Chapter 2, examples can be found of the combination of CLT and LVL [32], where the inner layer of the CLT is replaced by a layer of softwood LVL. Using parellel-bonded LVL as longitudinal layers of a CLT element will improve the designs made in the previous chapter. Designs will have higher strength and stiffness than the all-CLT designs, possibly resulting in thinner cross sections, while it will also solve the issues found in the previous chapter for all-LVL designs. Those latter issues are summarized here once more.

To reach a suitable frequency and keep the wall thickness within current standard production limitations, pure LVL towers had to become very wide at the bottom. Aside from the negative visual impact these towers would have, (local) buckling became an issue. This issue could be solved by adding material and thus increasing the wall thickness, as well as other methods such as local stiffening (e.g. stiffening ribs, rings) which are beyond the scope of this research. The thicker sections tend not to exploit the higher strength and stiffness inherent to the LVL material and are not considered to be the optimal application of this material, aside from possible problems regarding production and costs of such thick elements.

By joining longitudinal layers of LVL with cross-layers of CLT in-between, current production limitations for LVL can be maintained. This combination of multiple layers will produce thicker cross sections, less prone to buckling, but slimmer than those used in all-CLT designs. It allows for the high strength and stiffness of the LVL to be used more efficiently, while potentially reducing cross sectional width or thickness compared to CLT designs, as will be shown by example later.

The cross sections will consists of longitudinal layers of LVL, up to 80 mm thick, joined by (a) cross layer(s) of CLT, with a thickness up to 50 mm. Both values mentioned are the current production limitations for the respective materials, although one could easily join two layers of CLT to increase the width of 'one' cross-layer. First, the stress calculations in such an element are made clear.

9-3-2   Stress calculations

The maximum tensile and compression stresses in the material have to be lower than the ultimate strength of the LVL in longitudinal direction. The CLT cross layer does not contribute to the strength in this direction. This leads to:

$$\frac{\sigma_{t,net,max,d}}{f_{t,0,LVL,net,d}} \tag{9-3a}$$

$$\frac{\sigma_{c,net,max,d}}{f_{c,0,LVL,net,d}} \tag{9-3b}$$

Or, put in another form, consistent with Chapter 7:

$$\frac{1}{k_{net}} \frac{\sigma_{t,max,d}}{f_{t,0,LVL,net,d}}$$
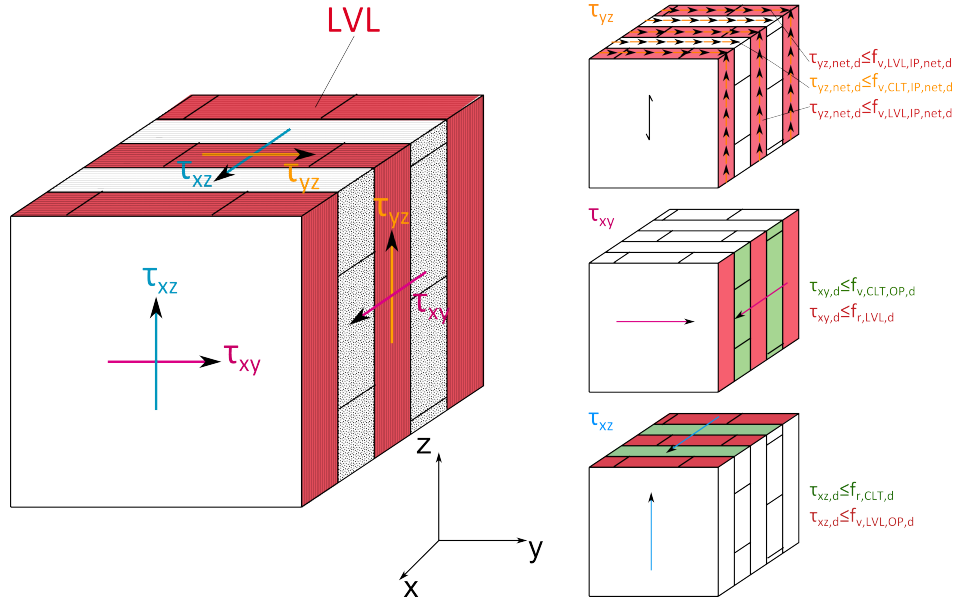
Figure 9-3: Shear mechanism in an LVL-CLT hybrid when the longitudinal layers are replaced

$$\frac{1}{k_{net}}\frac{\sigma_{c,max,d}}{f_{c,0,LVL,net,d}}$$

By making use of k_{net}, the same calculation model can be used as in the previous chapter. Design shear strengths and average density of the material have to be (re)calculated separately before the results from the FEM part of the model can be assessed.

Again, as with previous calculations, the maximum shear stresses are assumed present along the entire cross section, for all directions. Reference is made to Figure 9-3, where for the top face the in-plane shear strength of the hybrid material could be taken as the weighted average of both materials:

$$\frac{|\tau_{yz,max,d|}}{k_{net}f_{v,LVL,IP,d} + (1 - k_{net})f_{v,CLT,IP,d}} \leq 1$$

For the side face, however, the in-plane shear strength of the CLT is not taken into account, as is common for CLT [56]. In this way the governing unity check for τ_{yz} becomes:

$$\frac{|\tau_{yz,max,d|}}{k_{net}f_{v,LVL,IP,d}} \leq 1 \tag{9-3c}$$

For the other two shear stresses, the weakest layer is considered governing, as it was in Chapter 7, and the unity checks to be performed are:

$$\frac{|\tau_{xz}|}{\min\left[f_{r,CLT,d};\ f_{v,LVL,OP,d}\right]} \leq 1 \tag{9-3d}$$

$$\frac{|\tau_{xy}|}{\min\left[f_{r,LVL,d};\ f_{v,CLT,OP,d}\right]} \leq 1 \tag{9-3e}$$

9-3-3   Examples and comparison

To make the possible gains clear, a comparison is made between three different types of cross sections:

1. A pure softwood CLT cross section;

2. A cross section made of Kerto LVL and softwood CLT, where all longitudinal layers are made of Kerto-S;

3. A cross section made of BauBuche LVL and softwood CLT, where all longitudinal layers are made of BauBuche-S.

The comparisons have been shown in Figures 9-4 through 9-7, where the last three figures are expansions of those in the previous chapter.

Equal tower width

Keeping the tower width similar means that the wall thickness could decrease for cross section types 2 and 3 (Figures 9-4 and 9-5) compared to CLT, while shear and buckling strength remained sufficient. The high strength of the LVL material is not used to its full potential here though and the relatively large diameter at the base is still present. The same amount of LVL is used in the hybrid designs in Figure 9-5 as in the comparable all-LVL designs in the same figure, but the hybrid cross section walls are thicker due to the CLT cross layers. Peak normal stresses remained the same for both the hybrid and all-LVL towers, while shear stresses were slightly lower in the hybrid tower.

As was stated in the previous chapter, connections might prove to be a bottleneck for thinner-walled designs, especially when high stresses in the material are present. With this in mind, the thicker walled hybrid designs may reduce potential problems in this area by allowing wider or more connectors, without adding more (expensive) LVL.

Stresses in the hybrid designs are slightly higher than those in the all-LVL towers.

Equal wall thickness

Keeping the wall thickness the same, as is shown in Figures 9-6 and 9-7, allows for a reduction in tower width, while maintaining sufficient strength and meeting frequency demands. The effects are less severe than for a pure LVL-design, as can be seen in the figures.

High stress levels

A final comparison was made to see what would happen if one tries to make use of the higher strength present in the LVL. This is done in models HC1 and HC2, which are not shown graphically but can be found in Appendix C. This required towers to become wider and thinner than the comparable CLT design, like was observed in the previous chapter. These
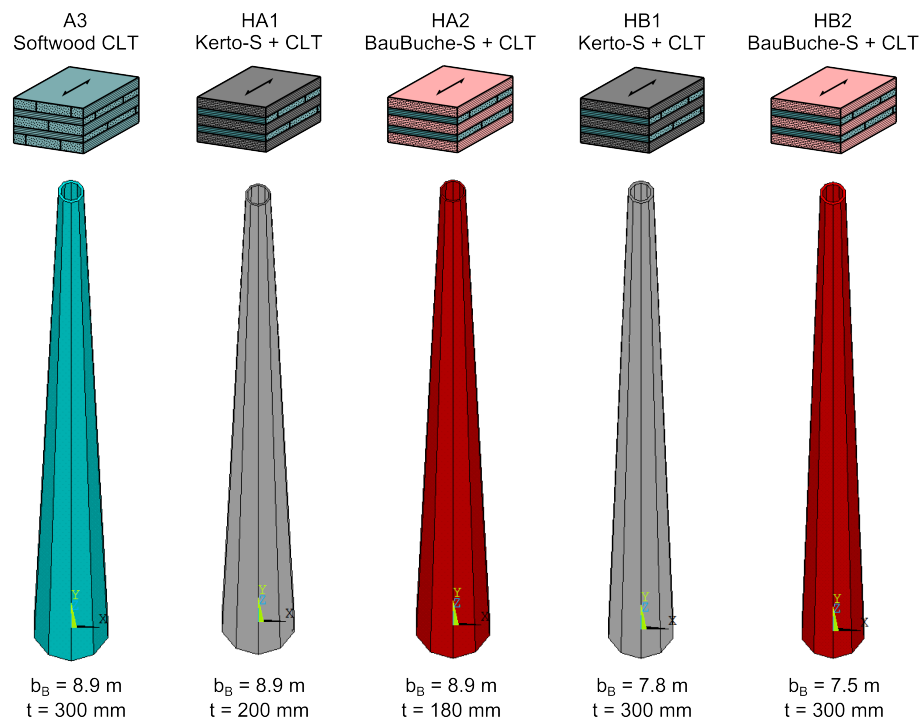
Figure 9-4: A comparison between CLT and hybrid towers with either an equal tower width or equal wall thickness, for the 3 MW turbine at 100 m

resulting wide, thin-walled towers are not considered favourable for reasons mentioned several times before.

For the hybrid hardwood LVL cross section, no design could be found that satisfied both buckling and frequency demands, while maintaining this sought-after high stress level.

9-3-4   Potential

The potential gains in constructing hybrid panels with LVL over all-CLT towers lies in either

- the reduction of the base width of the tower, while maintaining the same thickness that was found for all-CLT designs (Figures 9-6 and 9-7);

- or in reducing the wall thickness for a similar tower width (Figure 9-5), similar to the advantages of using all-LVL cross sections over all-CLT ones.

The higher strength of LVL will not be put to full use in the first case, but its higher stiffness allows for designs with smaller base diameters than equivalent all-CLT towers. This is considered beneficial, since turbine towers made of timber are by default wider than equally strong steel ones, catching more direct wind and having a higher (negative) visibility. This advantage was even stronger present in all-LVL designs, making those designs more favourable over the hybrid ones from that point of view. Both designs HD2 and HF2 contain around the same amount of LVL as their all-LVL counterparts X4 and X5, while normal stresses remained the same. Although shear stresses decreased for the hybrid tower, they were not
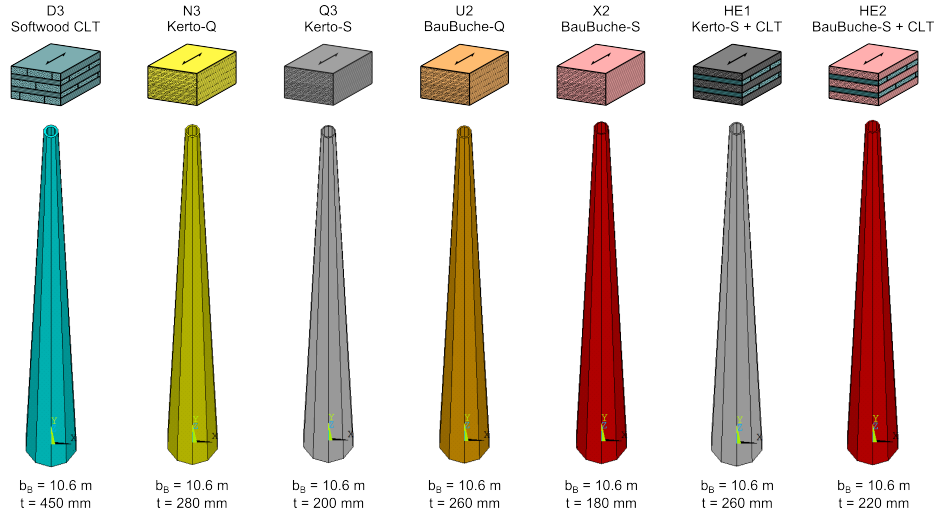
Figure 9-5: A comparison between towers with an equal tower width in different materials, for the 3 MW turbine at 125 m
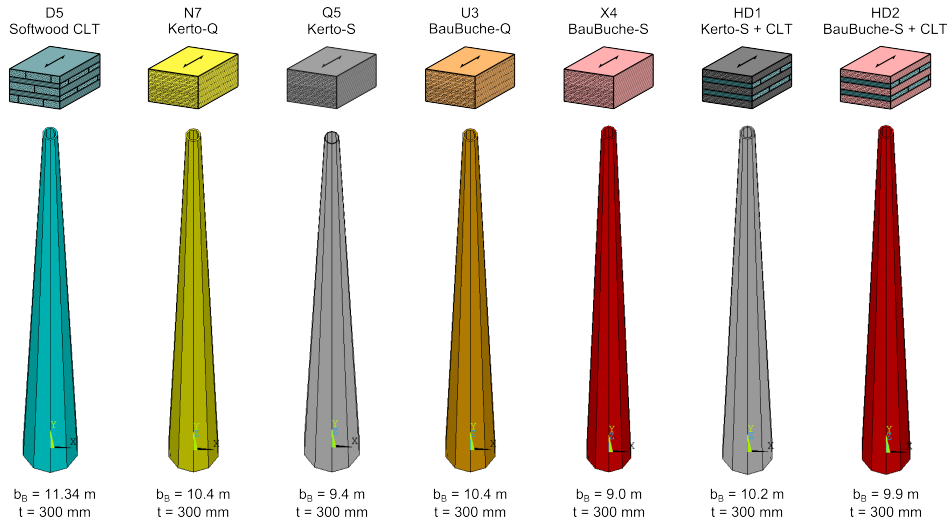
Figure 9-6: A comparison between towers with a wall thickness of 300 mm in different materials, for the 3 MW turbine at 125 m
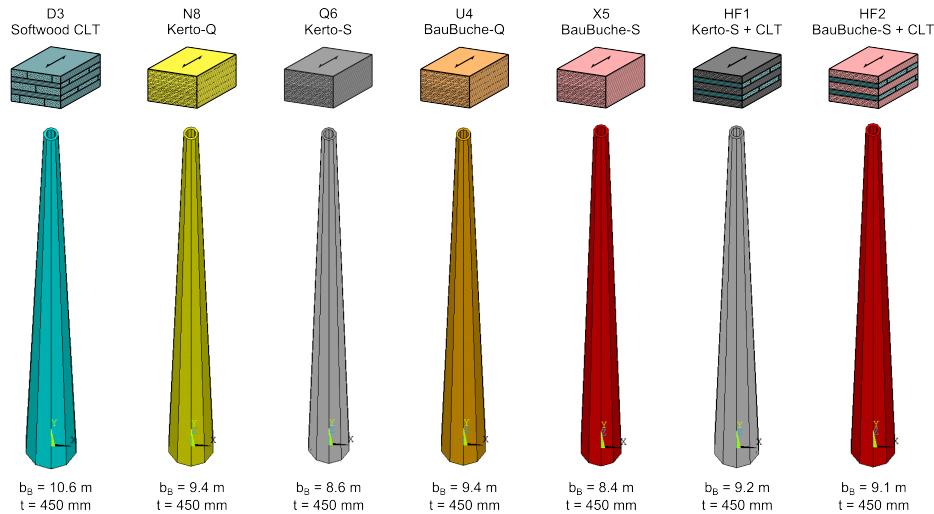
Figure 9-7: A comparison between towers with a wall thickness of 450 mm in different materials, for the 3 MW turbine at 125 m

found to be governing. From point of material use the hybrids considered here are therefore not favourable over all-LVL designs either.

The second case, where the wall thickness was reduced for a similar tower width, is not considered to be a significant improvement over the all-CLT designs. Stresses increase, while the amount of material in the cross section decreases, increasing the required capacity for a single connector. However, when comparing the hybrids with all-LVL designs, the peak stresses and the amount of LVL used remain the same, while the thicker walls might allow for a larger capacity of individual connectors in hybrid designs than in all-LVL designs.

This does not mean that no suitable connections for the all-LVL designs can be designed. However, when this turns out to be the case, the application of hybrid cross sections may prove to be a cheaper solution than simply increasing the amount of LVL.

9-4   Durability

There might be other advantages in the use of different timber products than those strength- and stiffness-related. Possible benefits of the natural durability of materials are discussed here. To do so, a short explanation of the different hazard and durability classes defined by the Eurocodes is given first.

9-4-1   Hazard classes

NEN-EN 335-1 defines five hazard classes to define the risk of biological attack by fungi and insects. One important aspect associated with this risk is the exposure to moisture. Sagot [65] summarizes the class definitions well:

> "*Hazard class 1*, situation in which timber of wood-based product is under cover, fully protected from the weather and not exposed to wetting;

Hazard class 2, situation in which timber or wood-based product is under cover and fully protected from the weather but where high environmental humidity can lead to occasional but not persistent wetting;

Hazard class 3, situation in which timber or wood-based product is not covered and not in contact with the ground. It is either continually exposed to the weather or is protected from the weather but subject to frequent wetting;

Hazard class 4, situation in which timber or wood-based product is in contact with the ground or fresh water and thus is permanently exposed to wetting;

Hazard class 5, situation in which timber or wood-based product is permanently exposed to salt water."

The original TimberTower uses standard PVC roof lining to cover the outside face of the tower, thus protecting the timber from the elements. Together with the concrete base, which avoids contact between the timber and the ground, and installations that regulate the relative humidity within the tower, the tower can be placed in hazard class 1. When the installations malfunction, it might pass into hazard class 2. Removing the lining and applying the timber unprotected would place it in hazard class 3.

9-4-2   Durability classes

Five durability classes are defined to classify the natural durability of a species, ranging from very durable (class 1) to not durable (class 5). Summarizing table 3 from [66] explains which durability classes may be used in the various hazard classes:

- Hazard class 1: all durability classes are allowed unprotected;

- Hazard class 2: durability classes 1 to 3 are allowed unprotected, classes 4 and 5 may be applied unprotected under most conditions;

- Hazard class 3: classes 1 and 2 unprotected, 3 under most conditions, 4 and 5 depend on the situation;

- Hazard class 4: class 1 unprotected, 2 under most conditions, other classes need to be treated;

- Hazard class 5: Only durability class 1 is allowed.

The durability classes for various species can be found in [66]. Most softwood has a low natural durability and is only applicable in hazard class 1, but often in class 2 as well. It is not allowed to apply softwood CLT in service class 3 [33], which corresponds to hazard classes 3 to 5 [65]. European beechwood, although high in strength and stiffness, has a very low natural durability (class 5). Iroko, which was used to define the hardwood CLT class CL40h, has a much higher natural durability and is considered to lie somewhere between durability classes 1 and 2.

9-4-3   Potential and discussion

The various materials used throughout this research show that only the iroko hardwood CLT may be applied unprotected at the outer face of the tower. The other materials could be chemically treated to reach a sufficient durability as well.

The iroko timber will have sufficient resistance against biological attacks from fungi and insects to allow it exposed to the elements, but the moisture content in the timber will then still vary. In research such as [67, 68, 69], it was found that the moisture content in the wood has an influence on the Young's modulus, with potential decreases up to 20% for high moisture contents. Figure A-7 shows the influence of the Young's modulus on the tower frequency, for one specific model. Here it can be found that a 20% decrease in Young's modulus lowers the first natural frequency by 10%. Although this is only considered for one particular model, the effect is expected to be similar for all towers within this range of stiffness values.

Since the tower frequency is one of its most important characteristics - potentially causing failure of the entire turbine through resonance when insufficient - the frequency should be kept as predictable and constant as possible. Because the tower is not a single sealed system in this unprotected case, but is in contact with the environment, the use of installations to control the moisture content in the timber are much less effective and variations will still occur when the timber is left exposed, even with these installations.

Even though the designs made throughout this research have a predicted natural frequency as far away from both the 1P and 3P frequency as possible, and could thus handle a possible 10% change in natural frequency, these variations are still not desirable. The variations are relatively large compared to the narrow frequency domain available and a 10% drop gets the frequency close to 1P. For instance, a 5 MW turbine with a tower frequency of 0.265 (model G2) could potentially drop to 0.239, which is a lot closer to the limit of 0.222, but still sufficient. However, when looking at several uncertainties in the frequency behaviour of the tower, such as the natural spread of the timber Young's modulus, this could potentially pose a problem.

The small-scale application of timber wind turbine towers so far makes for a limited correlation between practice and theory at this point in time. When more information is available about the actual frequency behaviour of timber turbine towers and how this compares to the theoretical predictions, a more substantial conclusion on this subject could be drawn. It is recommended for now that the frequency behaviour of the towers is first studied, using unexposed timber, before considering options such as an exposed timber outer surface.

To avoid the aforementioned problems, it is considered not feasible to apply uncovered timber until more knowledge on the frequency behaviour of actual towers is available, even when the timber has sufficient natural durability. Together with the small structural benefits to be gained from the application of hardwood, this material is deemed not to weigh up against the higher economical costs. The application of the LVL material types showed more promise on a structural level, but these will need to be covered.

Another argument against the use of uncovered timber could come from aesthetics, although this will always remain a subjective matter and is in not related to the structural feasibility of this option. Visibility plays a part in the possible acceptance of turbines by people in their direct environment and the greyish colour that most towers are painted in has been chosen

to blend in with the sky and surroundings. It is expected that a timber tower that has the brownish colour associated with wood will have problems getting accepted, apart from the potential structural complications it poses.

CHAPTER 10

Conclusions and recommendations

This thesis was set out to determine if it would be feasible to apply timber wind turbine towers in the Netherlands, from a structural point of view. So far only one timber turbine tower has been built, with a 1.5 MW turbine on top of a Cross Laminated Timber (CLT) design, on an inland location in Germany. No information is available on whether this design is also suited for the more severe wind conditions in the Netherlands. Neither is there knowledge on the possibilities of applying timber products other than softwood CLT in these turbine towers. The research sought to fill in these blanks by dealing with the following items:

1. Investigate what the demands and requirements for turbine towers set by codes, physics and the Dutch wind conditions are;

2. Determining which global structural system best satisfies these demands;

3. Verify if these designs can be further improved by the use of other timber products or species.

Detailed conclusions and results related to each of these sub-goals can be found below, after which the limitations of the research are discussed and recommendations for future approaches are made.

10-1 Conclusions

10-1-1 Demands and requirements on wind turbine towers

The International Electrotechnical Committee (IEC) has written a special design code for wind turbines in which turbine classes and corresponding load parameters are defined based on the mean wind velocity and turbulence intensity. These have been used as an upper limit to classify various locations throughout the country as either corresponding with turbine class IC, IIA or IIIA in Chapter 3. Based on the limited information on government plans, it was observed that new turbines will be built in locations that correspond with all three mentioned classes.

Structural verification of turbine towers

The codes prescribe several aspects of the tower to be checked, as described in Chapter 2:

– Frequency considerations

  The natural frequency is one of the most important characteristics of the tower. It should be kept as far away from the rotor frequency and the blade-passing frequency to prevent dynamic load amplification through resonance.

– Strength considerations

  Apart from the obvious extreme loads that have to be resisted by the structure and its connections, fatigue strength of turbine towers is crucial as well, since wind turbines are subjected to uniquely high amount of load cycles during their lifetime. However, fatigue strength of timber turbine towers is considered not to be governing over ultimate strength for timber turbine towers by several sources. Because of the limited time available for this thesis and the reason mentioned here, fatigue verifications have been excluded from calculations.

– Deformation considerations

  The blades and tower both deflect under the loads and may not collide at any time. The detailed time-displacement behaviour of both components is needed to judge whether this occurs and could not be obtained from the results in this research. Limits for the maximum tower deflection were set nonetheless and deflection calculations were performed to be able to judge at least an indication of the magnitude.

Load cases

The IEC describes many different load cases relating to all situations that might occur during the lifetime of the turbine. Eight different wind models are to be used throughout these load cases and all wind models should be checked using multiple computer simulations for each case. This was not deemed feasible for a large number of towers or considered necessary for the global design calculations performed in this research. Instead, three load cases were constructed that were considered to represent the extreme loads well:

1 Loads associated with operational wind speeds, to be able to obtain the value of the largest deflection during operation;

2a Loads associated with extreme wind speeds with a 50-year return period, to assess the highest occurring normal stresses in the tower;

2b Loads associated with extreme wind speeds with a 1-year return period and an extreme yaw misalignment, which would possibly lead to higher shear stresses than load case 2a.

Load cases regarding fatigue have not been taken into account, due to reasons mentioned in the previous paragraph.

10-1-2   Most suitable structural system

After theoretical consideration of several structural systems such as trusses, hyperboloid spaceframes and the original closed hollow section of the TimberTower, it was concluded that the latter is the most suited system for wind turbine towers made of timber. The other two mentioned here contain a large number of connections between individual members that introduce a certain amount of slip in the structure, that in turn will introduce undesired uncertainty in the tower natural frequency.

Designing new timber connections was left out of the scope of this research, while the perforated steel plate connections used in the original tower were assumed to be applicable to all designs considered. Other connection types may be suited for application in timber turbine towers as well, but have not been published yet.

10-1-3   Study of frequency behaviour

Because of the importance of the natural frequency of the tower, a study into the influence of several turbine tower-related parameters on this frequency was carried out. Quick estimations of the tower natural frequency were made using the Rayleigh-Ritz method, which overestimated the tower frequency with an average of 10 % compared to Finite Element (FEM) calculations using ANSYS. A parameter study showed that the timber towers behaved like expected, where adding mass would decrease the frequency and adding stiffness by either increasing the Young's modulus or enlarging the geometry would increase the frequency.

Only the first natural frequency of the tower lay in the range where problems with rotor resonance may occur, for all designs considered. This limited the amount of eigenmodes that had to be investigated to only one, saving time. Other investigations showed that for the global design calculations in this research, the influence of both foundation stiffness and connection stiffness on the tower frequency could be ignored.

10-1-4   Results from calculations of the various design cases

Designs were made for different combinations of the aforementioned parameters. The following parameters have been varied:

- IEC turbine class: IC, IIA and IIIA;

- Turbine type: NREL 5 MW turbine and a scaled down 3 MW version;

- Hub heights: 100 and 125 m for the 3 MW turbine and 125 m for the 5 MW turbine;

- Materials:

  - Mono-material towers made of CLT or Laminated Veneer Lumber (LVL), both having a softwood and a hardwood option;

  - Hybrid towers, made of the combination of CLT and LVL, also considering both hardwood and softwood.

The three aforementioned load cases were used to determine the validity of each design. The third load case was quickly dismissed after it was found that it did not provide higher stress conditions than the second one.

Calculation methods

Loads on the tower consisted of wind loading directly on the tower and three loads at hub height: a horizontal thrust force, an overturning moment and a torsional moment. Operational loads were calculated using the Blade Element Momentum Method. Loads during standstill, under extreme wind speeds, were made using a quasi-static method that included a gust factor to allow for turbulence and dynamic amplification. Wind loads along the tower were calculated using the common methods for structures from the Eurocodes. These wind loads were significantly higher for the timber designs than for comparable steel towers, which are more streamlined and have a smaller overall width for the same strength.

A very strong correspondence between both a simplified calculation model in Matlab and a Finite Element (FEM) model using ANSYS was present. Resulting loads from both models were compared with the limited data on real life turbines and were found to be on the conservative side and thus accepted for use throughout this research.

The tower designs were judged based on their natural frequency, normal stresses, shear stresses and buckling strength. Deflections were kept under close watch, but without time-displacement data of both tower and blade, no hard conclusions could be drawn there. Still, the deflection behaviour of the towers was considered to be sufficient.

Calculation results

For some towers with a large width-to-thickness ratio, local buckling (creasing) at the compression side at the bottom caused the design to be deemed inadequate. Decagonal towers showed better buckling behaviour than octagonal towers. This trend is expected to be present in dodecagons and higher polygons even more. The largest part of the stresses throughout the tower was caused by the thrust force at hub height.

The potential of the different materials that have been investigated varied and are described below.

Cross Laminated Timber
For the all-CLT designs first investigated, the tower frequency turned out to be the parameter that governed the required geometry of the tower, not the material strength. Using the higher strength classes of the material was therefore not necessary to design suitable towers. No reduction in material use could be achieved by replacing the entire cross section with hardwood that had an even higher strength, but similar stiffness, either. The same was found to hold for hybrid panels made from both softwood and hardwood layers. Both types have practically the same base stiffness and resulted in the same amount of material used to reach an adequate frequency.

Using the natural durability of hardwood to be able to leave the outside of the tower bare and exposed to the elements is not considered feasible. The moisture content in

the timber will vary, which in turn will influence the stiffness of the material and result in uncertain and varying natural frequencies. Although the designs made in CLT could deal with relatively large fluctuations in natural frequency, the resulting values would lie close to the limit value of 1P. This was, considering the uncertainty in the Young's modulus of the organic material, considered to be undesirable.

Wall thicknesses for all CLT designs were equal to or higher than that of the original TimberTower, so no problems in designing suitable connections are expected.

Laminated Veneer Lumber

Two directions in the design of LVL towers were chosen.

Firstly, relatively thin-walled towers were designed, resulting in large base widths, high stress levels and often insufficient resistance against due to local buckling. This could partly be solved by increasing the local buckling strength in other ways than simply adding material, such as stiffening ribs and rings, but these are beyond the scope of this research and its calculation model. No suitable designs with thicknesses within the standard production limitations of LVL were found. From a structural point of view, the thinner-walled designs that did meet requirements made better use of the high strength of the material, but the high stress levels could pose problems concerning the required capacity of connectors. From a non-structural point of view, the large widths of these towers are considered undesirable due to aesthetics.

Secondly, designs with cross sectional widths comparable to the CLT designs were made, resulting in wall thicknesses much larger than the production standard of LVL, in order to reach a suitable frequency. Compared to CLT designs with similar wall thicknesses, the tower width could decrease. This meant a lower wind load directly on the tower and, from a non-structural point of view, improved aesthetics. Stress levels were low, so no problems designing suitable connections are expected. The high strength of the LVL was however not exploited.

It is expected that the structural optimum for all-LVL designs is somewhere in-between these two options, depending on the balance between connection strength and frequency.

Using LVL as longitudinal layers in a CLT element, effectively making a CLT-LVL hybrid cross section, did not turn out to improve material use compared to the LVL designs. It showed the same advantages over CLT designs - reduced width or thickness - as the all-LVL designs did, albeit to a lesser extent. Practically the same amount of LVL was found to be used in these hybrid towers as for LVL towers of the same width and frequency, while peak normal stresses remained the same. Shear stresses decreased slightly, but were not found to be governing for both options. The hybrid towers are effectively the same as the all-LVL towers, with a larger wall thickness because of the added cross layers made out of CLT, but with no benefit in the amount of LVL used.

10-2   Discussion and limitations of the research

One of the two biggest limitations of the conclusions drawn from this research can be found in the loads the towers have been subjected to. Not all load cases prescribed by the IEC have been considered and especially the fatigue strength of the designs has not been assessed.

Furthermore, simplified load calculations methods have been used, instead of using detailed stochastic load simulations. Although fatigue is not regarded as governing for timber towers and the applied load cases are considered to represent the extreme loads well, no definite conclusions on the feasibility can be drawn until all load aspects of the tower have been considered.

The other large limitation consists of the connections between the horizontal edges of the individual elements. Connections have been left out of the scope of this research, but may prove to be the governing component, as is found in many kinds of timber structures. Although the original connection of the TimberTower is not considered the only suitable connections for these towers, finding suitable connections may turn out to be difficult for towers with walls thinner than the original 300 mm of the TimberTower, due to the high loads they will have to transfer. Designs have not been rejected as long as their ultimate strength and buckling strength were sufficient, but cannot be labelled as definitely feasible until suitable connections are designed as well.

Maximum deflection of the tower has not been regarded as one of the critical properties, mainly because the rotor axis can be tilted slightly upwards to increase the clearance and prevent most deflection issues.

Many of the material properties used throughout this research are still under investigation. More could be gained from determining if higher strength CLT also has a higher shear strength than its lower strength classes. The technological feasibility of hybrid panels has been judged on the basis of a small amount of examples, the majority of which is still being researched. Many questions are yet to be answered, such as if there are possible reductions in strength from the combination of materials and whether or not suitable adhesives exist. Until these have been answered, the application of hybrid panels in turbine towers remains theoretical.

Aside from the application of panels that have a consistent layout throughout the entire tower, the use of higher-strength species or products in areas of higher stress could prove to be of economical interest, but has not been researched in this thesis.

Local buckling of the tower walls has in some cases been cited to reject designs, even though this may not always have to be a problem. The calculation models only allowed for either adding material or increasing the base material Young's moduli to influence the buckling behaviour, but this is not the only way to improve local buckling behaviour. One can think of adding stiffening rings or ribs to increase the local buckling strength, for example. Results also suggest that adding more faces to the tower, i.e. increasing the order of the polygonal shape, will improve buckling behaviour. The addition of stiffening elements will take away the opportunity to perform relatively simple load calculations, but might prove to decrease the total amount of material used, since towers with thinner walls may become feasible.

Higher visibility of towers with a large base diameter has been put forward as an argument against the application of these towers, but has no influence on the structural feasibility. It will not be an issue for remote areas where the amount of people being affected is neglectable, but such areas are rare in the Netherlands.

10-3   Recommendations

Several recommendations are made for the future:

– To be able to make definite statements on the feasibility of timber turbine towers in the Netherlands, it is recommended that the designs made are subjected to the entire load spectrum, including all unincluded load cases and fatigue.

– Further research into the conformation of higher shear strength of higher CLT strength classes is recommended as well, because this might reduce the amount of cross-layers needed.

– CLT designs could benefit further from base materials with higher Young's modulus. Research into the application of stiff timber species in CLT would support this potential benefit.

– Consulting manufacturers on the possibilities of making thicker LVL elements and determining the extent of volume effects is needed to confirm the thick-walled designs in LVL.

– Apart from structurally feasible, the towers will have to be economically viable as well. Although sources suggest that timber towers will be cheaper than conventional concepts, the economic differences between the designs need to be assessed and economic considerations have to be taken into account in design as well.

– More experience in practice should be gained in applying these kinds of towers. The construction of more prototypes is advised, not just in the Netherlands, in order to expand knowledge on and publicity of the subject and validate design assumptions and parameters.

10-4   Final words

It is considered structurally feasible to apply timber towers for contemporary wind turbines in the Netherlands. Various designs have been made using an hollow polygonal tower made of Cross Laminated Timber (CLT) and Laminated Veneer Lumber (LVL) that met the appropriate requirements from design codes and physics. The original softwood CLT design for the TimberTower was sufficient, but improvements in terms of reduced tower width were shown to be possible by using all-LVL towers or, to a lesser extent, by replacing longitudinal layers in the CLT with parallel-oriented LVL.

Appendices

The appendices are split into three parts. The first part (A to C) contains additional and more detailed results, supplementing the calculations and results in the main report. The second part (D to H) contains an overview of underlying formulas used in the calculations, as well as the complete code behind the software model used.

The appendices in the last part (I to M) are mostly written as stand-alone pieces, to provide the reader with additional information on subjects that were unknown to the author at the start of this research as well. For this reason, they might have some overlap with the main report. Appendices L and M are intended to be read in that specific order.

Additional and detailed results

Frequency analysis: parameter study results

This appendix is an extension of section 5-5, displaying the results of the study into the influence of several parameters on the natural frequencies of the tower. This part is limited to octagonal towers with a height of 125 m. Lower hub heights and decagonal tower shapes will display the same behaviour. Reference to Appendix E is made for the definition of geometric parameters.

On the next pages the data generated by both frequency calcultation methods is shown in both tabular and graphical form.

A-1   Thickness t

| t | ANSYS | | | | | | Rayleigh | | Rayleigh/ANSYS | |
| | Absolut value | | | Scaled | | | Absolut | Scaled | Absolut | Scaled |
	f_1	f_2	f_3	f_1	f_2	f_3	f_1	f_1	f_1	f_1
0.25	0.1933	1.7474	4.5722	0.8013	1.0129	0.9565	0.2122	0.8020	109.8%	100.1%
0.35	0.2205	1.7367	4.8372	0.9139	1.0067	1.0119	0.2419	0.9142	109.7%	100.0%
0.45	0.2412	1.7251	4.7803	1.0000	1.0000	1.0000	0.2646	1.0000	109.7%	100.0%
0.55	0.2577	1.7122	4.7224	1.0681	0.9925	0.9879	0.2827	1.0684	109.7%	100.0%
0.65	0.2709	1.6987	4.6652	1.1230	0.9847	0.9759	0.2973	1.1236	109.7%	100.1%
0.75	0.2817	1.6847	4.6090	1.1678	0.9766	0.9642	0.3094	1.1693	109.8%	100.1%
0.85	0.2906	1.6703	4.5538	1.2047	0.9682	0.9526	0.3195	1.2075	109.9%	100.2%

Table A-1: Natural frequencies vs thickness t
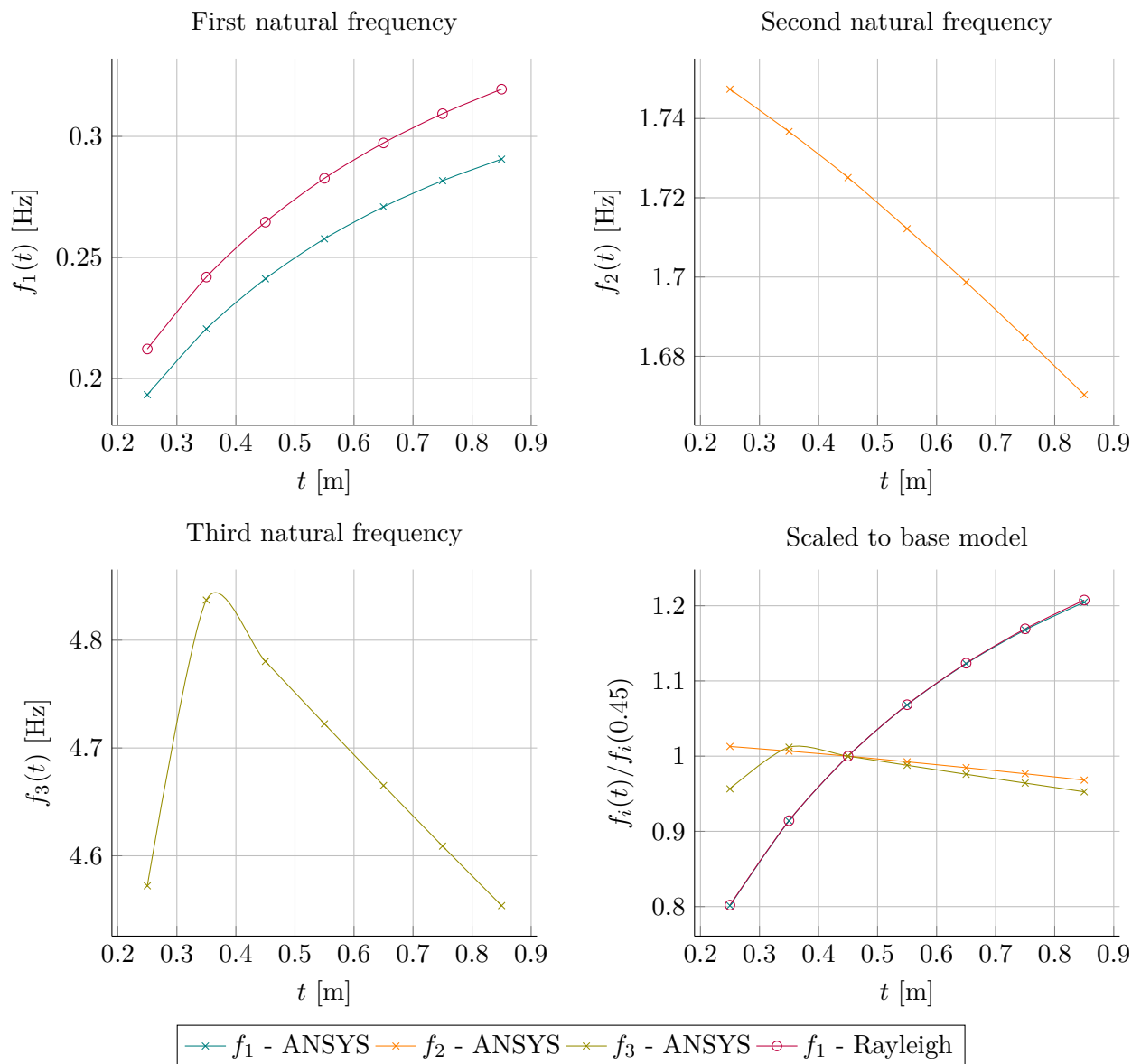
Figure A-1: The influence of wall thickness on the first three natural frequencies, comparing methods

A-2 Taper

| Taper | $a_{out,T}$ | ANSYS | | | | | | Rayleigh | | Rayleigh/ANSYS | |
| | | Absolut value | | | Scaled | | | Absolut | Scaled | Absolut | Scaled |
		f_1	f_2	f_3	f_1	f_2	f_3	f_1	f_1	f_1	f_1
1	4.00	0.3161	2.5128	5.5513	1.3105	1.4566	1.1613	0.3237	1.2247	1.024	0.935
2	2.00	0.2681	1.9535	5.4696	1.1113	1.1324	1.1442	0.2767	1.0469	1.032	0.942
3	1.33	0.2412	1.7251	4.7803	1.0000	1.0000	1.0000	0.2643	1.0000	1.096	1.000
4	1.00	0.2217	1.5829	4.3516	0.9190	0.9176	0.9103	0.2588	0.9792	1.167	1.066
5	0.80	0.2078	1.4920	4.0790	0.8613	0.8649	0.8533	0.2558	0.9678	1.231	1.124

Table A-2: First natural frequency vs taper
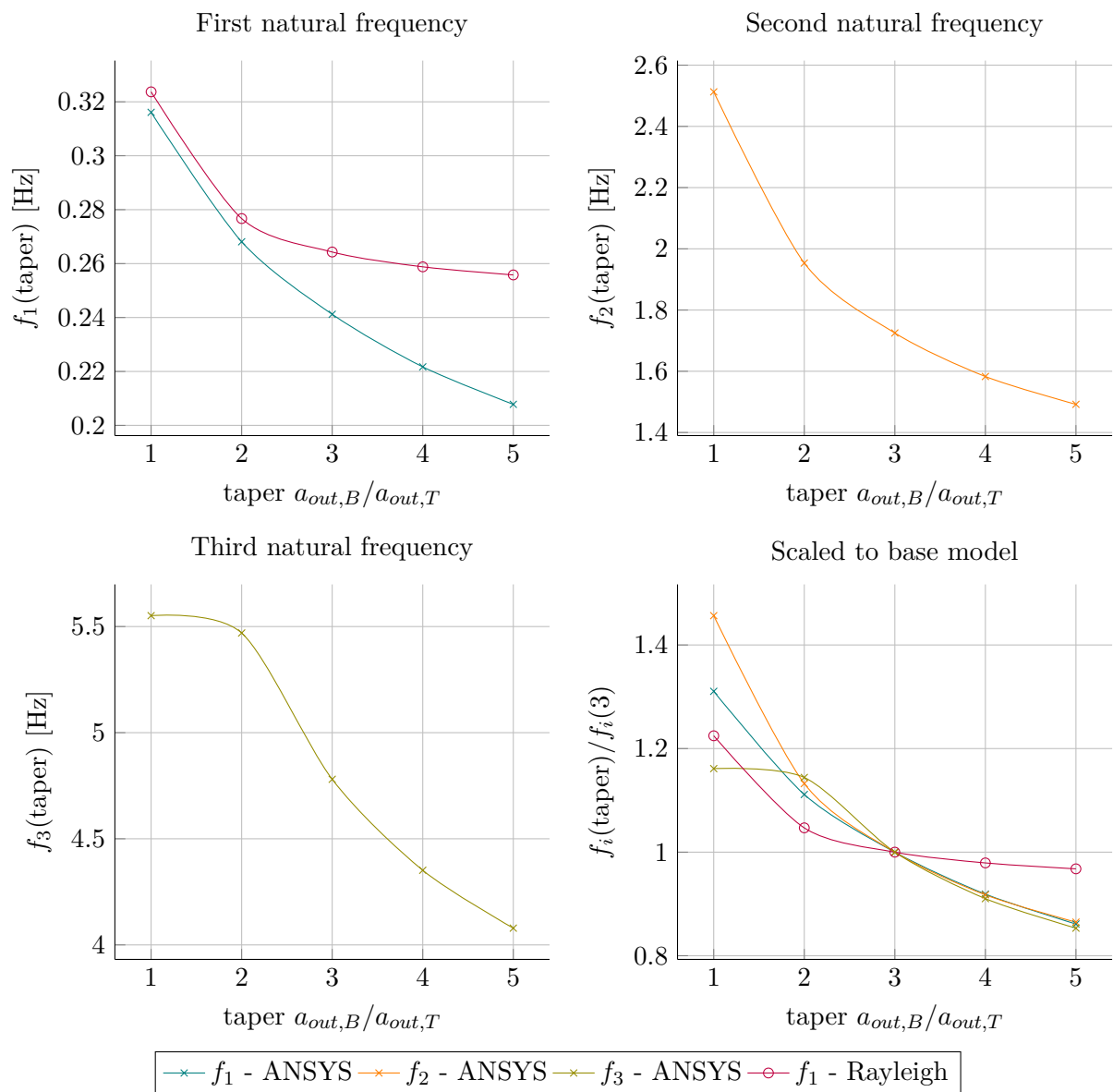
Figure A-2: The influence of the tapering of the tower on the first three natural frequencies, comparing methods

A-3 Overall geometry

| Multiplier | $a_{out,B}$ | $a_{out,T}$ | t | ANSYS | | | | | | Rayleigh | | Rayleigh/ANSYS | |
| | | | | Absolut value | | | Scaled | | | Absolut value | Scaled | Absolut | Scaled |
				f_1	f_2	f_3	f_1	f_2	f_3	f_1	f_1	f_1	f_1
0.5	2	0.675	0.225	0.0637	0.8497	2.4654	0.2639	0.4926	0.5157	0.0707	0.2672	1.111	1.012
0.75	3	1.0125	0.3375	0.1340	1.2832	3.6495	0.5555	0.7438	0.7634	0.1546	0.5843	1.154	1.052
1	4	1.35	0.45	0.2412	1.7251	4.7803	1.0000	1.0000	1.0000	0.2646	1.0000	1.097	1.000
1.25	5	1.6875	0.5625	0.3629	2.1754	5.8463	1.5044	1.2610	1.2230	0.3953	1.4940	1.089	0.993
1.5	6	2.025	0.675	0.5003	2.6318	6.8365	2.0738	1.5256	1.4301	0.5414	2.0461	1.082	0.987
1.75	7	2.3625	0.7875	0.6490	3.0922	7.5551	2.6904	1.7925	1.5805	0.6988	2.6409	1.077	0.982
2	8	2.7	0.9	0.8053	3.5518	8.6007	3.3382	2.0589	1.7992	0.8635	3.2634	1.072	0.978

Table A-3: Natural frequencies vs overall geometry
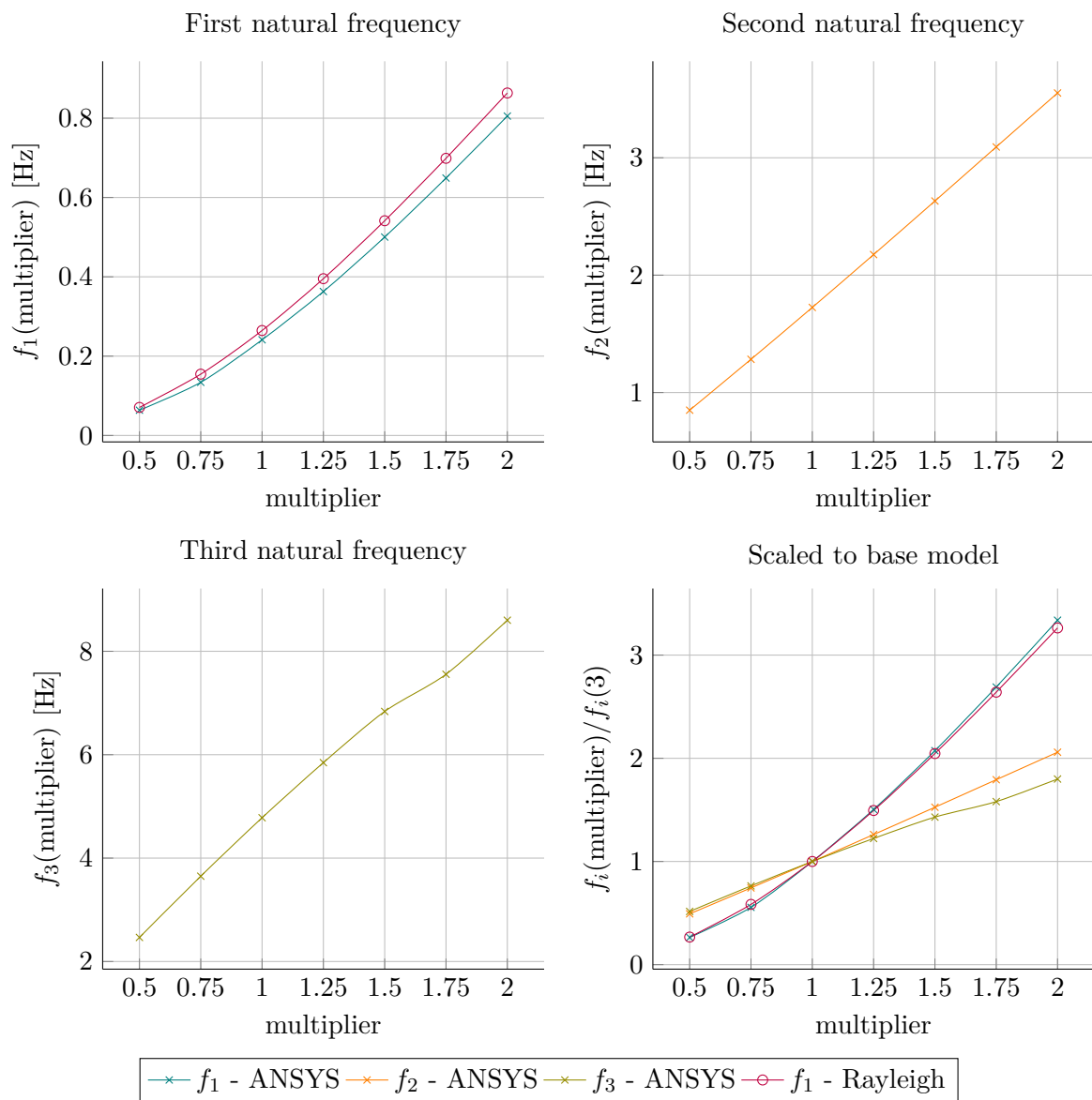
Figure A-3: The influence of the overall geometry of the tower on the first three natural frequencies, comparing methods

A-4 Overall width

| Multiplier | $a_{out,B}$ | $a_{out,T}$ | t | ANSYS | | | | | | Rayleigh | | Rayleigh/ANSYS | |
| | | | | Absolut value | | | Scaled | | | Absolut value | Scaled | Absolut | Scaled |
				f_1	f_2	f_3	f_1	f_2	f_3	f_1	f_1	f_1	f_1
0.5	2	0.675	0.45	0.0830	0.8024	2.3063	0.3440	0.4651	0.4825	0.0904	0.3416	1.089	0.993
0.75	3	1.0125	0.45	0.1546	1.2632	3.5746	0.6410	0.7322	0.7478	0.1712	0.6470	1.107	1.009
1	4	1.35	0.45	0.2412	1.7251	4.7803	1.0000	1.0000	1.0000	0.2646	1.0000	1.097	1.000
1.25	5	1.6875	0.45	0.3370	2.1815	5.8973	1.3971	1.2646	1.2337	0.3676	1.3893	1.091	0.994
1.5	6	2.025	0.45	0.4399	2.6273	6.7741	1.8237	1.5230	1.4171	0.4780	1.8065	1.087	0.991
1.75	7	2.3625	0.45	0.5485	3.0599	7.1184	2.2736	1.7738	1.4891	0.5946	2.2472	1.084	0.988
2	8	2.7	0.45	0.6614	3.4756	6.0469	2.7419	2.0147	1.2650	0.7136	2.6969	1.079	0.984

Table A-4: Natural frequencies vs overall width
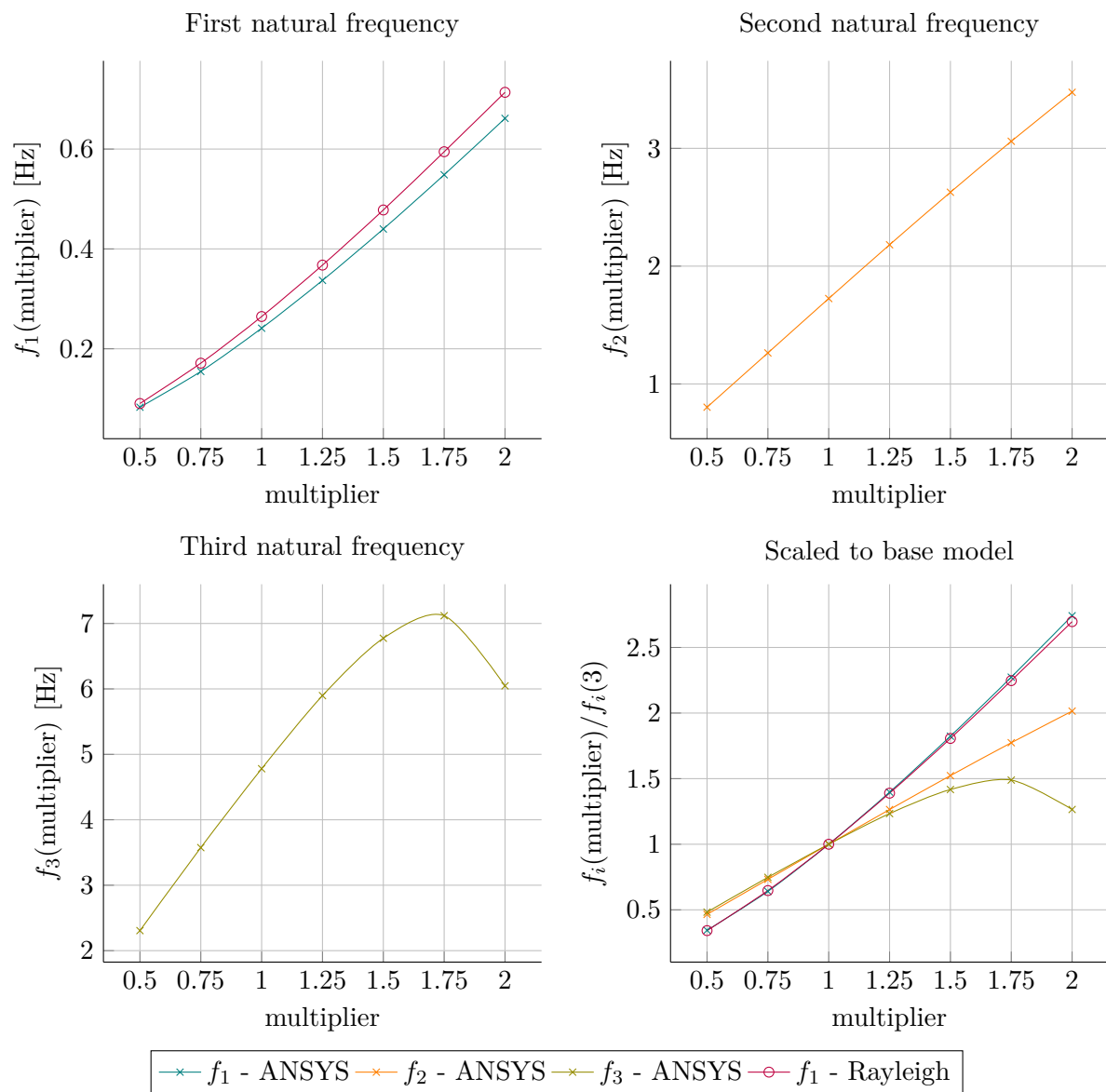
Figure A-4: The influence of the overall width of the tower on the first three natural frequencies, comparing methods

A-5   Top mass M_{top}

M_{top}	ANSYS						Rayleigh		Rayleigh/ANSYS	
	Absolut value			Scaled			Absolut	Scaled	Absolut	Scaled
	f_1	f_2	f_3	f_1	f_2	f_3	f_1	f_1	f_1	f_1
0	0.6344	2.5397	5.9940	2.6298	1.4722	1.2539	0.6466	2.4437	1.019	0.929
100000	0.3895	1.8604	4.9036	1.6148	1.0784	1.0258	0.4156	1.5707	1.067	0.973
200000	0.3041	1.7703	4.8196	1.2605	1.0262	1.0082	0.3300	1.2472	1.085	0.989
300000	0.2577	1.7355	4.7892	1.0682	1.0060	1.0019	0.2819	1.0654	1.094	0.997
400000	0.2276	1.7171	4.7735	0.9434	0.9954	0.9986	0.2502	0.9456	1.099	1.002
500000	0.2060	1.7057	4.7639	0.8540	0.9888	0.9966	0.2272	0.8587	1.103	1.005
600000	0.1896	1.6979	4.5960	0.7860	0.9842	0.9614	0.2096	0.7921	1.105	1.008
700000	0.1766	1.6923	4.2937	0.7320	0.9810	0.8982	0.1955	0.7389	1.107	1.009
1E+06	0.1493	1.6820	3.6519	0.6191	0.9750	0.7639	0.1658	0.6266	1.110	1.012
350000	0.2412	1.7251	4.7803	1.0000	1.0000	1.0000	0.2646	1.0000	1.097	1.000

Table A-5: Natural frequencies vs top mass

First natural frequency

Second natural frequency

Third natural frequency

Scaled to base model

f_1 - ANSYS f_2 - ANSYS f_3 - ANSYS f_1 - Rayleigh
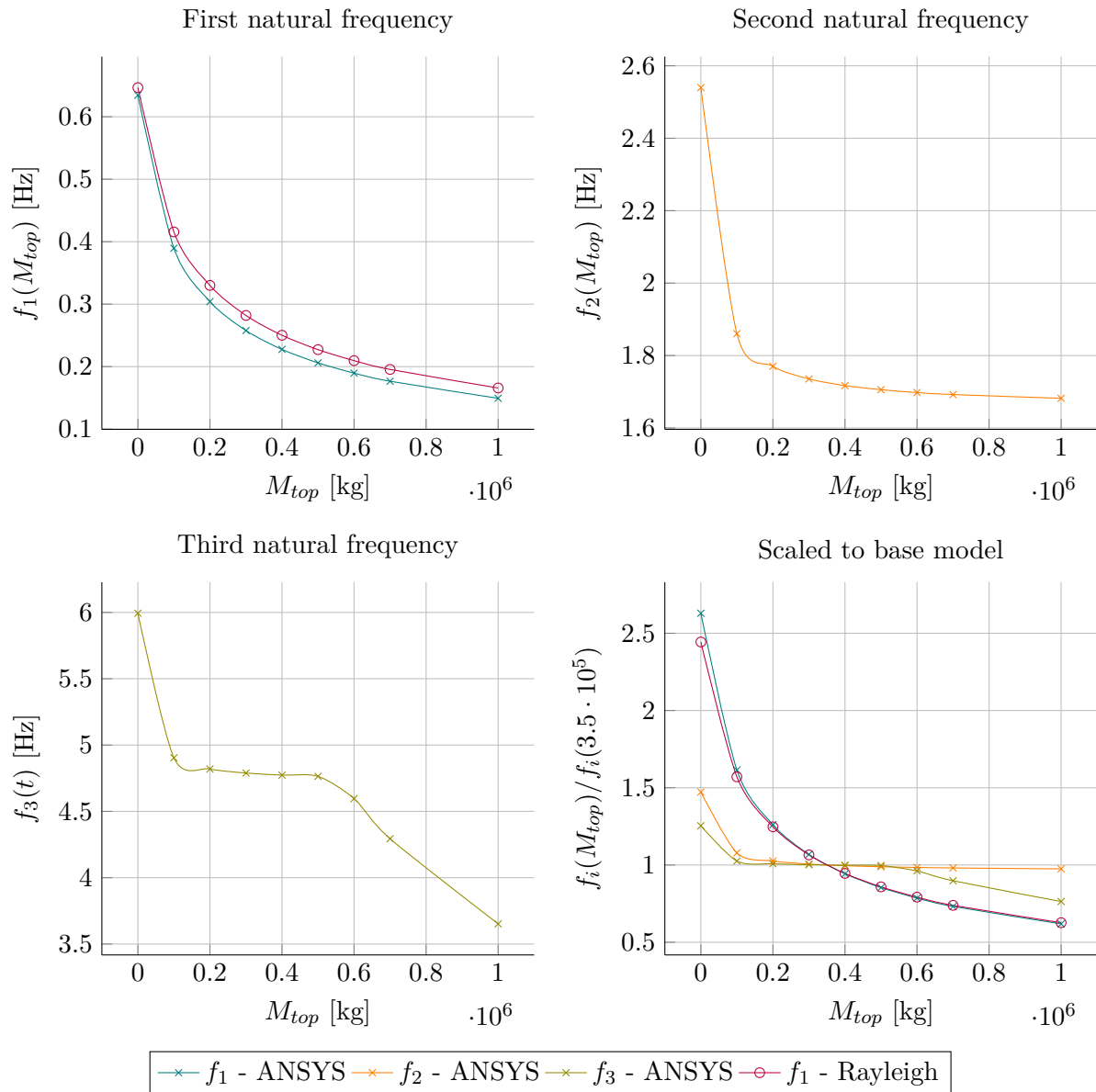
Figure A-5: The influence of top mass on the first three natural frequencies, comparing methods

A-6   Top mass inertia I_M

Rotational inertia of top mass I_M

Mass inertia	ANSYS					
	Absolut value			Scaled		
	f_1	f_2	f_3	f_1	f_2	f_3
0	0.2412	1.7251	4.7803	1.0000	1.0000	1.0000
35000	0.2412	1.7246	4.7776	1.0000	0.9997	0.9994
175000	0.2412	1.7228	4.7595	1.0000	0.9987	0.9956
350000	0.2412	1.7205	4.7385	0.9999	0.9973	0.9913
1750000	0.2411	1.7019	3.9810	0.9994	0.9866	0.8328
3500000	0.2409	1.6779	2.8744	0.9988	0.9726	0.6013
35000000	0.2382	0.9257	1.2576	0.9876	0.5366	0.2631

Table A-6: First natural frequency vs rotational inertia of the top mass
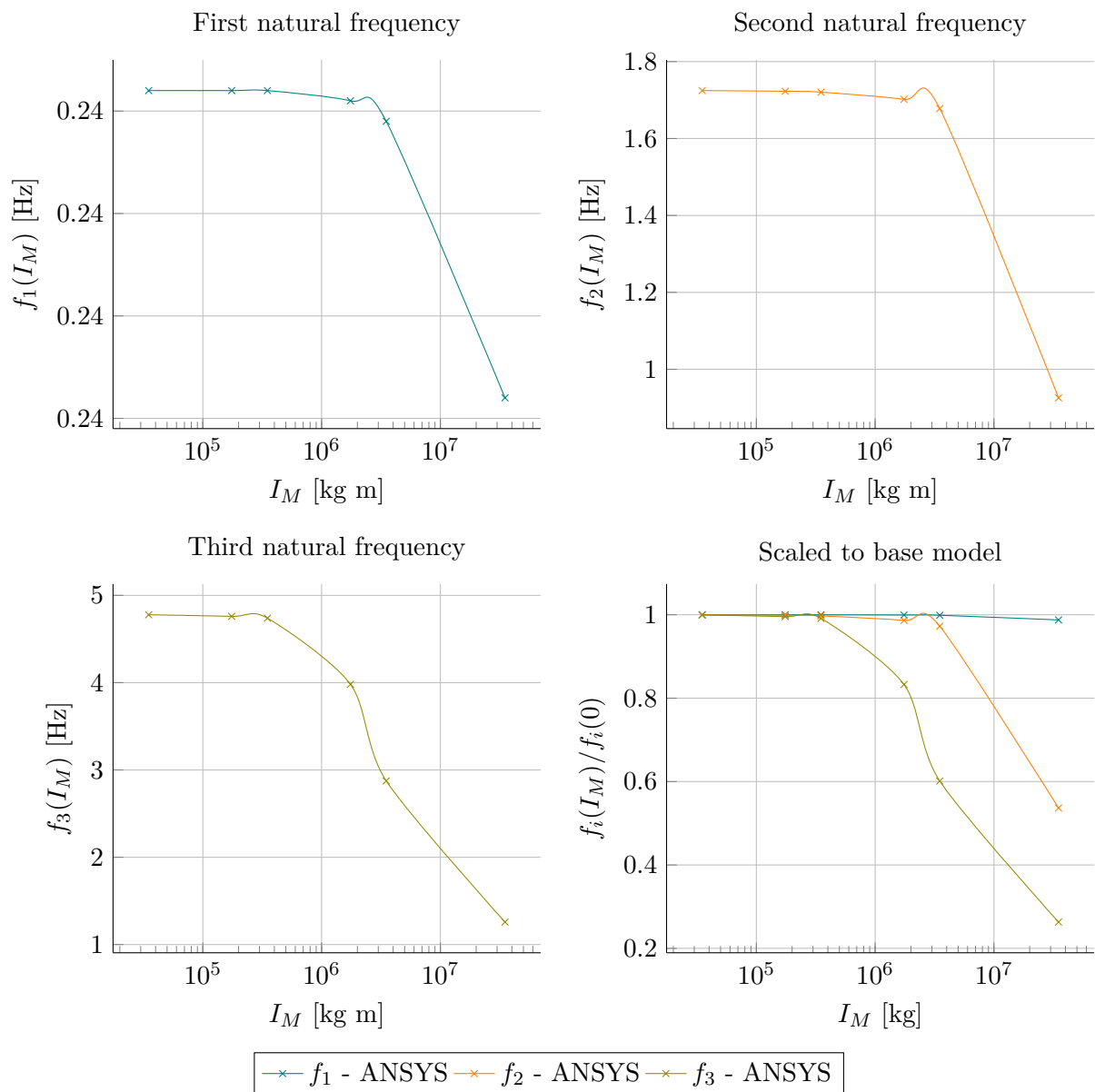
Figure A-6: The influence of top mass inertia on the first three natural frequencies, using ANSYS

A-7 Young's Modulus E

| E | ANSYS | | | | | | Rayleigh | | Rayleigh/ANSYS | |
| | Absolut value | | | Scaled | | | Absolut value | Scaled | Absolut | Scaled |
	f_1	f_2	f_3	f_1	f_2	f_3	f_1	f_1	f_1	f_1
2.00E+09	0.1150	0.8224	2.2789	0.4767	0.4767	0.4767	0.2162	0.8171	1.880	1.714
4.00E+09	0.1626	1.1630	3.2228	0.6742	0.6742	0.6742	0.1784	0.6742	1.097	1.000
6.00E+09	0.1992	1.4244	3.9472	0.8257	0.8257	0.8257	0.2185	0.8258	1.097	1.000
8.00E+09	0.2300	1.6448	4.5578	0.9535	0.9535	0.9535	0.2523	0.9535	1.097	1.000
1.00E+10	0.2572	1.8389	5.0958	1.0660	1.0660	1.0660	0.2821	1.0661	1.097	1.000
1.20E+10	0.2817	2.0144	5.5821	1.1678	1.1677	1.1677	0.3090	1.1678	1.097	1.000
1.40E+10	0.3043	2.1758	6.0294	1.2613	1.2613	1.2613	0.3338	1.2615	1.097	1.000
1.60E+10	0.3253	2.3261	6.4457	1.3484	1.3484	1.3484	0.3568	1.3485	1.097	1.000
1.80E+10	0.3450	2.4672	6.8367	1.4302	1.4302	1.4302	0.3785	1.4305	1.097	1.000

Table A-7: Natural frequencies vs Young's modulus
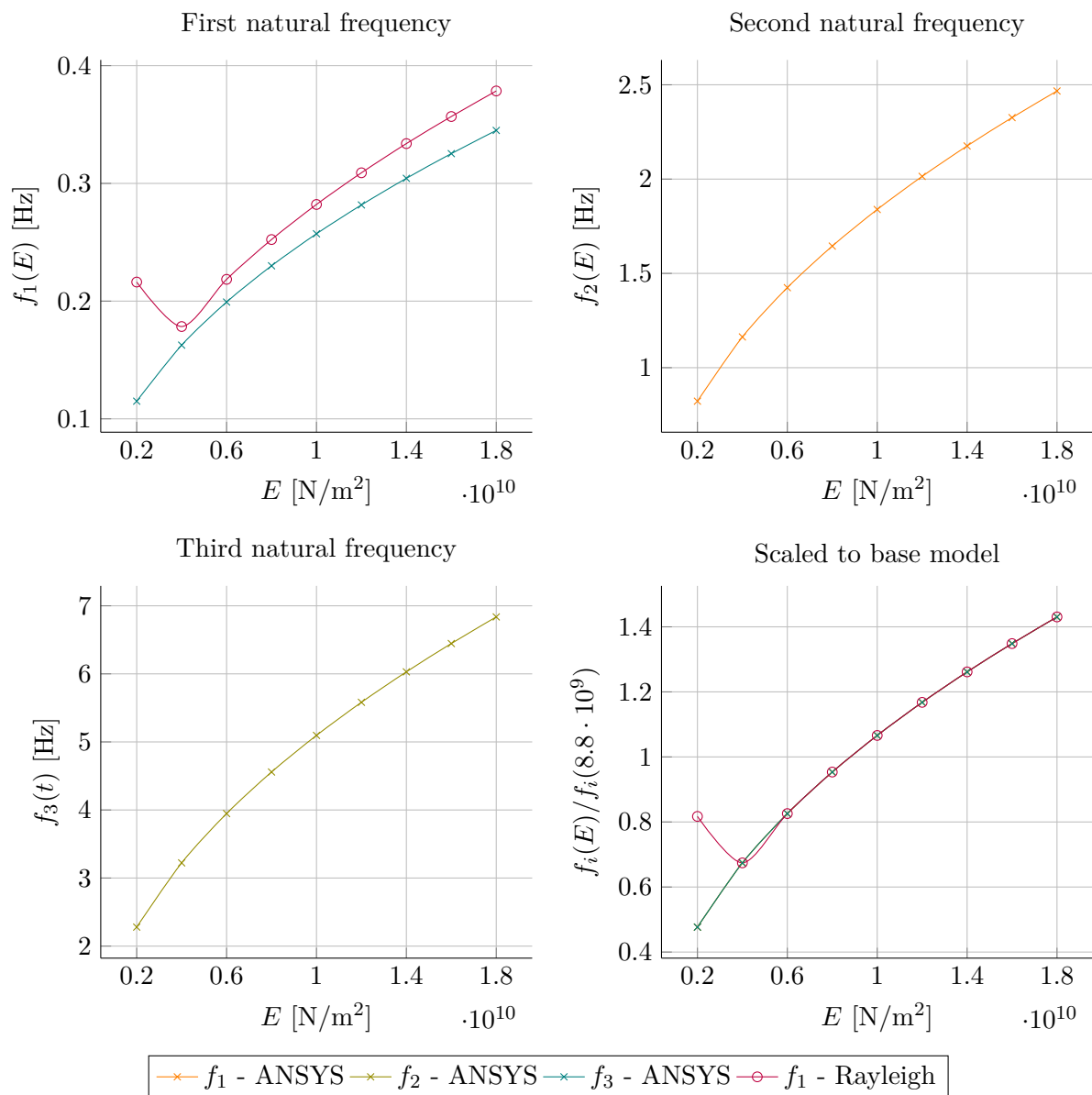
Figure A-7: The influence of the Young's modulus on the first three natural frequencies, comparing methods

A-8 Density ρ

| | ANSYS | | | | | | | Rayleigh | | Rayleigh/ANSYS | |
| | Absolut value | | | Scaled | | | | Absolut value | Scaled | Absolut | Scaled |
ρ	f_1	f_2	f_3	f_1	f_2	f_3		f_1	f_1	f_1	f_1
2.50E+02	0.2480	2.2018	6.0098	1.0282	1.2763	1.2572		0.2741	1.0359	1.105	1.007
3.00E+02	0.2460	2.0193	5.6377	1.0197	1.1705	1.1794		0.2712	1.0249	1.102	1.005
4.00E+02	0.2420	1.7646	4.8957	1.0032	1.0229	1.0241		0.2657	1.0042	1.098	1.001
5.00E+02	0.2382	1.5920	4.3905	0.9874	0.9228	0.9185		0.2605	0.9845	1.094	0.997
6.00E+02	0.2346	1.4654	4.0185	0.9723	0.8495	0.8406		0.2556	0.9660	1.090	0.993
4.20E+02	0.2412	1.7251	4.7803	1.0000	1.0000	1.0000		0.2646	1.0000	1.097	1.000

Table A-8: Natural frequencies vs density
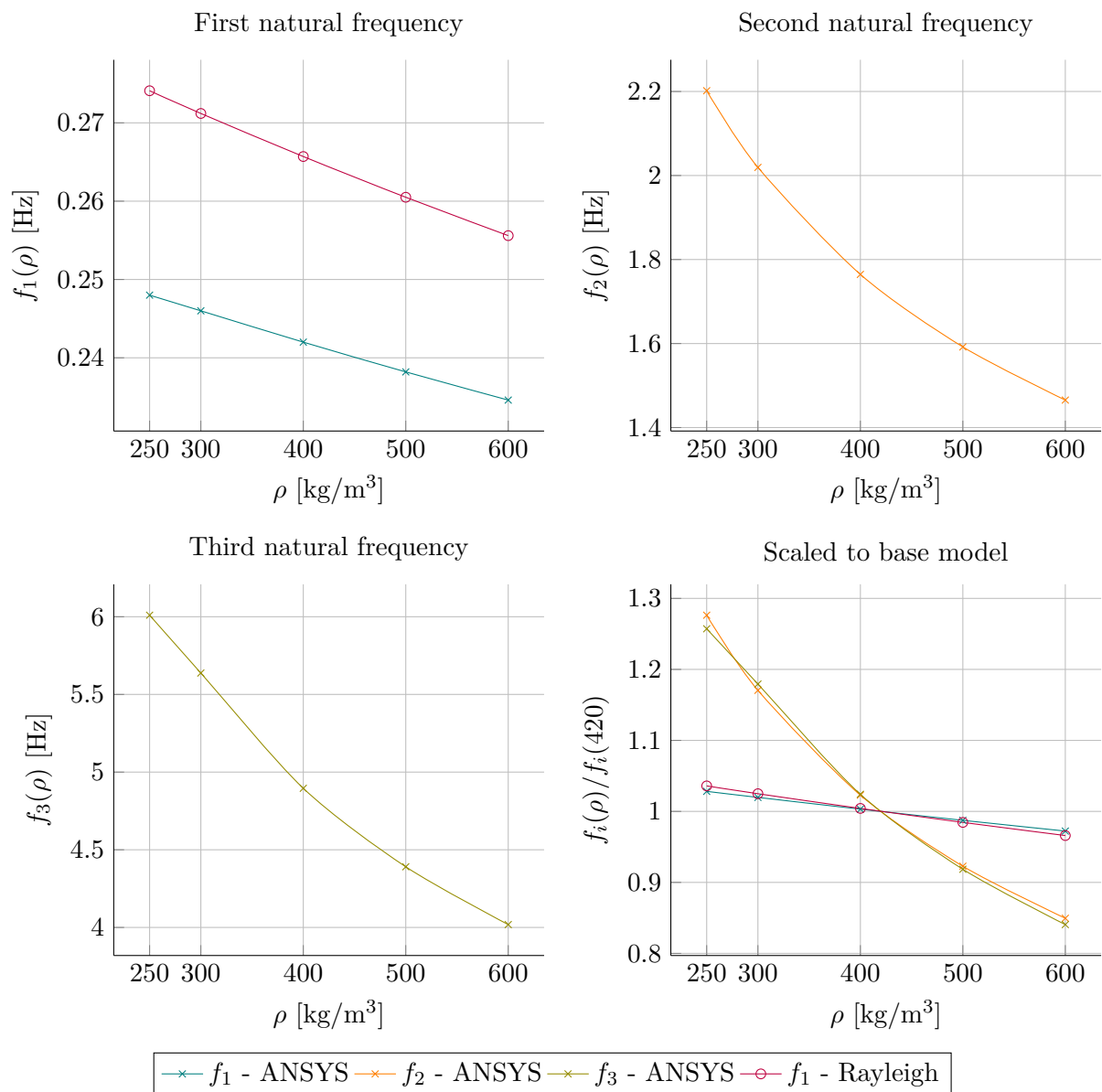
Figure A-8: The influence of density of the tower material on the first three natural frequencies, comparing methods

A-9 Isotropy and orthotropy

Model	$a_{out,B}$	$a_{out,T}$
1	3.00	1.01
2	4.00	1.35
3	5.00	1.70

Table A-9: Parameters altered within the three models used to investigate orthotropy

Model	Type	EX	EY	EZ	G	f_1	f_2	f_3	f_1	f_2	f_3
1	Iso	8800	8800	8800	3380	0.154	1.255	3.552	1.00	1.00	1.00
	Ortho	8800	8800	8800	650	0.153	1.178	3.148	0.99	0.94	0.89
	Ortho	450	2200	8800	650	0.153	1.197	3.199	0.99	0.95	0.90
2	Iso	8800	8800	8800	3380	0.240	1.171	4.742	1.00	1.00	1.00
	Ortho	8800	8800	8800	650	0.233	1.541	3.916	0.97	1.32	0.83
	Ortho	450	2200	8800	650	0.236	1.567	3.979	0.98	1.34	0.84
3	Iso	8800	8800	8800	3380	0.335	2.160	5.848	1.00	1.00	1.00
	Ortho	8800	8800	8800	650	0.320	1.855	4.216	0.96	0.86	0.72
	Ortho	450	2200	8800	650	0.325	1.893	4.216	0.97	0.88	0.72

Table A-10: Orthotropy versus isotropy, using ANSYS

Calculation methods – result examples

This appendix is a supplement to Chapter 6, here to provide examples of intermediate results for the quasi-static load calculation method (section B-2) and graphical examples of loads calculated with the methods from Chapter 6 along the tower height in sections B-3 and B-4.

B-1 Examples of the turbine class calculations in section 3-2

The following pages show two example calculations for the results in Table 3-1, based on the formulas from section L-2.

Wind area		I	
Terrain category		0	
Fundamental wind velocity			
Fundamental wind velocity	$V_{b,0}$	29.5	m/s
Directional factor	c_{dir}	1.0	
Seasonal factor	c_{season}	1.0	
Basic wind velocity	V_b	29.5	m/s
Mean wind speed at hub height			
Mean wind speed	$V_m(125)$	**48.31**	m/s
Roughness factor	$c_r(125)$	1.638	
Orography factor	$c_o(125)$	1.000	
Roughness length	z_0	0.005	m
Terrain factor	k_r	0.162	
Turbulence			
Turbulence intensity	I_v	**0.099**	
Standard deviation	σ_v	4.771	
Turbulence factor	k_l	1.0	

Table B-1: Calculation of the mean wind speed and turbulence parameters, according to Eurocode 1-1-4, for wind area I-0 at 125 m

Wind area		III	
Terrain category		II	
Fundamental wind velocity			
Fundamental wind velocity	$V_{b,0}$	24.5	m/s
Directional factor	c_{dir}	1.0	
Seasonal factor	c_{season}	1.0	
Basic wind velocity	V_b	24.5	m/s
Mean wind speed at hub height			
Mean wind speed	$V_m(100)$	**31.88**	m/s
Roughness factor	$c_r(100)$	1.301	
Orography factor	$c_o(100)$	1.000	
Roughness length	z_0	0.200	m
Terrain factor	k_r	0.209	
Turbulence			
Turbulence intensity	I_v	**0.161**	
Standard deviation	σ_v	5.129	
Turbulence factor	k_l	1.0	

Table B-2: Calculation of the mean wind speed and turbulence parameters, according to Eurocode 1-1-4, for wind area III-II at 100 m

B-2   Intermediate results for the quasi-static method in section 6-4-2

		Load	n_0	n^*	h	V_{10}	$\frac{n_0 L}{V_{10}}$	$f(n_0)$	$\frac{n_0 l}{V_{10}}$	k_r	k_b	ψ
100 m - 3 MW	IC	Blade load	1.7	0.699	142	52.0	0.85	0.28	25.17	0.51	0.82	1.91
		Axial force	0.45	0.32918	100	50.0	0.33	0.20	12.31	0.56	0.67	1.87
		Tilt moment	1.7	0.699	133	51.6	0.68	0.13	25.35	0.23	0.83	1.81
		Yaw moment	0	0	100	50.0	0.00	0.13	0.00	0.00	0.83	1.72
	IIA	Blade load	1.7	0.699	133	43.9	0.797	0.295	23.635	0.551	0.816	2.47
		Axial force	0.45	0.32918	100	42.5	0.387	0.177	11.483	0.511	0.649	2.35
		Tilt moment	1.7	0.699	133	43.9	0.797	0.117	23.635	0.219	0.816	2.28
		Yaw moment	0	0	100	42.5	0	0.117	0	0	0.816	2.13
	IIIA	Blade load	1.7	0.699	133	38.7	0.903	0.270	26.786	0.466	0.816	2.42
		Axial force	0.45	0.32918	100	37.5	0.439	0.160	13.015	0.428	0.649	2.30
		Tilt moment	1.7	0.699	133	38.7	0.903	0.107	26.786	0.185	0.816	2.26
		Yaw moment	0	0	100	37.5	0	0.107	0	0	0.816	2.13

		Load	n_0	n^*	h	V_{10}	$\frac{n_0 L}{V_{10}}$	$f(n_0)$	$\frac{n_0 l}{V_{10}}$	k_r	k_b	ψ
125 m - 5 MW	IC	Blade load	1.7	0.699	167	51.6	0.85	0.28	25.85	0.50	0.82	1.88
		Axial force	0.45	0.30506	125	50.0	0.38	0.18	11.64	0.51	0.65	1.83
		Tilt moment	1.7	0.699	167	51.6	0.85	0.11	25.85	0.20	0.82	1.78
		Yaw moment	0	0	125	50.0	0.00	0.11	0.00	0.00	0.82	1.70
	IIA	Blade load	1.7	0.699	167	43.9	1.004	0.249	25.470	0.445	0.801	2.35
		Axial force	0.45	0.30506	125	42.5	0.452	0.156	11.471	0.449	0.632	2.19
		Tilt moment	1.7	0.699	167	43.9	1.004	0.099	25.470	0.177	0.801	2.20
		Yaw moment	0	0	125	42.5	0	0.099	0	0	0.801	2.08
	IIIA	Blade load	1.7	0.699	167	38.7	1.138	0.227	28.866	0.374	0.801	2.31
		Axial force	0.45	0.30506	125	37.5	0.512	0.140	13.000	0.375	0.632	2.19
		Tilt moment	1.7	0.699	167	38.7	1.138	0.090	28.866	0.148	0.801	2.18
		Yaw moment	0	0	125	37.5	0	0.090	0	0	0.801	2.08

Table B-3: Intermediate results from the calculation examples of the quasi-static method for the both the 3 MW and 5 MW turbine

B-3   Examples for the wind load on the tower in section 6-5

The following pages show graphical examples of the resulting loads from wind loading directly on the tower, as described in section 6-5.
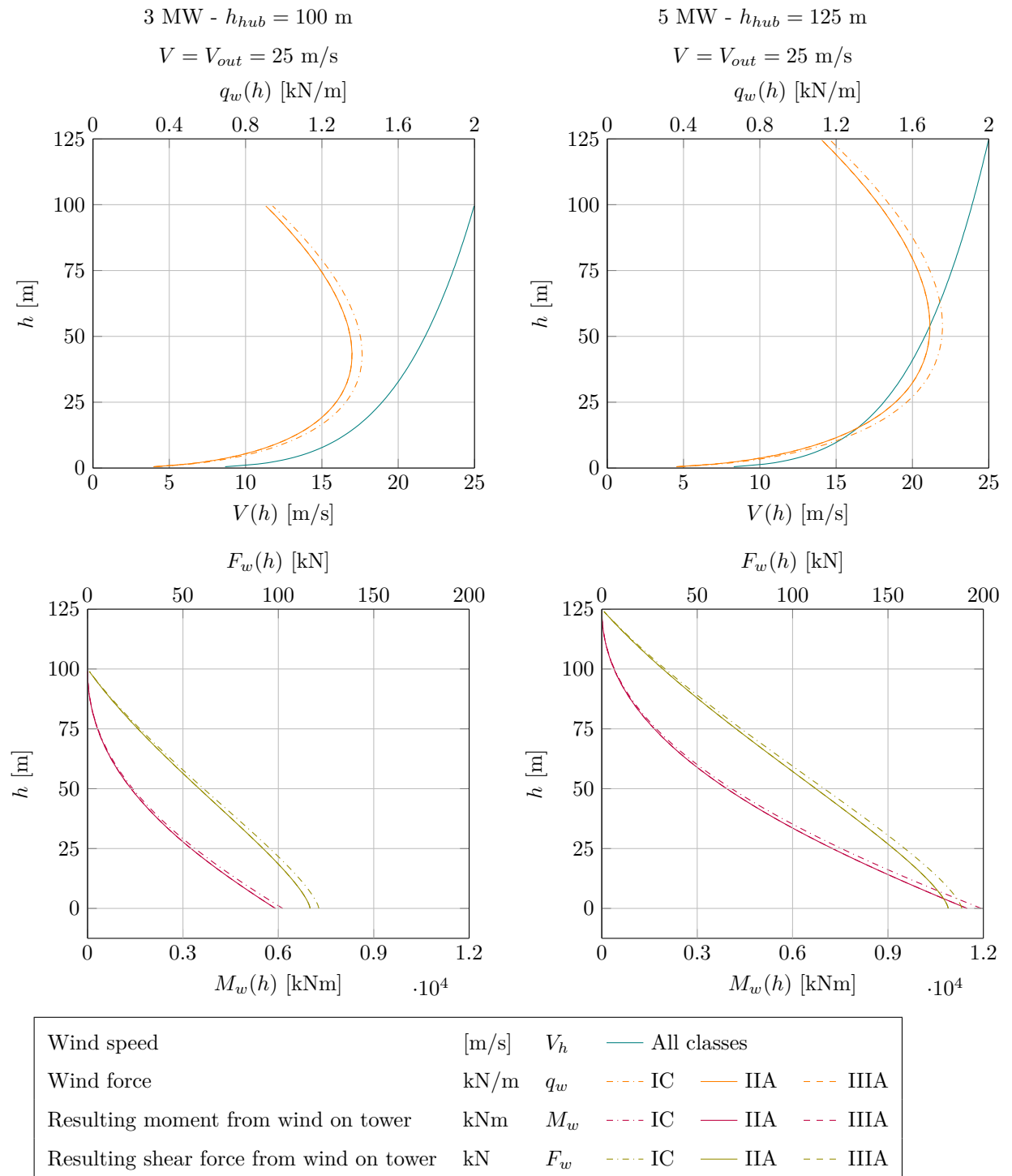
Figure B-1: Wind loads from wind loading directly on the tower, during operation (LC 1)
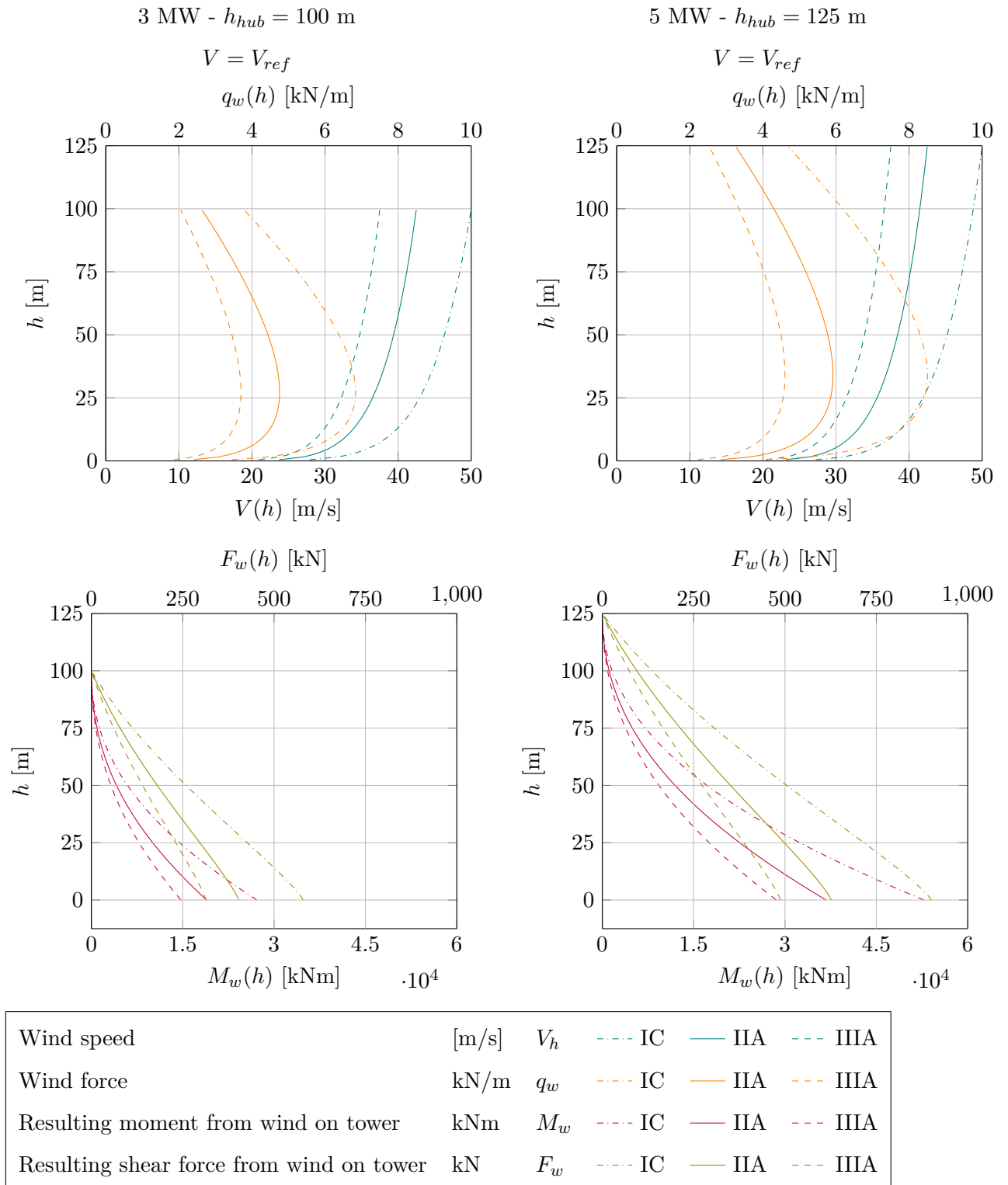
Figure B-2: Wind speed and loads from wind loading directly on the tower, during standstill (LC 2a)

B-4   Examples for resulting wind loads in section 6-6

The following pages show graphical examples of the total resulting loads as described in section 6-6.
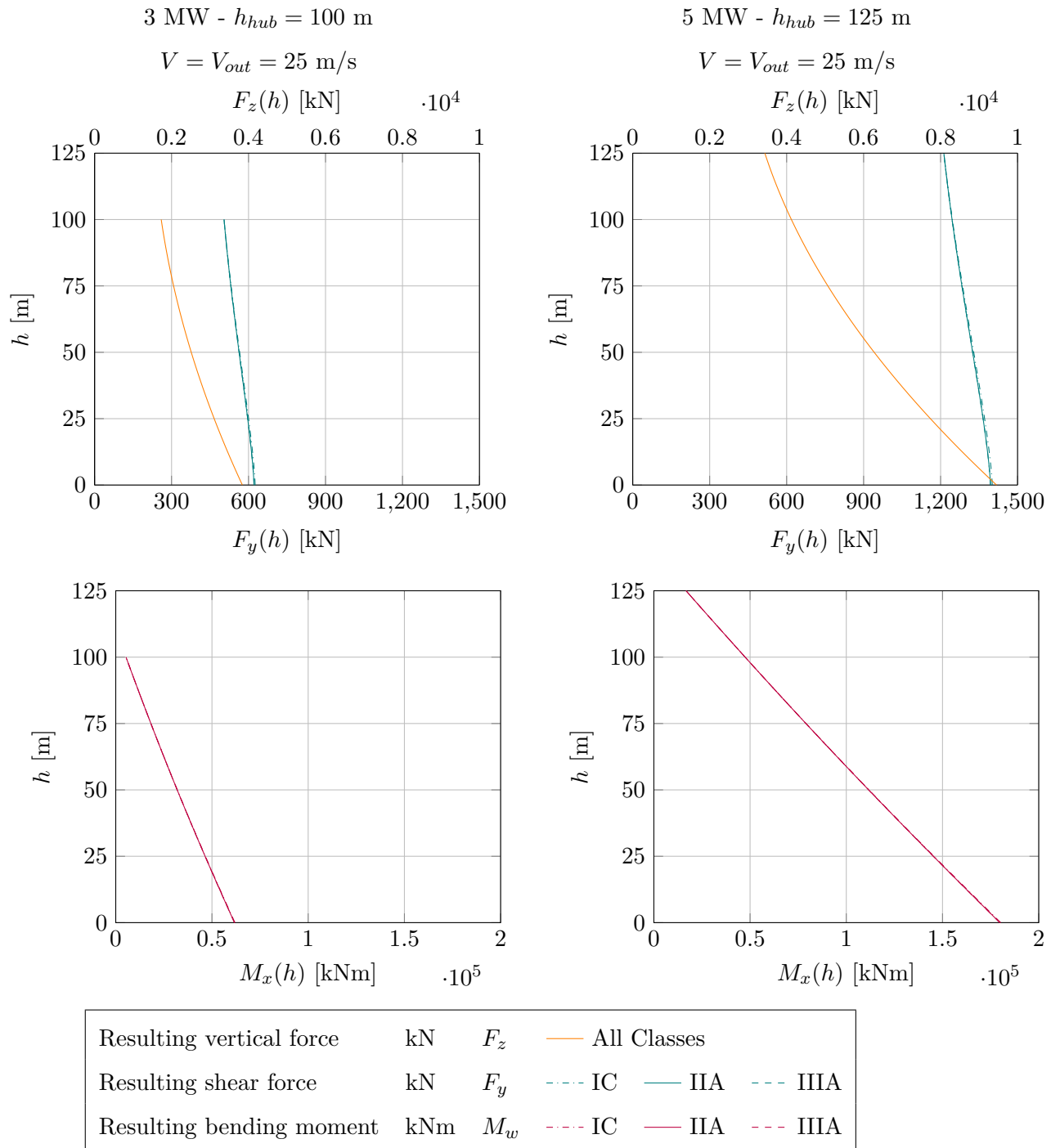
Figure B-3: Relevant resulting loads on the tower during operation (LC 1)
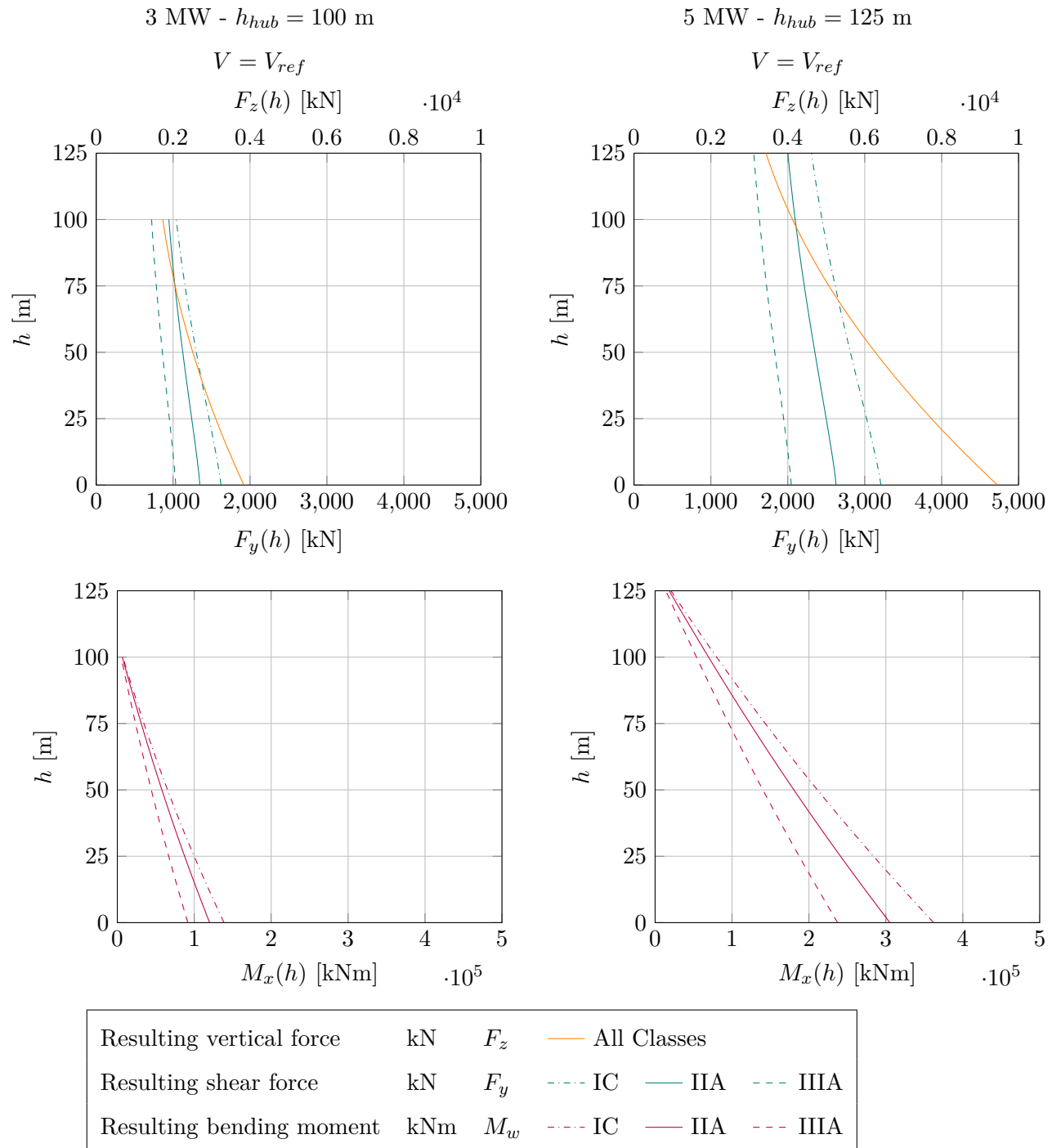
Figure B-4: Relevant resulting loads on the tower during standstill (LC 2a)

Design cases – detailed input and results

This appendix contains detailed calculation results and input for the designs discussed in Chapters 8 and 9, in tabular form. The parameters presented in the tables are explained on the next page.

Input

H	Hub height for the turbine;
Turbine	Either the 3 MW or 5 MW turbine;
Class	Turbine class according to the IEC;
Material	Type of material and strength class;
n_{sides}	The number of faces of the tower;
$a_{out,T}$	The width of one face at the top;
$a_{out,B}$	The width of one face at the bottom;
t	Tower wall thickness;
k_{net}	The amount of fibres in longitudinal direction (ranging from 0-1).

Output - Matlab

F_{yT}	Characteristic thrust force at hub height;
M_{xT}	Characteristic overturning moment at hub height;
M_{zT}	Characteristic vertical load at hub height;
f - Rayleigh	Frequency according to the Rayleigh-Ritz method;
$\sigma_{t,0,net,d,max}$	Maximum occurring net design tensile stress;
$f_{t,0,net,d}$	Design tensile strength of the material;
u.c. - tension	Unity check in tension, $\sigma_{t,0,net,d,max}/f_{t,0,net,d}$;
$\sigma_{c,0,net,d,max}$	Maximum occurring net compression stress;
$f_{c,0,net,d}$	Design compression strength of the material;
u.c. - compression	Unity check in compression, $\sigma_{c,0,net,d,max}/f_{c,0,net,d}$;
Max. allowable $\tau_{xy,d,max}$	The value of the denominator in the unity checks formulas found in section 7-3;
Max. allowable $\tau_{yz,d,max}$	Ditto;
Max. allowable $\tau_{xz,d,max}$	Ditto.

Output - ANSYS

f - ANSYS	First natural frequency according to ANSYS;
$\sigma_{t,0,d,max}$	The maximum occurring tensile normal stress for 5<z<(H-5);
$\sigma_{c,0,d,max}$	The maximum occurring compression stress for 5<z<(H-5);
$\sigma_{t,0,d,net,max}$	$\sigma_{t,0,d,max}/k_{net}$, for comparison with Matlab;
$\sigma_{c,0,d,net,max}$	$\sigma_{c,0,d,max}/k_{net}$;
$\tau_{xy,d,max}$	The maximum occurring shear stress in x-y plane for 5<z<(H-5);
$\tau_{yz,d,max}$	The maximum occurring shear stress in y-z plane for 5<z<(H-5);
$\tau_{xz,d,max}$	The maximum occurring shear stress in x-z plane for 5<z<(H-5);
Buckling factor	The actual buckling factor, see also section H-2-2;
Buckling factor, $\lambda = 1$	The buckling factor ANSYS provides for $\lambda = 1$, which is incorrect;
Maximum deflection	The deflection of the top of the tower, using characteristic material values and design load values.

Comparison ANSYS/Matlab

Here the resulting maximum tensile and compression stresses from ANSYS are divided by the results from Matlab to determine the conformity.

The following footnotes are made throughout the tables, regarding the buckling factor:

^{a} To save time, the buckling factors for load case 1 and 2b, denoted by ^{a}, are not always calculated. It was found that 2a is the governing situation for buckling. Buckling will in general not be an issue for the CLT designs.

^{b} Not all buckling factors for load case 2b have been calculated. The observation could be made from all other designs that when the buckling factor for $\lambda = 1$ is sufficient, the actual factor will be sufficient as well.

^{c} Not all buckling factors for load case 2b have been calculated. The observation could be made from all other designs that when the buckling factor for $\lambda = 1$ is insufficient, the actual factor will be insufficient as well.

C-1   Regular softwood CLT

C-1-1   3 MW turbine at 100 m

Model no.		A1	A2	A3	A4
Input	Load case	1 Operation	2a Extreme	2a Extreme	2b Torsion
H	[m]	100			
Turbine		3MW			
Class		IC			
Material		CL28h			
n_{sides}		8	8	10	8
$a_{out,T}$	[m]	1.15	1.15	0.93	1.15
$a_{out,B}$	[m]	3.40	3.40	2.74	3.40
t	[m]	0.30	0.30	0.30	0.30
k_{net}		0.75	0.75	0.75	0.75
Output - Matlab					
F_{yT}	[kN]	505	1042	1039	647
M_{xT}	[kNm]	5333	7281	7281	4442
M_{zT}	[kNm]	0	581	579	671
f - Rayleigh	[Hz]	0.330	0.330	0.337	0.330
$\sigma_{t,0,net,d,max}$	[N/mm^2]	8.50	13.84	13.74	10.89
$f_{t,0,net,d}$	[N/mm^2]	16.63	16.63	16.63	16.63
u.c. - tension		0.51	0.83	0.83	0.65
$\sigma_{c,0,net,d,max}$	[N/mm^2]	-10.13	-15.19	-15.08	-12.37
$f_{c,0,net,d}$	[N/mm^2]	24.64	24.64	24.64	24.64
u.c. - compression		0.41	0.62	0.61	0.50
Max. allowable $\tau_{xy,d,max}$	[N/mm^2]	1.10	1.10	1.10	1.10
Max. allowable $\tau_{yz,d,max}$	[N/mm^2]	1.10	1.10	1.10	1.10
Max. allowable $\tau_{xz,d,max}$	[N/mm^2]	1.10	1.10	1.10	1.10
Output - ANSYS					
f - Ansys	[Hz]	0.301	0.301	0.308	0.301
$\sigma_{t,0,d,max}$	[N/mm^2]	6.14	10.50	10.20	7.97
$\sigma_{c,0,d,max}$	[N/mm^2]	-7.59	-11.50	-11.20	-9.25
$\sigma_{t,0,d,net,max}$	[N/mm^2]	8.19	14.00	13.60	10.63
$\sigma_{c,0,d,net,max}$	[N/mm^2]	-10.12	-15.33	-14.93	-12.33
$\tau_{xy,d,max}$	[N/mm^2]	0.01	0.03	0.04	0.03
$\tau_{yz,d,max}$	[N/mm^2]	0.44	1.02	1.03	0.92
$\tau_{xz,d,max}$	[N/mm^2]	0.21	0.37	0.36	0.31
Buckling factor		59.0	31.0	38.0	38.0
Buckling factor for $\lambda = 1$		17.2	19.1	20.1	16.8
Maximum deflection	[m]	1.22	2.11	2.01	1.68
Comparison - ANSYS/Matlab					
Tensile stresses		0.96	1.01	0.99	0.98
Compression stresses		1.00	1.01	0.99	1.00

Input	Model no.	B1	B2	B3	B4	C
	Load case	1 Operation	2a Extreme	2a Extreme	2b Torsion	
H	[m]	100				100
Turbine		3MW				3 MW
Class		IIA				IIIA
Material		CL24h				CL24h
n_{sides}		8	8	10	8	
$a_{out,T}$	[m]	1.15	1.15	0.93	1.15	
$a_{out,B}$	[m]	3.40	3.40	2.74	3.40	
t	[m]	0.30	0.30	0.30	0.30	
k_{net}		0.75	0.75	0.75	0.75	
Output - Matlab						
F_{yT}	[kN]	505	945	941	578	
M_{xT}	[kNm]	5333	6563	6563	3974	The same
M_{zT}	[kNm]	0	527	525	227	model as
f - Rayleigh	[Hz]	0.330	0.330	0.337	0.330	for IIA
$\sigma_{t,0,net,d,max}$	[N/mm^2]	8.50	12.29	12.20	9.38	will
$f_{t,0,net,d}$	[N/mm^2]	14.78	14.78	14.78	14.78	suffice
u.c. - tension		0.57	0.83	0.83	0.63	
$\sigma_{c,0,net,d,max}$	[N/mm^2]	-10.12	-13.65	-13.55	-10.88	
$f_{c,0,net,d}$	[N/mm^2]	21.12	21.12	21.12	21.12	
u.c. - compression		0.48	0.65	0.64	0.52	
Max. allowable $\tau_{xy,d,max}$	[N/mm^2]	1.10	1.10	1.10	1.10	
Max. allowable $\tau_{yz,d,max}$	[N/mm^2]	1.10	1.10	1.10	1.10	
Max. allowable $\tau_{xz,d,max}$	[N/mm^2]	1.10	1.10	1.10	1.10	
Output - ANSYS						
f - Ansys	[Hz]	0.301	0.301	0.308	0.301	
$\sigma_{t,0,d,max}$	[N/mm^2]	6.13	9.24	9.00	6.83	
$\sigma_{c,0,d,max}$	[N/mm^2]	-7.59	-10.30	-10.10	-8.14	
$\sigma_{t,0,d,net,max}$	[N/mm^2]	8.17	12.32	12.00	9.11	The same
$\sigma_{c,0,d,net,max}$	[N/mm^2]	-10.12	-13.73	-13.47	-10.85	model as
$\tau_{xy,d,max}$	[N/mm^2]	0.01	0.03	0.03	0.02	for IIA
$\tau_{yz,d,max}$	[N/mm^2]	0.44	0.93	0.93	0.81	will
$\tau_{xz,d,max}$	[N/mm^2]	0.21	0.32	0.32	0.27	suffice
Buckling factor		59.0	36.0	45.0	45.0	
Buckling factor for $\lambda = 1$		17.2	19.6	20.6	17.0	
Maximum deflection	[m]	1.22	1.86	1.76	1.44	
Comparison - ANSYS/Matlab						
Tensile stresses		0.96	1.00	0.98	0.97	
Compression stresses		1.00	1.01	0.99	1.00	

C-1-2   3 MW turbine at 125 m

Input		D1	D2	D3	D4	D5
Model no.		D1	D2	D3	D4	D5
Load case		1 Operation	2a Extreme	2a Extreme	2b Torsion	2a Extreme
H	[m]	125				
Turbine		3MW				
Class		IC				
Material		CL24h				
n_{sides}		8	8	10	8	10
$a_{out,T}$	[m]	1.15	1.15	0.93	1.15	0.93
$a_{out,B}$	[m]	4.05	4.05	3.26	4.05	3.50
t	[m]	0.45	0.45	0.45	0.45	0.30
k_{net}		0.75	0.75	0.75	0.75	0.75
Output - Matlab						
F_{yT}	[kN]	505	1027	1024	639	1029
M_{xT}	[kNm]	5333	7114	7114	4338	7114
M_{zT}	[kNm]	0	573	571	663	574
f - Rayleigh	[Hz]	0.337	0.337	0.344	0.337	0.332
$\sigma_{t,0,net,d,max}$	[N/mm^2]	6.21	9.72	9.78	7.56	12.07
$f_{t,0,net,d}$	[N/mm^2]	14.78	14.78	14.78	14.78	14.78
u.c. - tension		0.42	0.66	0.66	0.51	0.82
$\sigma_{c,0,net,d,max}$	[N/mm^2]	-7.43	-10.75	-10.81	-8.70	-13.39
$f_{c,0,net,d}$	[N/mm^2]	21.12	21.12	21.12	21.12	21.12
u.c. - compression		0.35	0.51	0.51	0.41	0.63
Max. allowable $\tau_{xy,d,max}$	[N/mm^2]	1.10	1.10	1.10	1.10	1.10
Max. allowable $\tau_{yz,d,max}$	[N/mm^2]	1.10	1.10	1.10	1.10	1.10
Max. allowable $\tau_{xz,d,max}$	[N/mm^2]	1.10	1.10	1.10	1.10	1.10
Output - ANSYS						
f - Ansys	[Hz]	0.301	0.301	0.308	0.301	0.294
$\sigma_{t,0,d,max}$	[N/mm^2]	4.47	7.31	7.11	5.50	8.80
$\sigma_{c,0,d,max}$	[N/mm^2]	-5.57	-8.14	-7.93	-6.51	-9.84
$\sigma_{t,0,d,net,max}$	[N/mm^2]	5.96	9.75	9.48	7.33	11.73
$\sigma_{c,0,d,net,max}$	[N/mm^2]	-7.43	-10.85	-10.57	-8.68	-13.12
$\tau_{xy,d,max}$	[N/mm^2]	0.01	0.02	0.02	0.02	0.03
$\tau_{yz,d,max}$	[N/mm^2]	0.30	0.69	0.69	0.62	0.97
$\tau_{xz,d,max}$	[N/mm^2]	0.16	0.23	0.23	0.18	0.32
Buckling factor		114.0	71.0	76.0	85.0	N/A[c]
Buckling factor for $\lambda = 1$		20.5	23.6	24.7	20.3	21.5
Maximum deflection	[m]	1.10	1.94	1.84	1.56	2.11
Comparison - ANSYS/Matlab						
Tensile stresses		0.96	1.00	0.97	0.97	0.97
Compression stresses		1.00	1.01	0.98	1.00	0.98

Input	Model no.	E1	E2	E3	E4	F
	Load case	1 Operation	2a Extreme	2a Extreme	2b Torsion	
H	[m]	125				125
Turbine		3MW				3MW
Class		IIA				IIIA
Material		CL24h				CL24h
n_{sides}		8	8	10	8	
$a_{out,T}$	[m]	1.15	1.15	0.93	1.15	
$a_{out,B}$	[m]	4.05	4.05	3.26	4.05	
t	[m]	0.45	0.45	0.45	0.45	
k_{net}		0.75	0.75	0.75	0.75	
Output - Matlab						
F_{yT}	[kN]	505	919	916	565	
M_{xT}	[kNm]	5333	6341	6341	3838	The same
M_{zT}	[kNm]	0	513	511	586	model as
f - Rayleigh	[Hz]	0.337	0.337	0.344	0.337	for IIA
$\sigma_{t,0,net,d,max}$	[N/mm^2]	6.21	8.54	8.60	6.49	will
$f_{t,0,net,d}$	[N/mm^2]	14.78	14.78	14.78	14.78	suffice
u.c. - tension		0.42	0.58	0.58	0.44	
$\sigma_{c,0,net,d,max}$	[N/mm^2]	-7.43	-9.58	-9.63	-7.64	
$f_{c,0,net,d}$	[N/mm^2]	21.12	21.12	21.12	21.12	
u.c. - compression		0.35	0.45	0.46	0.36	
Max. allowable $\tau_{xy,d,max}$	[N/mm^2]	1.10	1.10	1.10	1.10	
Max. allowable $\tau_{yz,d,max}$	[N/mm^2]	1.10	1.10	1.10	1.10	
Max. allowable $\tau_{xz,d,max}$	[N/mm^2]	1.10	1.10	1.10	1.10	
Output - ANSYS						
f - Ansys	[Hz]	0.301	0.301	0.308	0.301	
$\sigma_{t,0,d,max}$	[N/mm^2]	4.47	6.39	6.21	4.69	
$\sigma_{c,0,d,max}$	[N/mm^2]	-5.57	-7.23	-7.04	-5.72	
$\sigma_{t,0,d,net,max}$	[N/mm^2]	5.96	8.52	8.28	6.25	The same
$\sigma_{c,0,d,net,max}$	[N/mm^2]	-7.43	-9.64	-9.39	-7.63	model as
$\tau_{xy,d,max}$	[N/mm^2]	0.01	0.02	0.02	0.02	for IIA
$\tau_{yz,d,max}$	[N/mm^2]	0.30	0.62	0.62	0.55	will
$\tau_{xz,d,max}$	[N/mm^2]	0.16	0.20	0.20	0.16	suffice
Buckling factor		113.0	82.0	86.0	103.0	
Buckling factor for $\lambda = 1$		20.5	24.0	25.2	20.4	
Maximum deflection	[m]	1.10	1.67	1.59	1.31	
Comparison - ANSYS/Matlab						
Tensile stresses		0.96	1.00	0.96	0.96	
Compression stresses		1.00	1.01	0.97	1.00	

C-1-3   5 MW turbine at 125 m

Model no.		G1	G2	G3	G4
Input	Load case	1 Operation	2a Extreme	2a Extreme	2b Torsion
H	[m]	125			
Turbine		5MW			
Class		IC			
Material		CL30h			
n_{sides}		8	8	10	8
$a_{out,T}$	[m]	1.45	1.45	1.17	1.45
$a_{out,B}$	[m]	4.25	4.25	3.42	4.25
t	[m]	0.45	0.45	0.45	0.45
k_{net}		0.75	0.75	0.75	0.75
Output - Matlab					
F_{yT}	[kN]	1213	2326	2319	1378
M_{xT}	[kNm]	16731	20659	20659	12728
M_{zT}	[kNm]	0	1622	1617	1786
f - Rayleigh	[Hz]	0.290	0.290	0.296	0.290
$\sigma_{t,0,net,d,max}$	[N/mm^2]	11.51	16.78	16.80	12.46
$f_{t,0,net,d}$	[N/mm^2]	19.01	19.01	19.01	19.01
u.c. - tension		0.61	0.88	0.88	0.66
$\sigma_{c,0,net,d,max}$	[N/mm^2]	-13.34	-18.33	-18.35	-14.19
$f_{c,0,net,d}$	[N/mm^2]	26.40	26.40	26.40	26.40
u.c. - compression		0.51	0.69	0.70	0.54
Max. allowable $\tau_{xy,d,max}$	[N/mm^2]	1.10	1.10	1.10	1.10
Max. allowable $\tau_{yz,d,max}$	[N/mm^2]	1.10	1.10	1.10	1.10
Max. allowable $\tau_{xz,d,max}$	[N/mm^2]	1.10	1.10	1.10	1.10
Output - ANSYS					
f - Ansys	[Hz]	0.265	0.265	0.271	0.265
$\sigma_{t,0,d,max}$	[N/mm^2]	8.35	12.60	12.30	9.09
$\sigma_{c,0,d,max}$	[N/mm^2]	-10.00	-13.80	-13.50	-10.60
$\sigma_{t,0,d,net,max}$	[N/mm^2]	11.13	16.80	16.40	12.12
$\sigma_{c,0,d,net,max}$	[N/mm^2]	-13.33	-18.40	-18.00	-14.13
$\tau_{xy,d,max}$	[N/mm^2]	0.02	0.03	0.03	0.03
$\tau_{yz,d,max}$	[N/mm^2]	0.58	1.27	1.28	1.08
$\tau_{xz,d,max}$	[N/mm^2]	0.27	0.37	0.37	0.29
Buckling factor		N/A[a]	40.0	47.0	N/A[a]
Buckling factor for $\lambda = 1$		16.4	18.4	19.2	16.2
Maximum deflection	[m]	1.83	2.85	2.71	2.16
Comparison - ANSYS/Matlab					
Tensile stresses		0.97	1.00	0.98	0.97
Compression stresses		1.00	1.00	0.98	1.00

Input	Model no.	H1	H2	H3	H4
	Load case	1 Operation	2a Extreme	2a Extreme	2b Torsion
H	[m]	125			
Turbine		5MW			
Class		IIA			
Material		CL28h			
n_{sides}		8	8	10	8
$a_{out,T}$	[m]	1.45	1.45	1.17	1.45
$a_{out,B}$	[m]	4.25	4.25	3.42	4.25
t	[m]	0.45	0.45	0.45	0.45
k_{net}		0.75	0.75	0.75	0.75
Output - Matlab					
F_{yT}	[kN]	1213	2090	2083	1281
M_{xT}	[kNm]	16731	18377	18377	11258
M_{zT}	[kNm]	0	1457	1452	1660
f - Rayleigh	[Hz]	0.280	0.280	0.285	0.280
$\sigma_{t,0,net,d,max}$	[N/mm^2]	11.51	14.86	14.88	11.24
$f_{t,0,net,d}$	[N/mm^2]	16.63	16.63	16.63	16.63
u.c. - tension		0.69	0.89	0.89	0.68
$\sigma_{c,0,net,d,max}$	[N/mm^2]	-13.32	-16.38	-16.40	-12.93
$f_{c,0,net,d}$	[N/mm^2]	24.64	24.64	24.64	24.64
u.c. - compression		0.54	0.66	0.67	0.52
Max. allowable $\tau_{xy,d,max}$	[N/mm^2]	1.10	1.10	1.10	1.10
Max. allowable $\tau_{yz,d,max}$	[N/mm^2]	1.10	1.10	1.10	1.10
Max. allowable $\tau_{xz,d,max}$	[N/mm^2]	1.10	1.10	1.10	1.10
Output - ANSYS					
f - Ansys	[Hz]	0.255	0.255	0.261	0.255
$\sigma_{t,0,d,max}$	[N/mm^2]	8.36	11.10	10.90	8.18
$\sigma_{c,0,d,max}$	[N/mm^2]	-9.98	-12.30	-12.10	-9.69
$\sigma_{t,0,d,net,max}$	[N/mm^2]	11.15	14.80	14.53	10.91
$\sigma_{c,0,d,net,max}$	[N/mm^2]	-13.31	-16.40	-16.13	-12.92
$\tau_{xy,d,max}$	[N/mm^2]	0.02	0.03	0.03	0.03
$\tau_{yz,d,max}$	[N/mm^2]	0.58	1.14	1.15	1.00
$\tau_{xz,d,max}$	[N/mm^2]	0.23	0.33	0.33	0.26
Buckling factor		N/A[a]	43.0	49.0	N/A[a]
Buckling factor for $\lambda = 1$		15.2	17.4	18.3	15.2
Maximum deflection	[m]	2.00	2.73	2.60	2.11
Comparison - ANSYS/Matlab					
Tensile stresses		0.97	1.00	0.98	0.97
Compression stresses		1.00	1.00	0.98	1.00

	Model no.	I1	I2	I3	I4
	Load case	1 Operation	2a Extreme	2a Extreme	2b Torsion
Input					
H	[m]	125			
Turbine		5MW			
Class		IIIA			
Material		CL24h			
n_{sides}		8	8	10	8
$a_{out,T}$	[m]	1.45	1.45	1.17	1.45
$a_{out,B}$	[m]	4.25	4.25	3.42	4.25
t	[m]	0.45	0.45	0.45	0.45
k_{net}		0.75	0.75	0.75	0.75
Output - Matlab					
F_{yT}	[kN]	1213	1558	1558	997
M_{xT}	[kNm]	16731	13980	13980	8499
M_{zT}	[kNm]	0	1086	1086	1293
f - Rayleigh	[Hz]	0.280	0.280	0.285	0.280
$\sigma_{t,0,net,d,max}$	[N/mm^2]	11.51	10.95	11.00	8.55
$f_{t,0,net,d}$	[N/mm^2]	14.78	14.78	14.78	14.78
u.c. - tension		0.78	0.74	0.74	0.58
$\sigma_{c,0,net,d,max}$	[N/mm^2]	-13.32	-12.48	-12.52	-10.25
$f_{c,0,net,d}$	[N/mm^2]	21.12	21.12	21.12	21.12
u.c. - compression		0.63	0.59	0.59	0.49
Max. allowable $\tau_{xy,d,max}$	[N/mm^2]	1.10	1.10	1.10	1.10
Max. allowable $\tau_{yz,d,max}$	[N/mm^2]	1.10	1.10	1.10	1.10
Max. allowable $\tau_{xz,d,max}$	[N/mm^2]	1.10	1.10	1.10	1.10
Output - ANSYS					
f - Ansys	[Hz]	0.255	0.255	0.261	0.255
$\sigma_{t,0,d,max}$	[N/mm^2]	8.36	8.17	8.00	6.17
$\sigma_{c,0,d,max}$	[N/mm^2]	-9.98	-9.41	-9.22	-7.68
$\sigma_{t,0,d,net,max}$	[N/mm^2]	11.15	10.89	10.67	8.23
$\sigma_{c,0,d,net,max}$	[N/mm^2]	-13.31	-12.55	-12.29	-10.24
$\tau_{xy,d,max}$	[N/mm^2]	0.02	0.02	0.02	0.02
$\tau_{yz,d,max}$	[N/mm^2]	0.58	0.85	0.86	0.78
$\tau_{xz,d,max}$	[N/mm^2]	0.27	0.26	0.26	0.21
Buckling factor		N/A[a]	57.0	65.0	N/A[a]
Buckling factor for $\lambda = 1$		15.2	18.3	19.1	15.5
Maximum deflection	[m]	2.00	2.05	1.95	1.64
Comparison - ANSYS/Matlab					
Tensile stresses		0.97	0.99	0.97	0.96
Compression stresses		1.00	1.01	0.98	1.00

C-2 Hardwood CLT

	Model no.	J1	J2	K1	K2
	Load case	1 Operation	2a Extreme	1 Operation	2a Extreme
Input					
H	[m]	100		125	
Turbine		3MW		3MW	
Class		IC		IC	
Material		CL40h		CL40h	
n_{sides}		10	10	10	10
$a_{out,T}$	[m]	0.93	0.93	0.93	0.93
$a_{out,B}$	[m]	2.74	2.74	3.26	3.26
t	[m]	0.30	0.30	0.45	0.45
k_{net}		0.75	0.75	0.75	0.75
Output - Matlab					
F_{yT}	[kN]	505	1045	505	1034
M_{xT}	[kNm]	5333	7281	5333	7114
M_{zT}	[kNm]	0	583	0	577
f - Rayleigh	[Hz]	0.323	0.323	0.321	0.321
$\sigma_{t,0,net,d,max}$	[N/mm^2]	8.43	13.73	6.25	9.79
$f_{t,0,net,d}$	[N/mm^2]	25.34	25.34	25.34	25.34
u.c. - tension		0.33	0.54	0.25	0.39
$\sigma_{c,0,net,d,max}$	[N/mm^2]	-10.17	-15.25	-7.57	-10.96
$f_{c,0,net,d}$	[N/mm^2]	35.20	35.20	35.20	35.20
u.c. - compression		0.29	0.43	0.22	0.31
Max. allowable $\tau_{xy,d,max}$	[N/mm^2]	1.10	1.10	1.10	1.10
Max. allowable $\tau_{yz,d,max}$	[N/mm^2]	1.10	1.10	1.10	1.10
Max. allowable $\tau_{xz,d,max}$	[N/mm^2]	1.10	1.10	1.10	1.10
Output - ANSYS					
f - Ansys	[Hz]	0.298	0.298	0.292	0.292
$\sigma_{t,0,d,max}$	[N/mm^2]	5.92	10.00	4.29	7.01
$\sigma_{c,0,d,max}$	[N/mm^2]	-7.47	-11.20	-5.47	-7.96
$\sigma_{t,0,d,net,max}$	[N/mm^2]	7.89	13.33	5.72	9.35
$\sigma_{c,0,d,net,max}$	[N/mm^2]	-9.96	-14.93	-7.29	-10.61
$\tau_{xy,d,max}$	[N/mm^2]	0.01	0.03	0.01	0.02
$\tau_{yz,d,max}$	[N/mm^2]	0.45	1.03	0.31	0.70
$\tau_{xz,d,max}$	[N/mm^2]	0.21	0.30	0.16	0.23
Buckling factor		N/A[a]	40.0	N/A[a]	75.0
Buckling factor for $\lambda = 1$		16.8	19.0	19.2	22.4
Maximum deflection	[m]	1.16	1.97	1.05	1.80
Comparison - ANSYS/Matlab					
Tensile stresses		0.94	0.97	0.92	0.95
Compression stresses		0.98	0.98	0.96	0.97

	Model no.	L1	L2
	Load case	1	2a
Input		Operation	Extreme
H	[m]	125	
Turbine		5MW	
Class		IC	
Material		CL40h	
n_{sides}		10	10
$a_{out,T}$	[m]	1.17	1.17
$a_{out,B}$	[m]	3.42	3.42
t	[m]	0.45	0.45
k_{net}		0.75	0.75
Output - Matlab			
F_{yT}	[kN]	1213	2347
M_{xT}	[kNm]	16731	20659
M_{zT}	[kNm]	0	1637
f - Rayleigh	[Hz]	0.272	0.272
$\sigma_{t,0,net,d,max}$	[N/mm^2]	11.54	16.90
$f_{t,0,net,d}$	[N/mm^2]	25.34	25.34
u.c. - tension		0.46	0.67
$\sigma_{c,0,net,d,max}$	[N/mm^2]	-13.49	-18.60
$f_{c,0,net,d}$	[N/mm^2]	35.20	35.20
u.c. - compression		0.38	0.53
Max. allowable $\tau_{xy,d,max}$	[N/mm^2]	1.10	1.10
Max. allowable $\tau_{yz,d,max}$	[N/mm^2]	1.10	1.10
Max. allowable $\tau_{xz,d,max}$	[N/mm^2]	1.10	1.10
Output - ANSYS			
f - Ansys	[Hz]	0.251	0.251
$\sigma_{t,0,d,max}$	[N/mm^2]	8.20	12.20
$\sigma_{c,0,d,max}$	[N/mm^2]	-9.85	-13.60
$\sigma_{t,0,d,net,max}$	[N/mm^2]	10.93	16.27
$\sigma_{c,0,d,net,max}$	[N/mm^2]	-13.13	-18.13
$\tau_{xy,d,max}$	[N/mm^2]	0.02	0.03
$\tau_{yz,d,max}$	[N/mm^2]	0.60	1.29
$\tau_{xz,d,max}$	[N/mm^2]	0.27	0.38
Buckling factor		N/A[a]	43.5
Buckling factor for $\lambda = 1$		14.7	16.7
Maximum deflection	[m]	1.91	2.93
Comparison - ANSYS/Matlab			
Tensile stresses		0.95	0.96
Compression stresses		0.97	0.97

C-3 Softwood LVL

C-3-1 Kerto-Q

Model no.		M1	M2	N1	N2
Input	Load case	1 Operation	2a Extreme	1 Operation	2a Extreme
H	[m]	100		125	
Turbine		3MW		3MW	
Class		IC		IC	
Material		KERTO-Q		KERTO-Q	
n_{sides}		10	10	10	10
$a_{out,T}$	[m]	0.93	0.93	0.93	0.93
$a_{out,B}$	[m]	2.70	2.70	3.05	3.05
t	[m]	0.21	0.21	0.35	0.35
k_{net}		1.00	1.00	1.00	1.00
Output - Matlab					
F_{yT}	[kN]	505	1045	505	1034
M_{xT}	[kNm]	5333	7281	5333	7114
M_{zT}	[kNm]	0	583	0	577
f - Rayleigh	[Hz]	0.322	0.322	0.321	0.321
$\sigma_{t,0,net,d,max}$	[N/mm^2]	8.62	14.25	5.96	9.63
$f_{t,0,net,d}$	[N/mm^2]	21.64	21.64	21.64	21.64
u.c. - tension		0.40	0.66	0.28	0.45
$\sigma_{c,0,net,d,max}$	[N/mm^2]	-10.23	-15.58	-7.07	-10.59
$f_{c,0,net,d}$	[N/mm^2]	23.83	23.83	23.83	23.83
u.c. - compression		0.43	0.65	0.30	0.44
Max. allowable $\tau_{xy,d,max}$	[N/mm^2]	0.55	0.55	0.55	0.55
Max. allowable $\tau_{yz,d,max}$	[N/mm^2]	4.13	4.13	4.13	4.13
Max. allowable $\tau_{xz,d,max}$	[N/mm^2]	1.19	1.19	1.19	1.19
Output - ANSYS					
f - Ansys	[Hz]	0.296	0.296	0.292	0.292
$\sigma_{t,0,d,max}$	[N/mm^2]	8.19	14.00	5.58	9.34
$\sigma_{c,0,d,max}$	[N/mm^2]	-10.10	-15.40	-6.90	-10.30
$\sigma_{t,0,d,net,max}$	[N/mm^2]	8.19	14.00	5.58	9.34
$\sigma_{c,0,d,net,max}$	[N/mm^2]	-10.10	-15.40	-6.90	-10.30
$\tau_{xy,d,max}$	[N/mm^2]	0.02	0.04	0.01	0.02
$\tau_{yz,d,max}$	[N/mm^2]	0.63	1.44	0.41	0.91
$\tau_{xz,d,max}$	[N/mm^2]	0.32	0.55	0.18	0.28
Buckling factor		N/A[a]	21.0	N/A[a]	59.0
Buckling factor for $\lambda = 1$		16.6	18.0	19.6	22.4
Maximum deflection	[m]	1.29	2.18	1.18	2.03
Comparison - ANSYS/Matlab					
Tensile stresses		0.95	0.98	0.94	0.97
Compression stresses		0.99	0.99	0.98	0.97

Input	Model no.	N3	N4	N5	N6
	Load case	2a Extreme	2a Extreme	2a Extreme	2b Torsion
H	[m]	125			
Turbine		3MW			
Class		IC			
Material		KERTO-Q			
n_{sides}		10	10	10	10
$a_{out,T}$	[m]	0.93	0.93	0.93	0.93
$a_{out,B}$	[m]	3.26	4.10	5.10	3.26
t	[m]	0.28	0.14	0.08	0.28
k_{net}		1.00	1.00	1.00	1.00
Output - Matlab					
F_{yT}	[kN]	1032	1024	1015	641
M_{xT}	[kNm]	7114	7114	7114	4338
M_{zT}	[kNm]	575	571	566	665
f - Rayleigh	[Hz]	0.327	0.344	0.367	0.327
$\sigma_{t,0,net,d,max}$	[N/mm^2]	10.48	14.33	19.02	8.23
$f_{t,0,net,d}$	[N/mm^2]	21.64	21.64	21.64	21.64
u.c. - tension		0.48	0.66	0.88	0.38
$\sigma_{c,0,net,d,max}$	[N/mm^2]	-11.56	-16.17	-22.27	-9.42
$f_{c,0,net,d}$	[N/mm^2]	23.83	23.83	23.83	23.83
u.c. - compression		0.49	0.68	0.93	0.40
Max. allowable $\tau_{xy,d,max}$	[N/mm^2]	0.55	0.55	0.55	0.55
Max. allowable $\tau_{yz,d,max}$	[N/mm^2]	4.13	4.13	4.13	4.13
Max. allowable $\tau_{xz,d,max}$	[N/mm^2]	1.19	1.19	1.19	1.19
Output - ANSYS					
f - Ansys	[Hz]	0.293	0.294	0.299	0.293
$\sigma_{t,0,d,max}$	[N/mm^2]	10.20	14.10	18.60	7.91
$\sigma_{c,0,d,max}$	[N/mm^2]	-11.30	-16.00	-22.30	-9.24
$\sigma_{t,0,d,net,max}$	[N/mm^2]	10.20	14.10	18.60	7.91
$\sigma_{c,0,d,net,max}$	[N/mm^2]	-11.30	-16.00	-22.30	-9.24
$\tau_{xy,d,max}$	[N/mm^2]	0.03	0.11	0.32	0.03
$\tau_{yz,d,max}$	[N/mm^2]	1.08	1.76	2.48	0.96
$\tau_{xz,d,max}$	[N/mm^2]	0.37	0.64	1.29	0.33
Buckling factor		36.0	4.9	0.9	N/A[a]
Buckling factor for $\lambda = 1$		22.0	4.9	0.9	19.0
Maximum deflection	[m]	2.09	2.27	2.33	1.68
Comparison - ANSYS/Matlab					
Tensile stresses		0.97	0.98	0.98	0.96
Compression stresses		0.98	0.99	1.00	0.98

	Model no.	N7	N8	O1	O2
Input	Load case	2a Extreme	2a Extreme	1 Operation	2a Extreme
H	[m]	125		125	
Turbine		3MW		5MW	
Class		IC		IC	
Material		KERTO-Q		KERTO-Q	
n_{sides}		10	10	10	10
$a_{out,T}$	[m]	0.93	0.93	1.17	1.17
$a_{out,B}$	[m]	3.20	2.90	3.80	3.80
t	[m]	0.30	0.45	0.25	0.25
k_{net}		1.00	1.00	1.00	1.00
Output - Matlab					
F_{yT}	[kN]	1032	1033	1213	2318
M_{xT}	[kNm]	7114	7114	16731	20659
M_{zT}	[kNm]	576	576	0	1617
f - Rayleigh	[Hz]	0.326	0.323	0.296	0.296
$\sigma_{t,0,net,d,max}$	[N/mm^2]	10.16	8.62	12.26	17.63
$f_{t,0,net,d}$	[N/mm^2]	21.64	21.64	21.64	21.64
u.c. - tension		0.47	0.40	0.57	0.81
$\sigma_{c,0,net,d,max}$	[N/mm^2]	-11.20	-9.45	-14.43	-19.39
$f_{c,0,net,d}$	[N/mm^2]	23.83	23.83	23.83	23.83
u.c. - compression		0.47	0.40	0.61	0.81
Max. allowable $\tau_{xy,d,max}$	[N/mm^2]	0.55	0.55	0.55	0.55
Max. allowable $\tau_{yz,d,max}$	[N/mm^2]	4.13	4.13	4.13	4.13
Max. allowable $\tau_{xz,d,max}$	[N/mm^2]	1.19	1.19	1.19	1.19
Output - ANSYS					
f - Ansys	[Hz]	0.293	0.296	0.266	0.266
$\sigma_{t,0,d,max}$	[N/mm^2]	9.89	8.26	11.70	17.30
$\sigma_{c,0,d,max}$	[N/mm^2]	11.00	9.16	-14.20	-19.10
$\sigma_{t,0,d,net,max}$	[N/mm^2]	9.89	8.26	11.70	17.30
$\sigma_{c,0,d,net,max}$	[N/mm^2]	11.00	9.16	-14.20	-19.10
$\tau_{xy,d,max}$	[N/mm^2]	0.03	0.02	0.03	0.06
$\tau_{yz,d,max}$	[N/mm^2]	1.02	0.74	0.95	2.06
$\tau_{xz,d,max}$	[N/mm^2]	0.34	0.22	0.49	0.69
Buckling factor		N/A[c]	N/A[c]	N/A[a]	14.0
Buckling factor for $\lambda = 1$		22.2	23.6	15.8	13.3
Maximum deflection	[m]	2.06	1.88	0.03	2.95
Comparison - ANSYS/Matlab					
Tensile stresses		0.97	0.96	0.95	0.98
Compression stresses		-0.98	-0.97	0.98	0.99

C-3-2   Kerto-S

Model no.		P1	P2	Q1	Q2	Q3
Input	Load case	1 Operation	2a Extreme	1 Operation	2a Extreme	2a Extreme
H	[m]	100		125		
Turbine		3MW		3MW		
Class		IC		IC		
Material		KERTO-S		KERTO-S		
n_{sides}		10	10	10	10	10
$a_{out,T}$	[m]	0.93	0.93	0.93	0.93	0.93
$a_{out,B}$	[m]	3.00	3.00	3.50	3.50	3.26
t	[m]	0.12	0.12	0.16	0.16	0.20
k_{net}		1.00	1.00	1.00	1.00	1.00
Output - Matlab						
F_{yT}	[kN]	505	1038	505	1028	1030
M_{xT}	[kNm]	5333	7281	5333	7114	7114
M_{zT}	[kNm]	0	579	0	574	574
f - Rayleigh	[Hz]	0.339	0.339	0.334	0.334	0.331
$\sigma_{t,0,net,d,max}$	[N/mm^2]	12.46	20.19	9.68	15.43	13.92
$f_{t,0,net,d}$	[N/mm^2]	29.13	29.13	29.13	29.13	29.13
u.c. - tension		0.43	0.69	0.33	0.53	0.48
$\sigma_{c,0,net,d,max}$	[N/mm^2]	-15.05	-22.22	-11.71	-17.05	-15.28
$f_{c,0,net,d}$	[N/mm^2]	32.08	32.08	32.08	32.08	32.08
u.c. - compression		0.47	0.69	0.36	0.53	0.48
Max. allowable $\tau_{xy,d,max}$	[N/mm^2]	0.28	0.28	0.28	0.28	0.28
Max. allowable $\tau_{yz,d,max}$	[N/mm^2]	3.76	3.76	3.76	3.76	3.76
Max. allowable $\tau_{xz,d,max}$	[N/mm^2]	2.11	2.11	2.11	2.11	2.11
Output - ANSYS						
f - Ansys	[Hz]	0.304	0.304	0.294	0.294	0.296
$\sigma_{t,0,d,max}$	[N/mm^2]	11.90	20.00	9.20	15.20	13.70
$\sigma_{c,0,d,max}$	[N/mm^2]	-14.90	-21.90	-11.60	-16.80	-15.10
$\sigma_{t,0,d,net,max}$	[N/mm^2]	11.90	20.00	9.20	15.20	13.70
$\sigma_{c,0,d,net,max}$	[N/mm^2]	-14.90	-21.90	-11.60	-16.80	-15.10
$\tau_{xy,d,max}$	[N/mm^2]	0.04	0.09	0.02	0.07	0.05
$\tau_{yz,d,max}$	[N/mm^2]	0.96	2.22	0.75	1.71	1.46
$\tau_{xz,d,max}$	[N/mm^2]	0.56	0.85	0.42	0.63	0.54
Buckling factor		N/A[a]	5.8	N/A[a]	10.1	N/A[c]
Buckling factor for $\lambda = 1$		9.5	5.6	17.0	9.7	18.3
Maximum deflection	[m]	1.29	2.16	1.30	2.23	2.15
Comparison - ANSYS/Matlab						
Tensile stresses		0.95	0.99	0.95	0.98	0.98
Compression stresses		0.99	0.99	0.99	0.99	0.99

Input	Model no.	Q4	Q5	Q6
	Load case	2a Extreme	2a Extreme	2a Extreme
H	[m]	125		125
Turbine		3MW		3 MW
Class		IC		IC
Material		KERTO-S		KERTO-S
n_{sides}		10	10	10
$a_{out,T}$	[m]	0.93	0.93	0.93
$a_{out,B}$	[m]	3.62	2.90	2.65
t	[m]	0.14	0.30	0.45
k_{net}		1.00	1.00	1.00
Output - Matlab				
F_{yT}	[kN]	1029	1032	1031
M_{xT}	[kNm]	7114	7114	7114
M_{zT}	[kNm]	574	575	575
f - Rayleigh	[Hz]	0.332	0.326	0.327
$\sigma_{t,0,net,d,max}$	[N/mm^2]	16.70	11.66	9.82
$f_{t,0,net,d}$	[N/mm^2]	29.13	29.13	29.13
u.c. - tension		0.57	0.40	0.34
$\sigma_{c,0,net,d,max}$	[N/mm^2]	-18.50	-12.73	-10.71
$f_{c,0,net,d}$	[N/mm^2]	32.08	32.08	32.08
u.c. - compression		0.58	0.40	0.33
Max. allowable $\tau_{xy,d,max}$	[N/mm^2]	0.28	0.28	0.28
Max. allowable $\tau_{yz,d,max}$	[N/mm^2]	3.76	3.76	3.76
Max. allowable $\tau_{xz,d,max}$	[N/mm^2]	2.11	2.11	2.11
Output - ANSYS				
f - Ansys	[Hz]	0.290	0.298	0.303
$\sigma_{t,0,d,max}$	[N/mm^2]	16.50	11.40	9.44
$\sigma_{c,0,d,max}$	[N/mm^2]	-18.30	-12.50	10.40
$\sigma_{t,0,d,net,max}$	[N/mm^2]	16.50	11.40	9.44
$\sigma_{c,0,d,net,max}$	[N/mm^2]	-18.30	-12.50	10.40
$\tau_{xy,d,max}$	[N/mm^2]	0.09	0.03	0.02
$\tau_{yz,d,max}$	[N/mm^2]	1.89	1.07	0.77
$\tau_{xz,d,max}$	[N/mm^2]	0.69	0.37	0.22
Buckling factor		N/A[c]	N/A[c]	N/A[c]
Buckling factor for $\lambda = 1$		6.6	23.6	25.4
Maximum deflection	[m]	2.33	1.98	1.78
Comparison - ANSYS/Matlab				
Tensile stresses		0.99	0.98	0.96
Compression stresses		0.99	0.98	-0.97

	Model no.	R1	R2	S1
Input	Load case	1 Operation	2a Extreme	2a Extreme
H	[m]	125		125
Turbine		5MW		5MW
Class		IC		IIIA
Material		KERTO-S		KERTO-S
n_{sides}		10	10	10
$a_{out,T}$	[m]	1.17	1.17	1.17
$a_{out,B}$	[m]	3.70	3.70	4.20
t	[m]	0.19	0.19	0.13
k_{net}		1.00	1.00	1.00
Output - Matlab				
F_{yT}	[kN]	1213	2323	1558
M_{xT}	[kNm]	16731	20659	13980
M_{zT}	[kNm]	0	1620	1086
f - Rayleigh	[Hz]	0.292	0.292	0.296
$\sigma_{t,0,net,d,max}$	[N/mm^2]	15.97	23.30	18.35
$f_{t,0,net,d}$	[N/mm^2]	29.13	29.13	29.13
u.c. - tension		0.55	0.80	0.63
$\sigma_{c,0,net,d,max}$	[N/mm^2]	-18.67	-25.47	-21.42
$f_{c,0,net,d}$	[N/mm^2]	32.08	32.08	32.08
u.c. - compression		0.58	0.79	0.67
Max. allowable $\tau_{xy,d,max}$	[N/mm^2]	0.28	0.28	0.28
Max. allowable $\tau_{yz,d,max}$	[N/mm^2]	3.76	3.76	3.76
Max. allowable $\tau_{xz,d,max}$	[N/mm^2]	2.11	2.11	2.11
Output - ANSYS				
f - Ansys	[Hz]	0.264	0.264	0.260
$\sigma_{t,0,d,max}$	[N/mm^2]	15.30	23.00	18.00
$\sigma_{c,0,d,max}$	[N/mm^2]	-18.50	-25.20	-21.20
$\sigma_{t,0,d,net,max}$	[N/mm^2]	15.30	23.00	18.00
$\sigma_{c,0,d,net,max}$	[N/mm^2]	-18.50	-25.20	-21.20
$\tau_{xy,d,max}$	[N/mm^2]	0.04	0.08	0.09
$\tau_{yz,d,max}$	[N/mm^2]	1.24	2.67	2.33
$\tau_{xz,d,max}$	[N/mm^2]	0.64	0.93	0.81
Buckling factor		N/A[a]	8.4	4.2
Buckling factor for $\lambda = 1$		12.7	8.1	4.0
Maximum deflection	[m]	2.01	3.10	2.16
Comparison - ANSYS/Matlab				
Tensile stresses		0.96	0.99	0.98
Compression stresses		0.99	0.99	0.99

C-4 Hardwood LVL

C-4-1 BauBuche Q

Model no.		T1	T2	T3
Load case		1 Operation	2a Extreme	2a Extreme
Input				
H	[m]	100		
Turbine		3MW		
Class		IC		
Material		BAUBUCHE-Q		
n_{sides}		10	10	10
$a_{out,T}$	[m]	0.93	0.93	0.93
$a_{out,B}$	[m]	3.10	3.10	2.70
t	[m]	0.13	0.13	0.19
k_{net}		1.00	1.00	1.00
Output - Matlab				
F_{yT}	[kN]	505	1041	1047
M_{xT}	[kNm]	5333	7281	7281
M_{zT}	[kNm]	0	581	584
f - Rayleigh	[Hz]	0.331	0.331	0.318
$\sigma_{t,0,net,d,max}$	[N/mm^2]	11.14	17.92	15.51
$f_{t,0,net,d}$	[N/mm^2]	33.29	33.29	33.29
u.c. - tension		0.33	0.54	0.47
$\sigma_{c,0,net,d,max}$	[N/mm^2]	-13.68	-19.97	-17.11
$f_{c,0,net,d}$	[N/mm^2]	22.18	22.18	22.18
u.c. - compression		0.62	0.90	0.77
Max. allowable $\tau_{xy,d,max}$	[N/mm^2]	3.03	3.03	3.03
Max. allowable $\tau_{yz,d,max}$	[N/mm^2]	8.25	8.25	8.25
Max. allowable $\tau_{xz,d,max}$	[N/mm^2]	3.03	3.03	3.03
Output - ANSYS				
f - Ansys	[Hz]	0.298	0.298	0.294
$\sigma_{t,0,d,max}$	[N/mm^2]	10.60	17.70	15.20
$\sigma_{c,0,d,max}$	[N/mm^2]	-13.50	-19.70	-16.80
$\sigma_{t,0,d,net,max}$	[N/mm^2]	10.60	17.70	15.20
$\sigma_{c,0,d,net,max}$	[N/mm^2]	-13.50	-19.70	-16.80
$\tau_{xy,d,max}$	[N/mm^2]	0.03	0.09	0.05
$\tau_{yz,d,max}$	[N/mm^2]	0.87	2.04	1.57
$\tau_{xz,d,max}$	[N/mm^2]	0.54	0.78	0.61
Buckling factor		N/A[a]	6.2	18.0
Buckling factor for $\lambda = 1$		10.0	5.9	17.0
Maximum deflection	[m]	1.29	2.17	2.12
Comparison - ANSYS/Matlab				
Tensile stresses		0.95	0.99	0.98
Compression stresses		0.99	0.99	0.98

Input	Model no.	U1	U2	U3	U4
	Load case	1 Operation	2a Extreme	2a Extreme	2a Extreme
H	[m]	125			
Turbine		3MW			
Class		IC			
Material		BAUBUCHE-Q			
n_{sides}		10	10	10	10
$a_{out,T}$	[m]	0.93	0.93	0.93	0.93
$a_{out,B}$	[m]	3.26	3.26	3.20	2.90
t	[m]	0.26	0.26	0.30	0.45
k_{net}		1.00	1.00	1.00	1.00
Output - Matlab					
F_{yT}	[kN]	505	1035	1032	1035
M_{xT}	[kNm]	5333	7114	7114	7114
M_{zT}	[kNm]	0	577	575	577
f - Rayleigh	[Hz]	0.320	0.320	0.327	0.319
$\sigma_{t,0,net,d,max}$	[N/mm^2]	6.89	11.10	10.09	8.56
$f_{t,0,net,d}$	[N/mm^2]	33.29	33.29	33.29	33.29
u.c. - tension		0.21	0.33	0.30	0.26
$\sigma_{c,0,net,d,max}$	[N/mm^2]	-8.37	-12.38	-11.28	-9.55
$f_{c,0,net,d}$	[N/mm^2]	22.18	22.18	22.18	22.18
u.c. - compression		0.38	0.56	0.51	0.43
Max. allowable $\tau_{xy,d,max}$	[N/mm^2]	3.03	3.03	3.03	3.03
Max. allowable $\tau_{yz,d,max}$	[N/mm^2]	8.25	8.25	8.25	8.25
Max. allowable $\tau_{xz,d,max}$	[N/mm^2]	3.03	3.03	3.03	3.03
Output - ANSYS					
f - Ansys	[Hz]	0.290	0.290	0.297	0.296
$\sigma_{t,0,d,max}$	[N/mm^2]	6.47	10.80	9.81	8.19
$\sigma_{c,0,d,max}$	[N/mm^2]	-8.23	-12.20	-11.10	-9.27
$\sigma_{t,0,d,net,max}$	[N/mm^2]	6.47	10.80	9.81	8.19
$\sigma_{c,0,d,net,max}$	[N/mm^2]	-8.23	-12.20	-11.10	-9.27
$\tau_{xy,d,max}$	[N/mm^2]	0.01	0.03	0.03	0.02
$\tau_{yz,d,max}$	[N/mm^2]	0.51	1.16	1.02	0.74
$\tau_{xz,d,max}$	[N/mm^2]	0.24	0.41	0.35	0.22
Buckling factor		N/A[a]	33.0	N/A[c]	N/A[c]
Buckling factor for $\lambda = 1$		19.1	21.6	23.0	23.8
Maximum deflection	[m]	1.16	1.99	1.83	1.67
Comparison - ANSYS/Matlab					
Tensile stresses		0.94	0.97	0.97	0.96
Compression stresses		0.98	0.99	0.98	0.97

Input	Model no.	V1	V2	V3	V4
	Load case	1 Operation	2a Extreme	2a Extreme	2a Extreme
H	[m]	125			
Turbine		5MW			
Class		IC		IIA	IIIA
Material		BAUBUCHE-Q			
n_{sides}		10	10	10	10
$a_{out,T}$	[m]	1.17	1.17	1.17	1.17
$a_{out,B}$	[m]	3.80	3.80	4.35	4.60
t	[m]	0.23	0.23	0.16	0.12
k_{net}		1.00	1.00	1.00	1.00
Output - Matlab					
F_{yT}	[kN]	1213	2321	2001	1558
M_{xT}	[kNm]	16731	20659	18377	13980
M_{zT}	[kNm]	0	1618	1395	1086
f - Rayleigh	[Hz]	0.294	0.294	0.307	0.293
$\sigma_{t,0,net,d,max}$	[N/mm^2]	13.11	18.91	19.05	17.74
$f_{t,0,net,d}$	[N/mm^2]	33.29	33.29	33.29	33.29
u.c. - tension		0.39	0.57	0.57	0.53
$\sigma_{c,0,net,d,max}$	[N/mm^2]	-15.54	-20.93	-21.76	-21.22
$f_{c,0,net,d}$	[N/mm^2]	22.18	22.18	22.18	22.18
u.c. - compression		0.70	0.94	0.98	0.96
Max. allowable $\tau_{xy,d,max}$	[N/mm^2]	3.03	3.03	3.03	3.03
Max. allowable $\tau_{yz,d,max}$	[N/mm^2]	8.25	8.25	8.25	8.25
Max. allowable $\tau_{xz,d,max}$	[N/mm^2]	3.03	3.03	3.03	3.03
Output - ANSYS					
f - Ansys	[Hz]	0.266	0.266	0.270	0.255
$\sigma_{t,0,d,max}$	[N/mm^2]	12.50	18.60	18.70	17.40
$\sigma_{c,0,d,max}$	[N/mm^2]	-15.30	-20.70	-21.50	-21.00
$\sigma_{t,0,d,net,max}$	[N/mm^2]	12.50	18.60	18.70	17.40
$\sigma_{c,0,d,net,max}$	[N/mm^2]	-15.30	-20.70	-21.50	-21.00
$\tau_{xy,d,max}$	[N/mm^2]	0.03	0.07	0.10	0.11
$\tau_{yz,d,max}$	[N/mm^2]	1.02	2.22	2.43	2.37
$\tau_{xz,d,max}$	[N/mm^2]	0.54	0.76	0.86	0.95
Buckling factor		N/A[a]	12.4	5.2	2.6
Buckling factor for $\lambda = 1$		15.7	11.7	4.9	2.6
Maximum deflection	[m]	1.86	2.83	2.46	2.21
Comparison - ANSYS/Matlab					
Tensile stresses		0.95	0.98	0.98	0.98
Compression stresses		0.98	0.99	0.99	0.99

C-4-2   BauBuche S

Model no.		W1	W2	W3	W4	W5
Input	Load case	1 Operation	2a Extreme	2a Extreme	2a Extreme	2a Extreme
H	[m]	100				
Turbine		3MW				
Class		IC				
Material		BAUBUCHE-S				
n_{sides}		10	10	10	10	10
$a_{out,T}$	[m]	0.93	0.93	0.93	0.93	0.93
$a_{out,B}$	[m]	2.75	2.70	2.75	2.90	3.30
t	[m]	0.12	0.14	0.12	0.10	0.08
k_{net}		1.00	1.00	1.00	1.00	1.00
Output - Matlab						
F_{yT}	[kN]	505	1039	1044	1045	1033
M_{xT}	[kNm]	5333	7281	7281	7281	7281
M_{zT}	[kNm]	0	579	583	583	576
f - Rayleigh	[Hz]	0.324	0.337	0.324	0.323	0.350
$\sigma_{t,0,net,d,max}$	[N/mm^2]	13.76	20.32	22.91	25.18	25.89
$f_{t,0,net,d}$	[N/mm^2]	49.94	49.94	49.94	49.94	49.94
u.c. - tension		0.28	0.41	0.46	0.50	0.52
$\sigma_{c,0,net,d,max}$	[N/mm^2]	-16.43	-22.28	-25.10	-27.68	-28.95
$f_{c,0,net,d}$	[N/mm^2]	38.13	38.13	38.13	38.13	38.13
u.c. - compression		0.43	0.58	0.66	0.73	0.76
Max. allowable $\tau_{xy,d,max}$	[N/mm^2]	1.51	1.51	1.51	1.51	1.51
Max. allowable $\tau_{yz,d,max}$	[N/mm^2]	7.33	7.33	7.33	7.33	7.33
Max. allowable $\tau_{xz,d,max}$	[N/mm^2]	7.33	7.33	7.33	7.33	7.33
Output - ANSYS						
f - Ansys	[Hz]	0.297	0.310	0.297	0.293	0.310
$\sigma_{t,0,d,max}$	[N/mm^2]	13.20	20.10	22.70	25.10	25.90
$\sigma_{c,0,d,max}$	[N/mm^2]	-16.30	-22.00	-24.80	-27.30	-29.00
$\sigma_{t,0,d,net,max}$	[N/mm^2]	13.20	20.10	22.70	25.10	25.90
$\sigma_{c,0,d,net,max}$	[N/mm^2]	-16.30	-22.00	-24.80	-27.30	-29.00
$\tau_{xy,d,max}$	[N/mm^2]	0.03	0.07	0.09	0.13	0.21
$\tau_{yz,d,max}$	[N/mm^2]	1.03	2.04	2.33	2.67	2.99
$\tau_{xz,d,max}$	[N/mm^2]	0.53	0.80	0.91	1.03	1.13
Buckling factor		N/A[a]	11.0	7.0	4.0	2.0
Buckling factor for $\lambda = 1$		11.5	10.5	6.7	3.9	2.0
Maximum deflection	[m]	1.14	1.97	2.18	2.29	2.08
Comparison - ANSYS/Matlab						
Tensile stresses		0.96	0.99	0.99	1.00	1.00
Compression stresses		0.99	0.99	0.99	0.99	1.00

Input	Model no.	X1	X2	X3	X4	X5
	Load case	1 Operation	2a Extreme	2a Extreme	2a Extreme	2a Extreme
H	[m]	125				
Turbine		3MW				
Class		IC				
Material		BAUBUCHE-S				
n_{sides}		10	10	10	10	10
$a_{out,T}$	[m]	0.93	0.93	0.93	0.93	0.93
$a_{out,B}$	[m]	3.26	3.26	4.10	2.80	2.58
t	[m]	0.18	0.18	0.08	0.30	0.45
k_{net}		1.00	1.00	1.00	1.00	1.00
Output - Matlab						
F_{yT}	[kN]	505	1027	1028	1032	1033
M_{xT}	[kNm]	5333	7114	7114	7114	7114
M_{zT}	[kNm]	0	573	574	576	576
f - Rayleigh	[Hz]	0.337	0.337	0.334	0.325	0.325
$\sigma_{t,0,net,d,max}$	[N/mm^2]	9.38	15.17	24.14	12.20	10.16
$f_{t,0,net,d}$	[N/mm^2]	49.94	49.94	49.94	49.94	49.94
u.c. - tension		0.19	0.30	0.48	0.24	0.20
$\sigma_{c,0,net,d,max}$	[N/mm^2]	-11.32	-16.80	-27.22	-13.49	-11.27
$f_{c,0,net,d}$	[N/mm^2]	38.13	38.13	38.13	38.13	38.13
u.c. - compression		0.30	0.44	0.71	0.35	0.30
Max. allowable $\tau_{xy,d,max}$	[N/mm^2]	1.51	1.51	1.51	1.51	1.51
Max. allowable $\tau_{yz,d,max}$	[N/mm^2]	7.33	7.33	7.33	7.33	7.33
Max. allowable $\tau_{xz,d,max}$	[N/mm^2]	7.33	7.33	7.33	7.33	7.33
Output - ANSYS						
f - Ansys	[Hz]	0.303	0.303	0.286	0.301	0.306
$\sigma_{t,0,d,max}$	[N/mm^2]	8.89	14.90	23.90	11.90	9.74
$\sigma_{c,0,d,max}$	[N/mm^2]	-11.20	-16.60	-27.80	-13.30	-11.00
$\sigma_{t,0,d,net,max}$	[N/mm^2]	8.89	14.90	23.90	11.90	9.74
$\sigma_{c,0,d,net,max}$	[N/mm^2]	-11.20	-16.60	-27.80	-13.30	-11.00
$\tau_{xy,d,max}$	[N/mm^2]	0.02	0.06	0.26	0.02	0.01
$\tau_{yz,d,max}$	[N/mm^2]	0.71	1.60	2.90	1.09	0.78
$\tau_{xz,d,max}$	[N/mm^2]	0.36	0.60	1.09	0.38	0.22
Buckling factor		N/A[a]	17.5	1.5	N/A[c]	N/A[c]
Buckling factor for $\lambda = 1$		20.7	16.4	1.5	24.6	26.0
Maximum deflection	[m]	1.13	1.94	2.44	1.77	1.56
Comparison - ANSYS/Matlab						
Tensile stresses		0.95	0.98	0.99	0.98	0.96
Compression stresses		0.99	0.99	1.02	0.99	0.98

	Model no.	Y1	Y2	Y3	Y4
Input	Load case	1 Operation	2a Extreme	2a Extreme	2a Extreme
H	[m]	125			
Turbine		5MW			
Class		IC			
Material		BAUBUCHE-S			
n_{sides}		10	10	10	10
$a_{out,T}$	[m]	1.17	1.17	1.17	1.17
$a_{out,B}$	[m]	3.70	3.42	4.00	3.70
t	[m]	0.16	0.21	0.12	0.16
k_{net}		1.00	1.00	1.00	1.00
Output - Matlab					
F_{yT}	[kN]	1213	2322	2327	2322
M_{xT}	[kNm]	16731	20659	20659	20659
M_{zT}	[kNm]	0	1619	1623	1619
f - Rayleigh	[Hz]	0.293	0.293	0.289	0.293
$\sigma_{t,0,net,d,max}$	[N/mm^2]	18.56	23.62	32.17	27.17
$f_{t,0,net,d}$	[N/mm^2]	49.94	49.94	49.94	49.94
u.c. - tension		0.37	0.47	0.64	0.54
$\sigma_{c,0,net,d,max}$	[N/mm^2]	-21.82	-25.82	-35.53	-29.82
$f_{c,0,net,d}$	[N/mm^2]	38.13	38.13	38.13	38.13
u.c. - compression		0.57	0.68	0.93	0.78
Max. allowable $\tau_{xy,d,max}$	[N/mm^2]	1.51	1.51	1.51	1.51
Max. allowable $\tau_{yz,d,max}$	[N/mm^2]	7.33	7.33	7.33	7.33
Max. allowable $\tau_{xz,d,max}$	[N/mm^2]	7.33	7.33	7.33	7.33
Output - ANSYS					
f - Ansys	[Hz]	0.265	0.270	0.257	0.265
$\sigma_{t,0,d,max}$	[N/mm^2]	17.80	23.30	31.90	26.80
$\sigma_{c,0,d,max}$	[N/mm^2]	-21.60	-25.50	-35.20	-29.50
$\sigma_{t,0,d,net,max}$	[N/mm^2]	17.80	23.30	31.90	26.80
$\sigma_{c,0,d,net,max}$	[N/mm^2]	-21.60	-25.50	-35.20	-29.50
$\tau_{xy,d,max}$	[N/mm^2]	0.05	0.07	0.16	0.10
$\tau_{yz,d,max}$	[N/mm^2]	1.44	2.54	3.85	3.10
$\tau_{xz,d,max}$	[N/mm^2]	0.76	0.91	1.33	1.09
Buckling factor		N/A[a]	13.5	2.6	6.2
Buckling factor for $\lambda = 1$		9.3	12.9	2.6	6.0
Maximum deflection	[m]	1.94	2.77	3.26	2.97
Comparison - ANSYS/Matlab					
Tensile stresses		0.96	0.99	0.99	0.99
Compression stresses		0.99	0.99	0.99	0.99

C-5 CLT-LVL hybrid cross sections

Designs with equal base width

Input		Equal base width		
Model no.		A3	HA1	HA2
Load case		2a Extreme	2a Extreme	2a Extreme
H	[m]	100		
Turbine		3 MW		
Class		IC		
Material		CL28h	KERTOS+CLT	BBS+CLT
n_{sides}		10	10	10
$a_{out,T}$	[m]	0.93	0.93	0.93
$a_{out,B}$	[m]	2.74	2.74	2.74
t	[m]	0.30	0.20	0.18
k_{net}		0.75	0.80	0.78
Output - Matlab				
F_{yT}	[kN]	1039	1041	1040
M_{xT}	[kNm]	7281	7281	7281
M_{zT}	[kNm]	579	581	580
f - Rayleigh	[Hz]	0.337	0.331	0.335
$\sigma_{t,0,net,d,max}$	[N/mm^2]	13.74	18.13	20.35
$f_{t,0,net,d}$	[N/mm^2]	16.63	29.13	49.94
u.c. - tension		0.83	0.62	0.41
$\sigma_{c,0,net,d,max}$	[N/mm^2]	-15.08	-19.85	-22.46
$f_{c,0,net,d}$	[N/mm^2]	24.64	32.08	38.13
u.c. - compression		0.61	0.62	0.59
Max. allowable $\tau_{xy,d,max}$	[N/mm^2]	1.10	0.28	1.51
Max. allowable $\tau_{yz,d,max}$	[N/mm^2]	1.10	3.01	5.70
Max. allowable $\tau_{xz,d,max}$	[N/mm^2]	1.10	1.10	1.10
ρ_{tow}	[kg/m^3]	420	468	670
Suggested layering		75-37-75-37-75	80-40-80	70-40-70
Output - ANSYS				
f - Ansys	[Hz]	0.308	0.303	0.310
$\sigma_{t,0,d,max}$	[N/mm^2]	10.20	14.30	15.60
$\sigma_{c,0,d,max}$	[N/mm^2]	-11.20	-15.60	-17.20
$\sigma_{t,0,d,net,max}$	[N/mm^2]	13.60	17.88	20.06
$\sigma_{c,0,d,net,max}$	[N/mm^2]	-14.93	-19.50	-22.11
$\tau_{xy,d,max}$	[N/mm^2]	0.03	0.04	0.05
$\tau_{yz,d,max}$	[N/mm^2]	1.03	1.49	1.63
$\tau_{xz,d,max}$	[N/mm^2]	0.36	0.57	0.63
Buckling factor		38.0	N/A[b]	N/A[b]
Buckling factor for $\lambda = 1$		20.1	18.7	16.5
Maximum deflection	[m]	2.01	1.86	1.94
Comparison - ANSYS/Matlab				
Tensile stresses		0.99	0.99	0.99
Compression stresses		0.99	0.98	0.98

		Equal base width		
	Model no.	D3	HE1	HE2
Input	Load case	2a Extreme	2a Extreme	2a Extreme
H	[m]	125		
Turbine		3 MW		
Class		IC		
Material		CL24h	KERTOS+CLT	BBS+CLT
n_{sides}		10	10	10
$a_{out,T}$	[m]	0.93	0.93	0.93
$a_{out,B}$	[m]	3.26	3.26	3.26
t	[m]	0.45	0.26	0.22
k_{net}		0.75	0.80	0.80
Output - Matlab				
F_{yT}	[kN]	1024	1032	1033
M_{xT}	[kNm]	7114	7114	7114
M_{zT}	[kNm]	571	576	576
f - Rayleigh	[Hz]	0.344	0.326	0.323
$\sigma_{t,0,net,d,max}$	[N/mm^2]	9.78	13.92	15.97
$f_{t,0,net,d}$	[N/mm^2]	14.78	29.13	49.94
u.c. - tension		0.66	0.48	0.32
$\sigma_{c,0,net,d,max}$	[N/mm^2]	-10.81	-15.35	-17.76
$f_{c,0,net,d}$	[N/mm^2]	21.12	32.08	38.13
u.c. - compression		0.51	0.48	0.47
Max. allowable $\tau_{xy,d,max}$	[N/mm^2]	1.10	0.28	1.51
Max. allowable $\tau_{yz,d,max}$	[N/mm^2]	1.10	3.76	5.87
Max. allowable $\tau_{xz,d,max}$	[N/mm^2]	1.10	2.11	1.10
ρ_{tow}	[kg/m^3]	420	468	676
Suggested layering		112-56-112-56-112	70-25-70-25-70	60-20-60-20-60
Output - ANSYS				
f - Ansys	[Hz]	0.308	0.292	0.292
$\sigma_{t,0,d,max}$	[N/mm^2]	7.11	10.90	12.50
$\sigma_{c,0,d,max}$	[N/mm^2]	-7.93	-12.10	-14.00
$\sigma_{t,0,d,net,max}$	[N/mm^2]	9.48	13.63	15.63
$\sigma_{c,0,d,net,max}$	[N/mm^2]	-10.57	-15.13	-17.50
$\tau_{xy,d,max}$	[N/mm^2]	0.19	0.03	0.04
$\tau_{yz,d,max}$	[N/mm^2]	0.69	1.15	1.35
$\tau_{xz,d,max}$	[N/mm^2]	0.23	0.41	0.50
Buckling factor		76.0	N/A[c]	N/A[c]
Buckling factor for $\lambda = 1$		24.7	21.6	21.5
Maximum deflection	[m]	1.84	2.12	2.03
Comparison - ANSYS/Matlab				
Tensile stresses		0.97	0.98	0.98
Compression stresses		0.98	0.99	0.99

Designs with equal thickness

Input		Equal thickness		
	Model no.	A3	HB1	HB2
	Load case	2a	2a	2a
		Extreme	Extreme	Extreme
H	[m]	100		
Turbine		3 MW		
Class		IC		
Material		CL28h	KERTOS+CLT	BBS+CLT
n_{sides}		10	10	10
$a_{out,T}$	[m]	0.93	0.93	0.93
$a_{out,B}$	[m]	2.74	2.40	2.30
t	[m]	0.30	0.30	0.30
k_{net}		0.75	0.80	0.80
Output - Matlab				
F_{yT}	[kN]	1039	1046	1046
M_{xT}	[kNm]	7281	7281	7281
M_{zT}	[kNm]	579	583	584
f - Rayleigh	[Hz]	0.337	0.321	0.320
$\sigma_{t,0,net,d,max}$	[N/mm^2]	13.74	15.86	16.92
$f_{t,0,net,d}$	[N/mm^2]	16.63	29.13	49.94
u.c. - tension		0.83	0.54	0.34
$\sigma_{c,0,net,d,max}$	[N/mm^2]	-15.08	-17.23	-18.61
$f_{c,0,net,d}$	[N/mm^2]	24.64	32.08	38.13
u.c. - compression		0.61	0.54	0.49
Max. allowable $\tau_{xy,d,max}$	[N/mm^2]	1.10	0.28	1.51
Max. allowable $\tau_{yz,d,max}$	[N/mm^2]	1.10	3.76	5.87
Max. allowable $\tau_{xz,d,max}$	[N/mm^2]	1.10	2.11	1.10
ρ_{tow}	[kg/m^3]	420	468	676
Suggested layering		75-37-75-37-75	80-30-80-30-80	80-30-80-30-80
Output - ANSYS				
f - Ansys	[Hz]	0.308	0.301	0.306
$\sigma_{t,0,d,max}$	[N/mm^2]	10.20	12.40	13.20
$\sigma_{c,0,d,max}$	[N/mm^2]	-11.20	-13.50	-14.60
$\sigma_{t,0,d,net,max}$	[N/mm^2]	13.60	15.50	16.50
$\sigma_{c,0,d,net,max}$	[N/mm^2]	-14.93	-16.88	-18.25
$\tau_{xy,d,max}$	[N/mm^2]	0.03	0.02	0.02
$\tau_{yz,d,max}$	[N/mm^2]	1.03	1.11	1.13
$\tau_{xz,d,max}$	[N/mm^2]	0.36	0.38	0.39
Buckling factor		38.0	N/A[b]	N/A[b]
Buckling factor for $\lambda = 1$		20.1	20.0	21.0
Maximum deflection	[m]	2.01	2.01	1.83
Comparison - ANSYS/Matlab				
Tensile stresses		0.99	0.98	0.98
Compression stresses		0.99	0.98	0.98

		Equal thickness		
	Model no.	D5	HD1	HD2
	Load case	2a Extreme	2a Extreme	2a Extreme
Input				
H	[m]		125	
Turbine			3 MW	
Class			IC	
Material		CL24h	KERTOS+CLT	BBS+CLT
n_{sides}		10	10	10
$a_{out,T}$	[m]	0.93	0.93	0.93
$a_{out,B}$	[m]	3.50	3.15	3.05
t	[m]	0.30	0.30	0.30
k_{net}		0.75	0.80	0.80
Output - Matlab				
F_{yT}	[kN]	1029	1031	1032
M_{xT}	[kNm]	7114	7114	7114
M_{zT}	[kNm]	574	575	575
f - Rayleigh	[Hz]	0.332	0.327	0.327
$\sigma_{t,0,net,d,max}$	[N/mm^2]	12.07	12.97	13.47
$f_{t,0,net,d}$	[N/mm^2]	14.78	29.13	49.94
u.c. - tension		0.82	0.45	0.27
$\sigma_{c,0,net,d,max}$	[N/mm^2]	-13.39	-14.27	-14.99
$f_{c,0,net,d}$	[N/mm^2]	21.12	32.08	38.13
u.c. - compression		0.63	0.44	0.39
Max. allowable $\tau_{xy,d,max}$	[N/mm^2]	1.10	0.28	1.51
Max. allowable $\tau_{yz,d,max}$	[N/mm^2]	1.10	3.76	5.87
Max. allowable $\tau_{xz,d,max}$	[N/mm^2]	1.10	2.11	1.10
ρ_{tow}	[kg/m^3]	420	468	676
Suggested layering		75-37-75-37-75	80-30-80-30-80	80-30-80-30-80
Output - ANSYS				
f - Ansys	[Hz]	0.294	0.295	0.299
$\sigma_{t,0,d,max}$	[N/mm^2]	8.80	10.10	10.50
$\sigma_{c,0,d,max}$	[N/mm^2]	-9.84	-11.20	-11.80
$\sigma_{t,0,d,net,max}$	[N/mm^2]	11.73	12.63	13.13
$\sigma_{c,0,d,net,max}$	[N/mm^2]	-13.12	-14.00	-14.75
$\tau_{xy,d,max}$	[N/mm^2]	0.03	0.02	0.03
$\tau_{yz,d,max}$	[N/mm^2]	0.97	1.03	1.05
$\tau_{xz,d,max}$	[N/mm^2]	0.32	0.35	0.36
Buckling factor		N/A[c]	N/A[c]	N/A[c]
Buckling factor for $\lambda = 1$		21.5	22.6	23.7
Maximum deflection	[m]	2.11	2.03	1.80
Comparison - ANSYS/Matlab				
Tensile stresses		0.97	0.97	0.97
Compression stresses		0.98	0.98	0.98

		Equal thickness		
	Model no.	D3	HF1	HF2
Input	Load case	2a Extreme	2a Extreme	2a Extreme
H	[m]	125		
Turbine		3 MW		
Class		IC		
Material		CL24h	KERTOS+CLT	BBS+CLT
n_{sides}		10	10	10
$a_{out,T}$	[m]	0.93	0.93	0.93
$a_{out,B}$	[m]	3.26	2.85	2.80
t	[m]	0.45	0.45	0.45
k_{net}		0.75	0.80	0.80
Output - Matlab				
F_{yT}	[kN]	1024	1033	1032
M_{xT}	[kNm]	7114	7114	7114
M_{zT}	[kNm]	571	576	576
f - Rayleigh	[Hz]	0.344	0.324	0.325
$\sigma_{t,0,net,d,max}$	[N/mm^2]	9.78	11.04	11.22
$f_{t,0,net,d}$	[N/mm^2]	14.78	29.13	49.94
u.c. - tension		0.66	0.38	0.22
$\sigma_{c,0,net,d,max}$	[N/mm^2]	-10.81	-12.09	-12.51
$f_{c,0,net,d}$	[N/mm^2]	21.12	32.08	38.13
u.c. - compression		0.51	0.38	0.33
Max. allowable $\tau_{xy,d,max}$	[N/mm^2]	1.10	0.28	1.51
Max. allowable $\tau_{yz,d,max}$	[N/mm^2]	1.10	3.76	7.33
Max. allowable $\tau_{xz,d,max}$	[N/mm^2]	1.10	2.11	7.33
ρ_{tow}	[kg/m^3]	420	468	676
Suggested layering		112-56-112-56-112	120-45-120-45-120	120-45-120-45-120
Output - ANSYS				
f - Ansys	[Hz]	0.308	0.297	0.302
$\sigma_{t,0,d,max}$	[N/mm^2]	7.11	8.47	8.60
$\sigma_{c,0,d,max}$	[N/mm^2]	-7.93	-9.38	-9.72
$\sigma_{t,0,d,net,max}$	[N/mm^2]	9.48	10.59	10.75
$\sigma_{c,0,d,net,max}$	[N/mm^2]	-10.57	-11.73	-12.15
$\tau_{xy,d,max}$	[N/mm^2]	0.19	0.02	0.02
$\tau_{yz,d,max}$	[N/mm^2]	0.69	0.75	0.75
$\tau_{xz,d,max}$	[N/mm^2]	0.23	0.22	0.22
Buckling factor		76.0	N/A[c]	N/A[c]
Buckling factor for $\lambda = 1$		24.7	23.9	25.0
Maximum deflection	[m]	1.84	1.86	1.59
Comparison - ANSYS/Matlab				
Tensile stresses		0.97	0.96	0.96
Compression stresses		0.98	0.97	0.97

Designs which exploit at least 80% of the longitudinal material strength

		u.c. < 0.8		
	Model no.	A3	HC1	HC2
Input	Load case	2a Extreme	2a Extreme	2a Extreme
H	[m]	100		
Turbine		3 MW		
Class		IC		
Material		CL28h	KERTOS+CLT	BBS+CLT
n_{sides}		10	10	10
$a_{out,T}$	[m]	0.93	0.93	0.93
$a_{out,B}$	[m]	2.74	3.20	3.20
t	[m]	0.30	0.13	0.10
k_{net}		0.75	0.77	0.80
Output - Matlab				
F_{yT}	[kN]	1039	1039	1042
M_{xT}	[kNm]	7281	7281	7281
M_{zT}	[kNm]	579	580	581
f - Rayleigh	[Hz]	0.337	0.336	0.330
$\sigma_{t,0,net,d,max}$	[N/mm^2]	13.74	22.38	27.44
$f_{t,0,net,d}$	[N/mm^2]	16.63	29.13	49.94
u.c. - tension		0.83	0.77	0.55
$\sigma_{c,0,net,d,max}$	[N/mm^2]	-15.08	-24.89	-30.60
$f_{c,0,net,d}$	[N/mm^2]	24.64	32.08	38.13
u.c. - compression		0.61	0.78	0.80
Max. allowable $\tau_{xy,d,max}$	[N/mm^2]	1.10	0.28	1.51
Max. allowable $\tau_{yz,d,max}$	[N/mm^2]	1.10	3.76	5.87
Max. allowable $\tau_{xz,d,max}$	[N/mm^2]	1.10	2.11	1.10
ρ_{tow}	[kg/m^3]	420	466	676
Suggested layering		75-37-75-37-75	50-30-50	40-20-40
Output - ANSYS				
f - Ansys	[Hz]	0.308	0.298	0.296
$\sigma_{t,0,d,max}$	[N/mm^2]	10.20	17.00	21.80
$\sigma_{c,0,d,max}$	[N/mm^2]	-11.20	-18.90	-24.20
$\sigma_{t,0,d,net,max}$	[N/mm^2]	13.60	22.10	27.25
$\sigma_{c,0,d,net,max}$	[N/mm^2]	-14.93	-24.57	-30.25
$\tau_{xy,d,max}$	[N/mm^2]	0.03	0.09	0.14
$\tau_{yz,d,max}$	[N/mm^2]	1.03	1.99	2.52
$\tau_{xz,d,max}$	[N/mm^2]	0.36	0.75	0.96
Buckling factor		38.0	N/A[b]	N/A[c]
Buckling factor for $\lambda = 1$		20.1	5.3	3.1
Maximum deflection	[m]	2.01	2.24	2.75
Comparison - ANSYS/Matlab				
Tensile stresses		0.99	0.99	0.99
Compression stresses		0.99	0.99	0.99

Underlying formulas and software codes

APPENDIX D

Material properties

The material properties for Cross Laminated Timber (CLT) and Laminated Veneer Lumber (LVL) in this appendix are used for calculations in Chapters 8 and 9 . For regular (softwood) CLT, the values and formulas are based on results and recommendations of Univ.-Prof. Dipl-Ing. Dr. Gerhard Schickhofer of TU Graz [6]. These same formulas have been used to determine representative properties for a hardwood version of CLT. For LVL, information provided by manufacturers has been used [11, 12].

This appendix only contains values and formulas for properties used within the design calculations. Material strengths perpendicular to the grain, or shear moduli, for example, are not provided because they are not used, but can be found in the sources named above.

D-1 Softwood Cross Laminated Timber

D-1-1 Base material properties

The base material properties for all four defined strength classes of softwood Cross Laminated Timber (CLT) can be found in Table D-1. These are the properties of the individual boards (or lamellas) that CLT panels are made up of. Combining these boards into CLT panels leads to slightly higher characteristic strengths, which are given in section D-1-2.

D-1-2 Characteristic material properties

With the formulas provided below, the characteristic material properties for CLT panels are calculated based on the tensile strength of the individual boards. Values are provided in Table D-2, partial factors used are later defined in section D-1-4. These properties are only valid for the net cross section, i.e. the part of the cross section where the fibres are in the direction under consideration.

Bending strength
In bending calculations, which will not occur in this research, the strength of layers perpendicular to the loading direction is ignored. The bending strength of the layers parallel to the loading direction:

$$f_{m,CLT,k} = k_{m,CLT} \cdot f_{t,0,l,k}^{0.8} \tag{D-1}$$

Tensile strength
The tensile strength of layers with their grains parallel to the load direction:

$$f_{t,0,CLT,net,k} = k_{sys,t,0} \cdot f_{t,0,l,k} \tag{D-2}$$

Compression strength
The compression strength of layers with their grains parallel to the load direction:

$$f_{c,0,CLT,net,k} = f_{m,CLT,k} \tag{D-3}$$

Shear strength
The characteristic shear strengths of CLT are provided in Table D-2. No distinction is made between the different strength classes by codes and proposals (yet), although some sources [70] suggest higher values in general. Chapter 7 provides a detailed description of how the net shear strengths are calculated within this research.

D-1-3 Design material properties

The design material properties are calculated from the characteristic values using the formulas below. Partial factors used in the formulas are defined in section D-1-4. Since some of these, such as the height factor k_h, depend on the chosen element or cross section, the design material properties will differ per calculation and no specific values are provided here.

Strength class		CL24h	CL28h	CL30h	CL34h
Lamella class		T14		T18	
Dispersion of lamella strength	CV [ft,0,l]	$25\% \pm 5\%$	$30\% \pm 5\%$	$25\% \pm 5\%$	$30\% \pm 5\%$
Lamella tensile strength	$f_{t,0,l,k}$	14 N/mm^2		18 N/mm^2	

Table D-1: Base material properties according to Schickhofer [6]

	Strength Class		CL24h	CL28h	CL30h	CL34h
Bending strength	$f_{m,CLT,k}$	N/mm^2	24	28	30	34
Tensile strength	$k_{sys,t,0}$		1.2	1.35	1.2	1.35
	$f_{t,0,CLT,net,k}$	N/mm^2	16.8	18.9	21.6	24.3
Compression strength	$f_{c,0,CLT,net,k}$	N/mm^2	24	28	30	34
Shear strength (in plane)	$f_{v,CLT,IP,k}$	N/mm^2	5.0			
	$f_{T,CLT,k}$	N/mm^2	2.5			
Shear strength (out of plane)	$f_{v,CLT,OP,k}$	N/mm^2	4.0			
	$f_{r,CLT,k}$	N/mm^2	1.25			
Young's Modulus	$E_{0,mean}$	N/mm^2	11000		12000	
Density	ρ_{mean}	kg/m^3	420		460	

Table D-2: Characteristic material strength values for the various CLT strength classes

Bending strength

The bending strength of layers with their grains parallel to the load direction:

$$f_{m,CLT,d} = k_{mod} \cdot k_h \cdot \frac{f_{m,CLT,k}}{\gamma_M \cdot \gamma_n} \tag{D-4}$$

Tensile strength

The tensile strength of layers with their grains parallel to the load direction:

$$f_{t,0,CLT,net,d} = k_{mod} \cdot k_h \cdot \frac{f_{t,0,CLT,net,k}}{\gamma_M \cdot \gamma_n} \tag{D-5}$$

When determining the average tensile strength of the cross section, cross layers are assumed to have no strength. The equivalent tensile strength for the entire cross section then becomes:

$$f_{t,0,CLT,d} = k_{net} \cdot f_{t,0,CLT,net,d} \tag{D-6}$$

k_{net} is defined in Figure 5-10.

Compression strength

The compression strength of layers with their grains parallel to the load direction:

$$f_{c,0,CLT,net,d} = k_{mod} \cdot \frac{f_{c,0,CLT,net,k}}{\gamma_M \cdot \gamma_n} \tag{D-7}$$

When determining the average compression strength of the cross section, cross layers are assumed to have no strength. The equivalent compression strength for the entire cross section then becomes:

$$f_{c,0,CLT,d} = k_{net} \cdot f_{c,0,CLT,net,d} \tag{D-8}$$

Shear strength

$$f_{v,CLT,i,d} = k_{mod} \cdot \frac{f_{v,CLT,i,k}}{\gamma_M \cdot \gamma_n} \tag{D-9}$$

Where $f_{v,CLT,i,k}$ can be any of the characteristic shear strengths (in-plane, out-of-plane, rolling shear). A detailed description of how shear stress calculations should be made is found in Chapter 7.

D-1-4   Partial factors

The factors described in this section are used to calculate the characteristic and design material properties in sections D-1-2 and D-1-3 respectively. They have been divided into three categories:

– Partial factors for bending strength, which will be used to calculate the characteristic panel bending strength from the tensile strength of the individual boards;

– Partial factors for tensile strength, which will be used to calculate the characteristic panel tensile strength from the tensile strength of the individual boards;

– General partial factors, which have to be included in the calculation of all design material properties from the characteristic properties.

Partial factors for bending strength

The overall factor for bending strength is given by:

$$k_{m,CLT} = k_{sys,CLT} \cdot k_{CLT/GLT} \cdot k_{h,CLT} \cdot k_{CV_t} \tag{D-10}$$

This is based on a similar factor for Glued Laminated Timber (GLT) and is made up out of the following factors:

– **System factor**
This takes into account the system effect of parallel arranged boards in bending:

$$k_{sys,CLT} = 1.1 \tag{D-11}$$

– **Homogenization factor**
Factor to take into account the homogenization, which is compared to the one used for GLT:

$$k_{CLT/GLT} = 0.94 \tag{D-12}$$

It includes the layers perpendicular to the grain.

– **Reference height factor**
Factor for adjusting the reference height of CLT, again compared to the one used for GLT:

$$k_{h,CLT} = 1.15 \tag{D-13}$$

– **Material dispersion**
Factor to take into account the dispersion of the base material:

$$k_{CV_T} = \begin{cases} 2.54 & \text{for dispersion 25 \%} \\ 2.97 & \text{for dispersion 35 \%} \end{cases} \tag{D-14}$$

Partial factors for tensile strength

Here, a single system factor takes into account the system effect of parallel arranged boards in tension:

$$k_{sys,t,0} = \begin{cases} \min\left(0.075 \cdot \ln(n) + 1; 1.20\right) & \text{for } CV[f_{t,0,l}] = 25\% \pm 5\% \\ \min\left(0.130 \cdot \ln(n) + 1; 1.35\right) & \text{for } CV[f_{t,0,l}] = 35\% \pm 5\% \end{cases} \tag{D-15}$$

The large dimensions of the structure are expected to result in n (number of boards) > 15, so this will lead to $k_{sys,t,0} = 1.20$ or 1.35, depending on the strength class.

General partial factors

These are to be applied to all characteristic material properties, to obtain the design values. Height factor k_h is an exception, only applied in case of bending or tension.

– **Material factor**
The partial factor for material properties and resistances, taken from Eurocode 5:

$$\gamma_M = 1.25 \tag{D-16}$$

– **Component factor**
The consequence of failure factor from the IEC-61400, component class 2:

$$\gamma_n = 1.0 \tag{D-17}$$

– **Modification factor for load duration**

$$k_{mod} = \begin{cases} \text{Permanent} & 0.6 \\ \text{Long term} & 0.7 \\ \text{Medium} & 0.8 \\ \text{Short term} & 0.9 \\ \text{Instantaneous} & 1.1 \end{cases} \tag{D-18}$$

– **Height factor**
Volume effects are taken into account for when $t < 150$ (bending) or $b < 600$ mm (tension):

$$k_h = \min\left(\left(\frac{150}{h}\right)^{0.1} ; 1.1 \right) \tag{D-19}$$

D-1-5 Production limitations

For panels made from CLT, the following limitations are provided by Impressum [71]:

– Standard thickness up to 300 mm, with possibilities to go up to 500 mm;

– Standard widths up to 2950 mm, but up to 4850 mm on request;

– Lengths up to 20 m, on request.

Strength class		CL40h
Lamella class		T24
Lamella tensile strength	$f_{t,0,l,k}$	24 N/mm^2

Table D-3: Base material properties for hardwood CLT, based on [7], [8]

D-2   Hardwood Cross Laminated Timber

Cross Laminated Timber made of timber with higher strength properties than the Norway Spruce used in 'regular' CLT, could possibly lead to higher or structurally more efficient towers. Some new research into CLT made of hardwood is being conducted, but no definitive results or material properties can be found as of yet. For the London Design Festival in 2013, one exposition used and tested tulipwood CLT [72]. Some material properties were provided, but no information is given about the tests performed or about the validity of these values. The small number of tests further reduces the potential of using these values in this research.

Instead, it is decided to apply the formulas from section D-1 on a hardwood species, in this case iroko. Iroko has been successfully glued together into glulam elements in multiple projects. Other examples of hardwood species being used in glulam exist as well. "[A]sh, locust tree, oak and many tropical timbers have been glued in the past based on the basis of an individual case approval" [64], although it requires an experiences manufacturer to make these elements.

Iroko is often applied unprotected, as it is of durability class 1 or 2 [7]. This further increases its potential, as the timber then will need minimal protection from the elements, unlike regular CLT. Contacts from practice [33] confirm that suitable adhesives for hardwood CLT exist, although currently only as an additional primer to the regular adhesives.

When comparing results for clearwood specimens of spruce and iroko in the Wood Handbook [9], it becomes clear that iroko has a substantially higher strength. Iroko is normally graded into strength class D40 [7], with tensile strength $f_{t,0,l,k} = 24$ N/mm^2 [8], as can be seen in Table D-3.

Shear strengths for CLT in general are still not well-documented. Even though figures from Green et al. [9] might suggest that iroko has a higher shear strength, this has only been shown for clearwood. Without additional reasons to increase the shear capacity of the timber, the same values as for softwood CLT are used, as can be seen in the characteristic material properties in Table D-4. The design material properties are also calculated according to the same formulas as for softwood CLT, using the same partial factors.

The values used here are only estimated and unconfirmed by tests, so conclusions drawn from calculations containing these values should be considered as such. It should be further noted that even though glued laminated timber from other species such as beechwood has been developed [63], iroko has been chosen to also be able to investigate possible benefits from its high natural durability.

	Strength Class		CL40h
Bending strength	$f_{m,CLT,k}$	N/mm^2	40
Tensile strength	$k_{sys,t,0}$		1.2
	$f_{t,0,CLT,net,k}$	N/mm^2	28.8
Compression strength	$f_{c,0,CLT,net,k}$	N/mm^2	40
Shear strength (in plane)	$f_{v,CLT,IP,k}$	N/mm^2	5.0
	$f_{T,CLT,k}$	N/mm^2	2.5
Shear strength (out of plane)	$f_{v,CLT,OP,k}$	N/mm^2	4.0
	$f_{r,CLT,k}$	N/mm^2	1.25
Young's Modulus	$E_{0,mean}$	N/mm^2	11000
Density	ρ_{mean}	kg/m^3	650

Table D-4: Characteristic material strength values for hardwood CLT, based on [9], [10], [7] and [8]

	Material	Kerto S	Kerto Q
Bending strength (in plane)	$f_{m,0,LVL,IP,k}$ N/mm^2	44	32
Bending strength (out of plane)	$f_{m,0,LVL,OP,k}$ N/mm^2	50	36
Tensile strength	$f_{t,0,LVL,k}$ N/mm^2	35	26
Compression strength	$f_{c,0,LVL,k}$ N/mm^2	35	26
Shear strength (in plane)	$f_{v,LVL,IP,k}$ N/mm^2	4.1	4.5
Shear strength (out of plane)	$f_{v,LVL,OP,k}$ N/mm^2	2.3	1.3
Rolling shear strength	$f_{r,LVL,k}$ N/mm^2	0.3[a]	0.6
Young's Modulus	$E_{0,mean}$ N/mm^2	13,800	10,500
Density	ρ_{mean} kg/m^3	480	

Table D-5: Characteristic material properties for softwood (Kerto) LVL according to Metsä Wood [11]

[a] The value for $f_{r,LVL,k}$ is not provided by the manufacturer for Kerto S, because shear in this direction would not occur in normal applications of Kerto S (bar-like elements). Since shear stresses occur in all direction in the turbine tower designs, a value is required and is taken as 50% of the rolling shear strength of Kerto Q.

D-3   Softwood LVL

This section describes the material properties of regular softwood Laminated Veneer Lumber (LVL). The material properties are taken from Metsä Wood's Kerto line [11], which comes in two types. The S variant contains only layers in the longitudinal direction, while Kerto Q also contains crosswise layers. Unlike with CLT, the orientation of the layers is set and taken into account by the manufacturers when calculating the material properties. k_{net} will therefore not be used in LVL calculations, but instead will be set to unity.

D-3-1   Characteristic material properties

The characteristic properties are displayed in Table D-5.

D-3-2   Design material properties

The design material properties are calculated using the following formulas. The factors used in these formulas are defined in section D-3-3. Since some factors, such as k_h, depend on the chosen element or cross section, they will differ per calculation and no specific values are provided here.

Bending strength

$$f_{m,LVL,i,d} = k_{mod} \cdot k_h \cdot \frac{f_{m,LVL,i,k}}{\gamma_M \cdot \gamma_n} \tag{D-20}$$

Tensile strength

$$f_{t,0,LVL,d} = k_{mod} \cdot k_l \cdot \frac{f_{t,0,LVL,k}}{\gamma_M \cdot \gamma_n} \tag{D-21}$$

Compression strength

$$f_{c,0,LVL,d} = k_{mod} \cdot \frac{f_{c,0,LVL,k}}{\gamma_M \cdot \gamma_n} \tag{D-22}$$

Shear strength

$$f_{v,LVL,i,d} = k_{mod} \cdot \frac{f_{v,LVL,i,k}}{\gamma_M \cdot \gamma_n} \tag{D-23}$$

D-3-3   Partial factors

The partial factors specific for LVL are defined by Eurocode 5 [14]. Other factors, such as the component factor are defined by the IEC [2]. They are used in section D-3-2 to calculate the design material properties, based on the characteristic material properties of section D-3-1.

Material factor
    The partial factor for material properties and resistances, taken from Eurocode 5:

$$\gamma_M = 1.2 \tag{D-24}$$

Component factor
    The consequence of failure factor from the IEC-61400, component class 2:

$$\gamma_n = 1.0 \tag{D-25}$$

Modification factor for load duration

$$k_{mod} = \begin{cases} \text{Permanent} & 0.5 \\ \text{Long term} & 0.5 \\ \text{Medium} & 0.65 \\ \text{Short term} & 0.8 \\ \text{Instantaneous} & 1.1 \end{cases} \tag{D-26}$$

Height factors
    Volume effects for softwood LVL are taken into account by the height factors for bending and tension, given by:

$$k_h = \min\left(\left(\frac{300}{h}\right)^s ; 1.2\right) \tag{D-27}$$

for when $300 < h \leq 1000$ (bending) or

$$k_l = \min\left(\left(\frac{3000}{l}\right)^{s/2} ; 1.1\right) \tag{D-28}$$

when $l \neq 3000$ mm (tension). The s-factor can be taken as 0.12 for Kerto LVL [11].

D-3-4 Production limitations

For boards made from Kerto Q, the following limitations are provided by Metsä Wood [11]:

– Standard thicknesses available are between 27 and 69 mm, in steps of 6 mm;

– Widths are possible up to 2500 mm;

– Standard lengths up to 12 m, with longer lengths up to 25 m on request.

	Material		Baubuche S	Baubuche Q
Bending strength (in plane)	$f_{m,0,LVL,IP,k}$	N/mm^2	70	60
Bending strength (out of plane)	$f_{m,0,LVL,OP,k}$	N/mm^2	65	45
Tensile strength	$f_{t,0,LVL,k}$	N/mm^2	60	40
Compression strength	$f_{c,0,LVL,k}$	N/mm^2	41.6	24.2
Shear strength (edgewise)	$f_{v,LVL,IP,k}$	N/mm^2	8	9
Shear strength (flapwise)	$f_{v,LVL,OP,k}$	N/mm^2	8	3.3
Rolling shear strength	$f_{r,LVL,k}$	N/mm^2	1.65[b]	3.3
Young's Modulus	$E_{0,mean}$	N/mm^2	16,800	11,800
Density	ρ_{mean}	kg/m^3	740	

Table D-6: Characteristic material properties for BauBuche LVL according to Pollmeier [12]

[b] The value for $f_{r,LVL,k}$ is not provided by the manufacturer for BauBuche S, because shear in this direction would not occur in normal applications (bar-like elements). Since shear stresses occur in all direction in the turbine tower designs, a value is required and is taken as 50% of the rolling shear strength of BauBuche Q.

D-4   Beechwood LVL

This section describes the material properties of the high-strength Baubuche (BB) material [12], LVL made of European beechwood. It has higher strength properties than regular softwood LVL and again comes in two forms, Baubuche S and Baubuche Q. The S variant contains only layers in the longitudinal direction, while Baubuche Q also contains crosswise layers, resulting in a higher tensile strength perpendicular to the grain. Because it is a form of LVL, the same formulas will apply as provided for softwood LVL. This section will only state the differences between softwood and beechwood LVL.

D-4-1   Characteristic material properties

The characteristic properties are displayed in Table D-6.

D-4-2   Design material properties

This design material properties are calculated in the same way as for softwood LVL in section D-3-2.

D-4-3 Partial factors

All partial factors are the same as those for softwood LVL found in section D-3-3. The same size effective parameter s can be used in the calculation of the height factor for BauBuche as for Kerto [12].

D-4-4 Production limitations

For boards made from BauBuche S or Q, the following limitations are provided by Pollmeier [12]:

– Standard thickness dimensions available are 40, 60, 80 mm;

– Widths are possible between 100 and 1850 mm;

– Lengths up to 18 m, with longer lengths on request.

An additional conversation with the producer revealed that wider panels should be possible through the use of finger joints. This should then also be possible for Kerto LVL.

Properties of regular polygons

This appendix describes certain properties of regular polygons that are used in design and calculation. Formulas are based on a set of general formulas found in Table A.1 of Young [73], where only general formulas and no numerical values were provided. Geometrical parameters are defined in Figure 5-1. All cross sectional properties are described in terms of number of sides n, angle α, side width a and (for hollow polygons) wall thickness t.

A division is made between general polygons, octagons and decagons.

E-1 General regular polygons

E-1-1 Dimensional properties of regular polygons

Outer radius

$$R = \frac{a}{2\sin\alpha} \tag{E-1}$$

Widest diameter

$$b = 2R = \frac{a}{\sin\alpha} \tag{E-2}$$

Inner radius

$$r = \frac{a}{2\tan\alpha} \tag{E-3}$$

Smallest diameter

$$d = 2r = \frac{a}{\tan\alpha} \tag{E-4}$$

E-1-2 Cross-sectional properties of solid regular polygons

Area

$$A = \frac{a^2 n}{4 \tan(\alpha)} \tag{E-5}$$

Moment of inertia

$$I_R = I_r = \frac{1}{24} A \left(6R^2 - a^2 \right) \tag{E-6}$$

Radius of gyration

$$i_R = i_r = \sqrt{\frac{1}{24} \left(6R^2 - a^2 \right)} \tag{E-7}$$

Section moduli

$$W_R = \frac{I_R}{R} \tag{E-8}$$

$$W_r = \frac{I_r}{r} \tag{E-9}$$

E-1-3 Cross-sectional properties of hollow regular polygons

Area

$$A = nat \left(1 - \frac{t \tan(\alpha)}{a} \right) \tag{E-10}$$

Moment of inertia

$$I_r = I_R = \frac{na^3 t}{8} \left(\frac{1}{3} + \frac{1}{\tan^2 \alpha} \right) \\ \left[1 - 3\frac{t \tan \alpha}{a} + 4 \left(\frac{t \tan \alpha}{a} \right)^2 - 2 \left(\frac{t \tan \alpha}{a} \right)^3 \right] \tag{E-11}$$

Radius of gyration

$$i_R = i_r = \frac{a}{\sqrt{8}} \sqrt{\frac{1}{3} + \frac{1}{\tan^2 \alpha} \left[1 - 2\frac{t \tan \alpha}{a} + 2 \left(\frac{t \tan \alpha}{a} \right)^2 \right]} \tag{E-12}$$

Section moduli

$$W_R = \frac{I_R}{R} \tag{E-13}$$

$$W_r = \frac{I_r}{r} \tag{E-14}$$

E-2 Regular octagons

For $n = 8$, $\alpha = \frac{1}{8}\pi$ so

$$\sin\left(\frac{1}{8}\pi\right) = \frac{1}{2}\sqrt{2 - \sqrt{2}}$$

$$\tan\left(\frac{1}{8}\pi\right) = \sqrt{2} - 1$$

$$\frac{1}{\tan\left(\frac{1}{8}\pi\right)} = \sqrt{2} + 1$$

$$\tan^2\left(\frac{1}{8}\pi\right) = 3 - 2\sqrt{2}$$

E-2-1 Dimensional properties of regular octagons

Outer radius

$$\begin{aligned} R =& \frac{1}{2}\sqrt{4 + 2\sqrt{2}}a \\ \approx& 1.30a \end{aligned} \tag{E-15}$$

$$\begin{aligned} R^2 =& \left(1 + \frac{1}{\sqrt{2}}\right)a^2 \\ \approx& 1.71a^2 \end{aligned} \tag{E-16}$$

Widest diameter

$$\begin{aligned} b =& 2R \\ =& \sqrt{4 + 2\sqrt{2}}a \\ \approx& 2.61a \end{aligned} \tag{E-17}$$

Inner radius

$$\begin{aligned} r =& \frac{1}{2}\left(1 + \sqrt{2}\right)a \\ \approx& 1.21a \end{aligned} \tag{E-18}$$

$$\begin{aligned} r^2 =& \left(\frac{3}{4} + \frac{1}{\sqrt{2}}\right)a^2 \\ \approx& 1.46a^2 \end{aligned} \tag{E-19}$$

Smallest diameter

$$\begin{aligned} d =& 2r \\ =& \left(1 + \sqrt{2}\right)a \\ \approx& 2.41a \end{aligned} \tag{E-20}$$

E-2-2   Cross-sectional properties of solid regular octagons

Area

$$A = 2\left(1 + \sqrt{2}\right)a^2$$
$$\approx 4.83a^2$$

(E-21)

Moment of inertia

$$I_R = I_r = \frac{1}{12}\left(11 + \frac{6}{\sqrt{2}} + 5\sqrt{2}\right)a^4$$
$$\approx 1.86a^4$$

(E-22)

Radius of gyration

$$i_R = i_r = \sqrt{\frac{5}{24} + \frac{1}{4\sqrt{2}}}\,a$$
$$\approx 0.62a$$

(E-23)

Section moduli

$$W_R = \frac{I_R}{R} \approx 1.42a^3$$

(E-24)

$$W_r = \frac{I_r}{r} = 1.54a^3$$

(E-25)

E-2-3   Cross-sectional properties of hollow regular octagons

Area

$$A = 8at\left(1 - \frac{t}{a}\left(\sqrt{2} - 1\right)\right)$$
$$= 8at - 8\sqrt{2}t^2 + 8t^2$$
$$\approx 8at - 3.31t^2$$

(E-26)

Moment of inertia

$$I_R = I_r = a^3 t\left(\frac{1}{3} + \frac{1}{3 - 2\sqrt{2}}\right)$$
$$\left[1 - 3\left(\sqrt{2} - 1\right)\frac{t}{a} + 4\left(3 - 2\sqrt{2}\right)\frac{t^2}{a^2}\right.$$
$$\left. - 2\left(5\sqrt{2} - 7\right)\frac{t^3}{a^3}\right]$$
$$= \left(\frac{1}{3} + \frac{1}{3 - 2\sqrt{2}}\right)a^3 t - \left(\frac{6\sqrt{2} - 7}{3 - 2\sqrt{2}} - 1\right)a^2 t^2$$
$$+ \left(8 - \frac{8}{3}\sqrt{2}\right)at^3 - \left(\frac{20\sqrt{2} - \frac{82}{3}}{3 - 2\sqrt{2}} - \frac{14}{3}\right)t^4$$
$$\approx 6.16a^3 t - 7.65a^2 t^2 + 4.23at^3 - 0.88t^4$$

(E-27)

Radius of gyration

$$i_R = i_r = \frac{a}{\sqrt{8}} \sqrt{\frac{1}{3} + \frac{1}{3 - 2\sqrt{2}} \left[1 - 2\frac{t}{a} \left(\sqrt{2} - 1 \right) + 2\frac{t^2}{a^2} \left(3 - 2\sqrt{2} \right) \right]}$$

$$= \sqrt{\left(\frac{1}{24} + \frac{1}{24 - 16\sqrt{2}} \right) a^2 - \left(\frac{1}{4} + \frac{1}{2\sqrt{2}} \right) ta + \frac{1}{4}t^2}$$

$$\approx \sqrt{0.77a^2 - 0.60ta + 0.25t^2}$$

$$(E\text{-}28)$$

Section moduli

$$W_R = \frac{I_R}{R} \approx 4.72a^2 t - 5.86at^2 + 3.24t^3 - 0.67\frac{t^4}{a} \tag{E-29}$$

$$W_r = \frac{I_r}{r} = \approx 5.10a^2 t - 6.34at^2 + 3.50t^3 - 0.73\frac{t^4}{a} \tag{E-30}$$

E-3   General regular decagons

For $n = 10$, $\alpha = \frac{1}{10}\pi$, so

$$\sin\left(\frac{1}{10}\pi\right) = \frac{1}{4}\left(\sqrt{5} - 1\right)$$

$$\tan\left(\frac{1}{10}\pi\right) = \frac{1}{5}\sqrt{25 - 10\sqrt{5}}$$

$$\frac{1}{\tan\left(\frac{1}{10}\pi\right)} = \sqrt{5 + 2\sqrt{5}}$$

$$\tan^2\left(\frac{1}{10}\pi\right) = 1 - \frac{2}{5}\sqrt{5}$$

E-3-1   Dimensional properties of regular decagons

Outer radius

$$R = \left(\frac{1}{2} + \frac{1}{2}\sqrt{5}\right)a$$
$$\approx 1.62a$$

(E-31)

$$R^2 = \left(\frac{3}{2} + \frac{1}{2}\sqrt{5}\right)a^2$$
$$\approx 2.62a^2$$

(E-32)

Widest diameter

$$b = 2R$$
$$= \left(1 + \sqrt{5}\right)a$$
$$\approx 3.24a$$

(E-33)

Inner radius

$$r = \frac{1}{2}\sqrt{5 + 2\sqrt{5}}a$$
$$\approx 1.54a$$

(E-34)

$$r^2 = \left(\frac{5}{4} + \frac{1}{2}\sqrt{5}\right)a^2$$
$$\approx 2.37a^2$$

(E-35)

Smallest diameter

$$d = 2r$$
$$= \sqrt{5 + 2\sqrt{5}}a$$
$$\approx 3.08a$$

(E-36)

E-3-2   Cross-sectional properties of solid regular decagons

Area

$$
\begin{aligned}
A =& \frac{10a^2}{4} \sqrt{5 + 2\sqrt{5}} \\
\approx& 7.69a^2
\end{aligned}
$$
(E-37)

Moment of inertia

$$
\begin{aligned}
I_R = I_r =& \left(\frac{10}{12} + \frac{5}{16}\sqrt{5} \right) \sqrt{5 + 2\sqrt{5}}\,a^4 \\
\approx& 4.71a^4
\end{aligned}
$$
(E-38)

Radius of gyration

$$
\begin{aligned}
i_R = i_r =& \sqrt{\frac{1}{3} + \frac{1}{8}\sqrt{5}}\,a \\
\approx& 0.78a
\end{aligned}
$$
(E-39)

Section moduli

$$
W_R = \frac{I_R}{R} \approx 2.91a^3
$$
(E-40)

$$
W_r = \frac{I_r}{r} = 3.06a^3
$$
(E-41)

E-3-3   Cross-sectional properties of hollow regular decagons

Area

$$
\begin{aligned}
A =& 10at - 2\sqrt{25 - 10\sqrt{5}}\,t^2 \\
\approx& 10at - 3.25t^2
\end{aligned}
$$
(E-42)

Moment of inertia

$$
\begin{aligned}
I_r = I_R =& \frac{10}{8}a^3 t \left(\frac{1}{3} + 5 + 2\sqrt{5} \right) \\
& \left[1 - \sqrt{9 - \frac{18}{5}\sqrt{5}}\frac{t}{a} + \left(4 + \frac{8}{5}\sqrt{5} \right) \frac{t^2}{a^2} \right. \\
& \left. - \left(\frac{1}{5}\sqrt{5} - \frac{2}{5} \right) \sqrt{5 + 2\sqrt{5}}\frac{t^3}{a^3} \right] \\
=& \left(\frac{20}{3} + \frac{5}{2}\sqrt{5} \right) a^3 t - \sqrt{1 - \frac{2}{5}\sqrt{5}} \left(20 + \frac{15}{2}\sqrt{5} \right) a^2 t^2 \\
& + \left(\frac{20}{3} - \frac{2}{3}\sqrt{5} \right) at^3 - \sqrt{5 + 2\sqrt{5}} \left(\frac{2}{3}\sqrt{5} - \frac{1}{3} \right) t^4 \\
\approx& 12.26a^3 t - 11.95a^2 t^2 + 5.18at^3 - 0.84t^4
\end{aligned}
$$
(E-43)

Radius of gyration

$$i_R = i_r = \sqrt{\left(\frac{1}{24} + \frac{1}{8 - \frac{16}{5}\sqrt{5}}\right)a^2 - \frac{1}{4}\sqrt{5 + 2\sqrt{5}}ta + \frac{1}{4}t^2}$$

$$\approx \sqrt{1.23a^2 - 0.77ta + 0.25t^2}$$

(E-44)

Section moduli

$$W_R = \frac{I_R}{R} \approx 7.57a^3t - 7.38a^2t^2 + 3.20at^3 - 0.52t^4$$

(E-45)

$$W_r = \frac{I_r}{r} \approx 7.96a^3t - 7.76a^2t^2 + 3.36at^3 - 0.55t^4$$

(E-46)

Frequency analysis: Rayleigh-Ritz tool for estimating natural frequency

This appendix displays the underlying formulas of the MS Excel tool developed by the Offshore Engineering section at the Department of Civil Engineering and Geosciences of Delft University of Technology [45] and its adjustments in the context of this thesis work. The resulting codes used for calculations that are based on this worksheet can be found in Appendix G.

In short, the Rayleigh-Ritz method for estimating the natural frequency of a structure assumes as a certain mode shape for the structure (in this case a sinusoidal shape) and calculates the natural frequency based on this shape. Unless the exact mode shape is used, the method will overestimate the actual frequency.

F-1 Input

The model does it calculations based on eight user-specified input values. The symbols and definitions can be found in Table F-1.

Figure F-1: Impression of the tool developed by TU Delft

Input fields	
L	Length of the tower in m, from the rigidly fixed base to the centre of gravity of the top mass
ρ	Density of the tower material in kg/m^3
E	Young's Modulus in N/m^2
n	Number of segments into which the structure is divided
d_{top}	Width of the cross section at the top
d_{bottom}	Width of the cross section at the bottom
t	Wall thickness
M_{top}	Total mass of the rotor and nacelle
l	Length of one segment (caculated automatically)

Table F-1: Definition of the input parameters for the frequency estimator

F-2   Calculations

Geometrical properties are calculated using the formulas for hollow octagons in Appendix E. This part differs from the original model for circular cross sections. The intermediate calculations parameters are shown in F-2.

F-3   Output

The method outputs the natural frequency and the associated natural period according to formulas that can be found in Table F-3.

Caculation columns		
Symbol	Description	Formula
j	Segment number	
$d, a, R, r,$ t, A, I	Geometrical properties for segment j	See Appendix E
E	Young's Modulus of segment j	
EI	Stiffness of segment j	$E \cdot I$
l	Length of segment j	
ρ	Density of the tower material for segment j	
μ	Mass per unit length of segment j	$A \cdot \rho$
x	Elevation of centre of segment j above rigid foundation in m	$L - (j - 0.5)l$
EI'	Bending stiffness of segment j multiplied by curvature of mode shape	$EIl \cos^2\left(\frac{\pi x}{2L}\right)$
m'	Mass of segment j multiplied by mode shape	$\mu l \left[1 - \cos^2\left(\frac{\pi x}{2L}\right)\right]$
m	Mass of segment j	μl

Table F-2: Intermediate calculated results for the frequency estimator

Output fields		
Symbol	Description	Formula
EI_{eq}	Equivalent bending stiffness of the support structure	$\frac{\Sigma EI'_j}{L}$
m_{eq}	Equivalent mass of the support structure	$\frac{\Sigma m'_j}{L}$
m_{beam}	Average mass of the beam in kg/m'	$\frac{\Sigma m_j}{L}$
T	Natural period of the structure associated with the natural frequency	$\frac{48}{\pi^4}\left(\frac{4\pi^2(M_{top}+m_{eq}L)L^3}{3EI_{eq}}\right)$
f	First natural frequency of the structure	$\frac{1}{T}$

Table F-3: Output generated by the frequency estimator

MATLAB code

This appendix contains the Matlab codes for calculation of loads, stresses and natural frequency. Actions to be performed by the user are simple. By inputting the correct values in *Input.m* and then executing *UC.m*, the frequency (according to Rayleigh-Ritz) and maximum tensile and compression stresses along the tower are checked, and the input for ANSYS is prepared.

G-1 Load calculation code written for this research

G-1-1 UC.m

This is the file to be executed when calculating a design. First, the correct parameters have to be input into *Input.m* function file (and saved). *UC.m* then calculates the unity checks for tension and compression as well as the height at which these unity check are highest. These are displayed along with the frequency (calculated according to the Rayleigh Ritz method) and a small list of parameters that are used to input in the ANSYS code for FEM-analysis. It also plots the design tension and compression stresses over the height, along with the design strength of the material, for easy graphical checks. An example is shown in Figure G-1.

The seperate functions called by *UC.m* will be included in this appendix.

```
1  clear,clc
2
3  %% Call all other functions needed
4  [Class,Mat,Op,Turb,H,n_sides,a_outT,a_outB,t,k_net,mnac,mhub,V,e]=Input(); %Read
       the input parameters from Input.m
5  [E,rho_tow,f_t0netd,f_c0netd,gamma_n,gamma_fN,gamma_fA,gamma_fUn,f_vnetIPd,
       f_vnetOPd,f_rnetd,f_Td,Mat2]=Material(Mat,t,k_net); %Calculate the material
       properties in Material.m
6  [B_outT,B_outB,B,A_tow,A_towh,A_tow0,I_tow,I_towh,I_tow0,W_tow,W_towh,W_tow0,
       q_towi,q_tow,q_tow0]=Geometry(H,n_sides,a_outT,a_outB,t,rho_tow); %Calculate
       the geometric properties in Geomtry.m
```
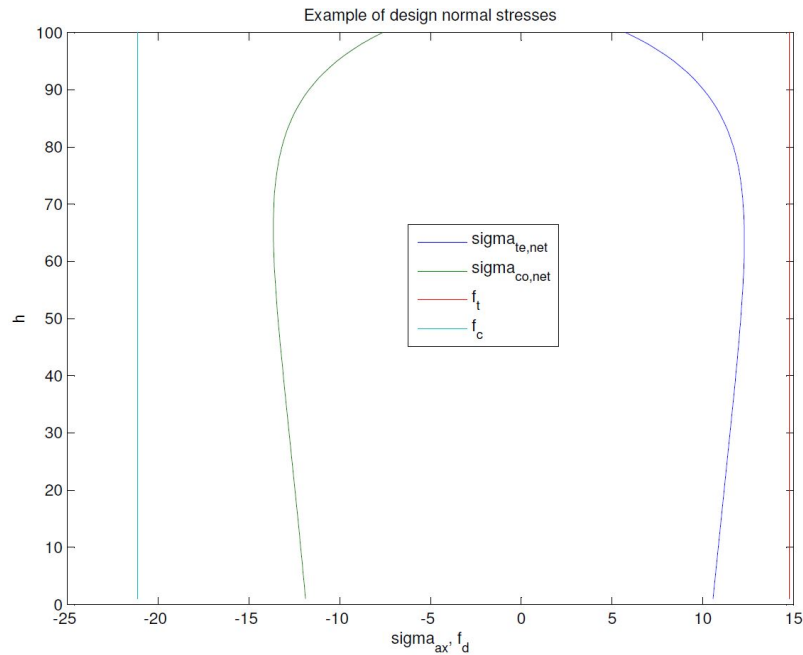
Figure G-1: Example of the graphical output of design stresses and strengths by *UC.m*

```matlab
 7  [f]=Frequency(H,mnac,mhub,E,rho_tow,A_tow,A_towh,I_tow); %Estimate the first
        natural frequency using Rayleigh-Ritz in frequency.m
 8  if strcmp(Turb,'NREL_5MW')
 9      [P1,P2,P3,P4]=NREL_5MW(f,mnac,mhub,q_towi,q_tow0); %Extract blade properties
            from NREL_5MW
10  elseif strcmp(Turb,'NREL_3MW')
11      [P1,P2,P3,P4]=NREL_3MW(f,mnac,mhub,q_towi,q_tow0); %Extract blade properties
            from NREL_3MW
12  end
13  [Dax,Mbeta,Mr,P,Cdax,Cp,a,theta,omr]=powercurve1(Turb,V,P1,P2,P3,P4); %Calculate
        the rotor forces in case of LC1 using powercurve1.m and its subfunctions
14  [T1,T2]=Blade_forces(Class,Turb,H,f,Op,P2,P3); %Calculate the rotor forces in
        case of LC2a and LC2b using Blade_forces.m
15  [F_zT,F_yT,F_xT,M_zT,M_yT,M_xT,M_rotx]=Top_Loads(Op,Turb,mnac,mhub,e,Dax,Mbeta,T2
        ); %Define and calculate the top loads in Top_Loads.m
16  [F_w,F_w0,M_w,M_w0,q_wi,F_wi,Vh]=Wind_tower(Class,Op,Turb,H,a_outT,a_outB,V,
        B_outT,B_outB,B,T1,Dax,n_sides,f); %Calculate the wind directly on the tower
        using Wind_tower.m
17  [F_x,M_x,F_y,M_y,F_z,M_z,F_x0,M_x0,F_y0,M_y0,F_z0,M_z0]=Resulting_loads(H,F_w,
        F_w0,M_w,M_w0,F_zT,F_yT,F_xT,M_zT,M_yT,M_xT,q_tow,q_tow0); %Calculate the
        resulting loads along the tower in Resulting_loads.m
18  [sigma_tenet,sigma_tenet0,sigma_conet,sigma_conet0,sigma_te,sigma_te0,sigma_co,
        sigma_co0]=Stresses(H,k_net,Op,M_x,M_x0,F_z,F_z0,A_towh,A_tow0,W_towh,W_tow0,
        gamma_fN,gamma_fUn,gamma_fA); %Calculate the resulting stresses along the
        tower height in Stresses.m
19
20  %% Construct and display the input for ANSYS
21  %First, a distinction is made between load cases 1 (Op=1), 2a (Op=2) and 2b (Op
        =3). In case of LC2a, accidential load factors are to be used
22  if Op==2
23      gamma=gamma_fA;
```

```matlab
24  else
25      gamma=gamma_fN;
26  end
27  %The following lines construct a table and displays it in such a way, that it is
        directly pasteable in the APDL code.
28  Names={'n_sides='; 'a_out_B='; 'a_out_T='; 'H='; 't='; 'M_top='; 'knet='; 'rho=';
        'YM='; 'FYT='; 'MXT='; 'MZT='; 'Grav='};
29  Vars=[n_sides; a_outB; a_outT; H; t; F_zT/9.81; k_net; rho_tow; E; gamma*F_yT;
        gamma*M_xT; gamma*M_zT; 9.81*gamma];
30  ANSYSINPUT=table(Vars,'RowNames',Names)
31
32  %The following lines calculate and store the wind load on the tower in a
        specified folder, in N/m^2. In this way, it can be directly applied on the
        tower in Ansys.
33  h=zeros(H,1);
34  for i=1:H
35      h(i)=i;
36  end
37  Height=h;
38  Wind=gamma*F_wi;
39  ANSYSWIND=table(Height,Wind);
40  writetable(ANSYSWIND,'C:\Users\Colin\Dropbox\Afstuderen\Final Report\Design\ANSYS
        \Wind.txt','Delimiter','\t','WriteRowNames',false);
41
42  %% Display the top forces
43  %To be able to check if the order of magnitude is correct
44  'F_yT = '
45  F_yT/1000
46  'kN'
47  'M_xT = '
48  M_xT/1000
49  'kNm'
50
51  %% Construct variables for easy plotting/checking
52  %The following lines store the design tension and compression strength, which
        will then be plotted along the stresses for easy graphical comparison
53  f_t=zeros(H,1);
54  f_c=zeros(H,1);
55  for i=1:H
56  f_t(i)=f_t0netd;
57  f_c(i)=-f_c0netd;
58  end
59
60  %% Maximum stresses
61  %Calculate the maximum tensile and compression stresses
62  sigma_temax=max(max(sigma_tenet),sigma_tenet0);
63  sigma_comax=min(min(sigma_conet),sigma_conet0);
64
65  %Calculate the heights for which the compression and tension strength is at its
        highest
66  h_te=find(sigma_tenet==sigma_temax);
67  h_co=find(sigma_conet==sigma_comax);
68  %If empty, then the maximum stress is at the bottom
69
70  %% Strength
71  %Calculate the unity checks, display their values and display if they are
        sufficient
```

```matlab
72  if sigma_temax<f_t0netd
73      disp('Tensile strength sufficient')
74  else disp('Tensile stress too high')
75  end
76  uc_t=sigma_temax/(f_t0netd)
77  sigma_temax
78  'Height of maximum tensile stress'
79  h_te
80  if abs(sigma_comax)<f_c0netd
81      disp('Compression strength sufficient')
82  else disp('Compression stress too high')
83  end
84  uc_c=abs(sigma_comax)/(f_c0netd)
85  sigma_comax
86  'Height of maximum compression stress'
87  h_co
88
89  %% Frequency
90  %Display the frequency and display whether or not it meets the demands set by 1P
        and 3P
91  f
92  if strcmp(Turb,'NREL_5MW')
93      if 0.104<f&f<0.222
94          disp('Frequency in range of 1P')
95      elseif 0.311<f&f<0.666
96          disp('Frequency in range of 3P')
97      else
98          disp('Frequency accepted')
99      end
100 elseif strcmp(Turb,'NREL_3MW')
101     if 0.120<f&f<0.256
102         disp('Frequency in range of 1P')
103     elseif 0.360<f&f<0.770
104         disp('Frequency in range of 3P')
105     else
106         disp('Frequency accepted')
107     end
108 end
109
110 %% Plot stresses
111 %Plot the design stresses and the design strength along the height
112 plot(sigma_te,h,sigma_co,h,f_t*k_net,h,f_c*k_net,h)
113 plot(sigma_tenet,h,sigma_conet,h,f_t,h,f_c,h)
114
115 %% Calculate maximum allowable shear stresses for Ansys
116 %Using the formulas from the Stress chapter, the maximum allowable shear stress
        is calculated, to which values from FEM-analysis will be compared
117 if strcmp(Mat2,'CLT')
118 tau_xz_allow=min(f_vnetOPd,f_rnetd);
119 tau_xy_allow=min(f_vnetOPd,f_rnetd);
120 tau_yz_allow=min(k_net*f_vnetIPd,(1-k_net)*f_vnetIPd);
121 elseif strcmp(Mat2,'LVL')
122 tau_xz_allow=f_vnetOPd;
123 tau_xy_allow=f_rnetd;
124 tau_yz_allow=f_vnetIPd;
125 else %Does not really matter if not CLT or LVL
126 tau_xz_allow=min(f_vnetOPd,f_rnetd);
```

```
127  tau_xy_allow=min(f_vnetOPd,f_rnetd);
128  tau_yz_allow=min(k_net*f_vnetIPd,(1-k_net)*f_vnetIPd);
129  end
130
131  %% Combine results for report
132  %These lines have only been included so that copying between Matlab, Excel and
         LaTeX was straight-forward and fast
133  RL=[F_x0 F_y0 F_z0 M_x0 M_y0 M_z0; F_x F_y F_z M_x M_y M_z]/1000;
134  RL2=[F_y0 F_z0 M_x0; F_y F_z M_x]/1000;
135  RT=[F_yT F_yT/1.1/1.25  M_rotx M_rotx/1.1/1.25 F_zT M_xT]/1000;
136  RW=[h q_wi/1000 Vh F_wi];
137  RW2=[0 F_w0 M_w0; h*1000 F_w M_w]/1000;
138  RF=[0 F_y0 F_z0 M_x0 ;h*1000 F_y F_z M_x ]/1000;
139  RF2=[F_yT; F_y0; F_w0;  M_x0; M_w0;  q_wi]/1000;
140  RS=[sigma_tenet0 sigma_conet0;sigma_tenet sigma_conet];
141  RI=[n_sides a_outT a_outB t k_net 0 F_yT/1000 M_xT/1000 M_zT/1000 f sigma_temax
         f_t0netd uc_t sigma_comax f_c0netd uc_c tau_xy_allow tau_yz_allow tau_xz_allow
         ]';
```

G-1-2 Input.m

Here the user is able to change the design case by altering the following parameters:

Class   Defines the turbine class, IC, IIA or IIIA;
Op   Defines the load case, 1, 2a or 2b;
Turb   Defines the turbine type, either 3 or 5 MW;
Mat   Defines the type and class of material, CLT, LVL or steel;
H   Defines the hub height;
n_sides   Defines the shape of the cross section, either octagonal, decagonal or circular;
a_outT   Defines the side width of the top cross section, see also Appendix E;
a_outB   Defines the side width of the bottom cross section;
t   Defines the wall thickness;
k_net   Defines the amount of fibres in longitudinal direction, which should be 1 for
             certain materials.

These are also displayed in Figure 6-5.

```
1   function [Class,Mat,Op,Turb,H,n_sides,a_outT,a_outB,t,k_net,mnac,mhub,V,e]=Input
        ();
2   %% Turbine user input
3   % Define the wind turbine class.
4   Class='IC'; %Available are 'IC','IIC','IIA' and 'IIIA'
5   % Define load case
6   Op=2; %Available are loads during operation (LC1, Op=1), bending during
        standstill (LC2a, Op=2) or torsion during standstill (LC2b Op=3)
7   %Define turbine type
8   Turb='NREL_3MW'; %Available are 'NREL_3MW' and 'NREL_5MW'
9
10  %% Tower user input
11  % Define the material
12  Mat='CL28h'; % Available are 'CL24h', 'CL28h', 'CL30h', 'CL34h', 'CL40h', 'KERTOS
        ', 'KERTOQ', 'BBS', 'BBQ' and 'Steel'.
```

```
13  %Define the geometrical parameters for the tower
14  H=100; %Hub height
15  n_sides=10; %Options: 0 (circular), 8 (octagon), 10 (decagon)
16  a_outT=0.93; %Side width at the top
17  a_outB=2.74; %Side width at the bottom
18  %a becomes the outer diameter for circular towers
19  t=0.3; %Wall thickness
20  k_net=0.75; %Part of the cross section with fibers in the longitudinal direction
        (1 for LVL and Steel)
21
22  %% End of user input
23
24  %% Turbine parameters
25  %These can be altered when needed
26  if strcmp(Turb,'NREL_5MW')
27      mnac=240000; %kg
28      mhub=110000; %kg
29  elseif strcmp(Turb,'NREL_3MW')
30      mnac=120000; %kg
31      mhub=56500; %kg
32  end
33  V_in=3; %m/s
34  V_out=25; %m/s
35  V=V_in:0.1:V_out;
36
37  %% Eccentricities
38  e_huby=5.01;
39  e_hubz=1.96;
40  h_transfer=5;
41  e_totz=h_transfer+e_hubz;
42  e_nacy=1.9;
43  e_nacz=1.75;
44  e=[e_huby e_hubz h_transfer e_totz e_nacy e_nacz];
45  if strcmp(Turb,'NREL_5MW')
46      e=e;
47  elseif strcmp(Turb,'NREL_3MW')
48      e=0.8*e; %Scaling down the NREL 5 MW eccentricities for the 3 MW turbine
49  end
```

G-1-3 Material.m

This function calculates the materials strengths based on the chosen material and cross section.

```
1  %Based on proposal by Schickhofer
2  function [E,rho_tow,f_t0netd,f_c0netd,gamma_n,gamma_fN,gamma_fA,gamma_fUn,
       f_vnetIPd,f_vnetOPd,f_rnetd,f_Td,Mat2]=Material(Mat,t,k_net)
3  %% Grouping of material classes
4  %For easier reference, strength classes are grouped under their material family
       in Mat2
5  if or(or(strcmp(Mat,'CL24h'),strcmp(Mat,'CL30h')),or(strcmp(Mat,'CL28h'),strcmp(
       Mat,'CL34h')))
6      Mat2='CLT';
7  elseif strcmp(Mat,'CL40h')
```

```matlab
 8         Mat2='CLT';
 9  elseif or(strcmp(Mat,'BBS'),strcmp(Mat,'BBQ'))
10         Mat2='LVL';
11  elseif or(strcmp(Mat,'KERTOS'),strcmp(Mat,'KERTOQ'))
12         Mat2='LVL';
13  elseif strcmp(Mat,'Steel')
14         Mat2='Steel';
15  end
16
17  %% Expected layout of CLT
18  %Some information about the layout of CLT panels, needed for strength calculation
19  n_lay=9; %Expected number of layers
20  n_boards=30; %Average number of boards in the direction of the tower axis, per
         element
21
22  %% Partial factors
23  %Material factors
24  if strcmp(Mat2,'CLT')
25         gamma_m=1.25; %Material factor for CLT
26  elseif strcmp(Mat2,'LVL')
27         gamma_m=1.2; %Material factor for LVL
28  elseif strcmp(Mat2,'Steel')
29         gamma_m=1.0; %Material factor for Steel
30  end
31
32  %Load factors
33  gamma_fN=1.35; %Normal load factor
34  gamma_fA=1.10; %Abnormal load factor
35  gamma_fUn=0.90; %Unfavorable load factor
36
37  %Component class factor
38  gamma_n=1.0; %Tower is component class 2.
39
40  %Modification factor, only used for timber materials
41  k_mod=1.1; %Short term action for all timber materials since the extreme gusts
         only last a couple of seconds
42
43  %Height factor for bending strength in timber
44  if strcmp(Mat2,'CLT')
45         if t<0.15
46             k_hb=min((150/(t*1000))^0.1,1.1);
47         else k_hb=1;
48         end
49  elseif strcmp(Mat2,'LVL')
50         k_hb=min((300/(t*1000))^(0.12),1.2);
51  end
52
53  %Height factor for tensile strength in timber
54  if strcmp(Mat2,'CLT')
55         if t<0.15
56             k_ht=k_hb;
57         else k_ht=1;
58         end
59  elseif strcmp(Mat2,'LVL')
60         k_ht=(3000/15000)^0.06;
61  end
62
```

```matlab
63  %System factor for tensile strength of CLT
64  if or(or(strcmp(Mat,'CL24h'),strcmp(Mat,'CL30h')),strcmp(Mat,'CL40h'))
65      k_syst0=min(0.075*log(n_boards)+1,1.20); %CV=25
66  elseif or(strcmp(Mat,'CL28h'),strcmp(Mat,'CL34h'))
67      k_syst0=min(0.130*log(n_boards)+1,1.35); %CV=35
68  elseif strcmp(Mat2,'LVL')
69      k_syst0=1;
70  elseif strcmp(Mat,'Steel')
71      k_syst0=1;
72  end
73
74  %% Base material properties and characteristic values
75  %Youngs Modulus and density
76  if or(strcmp(Mat,'CL24h'),strcmp(Mat,'CL28h'))
77      rho_tow=420; %kg/m^3
78      E=11e9*k_net; %N/m^2
79  elseif or(strcmp(Mat,'CL30h'),strcmp(Mat,'CL34h'))
80      rho_tow=460; %kg/m^3
81      E=12e9*k_net; %N/m^2
82  elseif strcmp(Mat,'CL40h')
83      rho_tow=650; %kg/m^3
84      E=11e9*k_net; %N/m^2
85  elseif strcmp(Mat,'KERTOS')
86      rho_tow=480;
87      E=13.8e9*k_net;
88  elseif strcmp(Mat,'KERTOQ')
89      rho_tow=480;
90      E=10.5e9*k_net;
91  elseif strcmp(Mat,'BBQ')
92      rho_tow=740;
93      E=11.8e9*k_net;
94  elseif strcmp(Mat,'BBS')
95      rho_tow=740;
96      E=16.8e9*k_net;
97  elseif strcmp(Mat,'Steel')
98      rho_tow=7850; %kg/m^3
99      E=2.1e11*k_net;
100 elseif strcmp(Mat,'HW')
101     rho_tow=552; %kg/m^3
102     E=12e9*k_net;
103 end
104
105 %Bending strength
106 if strcmp(Mat,'CL24h')
107     f_mk=24;% N/mm^2, CL24h
108 elseif strcmp(Mat,'CL28h')
109     f_mk=28;% N/mm^2, CL28h
110 elseif strcmp(Mat,'CL30h')
111     f_mk=30;% N/mm^2, CL30h
112 elseif strcmp(Mat,'CL34h')
113     f_mk=34;% N/mm^2, CL34h
114 elseif strcmp(Mat,'CL40h')
115     f_mk=40;% N/mm^2, CL40h
116 elseif strcmp(Mat,'BBS')
117     f_mk=65;% N/mm^2, BBS
118 elseif strcmp(Mat,'BBQ')
119     f_mk=45;% N/mm^2, BBQ
```

```matlab
120 elseif strcmp(Mat,'KERTOS')
121     f_mk=50;% N/mm^2, KERTO-S
122 elseif strcmp(Mat,'KERTOQ')
123     f_mk=36;% N/mm^2, KERTO-Q
124 elseif strcmp(Mat,'Steel')
125     f_mk=235;% N/mm^2, Steel
126 end
127
128 %Tensile strength
129 if or(strcmp(Mat,'CL24h'),strcmp(Mat,'CL28h'))
130     f_t0lk=14;% N/mm^2, T14
131 elseif or(strcmp(Mat,'CL30h'),strcmp(Mat,'CL34h'))
132     f_t0lk=18;% N/mm^2, T18
133 elseif strcmp(Mat,'CL40h')
134     f_t0lk=24;% N/mm^2, T24
135 elseif strcmp(Mat,'BBS')
136     f_t0lk=60;% N/mm^2, BBS
137 elseif strcmp(Mat,'BBQ')
138     f_t0lk=40;% N/mm^2, BBQ
139 elseif strcmp(Mat,'KERTOS')
140     f_t0lk=35;% N/mm^2, KERTOS
141 elseif strcmp(Mat,'KERTOQ')
142     f_t0lk=26;% N/mm^2, KERTOQ
143 elseif strcmp(Mat,'Steel')
144     f_t0lk=235;
145 end
146 f_t0netk=k_syst0*f_t0lk;
147
148 %Compression strength
149 if strcmp(Mat2,'CLT')
150     f_c0netk=f_mk;
151 elseif strcmp(Mat,'BBS')
152     f_c0netk=41.6;
153 elseif strcmp(Mat,'BBQ')
154     f_c0netk=24.2;
155 elseif strcmp(Mat,'KERTOS')
156     f_c0netk=35;
157 elseif strcmp(Mat,'KERTOQ')
158     f_c0netk=26;
159 elseif strcmp(Mat2,'Steel')
160     f_c0netk=235;
161 end
162
163 %Shear strength
164 if strcmp(Mat2,'CLT')
165     f_vnetIPk=5;
166     f_vnetOPk=3;
167     f_rnetk=1.25;
168     f_Tk=2.5;
169 elseif strcmp(Mat2,'Steel') %Can be ignored, here to prevent Matlab errors
170     f_vnetIPk=235/sqrt(3);
171     f_vnetOPk=235/sqrt(3);
172     f_rnetk=235/sqrt(3);
173     f_Tk=235/sqrt(3);
174 elseif strcmp(Mat,'BBS')
175     f_vnetIPk=8;
176     f_vnetOPk=8;
```

```matlab
177      f_rnetk=1.65;
178      f_Tk=8; %Can be ignored, here to prevent Matlab errors
179  elseif strcmp(Mat,'BBQ')
180      f_vnetIPk=9;
181      f_vnetOPk=3.3;
182      f_rnetk=3.3;
183      f_Tk=8; %Can be ignored, here to prevent Matlab errors
184  elseif strcmp(Mat,'KERTOS')
185      f_vnetIPk=4.1;
186      f_vnetOPk=2.3;
187      f_rnetk=0.3;
188      f_Tk=4.1; %Can be ignored, here to prevent Matlab errors
189  elseif strcmp(Mat,'KERTOQ')
190      f_vnetIPk=4.5;
191      f_vnetOPk=1.3;
192      f_rnetk=0.6;
193      f_Tk=4.5; %Can be ignored, here to prevent Matlab errors
194  end
195
196  %% Design material values
197  %Design value of material resistance is defined as Xd=k_mod*Xk/gamma_m for timber
198  if strcmp(Mat,'Steel') %Here to prevent errors
199      f_t0netd=235;
200      f_c0netd=235;
201      f_vnetIPd=235/sqrt(3);
202      f_vnetOPd=235/sqrt(3);
203      f_rnetd=235/sqrt(3);
204      f_Td=235/sqrt(3);
205  else
206      f_t0netd=k_ht*k_mod*f_t0netk/gamma_m/gamma_n;
207      f_c0netd=k_mod*f_c0netk/gamma_m/gamma_n;
208      f_vnetIPd=k_mod*f_vnetIPk/gamma_m/gamma_n;
209      f_vnetOPd=k_mod*f_vnetOPk/gamma_m/gamma_n;
210      f_rnetd=k_mod*f_rnetk/gamma_m/gamma_n;
211      f_Td=k_mod*f_Tk/gamma_m/gamma_n;
212  end
```

G-1-4   Geometry

Calculates the cross-sectional properties along the tower and loads resulting from self-weight.

```matlab
1  function [B_outT,B_outB,B,A_tow,A_towh,A_tow0,I_tow,I_towh,I_tow0,W_tow,W_towh,
       W_tow0,q_towi,q_tow,q_tow0]=Geometry(H,n_sides,a_outT,a_outB,t,rho_tow)
2  %The tower is divided into H elements of 1 m height
3
4  %% Calculate the width of the cross sections along the tower in the center of the
        elements (h=0.5,1.5,2.5,...)
5  %Devide the tower into H elements and calculate the parameter at the center of
       these elements
6  if n_sides==8
7      B_outT=sqrt(4+2*sqrt(2))*a_outT;
8      B_outB=sqrt(4+2*sqrt(2))*a_outB;
9  elseif n_sides==10
10      B_outT=(1+sqrt(5))*a_outT;
```

```matlab
11          B_outB=(1+sqrt(5))*a_outB;
12  elseif n_sides==0
13          B_outT=a_outT;
14          B_outB=a_outB;
15  end
16
17  B=zeros(H,1);
18  for i=1:H
19          B(i)=B_outB-(B_outB-B_outT)/H*(i-0.5);
20  end
21
22  %% %Calculate the cross-sectional area along the tower in the center of the
          elements (h=0.5,1.5,2.5,...)
23  Hi=zeros(H,1);
24  for i=1:H
25          Hi(i)=i-0.5;
26  end
27
28  a_outi=zeros(H,1);
29  for i=1:H
30          a_outi(i)=a_outB-(a_outB-a_outT)/H*Hi(i); %Side width at height i-0.5
31  end
32  a_out0=a_outB;
33
34  A_tow=zeros(H,1);
35  if n_sides==8
36          for i=1:H
37              A_tow(i)=8*a_outi(i)*t-3.31*t^2; %Area of each element center is at h=i-0
                  .5
38          end
39  elseif n_sides==10
40          for i=1:H
41              A_tow(i)=10*a_outi(i)*t-3.25*t^2;
42          end
43  elseif n_sides==0
44          for i=1:H
45              A_tow(i)=pi*((0.5*a_outi(i))^2-(0.5*a_outi(i)-t)^2);
46          end
47  end
48
49  %% %Calculate the cross-sectional area along the tower for the positions of
          calculations (h=1,2,3,...)
50  %Devide the tower into H elements and calculate the cross sectional area at the
          top of these elements
51  h=zeros(H,1);
52  for i=1:H
53          h(i)=i;
54  end
55
56  a_outh=zeros(H,1);
57  for i=1:H
58          a_outh(i)=a_outB-(a_outB-a_outT)/H*h(i); %Side width at height i
59  end
60
61  A_towh=zeros(H,1);
62  if n_sides==8
63          for i=1:H
```

```
64            A_towh(i)=8*a_outh(i)*t-3.31*t^2; %Area of each element, center is at h=i
65        end
66        A_tow0=t*a_out0*8-3.31*t^2;
67  elseif n_sides==10
68      for i=1:H
69            A_towh(i)=10*a_outh(i)*t-3.25*t^2;
70      end
71      A_tow0=t*a_out0*10-3.25*t^2;
72  elseif n_sides==0
73      for i=1:H
74            A_towh(i)=pi*((0.5*a_outh(i))^2-(0.5*a_outh(i)-t)^2);
75      end
76      A_tow0=pi*((0.5*a_out0)^2-(0.5*a_out0-t)^2);
77  end
78
79  %% Calculate the inner and outer radii of the cross sections along the tower for
         the center of the elements (h=0.5,1.5,2.5,...)
80  r=zeros(H,1);
81  R=zeros(H,1);
82  if n_sides==8
83      for i=1:H
84            r(i)=1.21*a_outi(i);
85            R(i)=1.30*a_outi(i);
86      end
87  elseif n_sides==10
88      for i=1:H
89            r(i)=1.54*a_outi(i);
90            R(i)=1.62*a_outi(i);
91      end
92  elseif n_sides==0
93          for i=1:H
94            r(i)=0.5*a_outi(i);
95            R(i)=0.5*a_outi(i);
96      end
97  end
98
99  %% Calculate the inner and outer radii of the cross sections along the tower for
         the positions of calculations (h=1,2,3,...)
100 rh=zeros(H,1);
101 Rh=zeros(H,1);
102 if n_sides==8
103     for i=1:H
104           rh(i)=1.21*a_outh(i);
105           Rh(i)=1.30*a_outh(i);
106     end
107     r0=1.21*a_outB;
108     R0=1.30*a_outB;
109 elseif n_sides==10
110         for i=1:H
111           rh(i)=1.54*a_outh(i);
112           Rh(i)=1.62*a_outh(i);
113     end
114     r0=1.54*a_outB;
115     R0=1.62*a_outB;
116 elseif n_sides==0
117         for i=1:H
118           rh(i)=0.5*a_outh(i);
```

```
119            Rh(i)=0.5*a_outh(i);
120        end
121        r0=0.5*a_outB;
122        R0=0.5*a_outB;
123  end
124
125  %% Calculate the cross sectional moment of inertia along the tower for the
          elements (h=0.5,1.5,2.5,...)
126  I_tow=zeros(H,1);
127  if n_sides==8
128        for i=1:H
129            I_tow(i)=6.16*a_outi(i)^3*t-7.65*a_outi(i)^2*t^2+4.23*a_outi(i)*t^3-0.88*
                  t^4; %For each element, centre is at h=i-0.5
130        end
131  elseif n_sides==10
132         for i=1:H
133            I_tow(i)=12.26*a_outi(i)^3*t-11.95*a_outi(i)^2*t^2+5.18*a_outi(i)*t^3-0
                  .84*t^4;
134         end
135  elseif n_sides==0
136        for i=1:H
137            I_tow(i)=pi/4*((0.5*a_outi(i))^4-(0.5*a_outi(i)-t)^4);
138        end
139  end
140
141  %% Calculate the cross sectional moment of inertia along the tower for the
          positions of calculations (h=1,2,3,...)
142  I_towh=zeros(H,1);
143  if n_sides==8
144        for i=1:H
145            I_towh(i)=6.16*a_outh(i)^3*t-7.65*a_outh(i)^2*t^2+4.23*a_outh(i)*t^3-0.88
                  *t^4; %For each element, center is at h=i
146        end
147        I_tow0=6.16*a_out0^3*t-7.65*a_out0^2*t^2+4.23*a_out0*t^3-0.88*t^4;
148  elseif n_sides==10
149        for i=1:H
150            I_towh(i)=12.26*a_outh(i)^3*t-12.95*a_outh(i)^2*t^2+5.18*a_outh(i)*t^3-0
                  .84*t^4;
151        end
152        I_tow0=12.26*a_out0^3*t-12.95*a_out0^2*t^2+5.18*a_out0*t^3-0.84*t^4;
153  elseif n_sides==0
154        for i=1:H
155            I_towh(i)=pi/4*((0.5*a_outh(i))^4-(0.5*a_outh(i)-t)^4);
156        end
157        I_tow0=pi/4*((0.5*a_out0)^4-(0.5*a_out0-t)^4);
158  end
159
160  %% Calculate the section modulus along the tower for the elements (h=0.5,1.5,2.5,
          ...)
161  W_tow=zeros(H,1);
162  if n_sides==8
163        for i=1:H
164            W_tow(i)=5.10*a_outh(i)^2*t-6.34*a_outh(i)*t^2+3.50*t^3-0.73*t^4/a_outh(i
                  );   %At each element, center is at h=i-0.5
165        end
166  elseif n_sides==10
167         for i=1:H
```

```matlab
168            W_tow(i)=7.57*a_outh(i)^2*t-7.38*a_outh(i)*t^2+3.20*t^3-0.52*t^4/a_outh(i
                   );
169        end
170 elseif n_sides==0
171     for i=1:H
172         W_tow(i)=pi/32*(a_outh(i)^4-(a_outh(i)-2*t)^4)/a_outh(i);
173     end
174 end
175
176 %% Calculate the section modulus along the tower for the positions of
        calculations (h=1,2,3,...)
177 W_towh=zeros(H,1);
178 for i=1:H
179     W_towh(i)=I_towh(i)/rh(i); %Area of each element, centre is at h=i
180 end
181 W_tow0=I_tow0/r0;
182
183 %% Calculate the self-weigth along the tower
184 %Calculate the self weigth of each element with its center at h=i-0.5
185 q_towi=zeros(H,1);
186 for i=1:H
187     q_towi(i)=A_tow(i)*rho_tow*9.81; %Self-weight per element in N, its center is
            at h=i+0.5
188 end
189
190 %Calculate the cumulative self-weigth along the tower in N
191 q_tow=zeros(H,1);
192 for i=1:H-1
193     q_t=zeros(H-1,1);
194     for j=i:H-1
195         q_t(j)=q_towi(j+1); %Store the weight of all elements above h=i
196     end
197     q_tow(i)=sum(q_t); %Summarize all elements above h=i
198 end
199 q_tow(H)=0;
200 q_tow0=sum(q_towi);
```

G-1-5   Frequency.m

Calculates the frequency of the tower, based on the geometrical and material input.

```matlab
1 function [f]=Frequency(H,mnac,mhub,E,rho_tow,A_tow,A_towh,I_tow)
2 % Uses the Rayleigh-Ritz method
3
4 %% Calculate the equivalent stiffness and mass(es)
5 Hi=zeros(H,1);
6 for i=1:H
7     Hi(i)=i-0.5;
8 end
9
10 mu=zeros(H,1);
11 for i=1:H
12     mu(i)=A_tow(i)*rho_tow; %Mass per unit length
13 end
```

```
14
15  EI=zeros(H,1);
16  for i=1:H
17      EI(i)=E*I_tow(i)*(cos((pi*Hi(i))/(2*H)))^2;
18  end
19  EIeq=sum(EI)/H; %Equivalent beam stiffness of the total support structure
20
21  m=A_towh*rho_tow;
22  mbeam=sum(m)/H; %Average beam mass
23
24  mh=zeros(H,1);
25  for i=1:H
26      mh(i)=mu(i)*(1-cos(pi*Hi(i)/(2*H)))^2;
27  end
28  meq=sum(mh)/H; %Equivalent mass of the total support structure
29
30  %% Calculate the natural period and frequency
31  T=sqrt(48/pi^4*((4*pi^2*H^3*(mnac+mhub+meq*H))/(3*EIeq))); %Natural period
32  f=1/T; %First natural frequency
```

G-1-6   Turbine types

This contains the properties of the considered turbine, among which are the dimensions, mass and aerodynamic properties of the blades.

NREL_5MW.m

This code already existed and was provided by DUWIND (the wind energy network of the Delft University of Technology) as part of their Windturbine Simulation package [74]. It has been slightly adjusted to be incorporated into the rest of the code.

```
1   function [P1,P2,P3,P4]=NREL_5MW(f,mnac,mhub,q_towi,q_tow0)
2   % Input of all required parameters of the NREL 5MW wind turbine
3   % Outputs
4   %     aerodynamic parameters P1=[rho,kp]
5   %     turbine parameters P2=[R,Nb,Jb,kb,mt,dt,kt,nu,Jr,dr,kr,...
6   %                           Jg,VLL,Pn,p,L_dfig]
7   %     blade geometry P3=[r;c;thetat]
8   %     nominal values P4=[Vn,lambdan,thetan]
9
10  %%Aerodynamic paramters
11  rho=1.25; % air density [kg/m3]
12  kp=0.9; % power loss factor [-]; correction factor for the simplifications in BEM
            [-], see listing 'bem.m'
13
14  P1=[rho,kp];
15
16  %% Turbine parameters
17  R=63; % rotor radius [m]
18  Nb=3; % number of blades [-]
19  mb=17740; % blade mass [kg]
20  mt=mnac+mhub+(sum(q_towi)+q_tow0)/9.81; % mass tower + nacelle [kg]
```

```matlab
21
22  Jb=11776047; % inertia blade (with respect to flapping hinge) [kg m^2]
23  omb=.668*2*pi;% the stiffness will be determined from the blade flap natural
        frequency omb [rad/s]
24  kb=Jb*omb^2; % stifness flap spring [Nm/rad]
25
26  omt=f*2*pi; % the stiffness will be determined from the tower natural frequency [
        rad/s]
27  kt=mt*omt^2;
28  dt=2*0.02*sqrt(kt*mt); % damping tower [N/(m/s)]; 2% critical damping assumed
29
30  Jg=534.116; % inertia generator [kg m^2]
31  Pn=4766949; % nominal (electrical) generator power [W]
32  eta=0.9; % efficiency generator [-]
33
34  nu=97; % transmission ratio [-]
35  Jr=Nb*Jb; % inertia rotor [kg m^2]
36  kr=867637000; % stiffness transmission [Nm/rad]
37  Jtot=(nu^2*Jg*Jr)/(nu^2*Jg+Jr); % total inertia transmission [kg m^2]
38  dr=2*0.05*sqrt(kr*Jtot);
39
40  P2=[R,Nb,Jb,kb,mt,dt,kt,nu,Jr,dr,kr,Jg,Pn,eta];
41
42  %% Blade properties
43  Ns=14; % number of blade elements [-]
44
45  % radial positions (with respect to rotor axis) of blade sections [m], not
        necessary equidistant.
46  % Note: the borders of the blade sections should be given; i.e. Ns+1 values
47  % First value is start of aerodynamic aerofoil, last value is blade tip (r=R)
48  r=[9.70 13.80 17.90 22.00 26.10 30.20 34.30 38.40 42.50 46.60 50.70 54.80 57.5333
        60.2667 63.00];
49
50  % chord of blade sections [m]
51  c=[4.348 4.625 4.580 4.356 4.131 3.878 3.624 3.379 3.133 2.887 2.641 2.400 2.218
        1.821 0.961];
52
53  % twist of blade sections [degrees];
54
55  thetat= [13.308 12.38 10.76 9.596 8.408 7.167 5.952 4.761 3.638 2.697 1.926 1.131
        0.593 0.215 0.0]; % by definition, the last value equals 0 (blade tip)
56
57  % check
58  if (length(r) ~= Ns+1),
59      error('number of radial positions not correct');
60  end
61  if (length(c) ~= Ns+1),
62      error('number of chord values not correct');
63  end
64  if (length(thetat) ~= Ns+1),
65      error('number of twist values not correct');
66  end
67
68  P3=[r;c;thetat];
69
70  %% Nominal values
71  Vn=11.4; % nominal (rated) wind speed [m/s]
```

```
72   lambdan=7.3; % nominal (rated) tip speed ratio [-]
73   thetan=-1.5; % nominal (rated) blade pitch angle [degrees]
74
75   P4=[Vn,lambdan,thetan];
```

NREL_3MW.m

The properties in this function have been scaled down from the 5 MW version according to Chapter 2.

```
1    function [P1,P2,P3,P4]=NREL_3MW(f,mnac,mhub,q_towi,q_tow0)
2    % Input of all required parameters of the scaled NREL 3MW wind turbine
3    % Outputs
4    %     aerodynamic parameters P1=[rho,kp]
5    %     turbine parameters P2=[R,Nb,Jb,kb,mt,dt,kt,nu,Jr,dr,kr,Jg,VLL,Pn,p,L_dfig]
6    %     blade geometry P3=[r;c;thetat]
7    %     nominal values P4=[Vn,lambdan,thetan]
8
9    %% Aerodynamic parameters
10   rho=1.25;% air density [kg/m3]
11   kp=0.9; % power loss factor [-]; correction factor for the simplifications in BEM
          [-], see listing 'bem.m'
12
13   P1=[rho,kp];
14
15   %% Turbine parameters
16   R=50; % rotor radius [m]
17   Nb=3; % number of blades [-]
18   mb=10500;% blade mass [kg]
19   mt=mnac+mhub+(sum(q_towi)+q_tow0)/9.81; % mass tower + nacelle [kg]
20
21   Jb=0.7*(100/126)^2*11776047; % inertia blade (with respect to flapping hinge) [kg
          m^2]
22   omb=.668*2*pi; % the stiffness will be determined from the blade flap natural
          frequency omb [rad/s]
23   kb=Jb*omb^2; % stifness flap spring [Nm/rad]
24
25   omt=f*2*pi; % the stiffness will be determined from the tower natural frequency [
          rad/s]
26   kt=mt*omt^2;
27   dt=2*0.02*sqrt(kt*mt); % damping tower [N/(m/s)]; 2% critical damping assumed
28
29   Jg=534.116; % inertia generator [kg m^2]
30   Pn=2766949; % nominal (electrical) generator power [W]
31   eta=0.9; % efficiency generator [-]
32
33   nu=97; % transmission ratio [-]
34   Jr=Nb*Jb; % inertia rotor [kg m^2]
35   kr=867637000; % stiffness transmission [Nm/rad]
36   Jtot=(nu^2*Jg*Jr)/(nu^2*Jg+Jr); % total inertia transmission [kg m^2]
37   dr=2*0.05*sqrt(kr*Jtot); % damping transmission [Nm/(rad/s)]; 5% critical damping
          assumed
38
39   P2=[R,Nb,Jb,kb,mt,dt,kt,nu,Jr,dr,kr,Jg,Pn,eta];
```

```
40
41  %% Blade geometry
42  Ns=14; % number of blade elements [-]
43
44  % radial positions (with respect to rotor axis) of blade sections [m], not
        necessary equidistant.
45  % Note: the borders of the blade sections should be given; i.e. Ns+1 values
46  % First value is start of aerodynamic aerofoil, last value is blade tip (r=R)
47  r=50/63*[9.70 13.80 17.90 22.00 26.10 30.20 34.30 38.40 42.50 46.60 50.70 54.80
        57.5333 60.2667 63.00];
48
49  % Chord of blade sections [m]
50  c=0.7*50/63*[4.348 4.625 4.580 4.356 4.131 3.878 3.624 3.379 3.133 2.887 2.641 2
        .400 2.218 1.821 0.961];
51
52  % twist of blade sections [degrees];
53  thetat= [13.308 12.38 10.76 9.596 8.408 7.167 5.952 4.761 3.638 2.697 1.926 1.131
         0.593 0.215 0.0]; % by definition, the last value equals 0 (blade tip)
54
55  % check
56  if (length(r) ~= Ns+1),
57      error('number of radial positions not correct');
58  end
59  if (length(c) ~= Ns+1),
60      error('number of chord values not correct');
61  end
62  if (length(thetat) ~= Ns+1),
63      error('number of twist values not correct');
64  end
65
66  P3=[r;c;thetat];
67
68  %% Nominal values
69  Vn=12; % nominal (rated) wind speed [m/s]
70  lambdan=73/Vn; % nominal (rated) tip speed ratio [-]
71  thetan=-1.5; % nominal (rated) blade pitch angle [degrees]
72
73  P4=[Vn,lambdan,thetan];
```

G-1-7   Blade_forces.m

Calculates the forces on the hub for load cases 2a and 2b, based on the quasi-static method described in section 2-2.

```
1  function [T1,T2]=Blade_forces(Class,Turb,H,f,Op,P2,P3)
2  %% Define values for class-related parameters
3  [V_ref,I_v,z_0,C,m]=feval(Class);
4
5  %% Collect blade properties
6  r=P3(1,:); %radial positions of blade elements
7  c=P3(2,:); %corresponding chord lengths for blade elements
8
9  %% Calculate total area of a single blade
10 x=zeros(1,length(r)); %Radial positions of center of blade elements
```

```matlab
11  x(1)=r(1)/2;
12  for i=2:length(x)
13      x(i)=(r(i)+r(i-1))/2;
14  end
15  y=zeros(1,length(c)); %Average chord per blade element
16  y(1)=c(1);
17  for i=2:length(y)
18      y(i)=(c(i)+c(i-1))/2;
19  end
20  A=zeros(1,length(c));
21  A(1)=y(1)*r(1);
22  for i=2:length(A)
23      A(i)=y(i)*(r(i)-r(i-1));
24  end
25  A_blade=sum(A);
26
27  %% Collect input parameters
28  z=H; %hub height
29  L=P2(1); %rotor radius
30  V_50=V_ref; %V_ref is also the 10-minute mean wind speed with a recurrence period
        of 50yrs
31  V_1=0.8*V_50; %Needed for load case 2b
32  C_max=1.5; %C_max is defined as the maximum of the drag coefficient and lift
        coefficient.
33  %The maximum for the considered blades is taken, which can be found in Jonkman.
34  rho=1.25; %air density
35
36  %% Define l using Kaimal, as in section 3.1.5 of DNV Riso
37  L_u=100*C*z^m; %Integral length scale
38  l=6.8*L_u;
39
40  %% Input parameters from section 4.5.3 of DNV Riso
41  %From here on, calculations will be done for all four considered design loads at
        the same time.
42  %These are 'blade loads', 'axial force', 'tilt moment' and 'yaw moment',
        respectively.
43  n_star=[1.7 0.45 1.7 0]; %Threshold values
44  n_0=[0.6993 f 0.6993 0]; %Eigenfrequencies corresponding to the considered design
        loads.
45  %The blade flap frequency is taken from Jonkman, the tower frequency is
        calculated with Frequency.m
46  h=[z+2/3*L z z+2/3*L z]; %Height corresponding to the considered design load
47
48  %% Determine wind speeds corresponding to the design loads
49  V_10=zeros(1,4);
50  if Op==2
51      for i=1:4
52          V_10(i)=V_50*(h(i)/z)^0.11; %Using the Extreme Wind Model (EWM) from the
                IEC 61400
53      end
54  elseif Op==3
55      for i=1:4
56          V_10(i)=V_1*(h(i)/z)^0.11; %Using the Extreme Wind Model (EWM) from the
                IEC 61400
57      end
58  end
59
```

```matlab
60  %% Aerodynamic admittance function
61  K1=zeros(1,4); %K1 is defined as n_0*L/V_10
62  for i=1:4
63      K1(i)=n_0(i)*L/V_10(i);
64  end
65  fa=zeros(1,4); %the aerodynamic admittance function
66  fa(1)=1/(1+3*K1(1));
67  fa(2)=1/(1+12*K1(2));
68  fa(3)=2.7*K1(3)/(1+4.4*K1(3)+21.8*K1(3)^2);
69  fa(4)=fa(3);
70
71  %% Define logarithmic increment of damping
72  zeta_0=0.02; %Estimated for timber as 2%
73  zeta_a=0.00477; %As defined by Jonkman, table 2-2
74  delta=2*pi*(zeta_0+zeta_a); %Logarithmic increment of damping
75
76  %% Calculate the resonance effect k_r
77  K2=zeros(1,4); %K2 is defined as n_0*l/V_10
78  for i=1:4
79      K2(i)=n_0(i)*l/V_10(i);
80  end
81  k_r=zeros(1,4);
82  for i=1:4
83      k_r(i)=K2(i)/(1+1.5*K2(i))^(5/3)*fa(i)*pi^2/(2*delta);
84  end
85
86  %% Calculate the background turbulence effect k_b
87  k_b=zeros(1,4);
88  k_b(1)=0.9-2.5*L/l;
89  k_b(2)=0.75-3*L/l;
90  k_b(3)=k_b(1);
91  k_b(4)=k_b(1);
92
93  %% Calculate the axial force F_thrust and the root moment M_root for all
        considered design loads for a single blade
94  F_thrust=zeros(1,4);
95  M_root=zeros(1,4);
96
97  %% Calculate the gust factor psi
98  psi=zeros(1,4);
99  for j=1:4
100     if K1(j)>n_star(j)
101         psi(j)=((log(z/z_0)+3.1)/log(z/z_0))^2;
102     else
103         psi(j)=1+3.9*(2*sqrt(k_b(j)+k_r(j)))/log(z/z_0);
104     end
105
106 %% Calculate blade force and root moment
107     F=zeros(1,length(c));
108     M=zeros(1,length(c));
109
110     for i=1:length(F)
111         F(i)=0.5*psi(j)*V_10(j)^2*A(i)*C_max; %Calculate the force on each blade
                segment
112     end
113     F_thrust(j)=sum(F);
114
```

```
115      M(1)=F(1)*x(1);
116      for i=2:length(A)
117          M(i)=F(i)*x(i); %Calculate the contribution of all the individual
                  elements to the root moment
118      end
119      M_root(j)=sum(M);
120  end
121
122  %% Collect intermediate results for easy reference and easy copying to report
123  T1=[n_star' n_0' h' V_10' K1' fa' K2' k_r' k_b' psi'];
124
125  %% %Collect final results for easy reference and easy copying to report (in N and
         Nm)
126  T2=[F_thrust' M_root'];
```

G-1-8   Turbine classes

IC.m

```
1  function [V_ref,I_V,z_0,C,m]=IC
2      V_ref=50; %V_ref is the considered reference wind speed at hub height
3      I_V=0.12; %The reference turbulence intensity
4      z_0=0.005; %z_0 is the Roughness length
5      C=1.83; %Using Figure 3.4 from DNV Riso
6      m=0.0885; %Using Figure 3.4 from DNV Riso
```

IIA.m

```
1  function [V_ref,I_v,z_0,C,m]=IIA
2      V_ref=42.5;
3      I_v=0.16;
4      z_0=0.2;
5      C=0.464;
6      m=0.336;
```

IIIA.m

```
1  function [V_ref,I_v,z_0,C,m]=IIIA
2      V_ref=37.5;
3      I_v=0.16;
4      z_0=0.2;
5      C=0.464;
6      m=0.336;
```

G-1-9   Top_Loads.m

Calculates the loads at the top of the tower, based on the results of either *powercurve.m* (LC1) or *Blade_forces.m* (LC 2a and 2b).

```matlab
function [F_zT,F_yT,F_xT,M_zT,M_yT,M_xT,M_rotx]=Top_Loads(Op,Turb,mnac,mhub,e,Dax
    ,Mbeta,T2)
%% %Define individual loads at the top
if Op==1
    F_yT=1.1*1.25*max(Dax); %Maximum thrust force in N, multiplied by 1.1 for
        faults and 1.25 for dynamic amplification
    b=find(Dax==max(Dax));
else
    F_yT=3*T2(2,1); %Thrust force in N
end

if Op==1
    M_rotx=1.1*1.25*Mbeta(b); %Corresponding with the highest Dax
else
    M_rotx=T2(3,2); %Tilt moment in Nm
end
F_nacz=mnac*9.81; %In N
F_hubz=mhub*9.81; %In N

%% %Define the eccentricities
e_huby=e(1);
e_nacy=e(5);
if Op==1
    e_yawm=0; %Yaw misalignment
elseif Op==2
    e_yawm=sind(8)*e_huby;
elseif Op==3
    e_yawm=sind(15)*e_huby;
end
%% %Calculate the resulting top loads at the top of the adapter in N and Nm
F_zT=F_nacz+F_hubz; %Used to calculate F_z(z)
F_yT=F_yT; %Used to calculate M_x(z) and F_y(z)
F_xT=0; %Not important for F_z(z), F_y(z) or M_x(z), set as 0
M_zT=e_yawm*F_yT; %Not important for F_z(z), F_y(z) or M_x(z), but it is for
    torsion and shear
M_yT=0; %Not important for F_z(z), F_y(z) or M_x(z), set as 0
M_xT=M_rotx+F_nacz*e_nacy-F_hubz*e_huby;%no F_yT*e_hubz
```

G-1-10   Wind_tower.m

Calculates the wind along the tower, based on the methods described in Chapter 6.

```matlab
function [F_w,F_w0,M_w,M_w0,q_wi,F_wi,Vh]=Wind_tower(Class,Op,Turb,H,a_outT,
    a_outB,V,B_outT,B_outB,B,T1,Dax,n_sides,f)
[V_ref,I_v,z_0,C,m]=feval(Class);

%% Various input parameters
```

```matlab
 5  k=0.001; %m
 6  r=0.05; %Corner radius of the polygon
 7  nu=10e-6; %Kinematic viscosity of air
 8  rho_a=1.25; %Density of air
 9  m_e=3763; %Average mass per unit of height, estimated from base model
10  n_1=f;
11
12  %% Define the heights of the center of the elements
13  %Divided into H elements, like in Geometry.m
14  Hi=zeros(H,1);
15  for i=1:H
16      Hi(i)=i-0.5;
17  end
18
19  %% Calculation of mean wind speeds
20  if Op==1
21      b=find(Dax==max(Dax)); %Highest top load
22      V_hub=max(V);   %Highest wind speed, conservative combination
23  else
24      V_50=V_ref; %For the turbulent extreme wind model, V_ref is also the 10-
                minute mean wind speed at hub height
25      V_hub=V_50;
26  end
27  Vh=zeros(H,1);
28  if Op==1
29      for i=1:H %Determine the mean wind speed at the center of the elements
30      Vh(i)=V_hub*((Hi(i))/H)^0.2;
31      end;
32  else
33      for i=1:H
34      Vh(i)=V_hub*((Hi(i))/H)^0.11;
35      end
36  end
37
38  %% Determine the force coefficient c_f using section 7.8 of Eurocode 1991 1-4.
39  Re=zeros(H,1); %Reynolds number
40  c_f0=zeros(H,1); %Force coefficient without end effects
41  for i=1:H
42  Re(i)=B(i)*Vh(i)/nu;
43      if n_sides==8
44          if r/B(i)<0.075
45              if Re(i)<2.4e5
46                  c_f0(i)=1.45;
47              elseif Re(i)>3e5
48                  c_f0(i)=1.30;
49              else
50                  c_f0(i)=(1.45+1.30)/2; %Not specified in EC1 1-4, so the average
                        is taken
51              end
52          else
53              if Re(i)<2e5
54                  c_f0(i)=1.30;
55              elseif Re(i)>7e5
56                  c_f0(i)=1.10;
57              else
58                  c_f0(i)=(1.30+1.10)/2; %Not specified in EC1 1-4, so the average
                        is taken
```

```matlab
59                end
60            end
61       elseif n_sides==10
62           c_f0(i)=1.3;
63       elseif n_sides==0
64               c_f0(i)=max(0.11/(Re(i)/10^6)^0.14,1.2+...
65                   (0.18*log10(10*k/B(i)))/(1+0.4*log10(Re(i)/10^6)));
66           if c_f0(i)>1.2
67               c_f0(i)=1.2;
68           elseif c_f0(i)<0.4
69               c_f0(i)=0.4;
70           else c_f0(i)=c_f0(i);
71           end
72       end
73 end
74 if n_sides==0
75     psi_lambda=0.78;
76 else
77 psi_lambda=0.9; %Factor that takes the end effects into account, based on figure
       7.36 of EC1 1-4
78 end
79 c_f=c_f0*psi_lambda; %Force coefficient including end effects
80
81 %% Determine cs
82 %Both conditions in 6.3.1(2) of EC1 1-4 are met so appendix C can be used
83 z_s=0.6*H; %Determine the turbulence length scale
84 L_zs=300*(z_s/200)^(0.67+0.05*log(z_0)); %Equation B.1 EC1 1-4
85 V_zs=Vh(z_s);
86
87 %Calculate the background responce factor
88 B_ave=(B_outT+B_outB)/2; %Use the average width to calculate the background
       factor
89 Bc=sqrt(1/(1+3/2*sqrt((B_ave/L_zs)^2+(H/L_zs)^2+((B_ave/L_zs)*(H/L_zs))^2))); %
       Equation C.1 EC1 1-4
90 Check1=Bc^2; %Should not be larger than 1
91
92 cs=(1+7*I_v*sqrt(Bc^2))/(1+7*I_v);
93
94 %% Determine cd
95 zeta_0=0.02; %Estimated for timber
96 zeta_a=mean(c_f)*rho_a*B_ave*V_zs/(2*n_1*m_e); %Equation F.18 from EC1 1-4
97 delta=2*pi*(zeta_0+zeta_a); %Logarithmic increment of damping
98
99 f_L=n_1*L_zs/V_zs;
100 S=6.8*f_L/((1+10.2*f_L)^(5/3)); %B.2 of EC1 1-4:
101 phi_y=11.5*B_ave*n_1/V_zs;
102 phi_z=11.5*H*n_1/V_zs;
103 G_y=1/2; G_z=3/8;
104 K_s=1/(1+sqrt((G_y*phi_y)^2+(G_z*phi_z)^2+(2/pi*G_y*phi_y*G_z*phi_z)^2)); %C.3 of
        EC1 1-4
105 Rc=sqrt(pi/(2*delta)*S*K_s); %C.2 of EC1 1-4
106 nu=f*sqrt(Rc^2/(Bc^2+Rc^2));
107 if nu<0.8
108     nu=0.8;
109 else
110     nu=nu;
111 end
```

```
112  k_p=sqrt(2*log(nu*600))+0.6/sqrt(2*log(nu*600));
113  if k_p<3
114      k_p=3;
115  else
116      k_p=k_p;
117  end
118
119  cd=(1+2*k_p*I_v*sqrt(Bc^2+Rc^2))/(1+7*I_v*sqrt(Bc^2));
120
121  %% Determine the structural factor cscd
122  cscd=cs*cd;
123  if cscd<0.85
124      cscd=0.85; %National Annex requires cscd to be at least 0.85
125
126  else
127      cscd=cs*cd;
128  end
129
130  %% Define the total factor C for each element
131  C=cscd*c_f;
132
133  %% Calculate the wind force per element (in N)
134  q_wi=zeros(H,1);
135  for i=1:H
136      q_wi(i)=0.75*1/2*rho_a*Vh(i)^2*B(i)*C(i)*1; %Center of each element is at h=i
                 -0.5, height of the element is 1 m
137  end
138  q_wik=q_wi/1000;
139  %One might plot(q_wik,Hi) to check the shape
140  Hi=zeros(H,1);
141  for i=1:H
142      Hi(i)=i-0.5;
143  end
144
145  a_outi=zeros(H,1);
146  for i=1:H
147      a_outi(i)=a_outB-(a_outB-a_outT)/H*Hi(i); %Side width at height i-0.5
148  end
149  a_out0=a_outB;
150  F_wi=zeros(H,1);
151  for i=1:H
152      F_wi(i)=q_wi(i)/a_outi(i); %Wind force in N/m^2 for Ansys
153  end
154
155  %% Calculate the cumulative wind force along the tower
156  F_w=zeros(H,1);
157  for i=1:H-1
158      q_s=zeros(H-1,1);
159      for j=i:H-1
160          q_s(j)=q_wi(j+1);
161      end
162      F_w(i)=sum(q_s);
163  end
164  F_w(H)=0;
165  F_w0=sum(q_wi);
166  F_wk=F_w/1000; %in kN
167
```

```
168  %% Calculate the moments along the tower caused by wind
169  M_w=zeros(H,1); %in Nm
170  %Since each element has a length of 1m, i can be used to depict the height above
         the ground when taken by steps of 1
171  for i=1:H-1 %Since the distributed wind load cannot cause a moment at i=H, i is
         taken only from 0 to H-1
172      M_wi=zeros(H,1);
173      for j=i:H-1
174          M_wi(j)=q_wi(j+1)*(Hi(j+1)-i); %Multiply the wind load on the elements
                 above height i with the distance of their center to height i
175      end
176      M_w(i)=sum(M_wi); %i = height above ground. So M_w(98) is the moment due to
             wind load at 98m above the ground
177  end
178  M_w(H)=0; %No moment occurs at height H, it is the end of the tower
179  M_wk=M_w/1000; %In kNm
180
181  M_w0i=zeros(H,1);
182  for i=1:H
183      M_w0i(i)=q_wi(i)*Hi(i); %Calculate the base moment separately
184  end
185  M_w0=sum(M_w0i);
```

G-1-11   Resulting_loads

Calculates the loads along the tower, based on the wind along the tower and the top loads,
using the formulas from Chapter 6.

```
1   function [F_x,M_x,F_y,M_y,F_z,M_z,F_x0,M_x0,F_y0,M_y0,F_z0,M_z0]=Resulting_loads(
        H,F_w,F_w0,M_w,M_w0,F_zT,F_yT,F_xT,M_zT,M_yT,M_xT,q_tow,q_tow0);
2   %% %Define variable h, height above ground, in stepts of 1m
3   h=zeros(H,1);
4   for i=1:H
5       h(i)=i;
6   end
7
8   %% Calculate the forces along the tower in N and Nm
9   %Using the formulas described in Chapter 6
10  F_x=zeros(H,1);
11  M_x=zeros(H,1);
12  F_y=zeros(H,1);
13  M_y=zeros(H,1);
14  F_z=zeros(H,1);
15  M_z=zeros(H,1);
16  for i=1:H
17      F_x(i)=F_xT;
18      M_x(i)=M_xT+F_yT*(H-i)+M_w(i);
19      F_y(i)=F_yT+F_w(i);
20      M_y(i)=M_yT;
21      F_z(i)=F_zT+q_tow(i);
22      M_z(i)=M_zT;
23  end
24
25  %% Calculate the forces at the bottom
```

```
26 | F_x0=F_xT;
27 | M_x0=M_xT+F_yT*H+M_w0;
28 | F_y0=F_yT+F_w0;
29 | M_y0=M_yT;
30 | F_z0=F_zT+q_tow0;
31 | M_z0=M_zT;
```

G-1-12 Stresses.m

Calculates the design stresses along the tower, based on the resulting loads.

```
1  | function [sigma_tenet,sigma_tenet0,sigma_conet,sigma_conet0,sigma_te,sigma_te0,
   |     sigma_co,sigma_co0]=Stresses(H,k_net,Op,M_x,M_x0,F_z,F_z0,A_towh,A_tow0,W_towh
   |     ,W_tow0,gamma_fN,gamma_fUn,gamma_fA)
2  | %% Determination of correct load factors
3  | if Op==1
4  |     gamma_f=gamma_fN;
5  | elseif Op==2
6  |     gamma_f=gamma_fA;
7  | elseif Op==3
8  |     gamma_f=gamma_fN;
9  | end
10 |
11 | %% Characteristic normal stresses due to F_z
12 | sigma_axnet=zeros(H,1);
13 | for i=1:H;
14 |     sigma_axnet(i)=-F_z(i)/(k_net*A_towh(i)*10^6); %In N/mm^2
15 | end
16 | sigma_axnet0=-F_z0/(k_net*A_tow0*10^6);
17 | sigma_ax=zeros(H,1);
18 | for i=1:H;
19 |     sigma_ax(i)=-F_z(i)/(A_towh(i)*10^6);
20 | end
21 | sigma_ax0=-F_z0/(A_tow0*10^6);
22 |
23 | %% Characteristic normal stresses due to M_x
24 | sigma_benet=zeros(H,1);
25 | for i=1:H;
26 |     sigma_benet(i)=M_x(i)*10^3/(k_net*W_towh(i)*10^9); %In N/mm^2
27 | end
28 | sigma_benet0=M_x0*10^3/(k_net*W_tow0*10^9);
29 | sigma_be=zeros(H,1);
30 | for i=1:H;
31 |     sigma_be(i)=M_x(i)*10^3/(W_towh(i)*10^9);
32 | end
33 | sigma_be0=M_x0*10^3/(W_tow0*10^9);
34 |
35 | %% Resulting design normal stresses, tension side
36 | sigma_tenet=zeros(H,1);
37 | for i=1:H
38 |     sigma_tenet(i)=gamma_fUn*sigma_axnet(i)+gamma_f*sigma_benet(i); %In case of
   |         tension, the self-weight is working favorable, hence the gamma_fUn
39 | end
40 | sigma_tenet0=gamma_fUn*sigma_axnet0+gamma_f*sigma_benet0;
```

```matlab
41  sigma_te=zeros(H,1);
42  for i=1:H
43      sigma_te(i)=gamma_fUn*sigma_ax(i)+gamma_f*sigma_be(i);
44  end
45  sigma_te0=gamma_fUn*sigma_ax0+gamma_f*sigma_be0;
46
47  %% Resulting design normal stresses, compression side
48  sigma_conet=zeros(H,1);
49  for i=1:H
50      sigma_conet(i)=gamma_f*sigma_axnet(i)-gamma_f*sigma_benet(i);
51  end
52  sigma_conet0=gamma_f*sigma_axnet0-gamma_f*sigma_benet0;
53  sigma_co=zeros(H,1);
54  for i=1:H
55      sigma_co(i)=gamma_f*sigma_ax(i)-gamma_f*sigma_be(i);
56  end
57  sigma_co0=gamma_f*sigma_ax0-gamma_f*sigma_be0;
```

G-2   Existing load calculation code

The following code was also written by DUWIND as part of their Windturbine Simulation package [74]. It has been used to calculate rotor loads according to the Blade Element Momentum Method. The only thing that has been adjusted is the syntax of the input of *powercurve.m*.

powercurve1.m

```matlab
1   function [Dax,Mbeta,Mr,P,Cdax,Cp,a,theta,omr]=powercurve1(Turb,V,P1,P2,P3,P4)
2   % syntax: function [Dax,Mbeta,Mr,P,Cdax,Cp,a,theta,omr]=...
3   % powercurve1(windturbine,V)
4   % Determination of the characteristics of a VARIABLE SPEED REGULATED...
5   % wind turbine
6   %    axial force versus wind speed                 Dax - V
7   %    aerodynamic flap moment versus wind speed     Mbeta - V
8   %    aerodynamic rotor torque versus wind speed    Mr - V
9   %    aerodynamic power versus wind speed           P - V
10  %    thrust coefficient versus wind speed          Cdax - V
11  %    power coefficient versus wind speed           Cp - V
12  %    induction factor versus wind speed            a - V
13  %    blade pitch angle versus wind speed           theta - V
14  %    rotor angular velocity versus wind speed      omr - V
15  % It is assumed that the wind turbine has an optimal lambda control, so:
16  %    Partial load (V<=Vn): lambda=lambdan, theta=thetan
17  %    Full load (V>Vn): omr=omrn; theta such that power equals nominal power
18  %
19  % Outputs:
20  %    Dax: axial force [N]
21  %    Mbeta: aerodynamic flap moment [Nm]
22  %    Mr: aerodynamic rotor torque [Nm]
23  %    P: aerodynamic power [W]
24  %    Cdax: thrust coefficient [-]
```

```
25 │ %      Cp: power coefficient [-]
26 │ %      a: induction factor [-]
27 │ %      theta: blade pitch angle [degrees]
28 │ %      omr: rotor angular velocity [rad/s]
29 │ % Inputs:
30 │ %      windturbine: name of file with wind turbine parameters (string)
31 │ %                   e.g.: 'LW50'
32 │ %      V: vector with wind speeds [m/s]
33 │
34 │ % required parameters
35 │ % rotor radius
36 │ R=P2(1);
37 │ % transmission ratio [-]
38 │ nu=P2(8);
39 │ % nominal wind speed [m/s]
40 │ Vn=P4(1);
41 │ % nominal tip speed ratio [-]
42 │ lambdan=P4(2);
43 │ % nominal blade pitch angle [degrees]
44 │ thetan=P4(3);
45 │
46 │ % stationary conditions: flap speed and tower top speed equal zero
47 │ betad=0;
48 │ xd=0;
49 │
50 │ % nominal rotor angular velocity
51 │ omrn=lambdan*Vn/R;
52 │ % nominal (mechanical) generator angular velocity
53 │ omgn=nu*omrn;
54 │ % nominal mechanical power Pn (wind speed equal to nominal wind speed;
55 │ % blade pitch angle equal to nominal blade pitch angle;
56 │ % rotor angular velocity equal to nominal rotor angular velocity)
57 │ [Dax,Mbeta,Mr,Pn,Cdax,Cp,a]=bem(Vn,thetan,betad,omrn,xd,P1,P2,P3);
58 │
59 │ N=length(V);
60 │ % calculation of aerodynamic forces, moments etc. for each wind speed
61 │ for i=1:N
62 │   if V(i) <= Vn
63 │      % partial load conditions (wind speed smaller or ...
64 │      % equal nominal wind speed)
65 │      % the tip speed ratio equals nominal tip speed ratio,
66 │      % so the rotor angular velocity equals:
67 │      omr(i)=lambdan*V(i)/R;
68 │      % the blade pitch angle equals nominal blade pitch angle
69 │      theta(i)=thetan;
70 │      % calculation of the aerodynamic forces, moments etc.
71 │      % by means of blade element-momentum method (BEM)
72 │      [Dax(i),Mbeta(i),Mr(i),P(i),Cdax(i),Cp(i),a(i)]=...
73 │          bem(V(i),theta(i),betad,omr(i),xd,P1,P2,P3);
74 │   else
75 │      % ful load conditions (wind speed larger than nominal wind speed)
76 │      % the rotor angular velocity is kept constant at nominal value
77 │      omr(i)=lambdan*Vn/R;
78 │      % the blade pitch angle should be such that the power ...
79 │      % equals nominal power;
80 │      % it is assumed that the blade pitch control is to zero-lift
81 │      % Use is made of the standard Matlab routine 'fzero' to find ...
```

```matlab
82        % a zero of the function 'fun_power.m'; 'fzero' varies
83        % the blade pitch angle (in the range thetan to 50) until 'fun_power'
84        % equals (about) zero.
85        warning off
86        options=optimset('Display','off');
87        theta(i)=fzero('fun_power',[thetan 50],options,V(i),Pn,P1,P2,P3,P4);
88        warning on
89        % since the blade pitch angle is determined,  the aerodynamic forces,
90        % moments and power can be calculated by means of the
91        % blade element - momentum method (BEM)
92        [Dax(i),Mbeta(i),Mr(i),P(i),Cdax(i),Cp(i),a(i)]=...
93            bem(V(i),theta(i),betad,omr(i),xd,P1,P2,P3);
94    end
95 end
```

bem.m

```matlab
 1 function [Dax,Mbeta,Mr,P,Cdax,Cp,a]=bem(V,theta,betad,omr,xd,P1,P2,P3);
 2 % syntax: function [Dax,Mbeta,Mr,P,Cdax,Cp,a]=
 3 % bem(V,theta,betad,omr,xd,P1,P2,P3);
 4 % Determintion of the aerodynamic forces, moments and power by means of the
 5 % blade element-momentum method (BEM); for known wind speed, pitch angle, etc.
 6 % Simplifications:
 7 %    - uniform flow (i.e. wind speed constant over rotor plane;
 8 %       no yawed flow, windshear or tower shadow)
 9 %    - no wake rotation (i.e. no tangential induction factor)
10 %    - no blade tip loss factor
11 %    - just one annular section (the total rotor plane)
12 %
13 % Output:
14 %    Dax: axial force [N]
15 %    Mbeta: aerodynamic flap moment [Nm]
16 %    Mr: aerodynamic rotor torque [Nm]
17 %    P: aerodynamic power [W]
18 %    Cdax: thrust coefficient [-]
19 %    Cp: power coefficient [-]
20 %    a: induction factor [-]
21 % Input:
22 %    V: undisturbed wind speed [m/s]
23 %    theta: pitch angle [degrees]
24 %    betad: flap velocity [rad/s]
25 %    omr: rotor angular velocity [rad/s]
26 %    xd: tower top velocity [m/s]
27 %    P1: aerodynamic parameters
28 %    P2: turbine parameters
29 %    P3: blade geometry
30
31
32 % Calculation of the inductionfactor a by means of BEM:
33 % Cdax according to the blade element method should be equal to Cdax
34 % according to the momentum theory
35 % Use is made of the standard Matlab routine 'fzero' to find a zero of
36 % the function 'fun_bem.m'; 'fzero' varies
37 % the induction factor a (in the range -0.5 to 2) until 'fun_bem' equals
```

```
38   % (about) zero.
39   warning off
40   options=optimset('Display','off');
41   a=fzero('fun_bem',[-0.5 2],options,V,theta,betad,omr,xd,P1,P2,P3);
42   warning on
43
44   % since the induction factor is determined, the aerodynamic forces,
45   % moments and power
46   % can be calculated by means of the blade element method
47   [Dax,Mbeta,Mr,P,Cdax,Cp]=aero2(a,V,theta,betad,omr,xd,P1,P2,P3);
```

fun_power.m

```
1    function Pd=fun_power(theta,V,Pn,P1,P2,P3,P4)
2    % syntax: function Pd=fun_power(theta,V,Pn,P1,P2,P3,P4)
3    % Determination of difference between aerodynamic power, for known blade
4    % pitch angle, and nominal power.
5    % This function is used by 'powercurve1' and 'equi'
6    %
7    % Output:
8    %    Pd: difference in power [W]
9    % Input:
10   %    theta: blade pitch anlge [degrees]
11   %    V: undisturbed wind speed [m/s]
12   %    Pn: nominal mechanical power [W]
13   %    P1: aerodynamic parameters
14   %    P2: turbine parameters
15   %    P3: blade geometry
16   %    P4: nominal values
17
18   % required parameters
19   % rotor radius
20   R=P2(1);
21   % nominal wind speed [m/s]
22   Vn=P4(1);
23   % nominal tip speed ratio [-]
24   lambdan=P4(2);
25
26   % stationary conditions: flap velocity and tower top velocity are equal zero
27   betad=0;
28   xd=0;
29
30   % the rotor angular velocity is kept constant at nominal value
31   omr=lambdan*Vn/R;
32
33   % power according to blade element-momentum method (BEM) for known blade
34   % pitch angle
35   [Dax,Mbeta,Mr,P,Cdax,Cp,a]=bem(V,theta,betad,omr,xd,P1,P2,P3);
36
37   % difference in power
38   Pd=P-Pn;
```

fun_bem.m

```matlab
function Cdaxd=fun_bem(a,V,theta,betad,omr,xd,P1,P2,P3)
% syntax: function Cdaxd=fun_bem(a,V,theta,betad,omr,xd,P1,P2,P3)
% Determination of the difference of the thrust coefficient Cdax
% according to the blade element method and the momentum theory;
% for known induction factor a.
% This function is used by 'bem.m'
%
% Output:
%     Cdaxd: difference in thrust coefficient [-]
% Inputs:
%     a: induction factor [-]
%     V: undisturbed wind speed [m/s]
%     theta: pitch angle [degrees]
%     betad: flap velocity [rad/s]
%     omr: rotor angular velocity [rad/s]
%     xd: tower top velocity [m/s]
%     P1: aerodynamic parameters
%     P2: turbine parameters
%     P3: blade geometry

% Cdax according to blade element method
[Dax,Mbeta,Mr,P,Cdax,Cp]=aero2(a,V,theta,betad,omr,xd,P1,P2,P3);

% Cdax according to momentum theory (the total rotor plane is treated as
% 1 annular section)
if (a > 0.5 & a < 1.62)
  % for these values of the induction factor a the momentum theory is
  % not valid;
  % instead an empirical relation is used
  Cdax2=1.49/(1.99-a);
else
  % momentum theory
  Cdax2=4*a*abs(1-a);
end

% difference in thrust coefficient Cdax according to
% blade element method and momentum theory
Cdaxd=Cdax-Cdax2;
```

aero2.m

```matlab
function [Dax,Mbeta,Mr,P,Cdax,Cp]=aero2(a,V,theta,betad,omr,xd,P1,P2,P3)
% syntax: function [Dax,Mbeta,Mr,P,Cdax,Cp]=...
%aero2(a,V,theta,betad,omr,xd,P1,P2,P3);
% 'Vector version' of the function 'aero.m';
% vector calculations are in Matlab much faster than for-loops
% See the listing of 'aero.m' for comments

rho=P1(1);
kp=P1(2);
```

```
10  R=P2(1);
11  Nb=P2(2);
12  Ns=length(P3)-1;
13  r=P3(1,:);
14  c=P3(2,:);
15  thetat=P3(3,:);
16
17  ri=(r(1:Ns)+r(2:Ns+1))/2;
18  ci=(c(1:Ns)+c(2:Ns+1))/2;
19  thetati=(thetat(1:Ns)+thetat(2:Ns+1))/2;
20  dr=r(2:Ns+1)-r(1:Ns);
21  Vp=V*(1-a).*ones(1,Ns)-betad.*ri-xd.*ones(1,Ns);
22  Vt=omr*ri;
23  W=sqrt(Vp.^2+Vt.^2);
24  phi=atan(Vp./Vt);
25  alpha=180/pi.*phi-(theta.*ones(1,Ns)+thetati);
26
27  Cl=lift(alpha);
28  dL=Cl.*0.5*rho.*W.^2.*ci.*dr;
29  Cd=drag(alpha);
30  dD=Cd.*0.5*rho.*W.^2.*ci.*dr;
31  dDax=Nb*(dL.*cos(phi)+dD.*sin(phi));
32  dMbeta=ri.*(dL.*cos(phi)+dD.*sin(phi));
33  dMr=Nb*ri.*(kp.*dL.*sin(phi)-dD.*cos(phi));
34
35  Dax=sum(dDax);
36  Mbeta=sum(dMbeta);
37  Mr=sum(dMr);
38
39  Cdax=Dax/(0.5*rho*pi*R^2*V^2);
40  P=omr*Mr;
41  Cp=P/(0.5*rho*pi*R^2*V^3);
```

lift.m

```
1   function Cl=lift(alpha)
2   % syntax: function Cl=lift(alpha)
3   % Lift curve of applied blade aerofoil
4   %
5   % Output:
6   %    Cl: lift coefficient [-]
7   % Input:
8   %    alpha: angle of attack [degrees]
9
10  % values in table format; 1st column alpha, 2nd column Cl
11
12  tabel=[
13  -180.0  -0.150
14  -178.0   0.186
15  -175.0   0.578
16  -173.0   0.727
17  -167.0   0.786
18  -163.0   0.644
19  -158.0   0.579
```

```
20   -153.0    0.722
21   -148.0    0.834
22   -143.0    0.912
23   -138.0    0.917
24   -133.0    0.866
25   -123.0    0.720
26   -113.0    0.513
27   -102.0    0.238
28    -93.0   -0.034
29    -83.0   -0.293
30    -72.0   -0.577
31    -62.0   -0.785
32    -52.0   -0.940
33    -45.0   -0.962
34    -36.0   -0.897
35    -33.0   -0.854
36    -29.0   -0.802
37    -25.0   -0.760
38    -20.0   -0.742
39    -16.0   -0.766
40    -14.0   -0.798
41    -10.0   -0.841
42     -9.0   -0.795
43     -8.0   -0.690
44     -6.0   -0.413
45     -4.0   -0.134
46     -2.0    0.135
47      0.0    0.391
48      2.0    0.654
49      4.0    0.908
50      6.0    1.153
51      8.0    1.337
52     10.0    1.400
53     12.0    1.450
54     14.0    1.498
55     16.0    1.535
56     17.0    1.497
57     19.0    1.443
58     21.0    1.403
59     23.0    1.367
60     26.0    1.322
61     29.0    1.284
62     32.0    1.249
63     35.0    1.229
64     42.0    1.240
65     47.0    1.200
66     52.0    1.123
67     57.0    1.021
68     62.0    0.910
69     67.0    0.761
70     71.0    0.634
71     77.0    0.454
72     82.0    0.311
73     87.0    0.145
74     92.0   -0.016
75     97.0   -0.147
76    102.0   -0.299
```

```
77    110.0  -0.529
78    118.0  -0.741
79    124.0  -0.897
80    129.0  -0.980
81    134.0  -1.024
82    141.0  -1.022
83    146.0  -0.938
84    152.0  -0.771
85    157.0  -0.689
86    161.0  -0.712
87    162.0  -0.825
88    163.0  -0.898
89    167.0  -0.937
90    172.0  -0.872
91    178.0  -0.458
92    180.0  -0.150];
93
94  % linear interpolation
95  Cl=interp1(tabel(:,1),tabel(:,2),alpha);
```

drag.m

```
1   function Cd=drag(alpha)
2   % syntax: function Cd=drag(alpha)
3   % Drag curve of applied blade aerofoil
4   %
5   % Output:
6   %    Cd: drag coefficient [-]
7   % Input:
8   %    alpha: angle of attack [degrees]
9
10  % values in table format; 1st column alpha, 2nd column Cd
11  tabel=[
12  -178.0   0.0266
13  -173.0   0.0513
14  -168.0   0.1368
15  -163.0   0.2546
16  -158.0   0.3940
17  -152.0   0.5814
18  -148.0   0.7146
19  -142.0   0.9036
20  -138.0   1.0332
21  -132.0   1.2078
22  -128.0   1.3316
23  -123.0   1.4602
24  -117.0   1.5714
25  -109.0   1.6864
26   -97.0   1.8003
27   -88.0   1.8174
28   -80.0   1.7452
29   -73.0   1.6625
30   -66.0   1.5486
31   -58.0   1.3543
32   -48.0   1.1106
```

```
33    -43.0    0.9647
34    -35.0    0.7420
35    -29.0    0.5672
36    -25.0    0.4427
37    -20.0    0.2983
38    -17.0    0.2070
39    -15.0    0.1340
40    -12.0    0.0657
41    -10.0    0.0383
42     -8.0    0.0161
43     -6.0    0.0094
44     -4.0    0.0082
45     -2.0    0.0076
46      0.0    0.0077
47      2.0    0.0078
48      4.0    0.0084
49      6.0    0.0092
50      8.0    0.0131
51     10.0    0.0221
52     12.0    0.0350
53     14.0    0.0550
54     16.0    0.0850
55     18.0    0.1280
56     20.0    0.1950
57     22.0    0.2600
58     25.0    0.3700
59     28.0    0.4900
60     32.0    0.6900
61     37.0    0.9348
62     42.0    1.1514
63     47.0    1.2993
64     52.0    1.4393
65     57.0    1.5507
66     62.0    1.6600
67     68.0    1.7684
68     77.0    1.8630
69     87.0    1.9186
70     94.0    1.9049
71     97.0    1.8828
72    104.0    1.7984
73    112.0    1.6853
74    121.0    1.5020
75    128.0    1.3281
76    132.0    1.2179
77    137.0    1.0649
78    142.0    0.9033
79    147.0    0.6956
80    152.0    0.5003
81    157.0    0.3474
82    162.0    0.2261
83    167.0    0.1083
84    172.0    0.0304
85    177.0    0.0221];
86
87  % linear interpolation
88  Cd=interp1(tabel(:,1),tabel(:,2),alpha);
```

G-3   Other Matlab code written in this research

Several other results have been calculated using Matlab. Their code and purpose are described below.

G-3-1   Influence of connection stiffness on frequency

The calculations on the influence of connection stiffness on the natural frequency in section 5-7 have been made using the code below.

```matlab
1  clear,clc
2  Mat='CL24h'; %The same materials as for the other calculations can be used
3  t_timber=[300 350 400 450 500 550 600]; %The calculations will be made
       simultaneously for different wall thicknesses
4  k_net=0.75; %Percentage of fibers in longitudinal direction
5  [E,rho_tow,f_t0netd,f_c0netd,gamma_n,gamma_fN,gamma_fA,gamma_fUn,f_vnetIPd,
       f_vnetOPd,f_rnetd,f_Td,Mat2]=Material(Mat,t_timber(1),k_net); %Uses
6  gamma_M=1.25;
7  k_mod=0.9; %Short term
8  eta_steel=0.6; %Percentage of net cross section of the steel plate
9  f_yd=235; %N/mm2
10 t_steel=2.5; %mm
11 k_con0=3.13e6*[0.1 0.5 1 2 5 10 ]; %The calculations will be made for different
       values of the connection stiffness simultaneously
12 l_timber=15000; %mm
13
14 l1=length(t_timber);
15 l2=length(k_con0);
16
17 b=zeros(l1,1);
18 E=zeros(l1,1);
19 for i=1:l1
20     [E,rho_tow,f_t0netd,f_c0netd,gamma_n,gamma_fN,gamma_fA,gamma_fUn,f_vnetIPd,
           f_vnetOPd,f_rnetd,f_Td,Mat2]=Material(Mat,t_timber(i),k_net); %Uses
           Material.m
21     E(i)=E;
22     b(i)=k_mod*(eta_steel*t_steel*f_yd)/(gamma_M*0.9*f_t0netd); %The 0.9*f_t0netd
           part can be adjusted to the appropriate stress level
23 end
24
25 A_timber=zeros(l1,l2);
26 k_con=zeros(l1,l2);
27 k_eq=zeros(l1,l2);
28 k_wall=zeros(l1,l2);
29 E_eq=zeros(l1,l2);
30 E_rel=zeros(l1,l2);
31 for i=1:l1
32     for j=1:l2
33         E_net=E(i)/10^6; %Change it from N/m^2 to N/mm^2
34         A_timber(i,j)=t_timber(i)*b(i);
35         k_con(i,j)=t_timber(i)/300*k_con0(j);
36         k_wall(i,j)=(E_net*A_timber(i,j))/(l_timber-t_timber(i));
37         k_eq(i,j)=1/(1/k_con0(j)+1/k_wall(i));
38         E_eq(i,j)=k_eq(i,j)*l_timber/A_timber(i,j);
```

```
39              E_rel(i,j)=E_eq(i,j)/(E_net);
40          end
41  end
```

G-3-2   Influence of foundation stiffness on frequency

The code behind the plots in Figure 5-5 is found below.

```
1   %Springs have been modeled underneath the model in Ansys.
2   %These have been given various stiffnesses, found below in k_v.
3   k_v=zeros(1,12); %k_v is the individual spring stiffness applied in Ansys.
4   for i=1:12
5       k_v(i)=10^(i+3); %Takes k_v from 10^4 to 10^15, which makes sure the total
            foundation stiffness varies as well
6   end
7   %For each calculation, the first natural frequency has been stored.
8   load('FoundationFreqs'); %In this file, the frequency results from Ansys are
        stored in a variable called 'Freqs'
9   %'Freqs' simply contains the individual spring stiffness applied in Ansys (which
        are the values in k_v), together with the first natural frequency of the tower
         for these values.
10  fi=zeros(1,12);
11  fi=flipud(Freqs(1:12,2)); %Load frequencies calculated in Ansys for all k_v's
        considered
12  %The code below will calculated the total K_phi for all values of k_v
13
14  load('Spring_coordinates_base_model'); %Coordinates of bottom nodes of FEM model,
         exported from Ansys
15  Ri=Springcoordinatesbasemodel(:,3); %Store these coordinates as Ri
16  Risq=zeros(length(Ri),1); %Square the coordinates
17  for i=1:length(Ri)
18      Risq(i)=Ri(i)^2;
19  end
20  for i=1:length(k_v)
21      Kphi(i)=sum(Risq)*k_v(i); %Calculate total rotational stiffness using k_phi=
            sum(k_v*R^2)
22  end
23
24  %% Plotting
25  finf=zeros(12,1)+0.24123; %Create a assymptotic line for the original freq
26  semilogx(Kphi,fi,Kphi,finf); %Plot to get a preview, x-axis is logarithmic
27
28  Extract=[Kphi' fi finf]; %For easy use in report
```

For the reference turbines in Vlissingen and the 'Zuidlob' park, as well as a base model,
foundation stiffness values have been calculated. This has been done using the code below.

Foundation stiffness for the base model

```
1  k=1.0e8; %Individual pile stiffness in N/m
2  R0=[11.5 9.5];        %Radial distances of pile rows to center. It is possible to
       add more rows.
3  Rcon=max(R0)+1.5; %Radius of the concrete slab, defined as 1.5 wider than the
       widest pile row
4  hcon=3.5;             %Height of the concrete slab
5  n=[40 24];            %Number of piles per row
6
7  F_y0=3600e3; %Design load in N
8  F_z0=8000e3; %Design load in N
9  M_x0=370000e3; %Design load Nm
10 F_slab=hcon*pi*Rcon^2*25000; %Total weight of the concrete slab in N
11
12 Kphii=zeros(1,length(n));
13 B1=zeros(max(n)/4,length(n));
14 B2=zeros(max(n)/4,length(n));
15
16 %Since the foundation is symmetrical, only 2 quarters will have to be
17 %calculated.
18 for j=1:length(n)
19     for i=1:n(j)/4 %For 0<_alpha<1/2pi
20         B1(i,j)=R0(j)*cos((i-1)*1/(n(j)/2)*pi);
21     end
22     for i=1:n(j)/4 %For -1/2pi<_alpha<0
23         B2(i,j)=R0(j)*cos((i-1)*1/(n(j)/2)*pi-0.5*pi);
24     end
25     Bsq=[B1;B2].^2; %Square all individual elements in R1 and R2
26     Kphii(j)=2*sum(Bsq(:,j))*k; %The foundation is symmetrical, hence the 2*, to
           incorporate both sides
27 end
28
29 Kphi=sum(Kphii);
30 I=Kphi/k;
31
32 %% Pile forces per quarter
33 %The suitability of the foundation layout will have to be judged according to the
        values of the pile forces, calculated below
34 F_pileslab=F_slab/sum(n); %Slab weight divided equally over the piles
35 F_pileFz=F_z0/sum(n); %Turbine weight divided equally over the piles
36 F_pilem=zeros(max(n)/4,length(n));
37 F_piletens=zeros(max(n)/4,length(n));
38 F_pilecomp=zeros(max(n)/4,length(n));
39
40 for j=1:length(n)
41     for i=1:n(j)/4
42     F_pilem(i,j)=M_x0/I*B1(i,j); %Individual pile loads due to M_x
43     F_piletens(i,j)=1/1000*(1.35*F_pilem(i,j)-0.9*F_pileslab-0.9*F_pileFz); %
           Resulting design pile load on the tension side. Favourable forces have
           been multiplied by 0.9
44     F_pilecomp(i,j)=1/1000*(-1.35*F_pilem(i,j)-1.35*F_pileslab-1.35*F_pileFz); %
           Resulting design pile load on the compression side
45     end
46 end
47
```

```
48  %Check pile distance as well
49  d=zeros(length(n),1);
50  for j=1:length(n)
51      d(j)=2*pi*R0(j)/n(j);
52  end
```

Foundation stiffness for the Vlissingen turbine

```
1   k=1.0e8; %Individual pile stiffness in N/m
2   R0=[11.5 9.5];         %Radial distances of pile rows to center. It is possible to
        add more rows.
3   Rcon=max(R0)+1.5; %Radius of the concrete slab, defined as 1.5 wider than the
        widest pile row
4   hcon=3.5;              %Height of the concrete slab
5   n=[40 24];             %Number of piles per row
6
7   F_y0=3600e3; %Design load in N
8   F_z0=8000e3; %Design load in N
9   M_x0=370000e3; %Design load Nm
10  F_slab=hcon*pi*Rcon^2*25000; %Total weight of the concrete slab in N
11
12  Kphii=zeros(1,length(n));
13  B1=zeros(max(n)/4,length(n));
14  B2=zeros(max(n)/4,length(n));
15
16  %Since the foundation is symmetrical, only 2 quarters will have to be
17  %calculated.
18  for j=1:length(n)
19      for i=1:n(j)/4 %For 0<_alpha<1/2pi
20          B1(i,j)=R0(j)*cos((i-1)*1/(n(j)/2)*pi);
21      end
22      for i=1:n(j)/4 %For -1/2pi<_alpha<0
23          B2(i,j)=R0(j)*cos((i-1)*1/(n(j)/2)*pi-0.5*pi);
24      end
25      Bsq=[B1;B2].^2; %Square all individual elements in R1 and R2
26      Kphii(j)=2*sum(Bsq(:,j))*k; %The foundation is symmetrical, hence the 2*, to
            incorporate both sides
27  end
28
29  Kphi=sum(Kphii);
30  I=Kphi/k;
31
32  %% Pile forces per quarter
33  %The suitability of the foundation layout will have to be judged according to the
         values of the pile forces, calculated below
34  F_pileslab=F_slab/sum(n); %Slab weight divided equally over the piles
35  F_pileFz=F_z0/sum(n); %Turbine weight divided equally over the piles
36  F_pilem=zeros(max(n)/4,length(n));
37  F_piletens=zeros(max(n)/4,length(n));
38  F_pilecomp=zeros(max(n)/4,length(n));
39
40  for j=1:length(n)
41      for i=1:n(j)/4
42      F_pilem(i,j)=M_x0/I*B1(i,j); %Individual pile loads due to M_x
```

```
43        F_piletens(i,j)=1/1000*(1.35*F_pilem(i,j)-0.9*F_pileslab-0.9*F_pileFz); %
              Resulting design pile load on the tension side. Favourable forces have
              been multiplied by 0.9
44        F_pilecomp(i,j)=1/1000*(-1.35*F_pilem(i,j)-1.35*F_pileslab-1.35*F_pileFz); %
              Resulting design pile load on the compression side
45    end
46 end
47
48 %Check pile distance as well
49 d=zeros(length(n),1);
50 for j=1:length(n)
51     d(j)=2*pi*R0(j)/n(j);
52 end
```

Foundation stiffness for the 'Zuidlob' turbine

```
1  k=1.0e8; %N/m
2  R0=[8.6];
3  n=[32];
4  Kphii=zeros(1,length(n));
5
6  for j=1:length(n)
7      B1=zeros(n(j)/4,1);
8      B2=zeros(n(j)/4,1);
9      for i=1:n(j)/4 %For 0<_alpha<1/2pi
10         B1(i)=R0(j)*cos((i-1)*1/(n(j)/2)*pi);
11     end
12     for i=1:n(j)/4 %For -1/2pi<_alpha<0
13         B2(i)=R0(j)*cos((i-1)*1/(n(j)/2)*pi-0.5*pi);
14     end
15     Bsq=[B1;B2].^2; %Square all individual elements in R1 and R2
16     Kphii(j)=2*sum(Bsq)*k;
17 end
18
19 Kphi=sum(Kphii)
```

APDL code for ANSYS

On the next pages the complete code that has been used in FEM calculations is provided. The separate components of this code will be discussed afterwards, reasoning behind them explained where necessary.

```
 1: !START INPUT
 2:      /CLEAR,START              !New project.
 3:      /CWD,'C:\Users\...\ANSYS' !The folder where Matlab stores the
 4:                                !wind pressure file.
 5:      /UIS,MSGPOP,3             !Lessens the amount of messages.
 6:
 7: !PREPROCESSING PHASE
 8:      /PREP7                    !Starts the preprocessing phase.
 9:
10: !USER INPUT
11:      !All units are in N, kg and m.
12:
13:   !INPUT PARAMETERS
14:      !Copy these from the Matlab model or adjust manually.
15:      n_sides=              8 !Number of sides of the cross section (8 or 10).
16:      a_out_B=              4 !Outer side width at the bottom.
17:      a_out_T=           1.15 !Outer side width at the top.
18:      H=                  125 !Height of the tower.
19:      t=                  0.4 !Wall thickness (constant over height).
20:      M_top=        1.765e+05 !Mass applied at the top (rotor+nacelle).
21:      knet=               0.7 !The ratio of fibers in the longitudinal direction.
22:      rho=                460 !Density of the tower material.
23:      YM=             8.4e+09 !Young's modulus of the tower material.
24:      FYT=         1.0211e+06 !Design horizontal force at hub height.
25:      MXT=         6.9746e+06 !Design overturning moment at hub height.
26:      MZT=           2.16e+05 !Design torsional moment at hub height.
27:      Grav=            10.791 !Gravitational constant multiplied by partial load factor.
28:
29:   !BUCKLING
30:
31:      lambda=1
32:
33:      !When lambda is set a 1, the buckling result from Ansys will also multiply gravity by
34:      !the factor it displays. Search manually for a lambda where Ansys displays
35:      !a buckling factor of 1.00. The input lambda is then the actual buckling factor.
36:      !Make sure this is set to 1 for regular calculations.
37:
38:   !OTHER INPUT
39:      !The Matlab model automatically stores the needed wind pressure loads on the
40:      !tower in a file called 'Wind.txt'. As long as the correct folder is
41:      !assigned here, it will read the values and store them for use in ANSYS.
42:
43:      *DIM,Windtow,TABLE,H,1,1,Height,Wind,  !Create a table to store the values.
44:      *TREAD,WINDTOW,'Wind','txt',,1,        !Fill the table.
45:
46:   !GEOMETRIC PROPERTIES
47:      !Here other parameters are defined or calculated based on the input.
48:
49:      !Fixed variables:
50:      nu=0.3                                 !Poisson's ratio.
51:      I_m=M_top*0                            !Rotary inertia of the top mass in kg*m.
52:
53:      !Calculate geometrical quantities for octagons:
54:      *IF,n_sides,EQ,8,THEN
55:      r_out_B=1.21*a_out_B                   !In m.
56:      r_in_B=r_out_B-t                       !In m.
57:      a_in_B=r_in_B/1.21                     !In m.
58:      r_out_T=1.21*a_out_T                   !In m.
59:      r_in_T=r_out_T-t                       !In m.
60:      a_in_T=r_in_T/1.21                     !In m.
61:      ratio1=a_out_T/a_out_B                 !Ratio between top width and bottom width,
62:                                             !outside.
63:      ratio2=a_in_T/a_in_B                   !Ratio between top width and bottom width,
64:                                             !inside.
65:      *ENDIF
66:
67:      !Calculate geometrical quantities for decagons:
68:      *IF,n_sides,EQ,10,THEN
69:      r_out_B=1.54*a_out_B                   !In m.
70:      r_in_B=r_out_B-t                       !In m.
71:      a_in_B=r_in_B/1.54                     !In m.
72:      r_out_T=1.54*a_out_T                   !In m.
73:      r_in_T=r_out_T-t                       !In m.
```

```
74:      a_in_T=r_in_T/1.54                       !In m.
75:      ratio1=a_out_T/a_out_B                   !Ratio between top width and bottom width,
76:                                               !outside.
77:      ratio2=a_in_T/a_in_B                     !Ratio between top width and bottom width,
78:                                               !inside.
79:      *ENDIF
80:
81: !ELEMENT DEFINITION
82:      !Define element types to be used throughout project:
83:      ET,1,PLANE183                            !8-node solid plane element.
84:      ET,2,SOLID186                            !20-node solid brick element.
85:      ET,3,MASS21                              !Dimensionless point mass element.
86:      ET,4,SOLID185                            !To prevent abnormalities around the supports,
87:                                               !midside nodes are removed at the bottom
88:                                               !later on.
89:                                               !SOLID185 does not have midside nodes and will
90:                                               !only be used there.
91:
92: !VIEW ADJUSTMENT
93:      !Set view for potential animations and easy graphical checks:
94:      /VIEW,1,,-1                              !Define for which window the view should
95:                                               !be adjusted.
96:      /ANG,1                                   !Adjust the viewing angles.
97:      /ANG,1,30,XS,1
98:      /ANG,1,30,XS,1
99:      /REP,FAST                                !Replot.
100:
101: !MATERIAL PROPERTIES
102:      !Apply isotropic material properties:
103:      MPTEMP,,,,,,,,                           !Undo previous selections.
104:      MPTEMP,1,0                               !Define properties for material 1.
105:      MPDATA,EX,1,,YM                          !Set Young's modulus.
106:      MPDATA,PRXY,1,,nu                        !Set Poisson's ratio.
107:      MPTEMP,,,,,,,,                           !Undo previous selections.
108:      MPTEMP,1,0                               !Define properties for material 1.
109:      MPDATA,DENS,1,,rho                       !Set density.
110:
111: !MASS PROPERTIES
112:      !Define the properties of the top mass:
113:      R,1,M_top,M_top,M_top,I_m,I_m,I_m
114:                                               !Defines real constant set 1 as mass M_top and
115:                                               !inertia I_m in all three directions.
116:
117: !CREATE GEOMETRY
118:      !Create hollow octagon cross section:
119:      Rpoly, n_sides,a_out_B                   !Create a regular polygon with n_sides,
120:                                               !side width a_out_B.
121:      Rpoly, n_sides,a_in_B                    !Create a regular polygon with n_sides,
122:                                               !side width a_in_B.
123:      ASEL,ALL                                 !Make sure all areas are selected,
124:                                               !undoing all previous selections.
125:      CSYS,1                                   !Set the coordinate system to cylindrical.
126:                                               !In this way, rotating the two octagonal areas
127:                                               !that were created is easier.
128:      AGEN, ,ALL, , , ,180/n_sides,0, , ,1
129:                                               !Rotates the areas so that one side is
130:                                               !perpendicular to the x-axis. In this way,
131:                                               !loads can be applied more easily.
132:      CSYS,0                                   !Set the coordinate system back to default.
133:      VEXT,1, , ,0,0,H,ratio1,ratio1,0
134:                                               !Extrude the outer polygon to height H,
135:                                               !tapering with ratio1.
136:      VEXT,2, , ,0,0,H,ratio2,ratio2,0,
137:                                               !Extrude the inner polygon to height H,
138:                                               !tapering with ratio2.
139:      VSBV,1,2                                 !Subtract the inner volume from the outer.
140:                                               !This will result in one volume, an octagonal
141:                                               !tube with a constant thickness.
142:
143: !MESHING
144:      !Because of the extrusion of the octagons vertical lines are readily created.
145:
146:   !SET ELEMENT SIZES ON VERTICAL LINE ELEMENTS
```

```
147:    LSEL,ALL                              !Make sure all lines are selected, undoing all
148:                                          !previous selections before defining a new
149:                                          !selection that is supposed to select from
150:                                          !all lines.
151:    LSEL,S,LOC,Z,1,H-1                    !Select the appropriate lines.
152:                                          !These are all the 'vertical' lines,
153:                                          !everything other than those at Z=0 and Z=H.
154:    LESIZE,ALL,,,H                        !Divide each line into H elements.
155:
156: !CREATE KEYPOINTS ON VERTICAL LINES
157:    LSEL,ALL                              !Make sure all lines are selected,
158:                                          !undoing all previous selections.
159:    LSEL,S,LOC,Z,1,H-1                    !Select the appropriate lines, see above.
160:
161:    !The following do-loops create keypoints on the vertical lines:
162:    *DO,j,3*n_sides+1,4*n_sides,1         !This selects the lines on the outside of the
163:                                          !polygon, independent of it beign an octagon
164:                                          !or decagon.
165:    *DO,i,1,H,1
166:    KL,j,i*(1/H)                          !Create a keypoint on line j at height i
167:    *ENDDO
168:    *ENDDO
169:    *DO,j,5*n_sides+1,6*n_sides,1         !This selects the lines on the inside of the
170:                                          !polygon, independent of it beign an octagon
171:                                          !or decagon.
172:    *DO,i,1,H,1
173:    KL,j,i*(1/H)                          !Create a keypoint on line j at height i.
174:    *ENDDO
175:    *ENDDO
176:       !These keypoints will be used to form the elements of the mesh.
177:
178: !CREATE HORIZONTAL LINES BETWEEN THE VERTICAL ONES
179:    LSEL,ALL                              !Make sure all lines are selected,
180:                                          !undoing all previous selections.
181:    *DO,i,1,H,1                           !Perform the same actions for all heights.
182:    KSEL,ALL                              !Make sure alle keypoints are selected,
183:                                          !undoing all previous selections.
184:    KSEL,S,LOC,Z,i                        !Select the keypoints at height i.
185:    *GET,MINKP,KP,,NUM,MIN                !The smallest keypoint number will be the start.
186:    *SET,KP1,MINKP                        !Store this as KP1.
187:    *DO,j,1,n_sides-1,1
188:    *GET,KP2,KP,KP1,NXTH                  !Get the next keypoint number, store as KP2.
189:    L,KP1,KP2                             !Create a line between KP1 and KP2.
190:    *SET,KP1,KP2                          !Set the keypoint number of KP2 as KP1.
191:    *ENDDO
192:    L,KP2,MINKP                           !Create a line between the last and
193:                                          !first keypoints.
194:    *ENDDO
195:
196: !SET ELEMENT SIZES ON HORIZONTAL LINE ELEMENTS
197:    LSEL,ALL                              !Make sure all lines are selected,
198:                                          !undoing all previous selections.
199:    LSEL,U,LOC,Z,1,H-1                    !Unselect all vertical lines.
200:    LESIZE,ALL,,,4                        !Set element size on these lines as 1/4
201:                                          !of length of line length.
202:
203: !CREATE SEPERATE VOLUMES
204:      !This will allow for easier selection of elements later on.
205:      !Each side will  become a seperate volume.
206:
207:    !Create lines between the corners at the top and bottom:
208:    LSEL,ALL                              !Make sure all lines are selected,
209:                                          !undoing all previous selections.
210:    KSEL,ALL                              !Make sure all keypoints are selected,
211:                                          !undoing all previous selections.
212:    *DO,i,1,n_sides,1                     !Create lines between the inner and
213:                                          !outer corners of the bottom.
214:    L,i,i+n_sides                         !Because of the way the model is constructed,
215:                                          !nodes 1 to n_sides will be the bottom nodes
216:                                          !at the outer corners.
217:                                          !Nodes n_sides+1 to 2*n_sides are the
218:                                          !inner corners.
219:    *ENDDO
```

```
220:
221:        *DO,i,n_sides*2+1,n_sides*3,1                  !Create lines between the inner and
222:                                                       !outer corners of the top.
223:        L,i,i+n_sides                                  !Because of the way the model is constructed,
224:                                                       !nodes 2*n_sides+1 o 3*n_sides will be the
225:                                                       !bottom nodes at the outer corners.
226:                                                       !Nodes 3*n_sides+1 to 4*n_sides will be the
227:                                                       !inner corners.
228:        *ENDDO
229:
230:        !Set element size for these new lines:
231:        *GET,LMAX,LINE,,NUM,MAXD                        !Store the maximum line number,
232:                                                       !which will be the last line created.
233:        LSEL,ALL                                       !Make sure all lines are selected,
234:                                                       !undoing all previous selections.
235:        LSEL,S,,,LMAX-2*n_sides+1,LMAX                 !Select the last created lines.
236:        LESIZE,ALL,,,1                                 !Set the element size to 1 times the
237:                                                       !line length.
238:
239:        !Create n_sides (8 or 10) volume elements that make up the walls:
240:        VDELE,3                                        !Delete the existing volume.
241:        VSEL,ALL                                       !Make sure all volumes are selected,
242:                                                       !undoing all previous selections.
243:        KSEL,ALL                                       !Make sure all keypoints are selected,
244:                                                       !undoing all previous selections.
245:        ESEL,ALL                                       !Make sure all elements are selected,
246:                                                       !undoing all previous selections.
247:        LSEL,ALL                                       !Make sure all lines are selected,
248:                                                       !undoing all previous selections.
249:        V,n_sides,1,n_sides+1,n_sides*2,n_sides*3,n_sides*2+1,n_sides*3+1,n_sides*4
250:                                                       !This creates the first volume,
251:                                                       !independent of 8 or 10 sides.
252:                                                       !The following do-loop will create
253:                                                       !the other volumes, independent of 8 or
254:                                                       !10 sides.
255:        *DO,i,1,n_sides-1
256:        V,i,i+1,i+1+n_sides,i+n_sides, n_sides*2+i,n_sides*2+i+1,n_sides*3+i+1,n_sides*3+i
257:        *ENDDO
258:
259:        !Set the element options:
260:        VSEL,ALL                                       !Make sure all volumes are selected,
261:                                                       !undoing all previous selections.
262:        TYPE,2                                         !Set elements to be created to be
263:                                                       !solid elements.
264:        MAT,1                                          !Apply material 1 to all elements to be created.
265:        REAL,1                                         !Apply real constant set 1 to all elements
266:                                                       !to be created.
267:
268:        !Mesh
269:        VSWEEP,ALL                                     !Mesh by sweeping the volumes
270:
271: !ELEMENT ADJUSTMENTS
272:        !Removing midside nodes:
273:          !To prevent unwanted behaviour at the base, the midside nodes in the
274:          !elements there are removed by replacing the elements there with
275:          !elements without midside nodes.
276:
277:        ESEL,ALL                                       !Make sure all elements are selected,
278:                                                       !undoing all previous selections.
279:        ESEL,S,CENT,Z,0,1                              !Select all elements between Z=0 and Z=1.
280:        EMODIF,ALL,TYPE,4                              !Modify the selected elements to become of
281:                                                       !type 4 (SOLID185).
282:
283:        !Create new coordinate systems:
284:        !These will be used to display results in the correct way.
285:        *DO,i,11,11+n_sides-2,1                        !This creates as many new coordinate systems
286:                                                       !as there are sides to the polygon, starting
287:                                                       !the numbering of the systems at 11.
288:        LOCAL,i,0,0,0,0,(i-10)*360/n_sides
289:                                                       !Creates a rotated coordinate system with n
290:                                                       !umbers as above, rotated 360/n_sides degrees
291:                                                       !further than the previous one.
292:        *ENDDO
```

```
293:    CSYS,0                                !Set the coordinate system back to default.
294:
295:    !Adjust element coordinate systems:
296:      !To be able to view the shear forces in all elements correctly, the element
297:      !coordinate systems of all elements will be rotated, so that the x-axis will
298:      !be perpendicular to the surface, independent of the orientation of the element.
299:
300:    *DO,j,11,11+n_sides-2,1                !The element coordinate systems will be adjusted
301:                                          !for n_sides-1 sides.
302:    CSYS,j                                 !Set the coordinate system to be one of the
303:                                          !new created systems.
304:    VSEL,S,,,j-9                           !Select the appropriate volume (one of the
305:                                          !newly created ones).
306:    ESLV,S                                 !Select all elements associated with these
307:                                          !volumes.
308:    EMODIF,ALL,ESYS,j                      !Modify the element coordinate systems of
309:                                          !these selected elements to coincide with the
310:                                          !selected coordinate systems.
311:    *ENDDO
312:    VSEL,ALL                              !Make sure all volumes are selected,
313:                                          !undoing all previous selections.
314:    CSYS,0                                 !Set the coordinate system back to default.
315:
316:    !Confine bottom rigidly
317:    ESEL,ALL                              !Make sure all elements are selected,
318:                                          !undoing all previous selections.
319:    ESEL,S,TYPE,,1                         !Select all plane elements (created because
320:                                          !the original areas were present when the
321:                                          !model was meshed).
322:    EDELE,ALL                             !Delete these plane elements.
323:    ESEL,ALL                              !Make sure all elements are selected,
324:                                          !undoing all previous selections.
325:    ESEL,S,CENT,Z,0,1                     !Select all elements between Z=0 and Z=1.
326:    NSLE,S,ALL                            !Select all nodes associated with
327:                                          !these elements.
328:                                          !In this way, only the corner nodes
329:                                          !are selected.
330:    NSEL,R,LOC,Z,0                        !Reselect all (corner) nodes at Z=0 from the
331:                                          !current selection.
332:    D,ALL, , , , , ,ALL, , , , ,          !Fix all degrees of freedom for these nodes,
333:                                          !clamping the tower at the base.
334:
335: !ADD ELEMENT ON TOP OF TOWER
336:    !Create the element:
337:    NSEL,ALL                              !Make sure all nodes are selected,
338:                                          !undoing all previous selections.
339:    *GET,eNum,NODE,,count                  !Store the current number of nodes in Enum.
340:    eNew=eNum+1                            !Store the next node number in eNew.
341:
342:    N,eNew ,,,H,,,,                        !Add a node at X=0, Y=0, Z=H, with number eNew.
343:    TYPE,   3                              !Set new elements to be MASS21 elements.
344:    MAT,    1                              !Define new elements to have material type 1.
345:    REAL,   1                              !Set new elements to have real constants set,
346:                                          !to define top mass.
347:    ESYS,   0                              !Set new elements to have the default
348:                                          !element coordinate system.
349:
350:    E,   eNew  , ,                         !Create the new element, with number eNew.
351:
352:    !Attach the mass to tower by creating a rigid region on top:
353:    NSEL,ALL                              !Make sure all nodes are selected,
354:                                          !undoing previous selections.
355:    NSEL,S,LOC,Z,H                        !Select all nodes at Z=H.
356:    CERIG,eNew,ALL,ALL                    !Rigidly link all these nodes,
357:                                          !using node eNew as the master node.
358: !FORCES
359:       !Because of buckling, all loads, except gravuity, will be multiplied
360:       !by a factor lambda. For regular calculations, this is set at 1.0.
361:       !For buckling, this is to be manually adjusted until ANSYS displays
362:       !1.000 as a result for the buckling factor. Lambda is then the
363:       !actual buckling factor.
364:
365:    !APPLY WIND LOAD
```

```
366:        /PSF,PRES,NORM,2,0,1                    !Makes sure pressure are displayed as arrows
367:                                                !from now on.
368:        *DO,i,1,H,1
369:        VSEL,ALL                                !Make sure all volumes are selected,
370:                                                !undoing all previous selections.
371:        VSEL,S,,,1                              !Select volume 1 (the side perpendicular to
372:                                                !the default x-axis).
373:        ESLV,S                                  !Select all elements associated with
374:                                                !this volume.
375:        ESEL,R,CENT,Z,i-1,i
376:        SFE,ALL,6,PRES,1,-lambda*WINDTOW(i)     !Apply the appropriate pressure to the selected
377:                                                !elements, on side 6, the outer surface
378:                                                !of the tower.
379:        *ENDDO
380:        ESEL,ALL                                !Make sure all elements are selected,
381:                                                !undoing all previous selections.
382:        VSEL,ALL                                !Make sure all volumes are selected,
383:                                                !undoing all previous selections.
384:
385:    !APPLY TOP THRUST FORCE
386:        F,eNew,FX,FYT*lambda                    !Apply F_yT on the mass located at the top
387:                                                !of the tower, which is node eNew.
388:
389:    !APPLY TOP OVERTURNING MOMENT
390:        ESEL,ALL                                !Make sure all elements are selected,
391:                                                !undoing all previous selections.
392:        NSEL,ALL                                !Make sure all nodes are selected,
393:                                                !undoing previous selections.
394:        ESEL,S,CENT,Z,H-1,H                     !Select all elements at the top,
395:                                                !between Z=H-1 and Z=H.
396:        NSLE,S,CORNER                           !Select only the corner nodes from
397:                                                !these elements.
398:        NSEL,R,LOC,Z,H                          !Reselect from this set, only the nodes at Z=H.
399:        NSEL,U,,,Enum+1                         !Unselect the mass node (node eNum+1)
400:                                                !from this set.
401:        !Basically, now all corner nodes on the top surface of the tower are selected.
402:
403:        *GET,NTOPNODES,NODE,,COUNT              !Count the number of nodes in the selected set.
404:        *GET,TOPNODEMIN,NODE,,NUM,MIN           !Store the lowest node number in the set.
405:        *DIM,XTOPNODES,,NTOPNODES               !Create an empty table called XTOPNODES
406:                                                !of NTOPNODES*1 dimensions.
407:
408:        TOPNODE1=TOPNODEMIN                     !Set the lowest node number to be TOPNODE1.
409:        *DO,i,1,NTOPNODES,1
410:        *GET,XTOPNODE1,NODE,TOPNODE1,LOC,X      !Get the x-coordinate of TOPNODE1.
411:        *SET,XTOPNODES(i,1),XTOPNODE1           !Store this in table XTOPNODES.
412:        *GET,TOPNODE2,NODE,TOPNODE1,NXTH        !Get the next node number in the set.
413:        *SET,TOPNODE1,TOPNODE2                  !Set this as TOPNODE 1 and repeat.
414:        *ENDDO
415:
416:        *DIM,XTOPSQ,,NTOPNODES                  !Create an empty table called XTOPSQ of
417:                                                !NTOPNODES*1 dimensions.
418:        *DO,i,1,NTOPNODES,1
419:        XTOPSQ(i,1)=XTOPNODES(i,1)*XTOPNODES(i,1)
420:                                                !Square the values in XTOPNODES.
421:        *ENDDO
422:
423:        *VSCFUN,ITOT,SUM,XTOPSQ                 !Sum the values in XTOPNODES, store as ITOT.
424:
425:        TOPNODE3=TOPNODEMIN                     !Set TOPNODE3 as the lowest node number
426:                                                !in the set.
427:        *DO,i,1,NTOPNODES,1
428:        F,TOPNODE3,FZ,-lambda*MXT*XTOPNODES(i,1)/ITOT
429:                                                !Apply a force at this node.
430:        *GET,TOPNODE4,NODE,TOPNODE3,NXTH        !Get the next node number in the set.
431:        TOPNODE3=TOPNODE4                       !Store the next node number as TOPNODE3
432:                                                !and repeat.
433:        *ENDDO
434:        NSEL,ALL                                !Make sure all nodes are selected,
435:                                                !undoing all previous selections.
436:        ESEL,ALL                                !Make sure all elements are selected,
437:                                                !undoing all previous selections.
438:
```

```
439:    !APPLY TOP TORSIONAL MOMENT
440:        B_cent=r_out_T+r_in_T                       !Define the width of the center line at the top,
441:                                                    !which is (B_out_T+B_in_T)/2.
442:        a_ave_T=(a_out_T+a_in_T)/2                  !Define the width of one side at the top,
443:                                                    !on this center line.
444:
445:        !The torsion moment will be applied as nodal forces to the nodes at the top
446:        !It is not possible to apply the moment at a single point without influencing
447:        !results negatively because of the concentrated load introductions.
448:        !Furthermore, the spread-out introduction of the load that is modelled here,
449:        !represents realitybetter than a concentrated load.
450:
451:        !Octagons:
452:        !Because of the symmetric shape, the torsion is applied to four sides,
453:        !because there are four sides parallel to the x or y-axis.
454:    *IF,n_sides,EQ,8,THEN
455:        ESEL,ALL                                    !Make sure all elements are selected,
456:                                                    !undoing all previous selections.
457:        NSEL,ALL                                    !Make sure all nodes are selected,
458:                                                    !undoing all previous selections.
459:        ESEL,S,CENT,Z,H-1,H                         !Select all elements at the top,
460:                                                    !between Z=H-1 and Z=H.
461:        NSLE,S,CORNER                               !Select only the corner nodes from
462:                                                    !these elements.
463:        NSEL,R,LOC,Z,H                              !Reselect from this set, only the nodes at Z=H.
464:        NSEL,U,,,Enum+1                             !Unselect the mass node (node eNum+1)
465:                                                    !from this set.
466:                                                    !The following two lines select the appropriate
467:                                                    !nodes to which the loads will be applied.
468:        NSEL,R,LOC,X,0.95*r_in_t,1.05*r_out_t
469:        NSEL,U,LOC,X,1.01*r_in_t,0.99*r_out_t
470:    *GET,NSIDENODES,NODE,,COUNT                     !Count the total number of nodes selected
471:                                                    !on one side.
472:                                                    !This will be the same for all sides,
473:                                                    !since the structure is symmetric.
474:
475:        !The nodal foce applied on each node is:
476:        FTOR=MZT/(2*B_cent)/(NSIDENODES)*lambda
477:                                                    !Based on MZT=2*F_SIDE*B_ave and
478:                                                    !FTOR=F_SIDE/NSIDENODES.
479:
480:        ESEL,ALL                                    !Make sure all elements are selected,
481:                                                    !undoing all previous selections.
482:        NSEL,ALL                                    !Make sure all nodes are selected,
483:                                                    !undoing all previous selections.
484:        ESEL,S,CENT,Z,H-1,H                         !Select all elements at the top,
485:                                                    !between Z=H-1 and Z=H.
486:        NSLE,S,CORNER                               !Select only the corner nodes from
487:                                                    !these elements.
488:        NSEL,R,LOC,Z,H                              !Reselect from this set, only the nodes at Z=H.
489:        NSEL,U,,,Enum+1                             !Unselect the mass node (node eNum+1)
490:                                                    !from this set.
491:        !The following two lines select the appropriate nodes to which the loads
492:        !will be applied:
493:        NSEL,R,LOC,X,0.95*r_in_t,1.05*r_out_t
494:        NSEL,U,LOC,X,1.01*r_in_t,0.99*r_out_t
495:        F,ALL,FY,FTOR                               !Apply the nodal force on the selected nodes.
496:
497:        ESEL,ALL                                    !Make sure all elements are selected,
498:                                                    !undoing all previous selections.
499:         NSEL,ALL                                   !Make sure all nodes are selected,
500:                                                    !undoing all previous selections.
501:        ESEL,S,CENT,Z,H-1,H                         !Select all elements at the top,
502:                                                    !between Z=H-1 and Z=H.
503:        NSLE,S,CORNER                               !Select only the corner nodes from
504:                                                    !these elements.
505:        NSEL,R,LOC,Z,H                              !Reselect from this set, only the nodes at Z=H.
506:        NSEL,U,,,Enum+1                             !Unselect the mass node (node eNum+1)
507:                                                    !from this set.
508:        !The following two lines select the appropriate nodes to which the loads
509:        !will be applied.
510:        NSEL,R,LOC,X,-0.95*r_in_t,-1.05*r_out_t
511:        NSEL,U,LOC,X,-1.01*r_in_t,-0.99*r_out_t
```

```
512:        F,ALL,FY,-FTOR                              !Apply the nodal force on the selected nodes.
513:
514:        ESEL,ALL                                    !Make sure all elements are selected,
515:                                                    !undoing all previous selections.
516:        NSEL,ALL                                    !Make sure all nodes are selected,
517:                                                    !undoing all previous selections.
518:        ESEL,S,CENT,Z,H-1,H                         !Select all elements at the top,
519:                                                    !between Z=H-1 and Z=H.
520:        NSLE,S,CORNER                               !Select only the corner nodes from
521:                                                    !these elements.
522:        NSEL,R,LOC,Z,H                              !Reselect from this set, only the nodes at Z=H.
523:        NSEL,U,,,Enum+1                             !Unselect the mass node (node eNum+1)
524:                                                    !from this set.
525:          !The following two lines select the appropriate nodes to which the loads
526:          !will be applied.
527:        NSEL,R,LOC,Y,-0.95*r_in_t,-1.05*r_out_t
528:        NSEL,U,LOC,Y,-1.01*r_in_t,-0.99*r_out_t
529:        F,ALL,FX,FTOR                               !Apply the nodal force on the selected nodes.
530:
531:        ESEL,ALL                                    !Make sure all elements are selected,
532:                                                    !undoing all previous selections.
533:        NSEL,ALL                                    !Make sure all nodes are selected,
534:                                                    !undoing all previous selections.
535:        ESEL,S,CENT,Z,H-1,H                         !Select all elements at the top,
536:                                                    !between Z=H-1 and Z=H.
537:        NSLE,S,CORNER                               !Select only the corner nodes from
538:                                                    !these elements.
539:        NSEL,R,LOC,Z,H                              !Reselect from this set, only the nodes at Z=H.
540:        NSEL,U,,,Enum+1                             !Unselect the mass node (node eNum+1)
541:                                                    !from this set.
542:          !The following two lines select the appropriate nodes to which the loads
543:          !will be applied.
544:        NSEL,R,LOC,Y,0.95*r_in_t,1.05*r_out_t
545:        NSEL,U,LOC,Y,1.01*r_in_t,0.99*r_out_t
546:        F,ALL,FX,-FTOR                              !Apply the nodal force on the selected nodes.
547:        ESEL,ALL                                    !Make sure all elements are selected,
548:                                                    !undoing all previous selections.
549:        *ENDIF
550:
551:        !Decagons:
552:          !Decagons are less ideal to apply the torsion in a simple way.
553:          !It is therefore only applied to two sides, since there are only two sides
554:          !that are parallel to the x or y-axis.
555:        *IF,n_sides,EQ,10,THEN
556:        ESEL,ALL                                    !Make sure all elements are selected,
557:                                                    !undoing all previous selections.
558:        NSEL,ALL                                    !Make sure all nodes are selected,
559:                                                    !undoing all previous selections.
560:        ESEL,S,CENT,Z,H-1,H                         !Select all elements at the top,
561:                                                    !between Z=H-1 and Z=H.
562:        NSLE,S,CORNER                               !Select only the corner nodes from
563:                                                    !these elements.
564:        NSEL,R,LOC,Z,H                              !Reselect from this set, only the nodes at Z=H.
565:        NSEL,U,,,Enum+1                             !Unselect the mass node (node eNum+1)
566:                                                    !from this set.
567:          !The following two lines select the appropriate nodes to which the loads
568:          !will be applied.
569:        NSEL,R,LOC,X,0.95*r_in_t,1.05*r_out_t
570:        NSEL,U,LOC,X,1.01*r_in_t,0.99*r_out_t
571:        NSEL,U,LOC,Y,0.6*a_in_T,2*a_in_T
572:        NSEL,U,LOC,Y,-0.6*a_in_T,-2*a_in_T
573:        *GET,NSIDENODES,NODE,,COUNT                 !Count the total number of nodes selected
574:                                                    !on one side.
575:        FTOR=MZT/(B_cent*NSIDENODES)*lambda         !Define the individual nodal force
576:                                                    !to produce MZT.
577:                                                    !Based on MZT=F_SIDE*B_ave and
578:                                                    !FTOR=F_SIDE/NSIDENODES.
579:        F,ALL,FY,FTOR                               !Apply the load to the selected nodes.
580:
581:        ESEL,ALL                                    !Make sure all elements are selected,
582:                                                    !undoing all previous selections.
583:        NSEL,ALL                                    !Make sure all nodes are selected,
584:                                                    !undoing all previous selections.
```

```
585:    ESEL,S,CENT,Z,H-1,H                    !Select all elements at the top,
586:                                           !between Z=H-1 and Z=H.
587:    NSLE,S,CORNER                          !Select only the corner nodes from
588:                                           !these elements.
589:    NSEL,R,LOC,Z,H                         !Reselect from this set, only the nodes at Z=H.
590:    NSEL,U,,,Enum+1                        !Unselect the mass node (node eNum+1)
591:                                           !from this set.
592:       !The following two lines select the appropriate nodes to which the loads
593:       !will be applied.
594:    NSEL,R,LOC,X,-0.95*r_in_t,-1.05*r_out_t
595:    NSEL,U,LOC,X,-1.01*r_in_t,-0.99*r_out_t
596:    NSEL,U,LOC,Y,0.6*a_in_T,2*a_in_T
597:    NSEL,U,LOC,Y,-0.6*a_in_T,-2*a_in_T
598:    F,ALL,FY,-FTOR                         !Apply the load to the selected nodes
599:    *ENDIF
600:
601:    !Gravity:
602:    ACEL,0,0,Grav                          !Define and apply gravity, including the
603:                                           !appropriate load factor.
604:                                           !Lambda is not included, because gravity is not
605:                                           !to be scaled for buckling calculations.
606:
607:    FINISH                                 !Ends the Preprocessing phase.
608:
609: !SOLUTION PHASE
610:    /SOL                                   !Enters the Solution phase.
611:    /NERR,
612:    /UIS, Label, VALUE
613:    /UIS, MSGPOP, 3
614:    /CONTOUR,ALL,100                       !Set al contour plots to have 100 colors.
615:                                           !The default is much lower,
616:                                           !making it harder to judge results.
617:
618:    !SOLVE FREQUENCY
619:    /SOL                                   !Enters the Solution phase
620:    ESEL,ALL                               !Make sure all elements are selected,
621:                                           !undoing all previous selections.
622:    NSEL,ALL                               !Make sure all nodes are selected,
623:                                           !undoing all previous selections.
624:       !Without these two lines, ANSYS will crash.
625:
626:    ANTYPE,MODAL                           !Set analysis mode to Modal analysis.
627:    MODOPT,LANB,6,0,0, ,ON                 !Set the calculation method to Block Lanczos,
628:                                           !to expand on a total number of 6 modes.
629:                                           !Normalize to unity.
630:    MXPAND,6, , ,0                         !Expand these 6 modes, to be able to
631:                                           !show results.
632:    SOLVE                                  !Run the model.
633:    FINISH                                 !Ends the Solution phase.
634:
635:    /POST1                                 !Enters the Post-processing phase.
636:    SET,LIST                               !Display the frequencies in a list.
637:    FINISH                                 !Ends the Post-processing phase.
638:
639:    !SOLVE FOR BUCKLING
640:    /SOL                                   !Enters the Solution phase.
641:    ESEL,ALL                               !Make sure all elements are selected,
642:                                           !undoing all previous selections.
643:    NSEL,ALL                               !Make sure all nodes are selected,
644:                                           !undoing all previous selections.
645:       !Without these two lines, ANSYS will crash.
646:
647:    !First, the static results are needed to later perform the buckling analysis:
648:    ANTYPE,0                               !Set analysis mode to Static analysis.
649:    SOLVE                                  !Run the model.
650:    FINISH                                 !Ends the Solution phase.
651:
652:    /SOL                                   !Enters the Solution phase.
653:    ESEL,ALL                               !Make sure all elements are selected,
654:                                           !undoing all previous selections.
655:    NSEL,ALL                               !Make sure all nodes are selected,
656:                                           !undoing all previous selections.
657:       !Without these two lines, ANSYS will crash.
```

```
658:
659:      !Now, the buckling analysis can be performed:
660:      ANTYPE,1                              !Set analysis mode to Modal analysis.
661:      PSTRES,ON                             !Set prestress effects to be included in
662:                                            !buckling analysis.
663:      BUCOPT,LANB,1,0,0,                    !Set the correct options for Block Lanczos
664:                                            !buckling analysis.
665:      SOLVE                                 !Run the model.
666:      FINISH                                !Ends the Solution phase.
667:
668:      /SOL                                  !Enters the Solution phase.
669:      EXPASS,1                              !Make ANSYS do an expansion pass.
670:      MXPAND,1,0,0,0,0.01,                  !Expand only the first buckling mode,
671:                                            !to the second decimal.
672:      SOLVE                                 !Run the model.
673:      FINISH                                !Ends the Solution phase.
674:
675:      /POST1                                !Enters the Post-processing phase.
676:      SET,LIST                              !Display the buckling factor in a list.
677:      FINISH                                !Ends the Post-processing phase.
678:
679:      !SOLVE FOR STATIC ANALYSIS
680:      /SOL                                  !Enters the Solution phase.
681:      ESEL,ALL                              !Make sure all elements are selected,
682:                                            !undoing all previous selections.
683:      NSEL,ALL                              !Make sure all nodes are selected,
684:                                            !undoing all previous selections.
685:        !Without these two lines, ANSYS will crash.
686:
687:      ANTYPE,0                              !Set analysis mode to Static analysis.
688:      SOLVE                                 !Run the model.
689:      FINISH                                !Ends the Solution phase.
690:
691:      /POST1                                !Enters the Post-processing phase.
692:      PRRSOL,F                              !Display the reaction forces, to be checked
693:                                            !against the reaction forces in Matlab
694:                                            !(mind the partial load factor).
695:      RSYS,SOLU                             !Set the result coordinate system to the element
696:                                            !coordinate systems.
697:      ESEL,S,CENT,Z,5,H-5                   !Select all elements except the top 5 m
698:                                            !and bottom 5m,
699:                                            !for displaying and analyzing the forces.
700:      PLNSOL,S,Z, 0,1.0                     !Plot the stresses in Z-direction.
701:      FINISH                                !Ends the Post-processing phase.
```

H-1 Starting phase (l. 1-8)

The only part in need of explanation is the folder in which the calculations are made (l. 3), which has to be the same folder as the one where the Matlab model stores the wind loads directly on the tower $q_w(h)$.

H-2 Input phase (l.10-79)

H-2-1 User input (l. 13-27)

Lines 15-27 are the parameters input by the user for each design. The easiest way is to copy the values from Matlab, which provides them in the right format. Manual adjustment is of course possible as well. The comments in the code explains the meaning of each parameter.

H-2-2 Buckling parameter (l. 29-37)

The buckling parameter displayed here will magnify the wind loads $M_{x,T}$, $M_{z,T}$, $F_{y,T}$ and $q_w(h)$ by a factor *lambda*, but not the gravitational constant *Grav* used to calculate gravity loads from the mass inputs. When *lambda* is set to 1, ANSYS will start increasing all loads, including gravity, until buckling first occurs. This is not the correct way to determine the buckling factor, since gravity should not be increased this way. By manually altering the *lambda*-factor, this is countered. The value of *lambda* for which ANSYS returns a buckling factor of 1.0 is the actual buckling factor.

H-2-3 Other input (l. 38-44)

These lines load the wind pressures on the tower for the specific parameters input in the Matlab model. It is imperative that the folder in which these are stored is the same as the one called upon in the starting phase of this model. Manually entering values is possible, but not recommended.

H-3 Definition of properties (l. 46-115)

H-3-1 Geometric properties (l. 46-79)

The Poisson's ratio and rotary inertia of the top mass are kept constant for all designs, but their influence on the natural frequency has been investigated in Chapter 5. ANSYS then will calculate several geometrical properties based on formulas from Appendix E, which will be used later in various sections of the code.

H-3-2   Element type definition (l.81-90)

Here four element types are defined for use throughout the model:

– PLANE183, an 8-node plane element for when areas are meshed;

– SOLID186, a 20-node solid brick element, the main element type for the tower walls;

– MASS21, a dimensionless point mass to add the weight of the rotor and nacelle to the top of the tower;

– SOLID185, like SOLID 186, but with the mid-side nodes removed, which will provide less abnormalities in reaction forces at the bottom.

During the study in Chapter 5, other elements have been used instead of the SOLID186 elements, but SOLID186 was found to be the best suited type.

H-3-3   View adjustment (l.92-99)

This part simply changes the default view in the program to one that makes it easy to see and judge the structure in terms of frequency and stresses.

H-3-4   Material and mass properties (l. 101-115)

Based on the input parameters, this code constructs the material properties for the tower elements and mass properties for the top mass element. When creating the elements later on, these properties will be called upon.

H-4   Geometry creation (l. 117-141)

The polygonal tube is created by constructing two polygonal areas at $Z = 0$ and rotating these in such a way that one of the sides is perpendicular to the X-axis. This makes the application of the wind pressure later much easier. Both areas are extruded into volumes up to $Z = H$ (Figure H-1a), after which they are subtracted from each other to create the hollow tube desired (Figure H-1b). The order in which the elements are build up determines the number of its lines, nodes and areas. This order is later used to construct the mesh.

H-5   Meshing (l.143-269)

The meshing part consists of the following steps:

– Setting the element size for the vertical lines to 1, so that the tower will vertically be divided into H elements.

– Creating keypoints on these lines, on the locations the element divisions (Figure H-1c).

– Creating horizontal lines, 1 m apart, between these vertical lines by using the keypoints (Figure H-1d). This is done for both the inner and the outer surface.

– Setting the element size for these new lines. Each line is divided into four equal parts.

– Creating *n_sides* number of volumes. Lines between the inner corners and outer corners are made (Figure H-1e, their element size division set to 1, which means that there will be only one element over the wall thickness. Each side will then be made a separate volume, which makes selecting elements in a later stage much easier (Figure H-1f).

– The material properties as defined before are called upon to be implemented for new elements.

– The actual meshing is done, which will create elements according to the element divisions defined in this phase (Figure H-1g).

H-6 Element adjustments

H-6-1 Removing mid-side nodes (l. 272-281)

Keeping mid-side nodes in the bottom elements, which will be confined later to provide the clamped support of the tower, will result in an unrealistic distribution of reaction forces. The bottom layer of elements is therefore changed from SOLID186 to SOLID185 elements.

H-6-2 Adjusting element coordinate systems (l. 283-314)

When unadjusted, ANSYS will plot element results in the global coordinate system. This makes the judging of stresses, especially shear stresses, very difficult. ANSYS has the option to display the results in the element coordinate systems, which, for now, are equal to the global coordinate system. By rotating the element coordinate systems in such a way that the X-axis is always perpendicular to the side face, a single plot is sufficient to judge a single output variable. The elements are easily selected because of the separate volumes created earlier. The result is shown in Figures H-1h and H-1i.

H-6-3 Adding the base support (l. 316-333)

The nodes at Z=0 are selected and restricted in translating and rotating in all three principle directions (Figure H-1j).

H-7 Adding the top mass (l. 335-356)

Since it is not reasonable to model the entire nacelle and rotor, they will be modelled as a point mass at the top of the tower. A new node is created at Z=H, X=0 and Y=0, with its number specified so that it can be easily called upon. A new point mass element is assigned at this node (Figure H-1k), with the mass properties specified in Real Constant Set 1 (see

section H-3-4). Finally, the new node is used as a master node in creating a rigid region at the top of the tower, making sure that when the tower moves, the mass moves as well, and vice versa (Figure H-1l).

H-8   Load application (l. 358-607)

All loads, except the gravity are multiplied by *lambda*, as is explained in section H-2-2.

H-8-1   Wind load on tower (l. 365-382)

Wind loads are loaded from the table defined before and applied to only one face of the polygon (the positive x-face), as is shown in Figure H-1m. Local stresses because of this load introduction are neglectable. Again, the previously defined separate volumes make selecting the appropriate elements simple.

H-8-2   Wind thrust force $F_{y,T}$ (l. 385-386)

The value for FYT from the input is applied on the new (mass) node, which is easily referred to because of its specified number (Figure H-1n).

H-8-3   Wind overturning moment $M_{x,T}$ (l. 389-437)

It is not possible to apply the top moment on the mass element, since it does not have dimensions and will not transfer the moment to the rest of the tower. Instead, the code displayed here will calculate and distribute vertical nodal loads that will have the desired effect.

First, only the corner nodes of the top surface are selected. Using their coordinates, the total moment of inertia of these nodes is calculated using $I_{tot} = \sum R_i^2$. The appropriate load $F_i = M_{x,T} R_i / I_{tot}$ is then applied on the selected nodes (Figure H-1o).

H-8-4   Wind torsional moment $M_{z,T}$ (l. 439-599)

What holds for the overturning moment, also applied to the torsional moment. It is not possible to apply it directly on one single node. Instead, the torsional moment is applied as a large number of nodal force having the same effect. Applying the correct forces on faces that are not parallel to either the x or y-axis are difficult, so a distinction between octagonal and decagonal towers is made. For octagonal towers four sides are used, for decagonal ones only two are used.

The average of the top tower width B_cent is used to calculate the force per side. For octagons this means that four forces with a magnitude of $MZT/(2B\_cent)$ and for decagons two forces of MZT/B_cent are used. The number of nodes is counted and the nodal loads calculated by dividing the forces by the number of nodes per face. An example for an octagonal shape is shown in Figure H-1p.

H-8-5   Gravity (l. 601-605)

Gravity is only applied in z-direction and is already multiplied by the appropriate load factor in the input (1.1 or 1.35). The resulting stresses will therefore be the design stresses, while the absence of *lambda* makes sure that gravity loads will remain the same during buckling analysis.

H-9   Solution and post-processing phase (l. 609-701)

Three different analyses have been used throughout this research and have all been included in the code at the end of this appendix.

- – Frequency analysis;

- – Buckling analysis;

- – Static analysis.

H-9-1   Frequency analysis (l. 618-637)

The default Block Lanczos solver is used to calculate the first six natural frequencies of the tower. These are displayed in a list for easy reference.

H-9-2   Buckling analysis (l. 639-677)

The use of buckling factor *lambda* has already been explained above. ANSYS will calculate the buckling factor based on the loads defined by the combination of input loads and *lambda*, but needs the static results to be able to do so. After a static analysis, the (first) buckling factor is calculated and displayed.

H-9-3   Static analysis (l. 679-701)

Static analysis is performed, after which the reaction forces are displayed, so that these can be checked against their counterparts in Matlab. After this, the bottom and top 5 m are removed from stress plots and, as a default, the stresses in z-direction (the normal stresses) are displayed.

H-10   Example calculation

Model A3 from Appendix C is taken as an example to explain the tables in Appendix C and the calculation model.
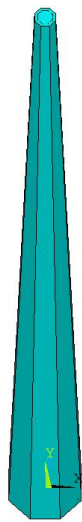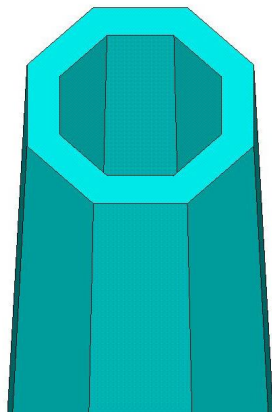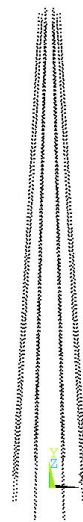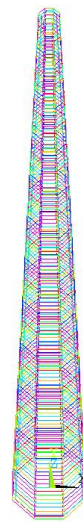
(a) (b) (c) (d)
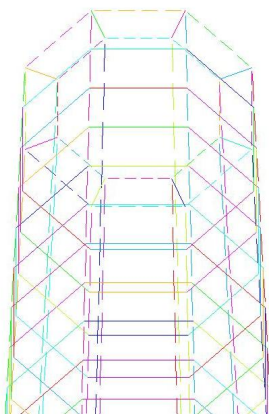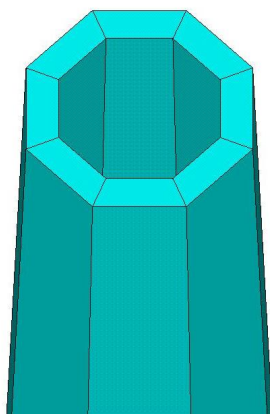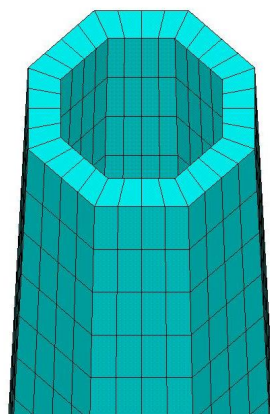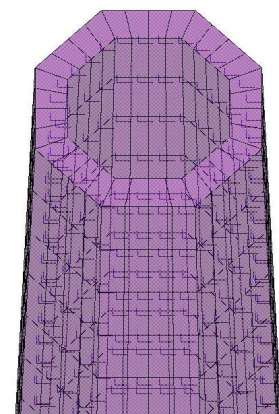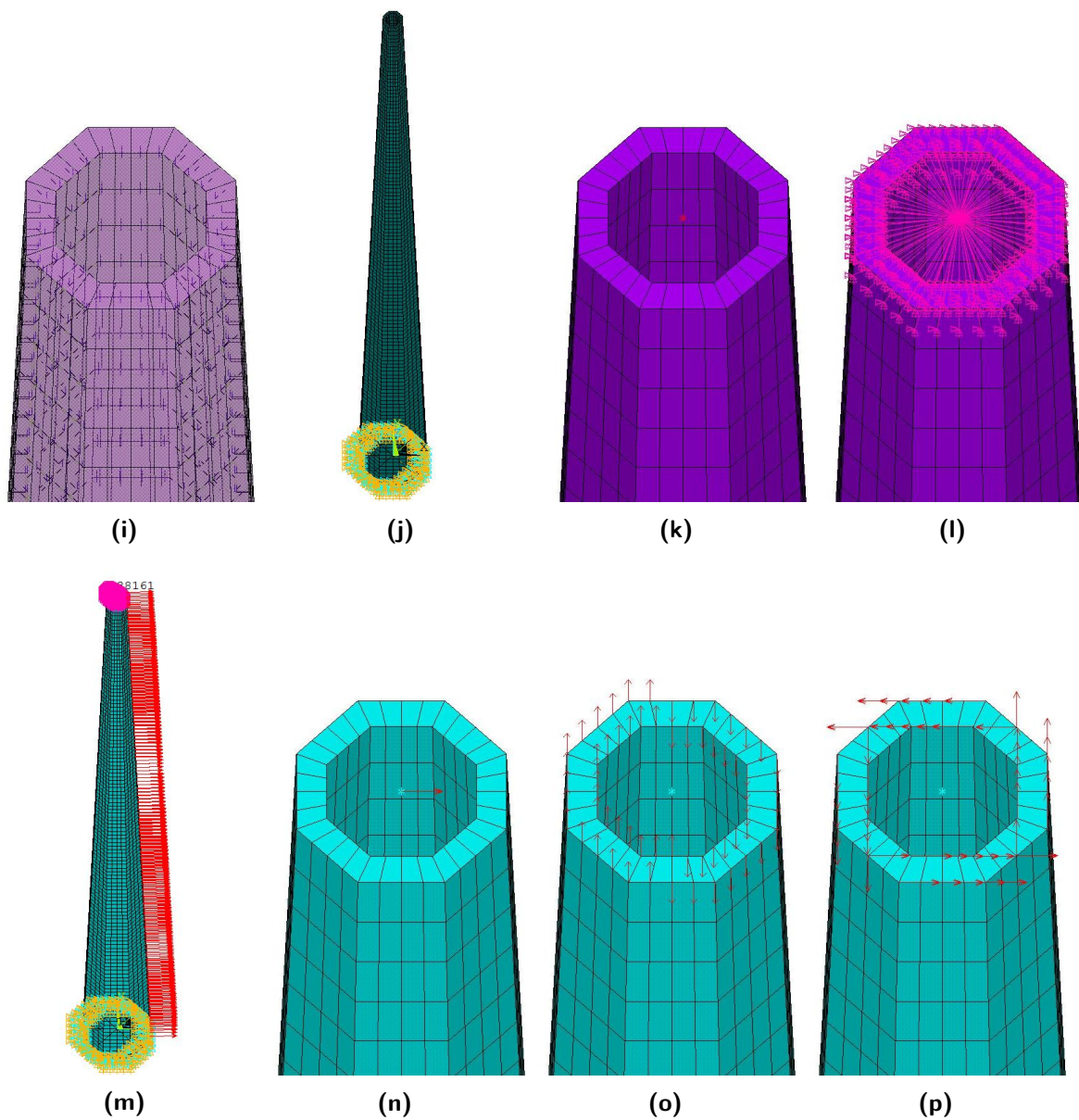
(e) (f) (g) (h)

Figure H-1: Screenshots of the model in various steps during the pre-processing phase of the model

H-10-1 Input - Matlab

The ten input parameters to put into *Input.m* from the Matlab part of the model are as follows for design A3:

- Class='1C';

- Op=2;

- Turb='NREL_3MW';

- Mat='CL28h';

- H=100;

- n_sides=10;

- a_outT=0.93;

- a_outB=2.74;

- t=0.3;

- k_net=0.75

H-10-2 Output - Matlab

When the *UC.m* file is then run, Matlab provides Figure H-2, along with the following information, which is shown raw in Figure H-3a:

- The tensile strength is sufficient. The maximum occurring tensile stress is $13.74\,\text{N/mm}^2$, at a height of 62 m. The unity check is 0.83.

- The compression strength is sufficient. The maximum occurring compression stress is $15.08\,\text{N/mm}^2$, at a height of 64 m. The unity check is 0.61.

- The frequency according to Rayleigh Ritz is 0.3371 Hz, which is within the limits set in Chapter 2.

The output in Figure H-2 allows for a quick graphical check of the normal stresses versus the design strength.

Even though normal stresses will later be checked in ANSYS, they are calculated here as well. Matlab provides the outcome within a matter of seconds, while the complete ANSYS model takes more than a minute to run. Since finding a suitable geometry that meets both the frequency and strength demands is a trial-and-error process, using Matlab to make initial normal stress calculations saves a lot of time. The bottom rows in Appendix C show that the correspondence between the normal stresses from both programs is very high.

One of the things created by the Matlab model is its parameter *RI* (arbitrarily named), which allows for easy copying and pasting into the tables in Appendix C. It contains the loads at
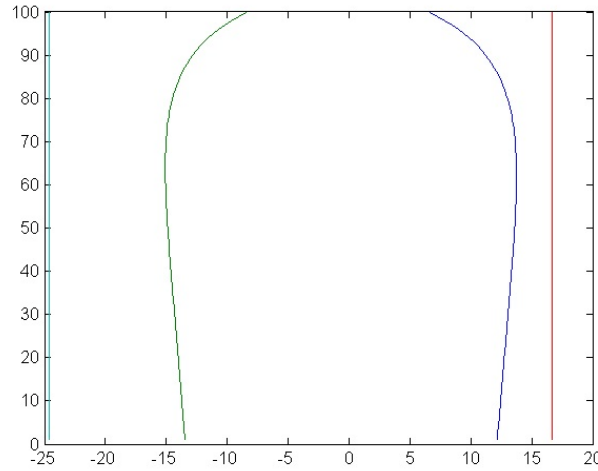
Figure H-2: The normal stresses and corresponding material strength Matlab shows (unedited figure)

the top of the tower, the tower frequency, normal stresses, design normal strengths calculated according to Appendix D and the unity checks in tension and compression. It also contains the maximum allowable values of the shear stresses found later in ANSYS, calculated according to Chapter 7, which will be explained later on.

As an example, the design tensile strength $f_{t,0,net,d} = 16.63$ N/mm^2 is calculated as follows:

$$f_{t,0,l,k} = 14 \text{ N/mm}^2$$

$$k_{sys,t,0} = \min\left(0.130 \cdot \ln(n) + 1; 1.35\right) = 1.35 \text{ Where } n > 15$$

$$f_{t,0,net,k} = k_{sys,t,0} f_{t,0,l,k} = 18.9 \text{ N/mm}^2$$

$$k_{mod} = 1.1 \quad \gamma_M = 1.25 \quad \gamma_n = 1.0 \quad k_h = 1.0$$

$$f_{t,0,net,d} = k_h k_{mod} \frac{f_{t,0,net,k}}{\gamma_M \gamma_n} = 16.63 \text{ N/mm}^2$$

This value is shown as a vertical line in Figure H-2. $f_{c,0,net,d}$ is calculated in a similar way.

H-10-3   Input - Ansys

Matlab further provides the required input data for the ANSYS model that differs for each design. Figure H-3b shows how Matlab outputs this in the Command Window, from where it can be copied into the top of the APDL code. The rest of the APDL code is written to use these values to calculate all other required parameters throughout the model. The input loads already include the partial safety factor for loads, which differs per load case. The gravitational constant is also multiplied by the correct load factor. Wind loading on the tower is automatically stored in a *.txt*-file by Matlab and automatically loaded by ANSYS, without interference of the user. Pasting the entire code into ANSYS makes the software calculate the natural frequency, stresses and buckling factor as described earlier.

```
Tensile strength sufficient        Compression strength sufficient     f =              n_sides=          10
                                                                                        a_out_B=         2.74
uc_t =                             uc_c =                        0.3371                 a_out_T=         0.93
                                                                                        H=                100
    0.8262                             0.6121                    Frequency accepted     t=                0.3
                                                                >>                      M_top=       1.765e+05
                                                                                        knet=            0.75
sigma_temax =                      sigma_comax =                                        rho=              420
                                                                                        YM=           8.25e+09
   13.7417                            -15.0831                                          FYT=        1.1424e+06
                                                                                        MXT=        8.0087e+06
ans =                              ans =                                                MZT=        6.3723e+05
                                                                                        Grav=          10.791
Height of maximum tensile stress   Height of maximum compression stress
```

(b) The input required
for the APDL code, in

h_te =   h_co =   the correct format. for

   62   64   model A3

(a) The resulting normal stresses and frequency as calculated by Matlab for
model A3

Figure H-3: The output in the Command Window of Matlab

The reason why Matlab and ANSYS are not automatically coupled (which would mean that Matlab would start the ANSYS calculation without the user manually doing so) is one of caution. Checking the values that are put into the ANSYS model allows for an additional check on validity, instead of it being a so-called 'black box'.

H-10-4 Output - Ansys

The default listed output of the code written are three unique lists, parts of which are presented in Figure H-4.

- The natural frequencies of the tower, which should be slightly lower than those found in the Matlab model.

- The total reaction forces. This allows for another check, where the total reaction force in Z-direction (1779 kN) in ANSYS should be equal to $\gamma_f F_z(0) = 1.1 \cdot 1617 = 1779$ kN from the Matlab model, which is the case. Likewise, the total reaction force in X-direction (4248 kN) should be equal to $\gamma_f F_y(0) = 1.1 \cdot 3879 = 4267$ kN from the Matlab model, which has a neglectable difference. The reaction forces in Y-direction should be 0, which is also the case.

- The buckling factor for $lambda=1.0$.

The default graphical output of the code are the normal stresses (stresses in Z-direction) for the middle part of the tower, as shown in Figure H-5. The stresses in the top and bottom 5 m are not plotted, because here other materials are assumed present. ANSYS plots the equivalent normal stresses described in Chapter 7 and the maximum values are shown on the legend bar at the bottom of the screen. By dividing these values by k_{net}, the net stresses are calculated according to Equation 7-4:

$$\sigma_{t,0,net,d} = \frac{\sigma_{t,0,d}}{k_{net}} = \frac{10.20}{0.75} = 13.60 \text{ N/mm}^2$$

```
SET   TIME/FREQ   LOAD STEP   SUBSTEP   CUMULATIVE
 1  0.30831           1          1           1
 2  0.30831           1          2           2
 3   2.2702           1          3           3
 4   2.2702           1          4           4
 5   6.2759           1          5           5
 6   6.2759           1          6           6
```

Natural frequencies

```
TOTAL VALUES
VALUE  -0.17789E+07 0.14412E-02 0.42477E+07
```

Total reaction forces in X, Y and Z direction

```
SET   TIME/FREQ   LOAD STEP   SUBSTEP   CUMULATIVE
 1   20.149            1          1           1
```

Buckling factor for lambda=1

Figure H-4: The listed outputs by ANSYS

$$\sigma_{c,0,net,d} = \frac{\sigma_{c,0,d}}{k_{net}} = \frac{11.20}{0.75} = 14.93 \text{ N/mm}^2$$

These values correspond with the Matlab model for 99%, which makes the Matlab model suited for normal stress calculations as well.

Selecting different stresses to plot lets one check the other stresses. Stresses in X- and Y-direction, perpendicular to the grain, only occur around the support and at the face where the tower wind load is introduced. They are neglectable in the rest of the tower and only occur due to modelling choices.

Not plotting the stresses in the top and bottom 5 m of the tower also makes sure that any irregularities caused by the boundary conditions do not show up in the shear stress results, which mostly occurs around the nodes that have been fixed by the boundary conditions.

Figure H-6a shows the shear stresses in the XY-plane for the entire tower. The largest positive value can be found at Z=28 m and the largest negative value at Z=95 m. The latter is shown in Figure H-6b. The biggest absolute value of these two, 0.03 N/mm^2 is checked against the corresponding shear strength in Equation 7-26b and 7-27b:

$$|\tau_{xy,d}| = 0.03 \leq f_{r,CLT,d} = k_{mod} \cdot \frac{f_{v,CLT,OP,k}}{\gamma_M \cdot \gamma_n} = 1.1 \cdot \frac{4}{1.25 \cdot 1.0} = 3.52 \text{ N/mm}^2$$

$$|\tau_{xy,d}| = 0.03 \leq f_{r,CLT,d} = k_{mod} \cdot \frac{f_{r,CLT,k}}{\gamma_M \cdot \gamma_n} = 1.1 \cdot \frac{1.25}{1.25 \cdot 1.0} = 1.10 \text{ N/mm}^2$$

These two equations are joined in Equation 7-28c. The minimum strength value of 1.10 N/mm^2 is governing and is used to check the maximum occurring $\sigma_{xy,d,max}$ of 0.03 N/mm^2 with, which is sufficiently low. The value of 1.10 is the result of the formula in the denominator of the unity check in Equation 7-28c and the one found as 'Max. allowable $\sigma_{xy,d,max}$' in the table in Appendix C.

The exact same thing is done for the shear stresses in the XZ-plane, which are shown in Figure H-8. The denominator in formula 7-28b is equal to that of 7-28c, so the same values

apply. $\sigma_{xz,d,max}$ is now 0.35 N/mm^2, which is still lower than the maximum allowable stress of 1.10 N/mm^2 and thus sufficiently low.

For shear stresses in the YZ-plane, the stresses are shown in Figure H-7 and Equation 7-20 is used:

$$\begin{aligned}
|\tau_{yz,max,d}| = 1.03 \leq k_{net} f_{v,CLT,IP,d} &= k_{net} \cdot k_{mod} \cdot \frac{f_{v,CLT,i,k}}{\gamma_M \cdot \gamma_n} \\
&= 0.75 \cdot 1.1 \cdot \frac{5.0}{1.25 \cdot 1.0} = 3.30 \text{ N/mm}^2
\end{aligned} \tag{H-2}$$

$$\begin{aligned}
|\tau_{yz,max,d}| = 1.03 \leq (1 - k_{net}) f_{v,CLT,IP,d} &= (1 - k_{net}) \cdot k_{mod} \cdot \frac{f_{v,CLT,i,k}}{\gamma_M \cdot \gamma_n} \\
&= 0.25 \cdot 1.1 \cdot \frac{5.0}{1.25 \cdot 1.0} = 1.10 \text{ N/mm}^2
\end{aligned} \tag{H-3}$$

The minimum value of these two is to be used, which at 1.10 N/mm^2 is coincidentally the same as the governing strength for the other two directions. These two equations are joined in Equation 7-28a.

One of the underlying assumptions is that the maximum occurring shear stresses are present along the entire tower, in the entire cross section. In reality, these peaks occur relatively locally, as can be seen in the various figures, making this a conservative assumption. Even though the stresses in the YZ-plane appear to be very close to the ultimate strength in this plane, in reality the average shear stresses are much lower and less concerning. However, calculating them in this way allows for a straight-forward and quick way of checking the shear stresses.
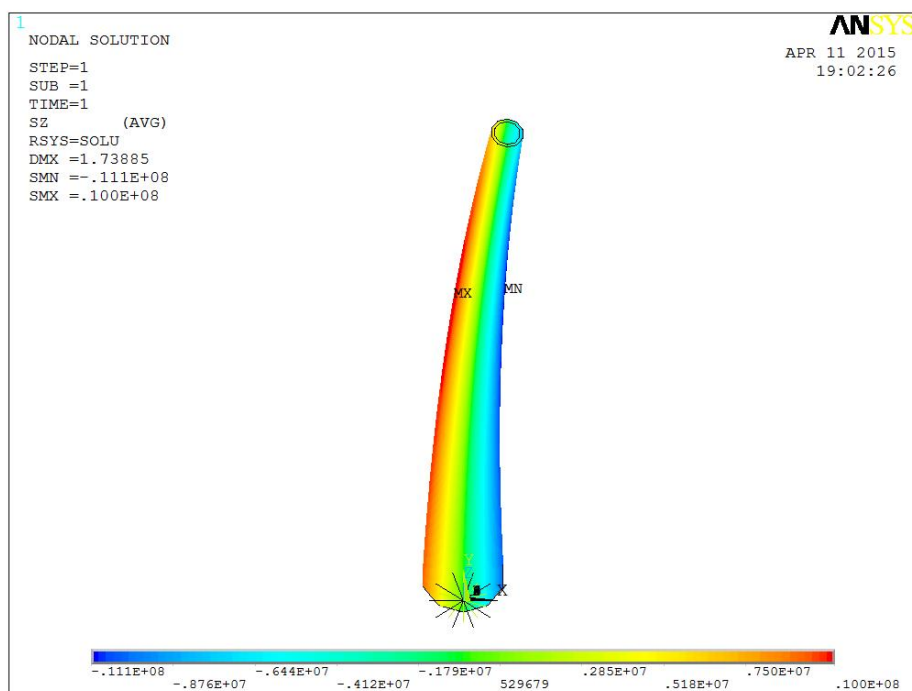
Figure H-5: Stresses in Z-direction for model A3
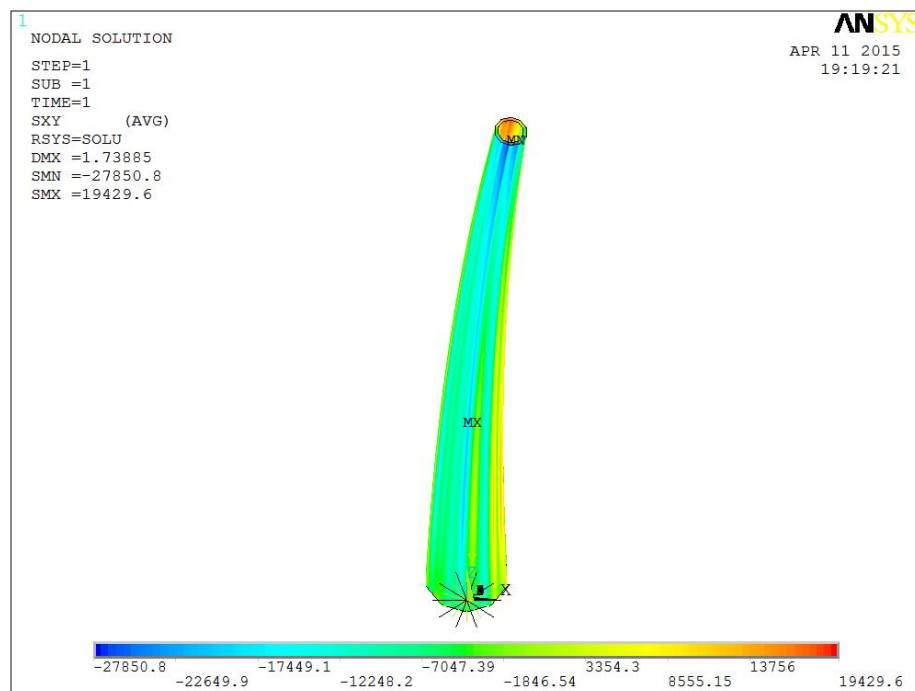
(a) H=5 to H=95 m
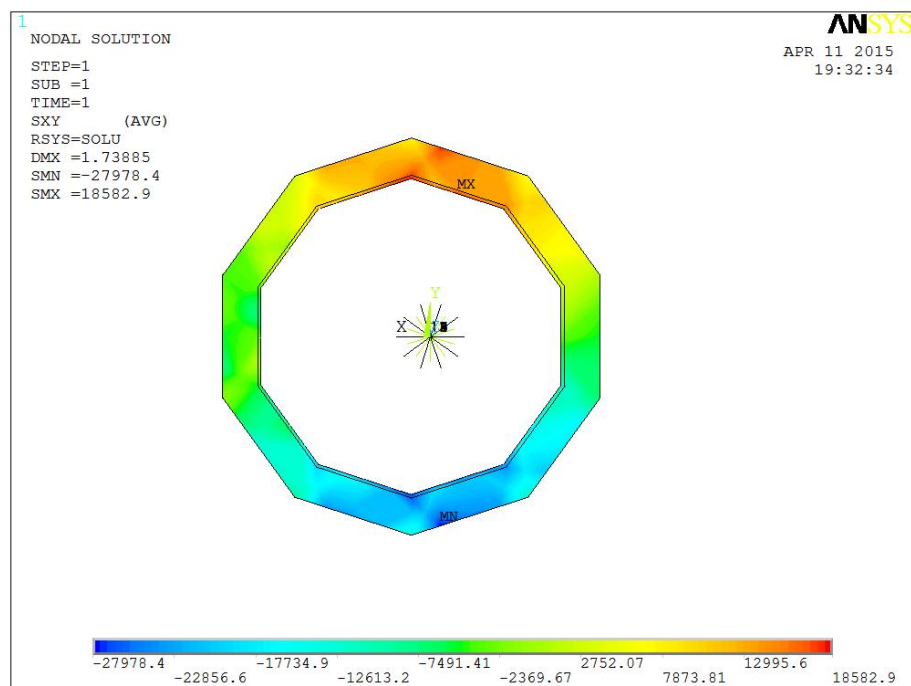
(b) H=95 m

Figure H-6: Shear stresses in the XY-plane for model A3
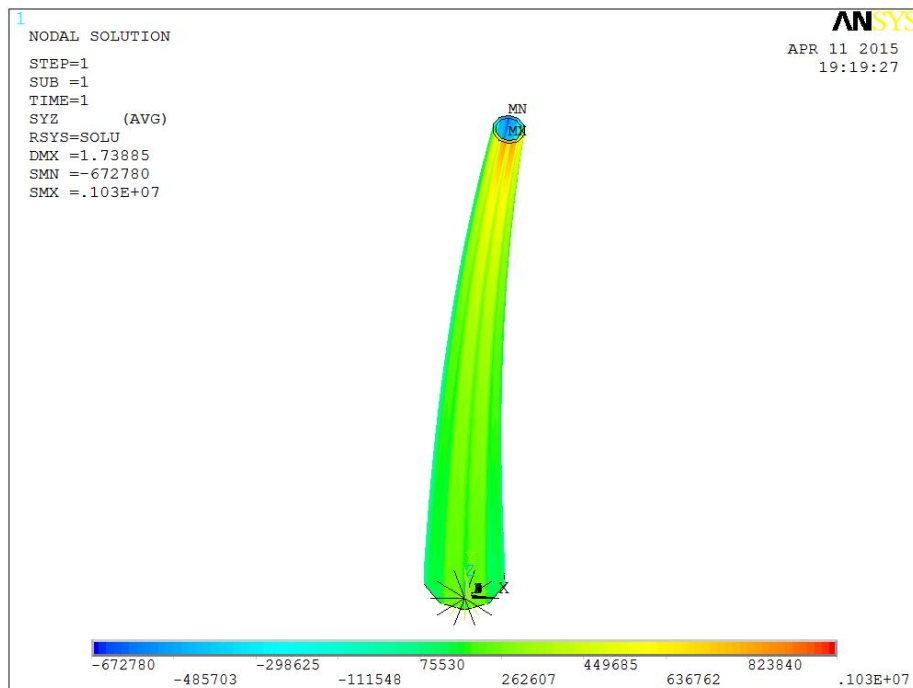
(a) Shear stresses in the YZ-plane for model A3
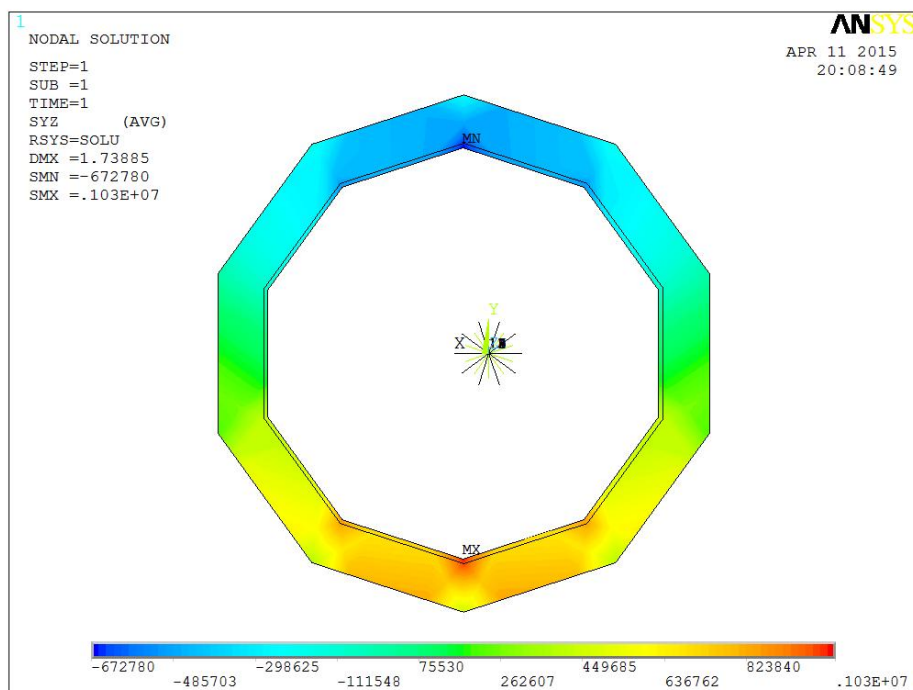
(b) H=95 m

Figure H-7: Shear stresses in the YZ-plane for model A3
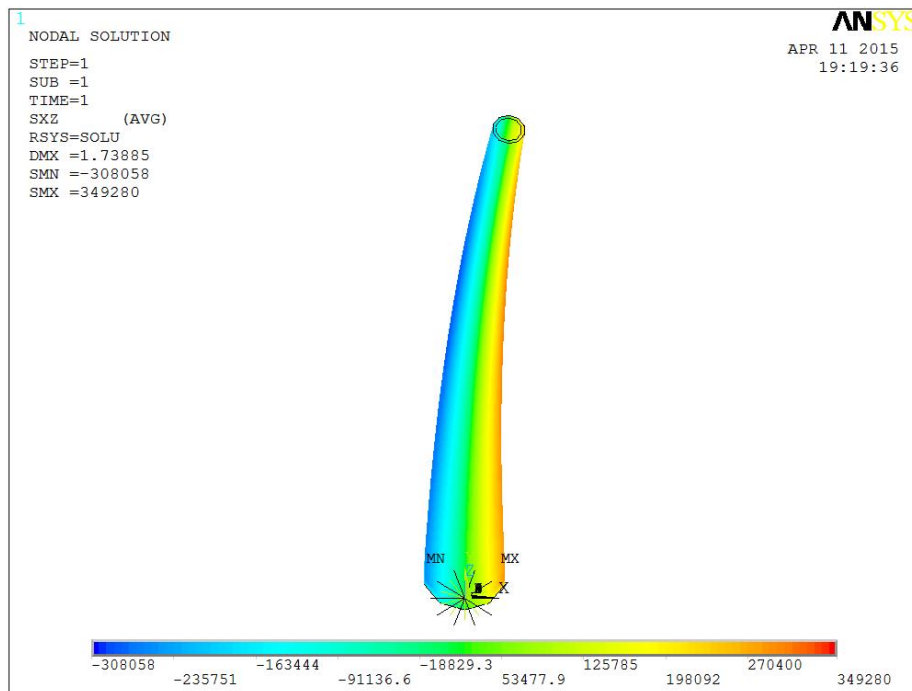
(a) H=5 to H=95 m
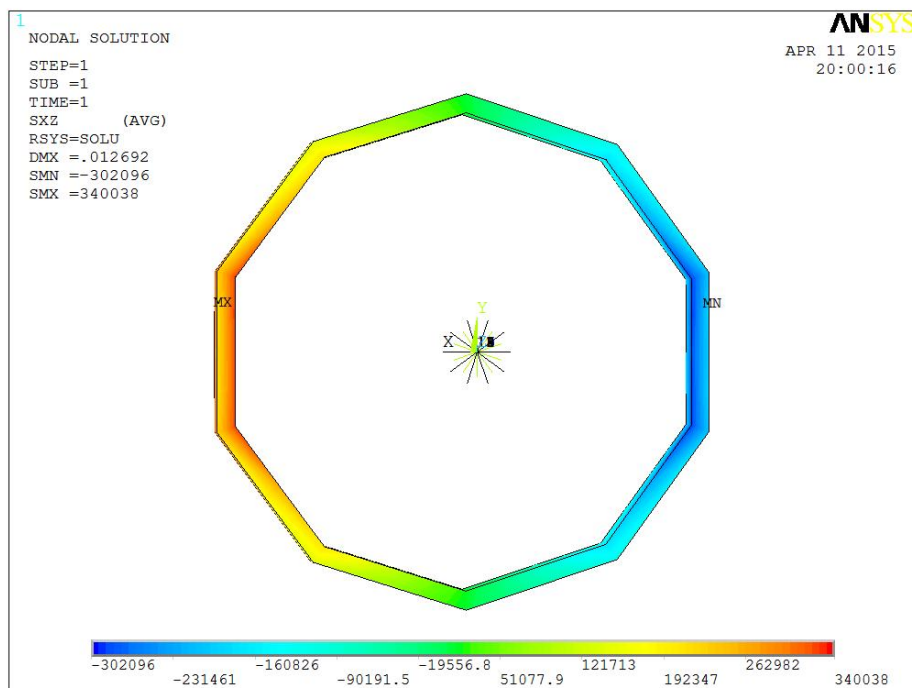
(b) H=5 m

Figure H-8: Shear stresses in the XZ-plane for model A3

Background information and further reading

Wind turbine terminology and operation

This appendix will explain some of the general terms related to wind turbines used in the rest of this report and make the reader familiar with the operation of a modern-day wind turbine. First, it will give a short introduction in the history of wind turbines.

I-1   History of wind turbines

I-1-1   Earliest developments

Mankind has been using the power of wind for their own purposes for thousands of years, whether it was to power ships, crush grain or to drain fields. Especially in the Netherlands, wind mills for pumping water and milling grain have become a part of our cultural heritage, some sources even claiming that the first mill in the Netherlands dates back to the 12th century [75]. In the 16th century it were the Dutch who started to make improvements on these first prototypes, resulting in the wind mills that symbolize our country today. These mills arrived at their technological perfection somewhere in the 19th century. For more information about the first wind mills, the reader is advised to read 'Wind Turbines: Fundamentals, Technologies, Application, Economics' by Hau [75].

I-1-2   Development of modern day wind turbines

With the technological progress of the 20th century, the extraction of energy from the wind became more efficient. Nowadays the term wind turbines describes "machines with rotating blades that convert the kinetic energy of wind into useful power" [5].

Although not the first to generate electricity from wind, many say modern day wind energy production was pioneered by Danish inventor Poul La Cour as early as 1891 [75]. His design was simple, where the turbines had rotors made out of four shutters sails supported by lattice
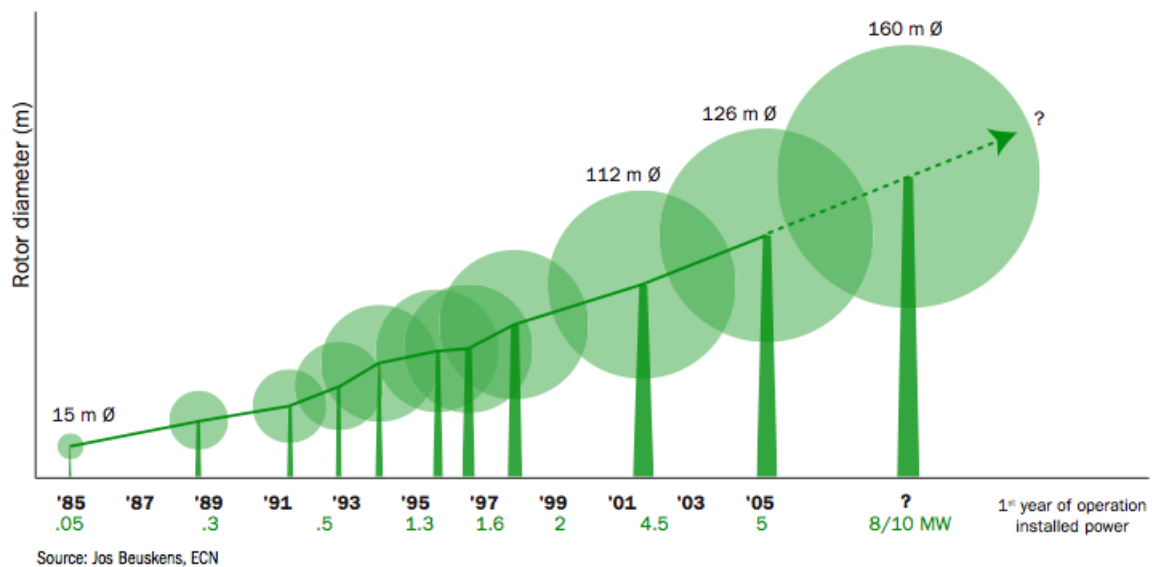
Figure I-1: An indication of the increase in size of individual turbines over the past years

towers. In the first decades of the 20th century, his design was applied in over a hundred turbines, with outputs from 10-35 kW.

During the forties, Danish company F.L. Schmidt started to develop two- and three-bladed rotors with aerodynamically shaped rotor blades, held up by either a steel lattice tower or concrete tower [75]. The high level of innovation by the Danish has resulted in the widespread application of the so-called "'Danish model"'[76, 29]. This light-weight three-bladed upwind turbine is what many nowadays picture when thinking of a wind turbine.

The oil crisis in 1973 changed the purpose of wind turbines drastically. Up until that point, turbines were almost exclusively used to power batteries for remote places, not yet connected to the electrical grid. The rising oil prices served a new incentive for research and development, mostly government-funded [29]. Besides the multi-megawatt turbines developed within these programs, privately funded wind farms in the western United States with a large number of smaller turbines (<100kW) also emerged.

I-1-3   The present state of wind turbines

Wind turbines are becoming taller and the diameter of the rotors is increasing as well, as long as technology permits it. Higher masts mean higher wind speeds on the hub. If the amount of wind is doubled, the amount of electricity that is produced becomes eight times as high. Doubling the diameter of the rotor also means quadrupling the amount of electricity produced [77]. With these figures, it is no surprise that there is a constant drive to increase the dimensions of the turbines, to increase the revenue of a single turbine. As can be seen from the list in the next section and Figure I-1, the scale of individual wind turbines has increased drastically over the years.

The first wind turbines of considerable height only had an output of 0,3 MW, but nowadays a large amount of turbines of over 8 MW have been erected. Multi-MW turbines have become

the standard. It leads to the fact that, with the speed of technological advancements, the economical lifespan of the current wind turbines is only 15 to 20 years [17]. Production and erection of the turbines requires energy and money, both earned back easily during operation. The energy needed is earned back in three to six months, while the economical investment takes between three and five years to break even.

I-1-4 Modern day records

Although the following list is taken from the less academical source that is Wikipedia [78], it should give a good idea how far the wind turbine industry has come in designing large scale turbines. The following records were found in April of 2014:

Largest capacity
The Vestas V164 has a rated capacity of 8.0 MW with a diameter of 164 m. It has been constructed for testing near Østerild in Denmark and is the world's largest-capacity wind turbine since its introduction in January of 2014.

Largest swept area
The turbine with the largest swept area is the Samsung S7.0-171, with a diameter of 171 m, giving a total sweep of 22966 m^2.

Tallest
The Vestas V164 is also the tallest wind turbine with the tips of its blades reaching 220 meters.

I-2 Classification of wind turbines

Over the years many different concepts and operating systems have been developed. Some have survived and dominate the field today, while others have disappeared completely. The following terms are often used to classify different types of wind turbines:

Horizontal- and vertical-axis turbines
Although horizontal-axis wind turbines (HAWT) dominate the horizon today, turbines with their axis perpendicular to the ground have also been applied on many occasions. An example of a vertical-axis wind turbine (VAWT) can be seen in figure I-2. The reader is expected to be familiar with the appearance of contemporary HAWT's, as can be seen in figure I-4.

Vertical-axis turbines allow for a more simple design and construction, since the main electrical components can be kept on the ground. This results in lower costs compared to HAWT's. Another advantage of VAWT's is that they do not need to be yawed (turned in order to optimize wind intake), but their many disadvantages still outweigh the advantages and limit their application [79, 5]:

– They must use an external power source to initiate rotation;
– They have a lower energy efficiency than HAWT's;

Figure I-2: An example of a Darrieus VAWT
Source: Wikipedia, http://en.wikipedia.org/wiki/Troposkein, accessed February 2015

- Their practical height is limited due to the fact that the axis is only supported at one end;

- When bearings or other components have to be replaced, the entire system has to be disassembled.

Upwind and downwind turbines

The difference between upwind and downwind HAWT's can best be seen in figure I-3. On upwind turbines the wind hits the rotor blades first, making a yawing system necessary to turn the rotors to face the wind. Although a downwind turbine is cheaper to make because of the lack of a yawing system and lower demands on blade stiffness, it is the upwind rotor that is applied almost everywhere today. This is because the wind on downwind turbines has to pass tower and nacelle, distorting the wind, resulting in fluctuating output and lower efficiency [79]. Other downsides to applying downwind turbines include potential higher fatigue loads and noise increase.

Capacity

Tong [79] devides wind turbines into several size groups based on their rated capacities:

- Micro turbines, ± 1 kW. Used for small-scale applications, such as lighting or powering a single small residence;

- Small turbines, <100 kW. Often used in rural areas for powering single large structures;

- Medium turbines, 100 kW - 1 MW. This is the type that has been extensively used in wind farms in the past, but in present times large turbines have taken over;

- Large turbines, >1 MW. The size that is applied most on the market today. Most modern-day, energy-producing turbines rate between 1 and 3 MW.;
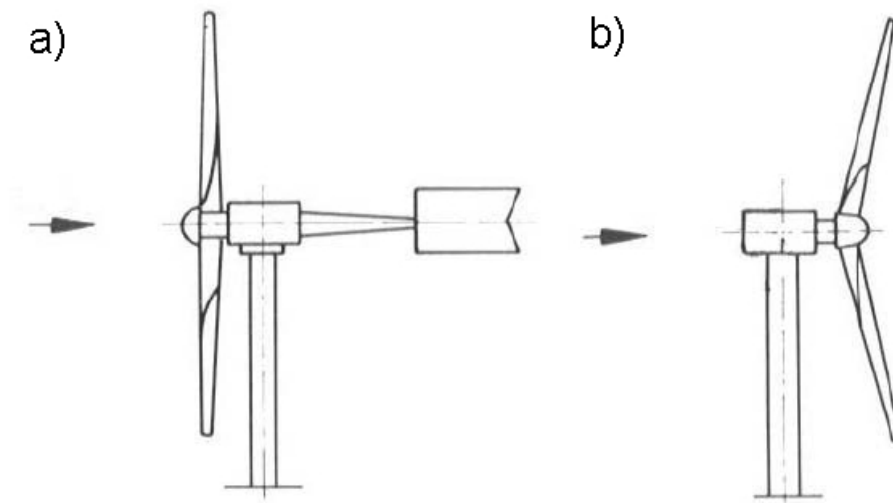
Figure I-3: Upwind (a) and downwind (b) turbines
Source: Acta Energetica, http://actaenergetica.org/en/science/innovations, accessed February 2015

– Ultra-large turbines, >10 MW. Although not yet applied at this moment, turbines
of up to 8 MW have already been built [80].

Onshore and offshore
This subdivision speaks for itself. Offshore application of wind turbines has taken big
steps in the last decades, the majority of the biggest turbines no longer being constructed
on land. Although onshore turbines are easier to erect and to connect to electrical grids,
making them cheaper, offshore turbines experience steadier and higher winds, allowing
for more operating hours and higher output [79].

Direct drive and geared
In direct drive turbines the (low-speed) rotational shaft is directly connected to the
generator, resulting in lower mechanical losses, lower noise emission, higher reliability
and simpler design than with a geared turbine [79]. In a geared turbine a multi-stage
gearbox turns the low-speed rotation of the rotor shaft into a high-speed rotation at
the generator for higher power output. Turbines with a gearbox are cheaper, smaller,
weigh less and have been the standard in design over the past decades. Lately, due to a
high number of gearbox failures, designs have also shifted towards direct drive solutions
[81, 82].

Stall-controlled and pitch-controlled blades
Power control is needed in order to enhance the efficiency of the conversion of wind
energy, stabilize power generation and protect the turbine in case of high winds. It has
three approaches [5]:

– A pitch-controlled system involves blades that are able to rotate around their axis,
usually using hydraulics. The blades are turned slightly out of the wind when the
wind speed becomes to high and turned back into the wind when it drops [79].

– Passive stall-control involves the optimized design of the aerodynamic profile of the
blades, which are fixed at their root to the hub. At higher wind speeds the profile

creates turbulence on the downwind side of the blade, causing it to stall [83].

– A combination of both pitch- and stall-control is called active stall control, where a pitch system is used to force the blades into deeper stall. It allows for turbines to run at rated power for most wind speeds [83].

Modern day turbines are predominantly equipped with pitch-controlled blades. Further explanation can be found in the section about power control on one of the next pages.

Variable and fixed rotor speeds

Due to easier design, stall-controlled turbines with a constant speed were dominant in the past. Variable speed turbines were seen as something of the future. But today "turbines with variable rotor speed are becoming increasingly more common in an attempt to optimize the energy capture, lower the loads, obtain better power quality, and enable more advanced power control aspects", according to DNV Risø[5].

I-3   Modern day horizontal axis wind turbines

Nowadays, the three-bladed, upwind, horizontal-axis wind turbine dominates the field. For this thesis, the considered turbine will be an upwind three-bladed onshore HAWT with a maximum capacity of 5 MW. The components and operation of such a turbine will be described below.

I-3-1   Components

The names of the major components used throughout this report can be found in figure I-4. The structure on top of the turbine tower can be roughly divided into two main components; the nacelle and the rotor. The nacelle houses important parts of the turbine, such as the gearbox, the generator and the controller. The rotor consists of the rotor blades and the hub, to which the blades are connected. The hub is connected to the low-speed shaft of the turbine. This shaft turns at around 20 to 30 revolutions per minute, whereas in the case of a geared turbine the high-speed shaft turns around 50 times as fast, thanks to the gearbox that is placed in-between [83]. The high speed shaft powers an induction generator that turns the rotational motion into electrical energy.

The last vital parts of the turbine to be mentioned here are the yaw mechanism, used to turn the rotor towards the wind, and the controller. The yaw system is operated by the controller, changing the direction of the turbine only a few degrees at a time. The term 'yaw error' refers to the rotor facing the wind under a slight angle. This will result in lower efficiency and higher fatigue loads [83]. The controller also monitors the turbine and controls the electrical and mechanical systems, aiming for the highest possible availability production rate.

I-3-2   Operation

General power production

The rotors slow down the wind to capture its kinetic energy and transform it into mechanical (rotational) energy. As stated before, the rotation of the shaft is converted into electrical
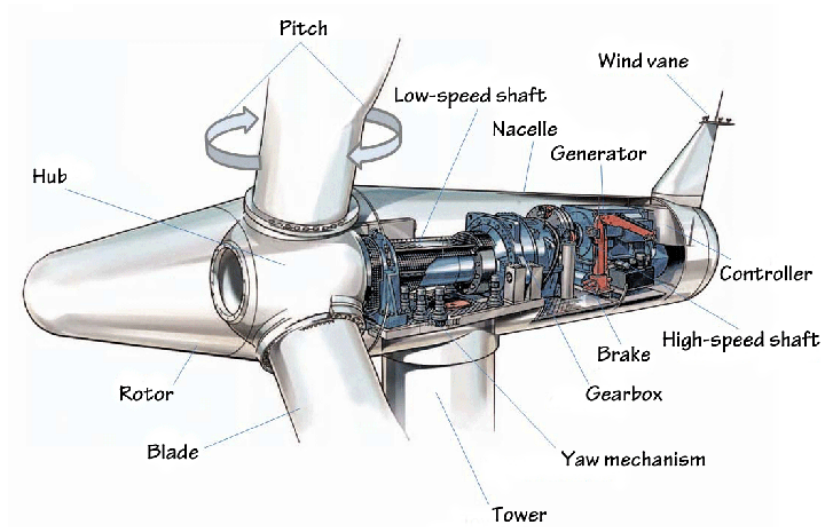
Figure I-4: The major components of a modern-day wind turbine
Source: Hamilton and Lining, http://www.bls.gov/green/wind_energy, accessed February 2015

energy by the generator within the nacelle, often with the aid of a gearbox. The energy content of wind varies with the cube of the wind speed V, which together with the rotor swept area A and the density of the surrounding air ρ can be found in the following formula for the power output of a turbine:

$$P = \frac{1}{2} C_p \rho A V^3 \tag{I-1}$$

Within a reader made by the 3TU cooperation [83], the following remarks can be found that should explain the power coefficient C_p, which has a theoretical maximum of 0.593.

"The Betz' law says that you can only convert a maximum of 16/27, or else 59.3%, of the kinetic energy in the wind to mechanical energy using a wind turbine" [83]. Part of the reason for this is the fact that a spinning rotor will actually deflect part of the wind coming towards it, even before it reaches the turbine. Besides, if a turbine would extract all the energy from the oncoming wind, the motionless air behind the rotors would block other in-flowing air. In practice, lower coefficients than the Betz limit are reached, due to various reasons not named here specifically [29].

The formula also shows the reason for the ever increasing size of individual turbines. Doubling the diameter will quadruple the potential output, whereas doubling the wind speed will increase the output eight-fold. Wind speeds are higher at higher altitudes, explaining the desire for increased tower heights. With the wind speed being so important, a lot of effort is also put into picking the right locations for turbines.
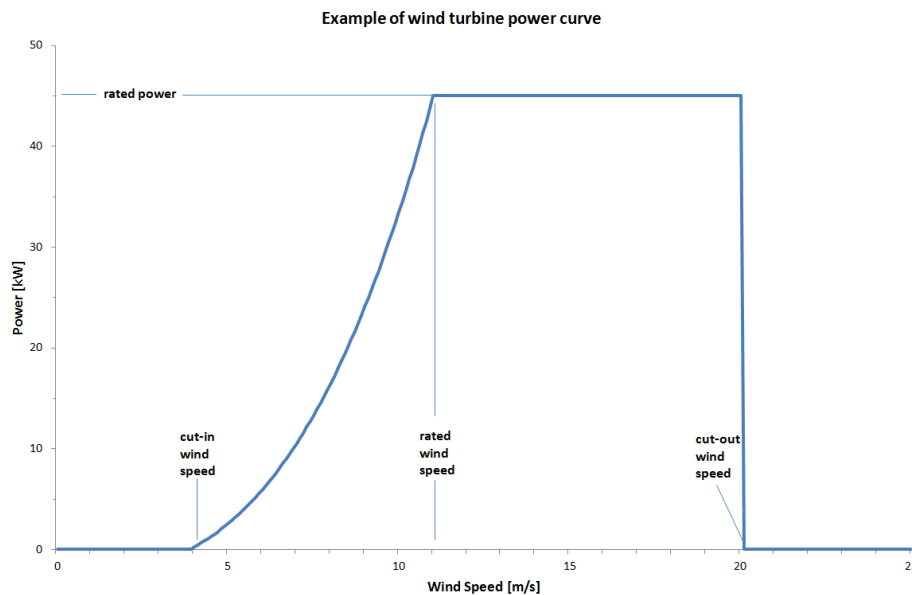
Figure I-5: Example of a wind turbine power curve
Source: Science and Technology Facilities Council, http://www.elm.eru.rl.ac.uk/ins4.html, accessed
February 2015

Rotor operation

Just like the wings of an airplane, turbine rotors move because of lift. Wind flowing over one side of the blade has a higher speed than the wind sliding along the other surface, creating a lift force perpendicular to the wind direction. When the angle of the blade relative to the airflow is increased (the so-called angle of attack), there will be a certain point where the wind flow on the downwind side will separate from the blade surface, causing turbulence and taking away the lift. This is called stall, one of the ways to control the power output of the turbine, as will be explained in the next section. Besides lift and stall, the drag force, caused by air resistance, is another main design point for rotor blades [83].

Power control and characteristic wind speeds

As can be found in Tong [83], the 'rated' or 'nominal' wind speed is the speed at which the turbine will reach its rated power output. Often this is also the maximum power output. For speeds below the rated speed (but above the cut-in speed), the turbine will not produce its maximum output and the power control system will try to optimize the power output [5]. Below the cut-in speed, the turbine does not produce usable energy.

For speeds above the rated speed, the power control system ensures the turbine will limit power output and try to keep it outputting at rated level, up to the cut-out speed [5]. The cut-out speed is the speed at which the turbine will shut down to "prevent loads and power from reaching damaging levels" [83]. This can be seen in the power curve in figure I-5.

As stated before, there are three approaches to power control. DNV Risø have published a report [5] explaining the operation, advantages and disadvantages of the different approaches.

Stall-controlled blades are fixed to the hub and rely on aerodynamic design to slow down. At a certain critical value, turbulence at the downwards side of the blade will reduce the lift force, preventing the rotor from gaining speed. The rotor can be made cheaper compared to other approaches, but is less efficient at lower wind speeds and stall controlled turbines often operate below rated power at high wind speeds.

Pitch-controlled blades have mostly been used in variable-speed turbines up to now. Through continuous monitoring of the power output and wind speed, the controller adjusts the angle of the blades, allowing for good power control. Apart from the added complexity, it also exhibits considerable power fluctuations at high wind speeds. Active stall also requires a more complex component to be installed, compared to passive stall, but the advantage of active stall is that it allows for very accurate power control. In this way the turbine is able to run at rated power for all high wind speeds.

Yawing

When the controller senses a change in wind direction, it uses the yaw mechanism to change the direction the rotor is facing. The yaw system consists of a number of components:

- Yaw bearing:
  Part of the connection between the nacelle and the tower that allows for rotation of the nacelle.

- Yaw drive:
  Nowadays almost always an electric motor and gearbox, providing the torque to turn the nacelle.

- Yaw break:
  Used to hold the nacelle in place when there is no yaw error.

Continuous yawing in one direction may lead to cable twisting, which is monitored by the controller and adjusted when needed [83].

Conventional tower concepts

This appendix will give a short overview of many of the structural materials and concepts that have been applied for large wind turbine towers. It will focus on onshore turbines. At the end a few statements about the economics of the different systems will be made. It should be noted that this chapter was already written in April of 2014, while in the meantime several developments and new tower designs have been applied which may not be included here.

Figure J-1 shows several examples of structural systems, of which the first three will be explained in more detail within this chapter. The guyed towers on the right are only used for small wind turbines [5].

| Tubular steel tower | Tubular concrete | Lattice tower | Three-legged tower | Guy-wired pole tower |

Figure J-1: Examples of different structural systems and materials
Source: Miceli, http://www.windfarmbop.com/tag/concrete-tower/, accessed February 2014
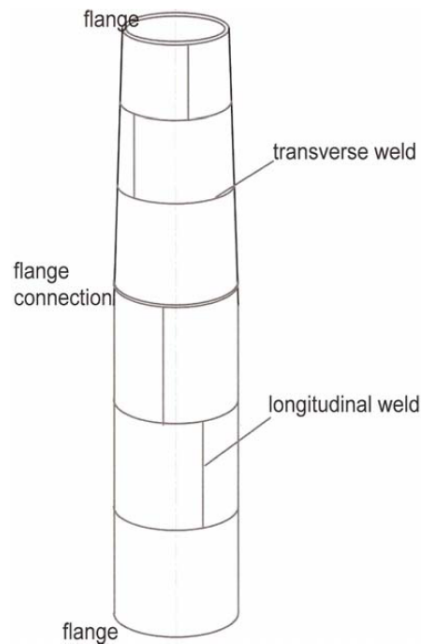
Figure J-2: Two sections of a welded tubular steel turbine tower
Source: Lyrner et al. [3]

J-1 Steel towers

J-1-1 Tubular welded steel shell tower

The tubular welded steel tower is the face of modern day wind turbines and is applied most throughout the field, because of its predictable dynamic and fatigue properties [3, 84]. For the traditional tubular tower several curved plate elements are welded together in the shop to form tower sections. Each sections begins and ends with a flange, which are bolted together on site. This can be seen in Figure J-3. The diameter of the tower decreases with height.

Tubular steel towers are dimensioned for failure in tension and buckling, as well as fatigue. The welds and flanges form the weak link in the fatigue behaviour, allowing for little to be gained by the application of higher steel grades, which is why regular steel grades are used [3].

Transportation restrictions on land lead to a maximum base diameter of around 4 to 4.5 m, depending on the country and turbine site. Larger hub heights have larger optimal diameters which cannot be achieved, resulting in uneconomical increases in wall thickness and mass to increase the stiffness and strength of the tower. It also results in difficulties transferring the loads to the foundation [3]. The maximum hub height where the design of the tower will remain economical, lies between 85 and 100 m, depending on the source [19, 3]. These restrictions do not apply offshore.
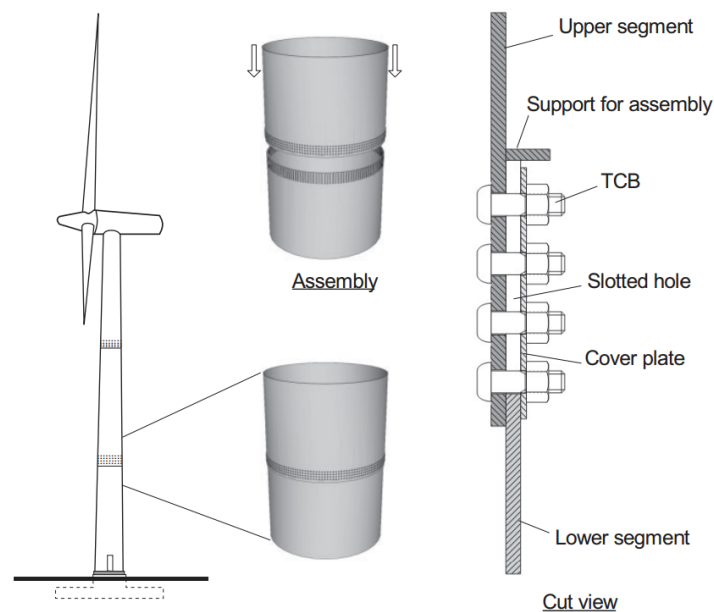
Figure J-3: Example of a lateral friction joint
Source: Veljkovic [85]

J-1-2 Tubular steel shell tower with friction joints

One way to solve the problem of base diameter restrictions, is to replace the shop welding with on-site friction joints. Tower plates are joint by bolts and nuts, relying on friction between elements to transfer loads. Since bolts have to be tightened from both sides, access to the outer end of the bolt is an obvious problem to this kind of system [3]. Friction joints can be applied both laterally and longitudinally.

Advantages of this type of steel tower are that it uses less material than a welded tower and base diameter restrictions no longer apply. It also takes away the weakness of welds in fatigue behaviour, possibly shifting the dominant failure mode towards ultimate strength instead of fatigue. Better energy dissipation and higher stiffness are also associated with these connections, compared to the system in Figure J-3 [86]. Downsides are the need for regular checks of the pretensioned bolts and the need for high accuracy in the cutting and drilling of the steel.

An example can be found in Siemens' concept, shown in Figure J-4, which also uses bolts in the longitudinal connections (placed on the inside of the tower) [25]. The concept is not widespread yet, but its application is increasing [3].

J-1-3 Steel lattice towers

Steel lattice towers have no restrictions on how large the base width can be made, giving them two major advantages: they are light-weight and cheap. Other advantages are the ease of transportation, allowing for applications in hard-to-reach areas, and the use of standardized
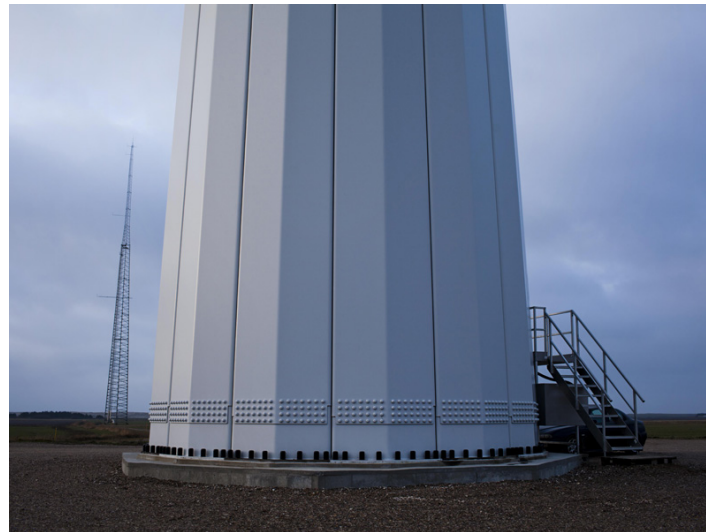
Figure J-4: The base of a bolted tower by Siemens
Source: Siemens, http://www.energy.siemens
.com/hq/en/renewable-energy/wind-power/wind-turbine-technology/tower.htm, accessed December
2013

materials and elements which are easier to dispose of than a large tubular tower. However, according to a report published by Elforsk [3], the many downsides are "equally strong":

– The number of bolts is high and they need periodic checking;

– Dynamic properties and torsional stiffness may be problematic to control;

– Large accumulation of ice may endanger the turbine;

– It is hard to maintain an acceptable level of safety for maintenance personnel;

– Its visual aspects are controversial.

Lattice towers often have 3, 4, 6 or 8 corner posts, various types of bracing and almost no restriction in height. The German Führlander company, for instance, has used lattice towers to reach hub heights up to almost 160 m. Their 2.5 MW turbine near Laasow used to be the tallest onshore wind turbine in the world, a title now borne by the Nowy Tomyśl Wind Turbines in Poland. Both 2.5 MW turbines located there are supported by a 160 m tall steel latice tower. The one is Laasow is shown in Figure J-5.

J-2   Other materials

J-2-1   Concrete

Concrete towers contain pre-tensioned tendons, running through ducts cast within the concrete or placed outside the concrete, in the latter case either inside or outside the tower, which allows for easier inspection. The concrete also contains regular reinforcement. Especially the

Figure J-5: The Führlander tower of 160 m

Source: Esser Systems, https://www.esser-systems.com/en/press/presse-detail/article/comprehensive-monitoring-additionally-provides-fire-protection-in-one-of-the-worlds-tallest-wind-tu.html, accessed April 2014

bottom part of the tower benefits from the application of concrete, where higher moments can be absorbed.

Fatigue is not of concern when designing concrete towers, so the dimensions are governed by the extreme load case [3]. In the ideal situation, the extreme load would not result in tension stresses within the concrete. Benefits of concrete towers are the lack of restrictions to the base diameter and the possibility for long lifetimes [3]. Downsides are longer erection times and larger weight, calling for heavier foundations.

Slip formed concrete towers have been around for a long time, but current towers are also built by assembling prefabricated parts. The latter is shown in Figure J-6. The following descriptions are based on the Elforsk report mentioned earlier.

Slip formed towers

Slip formed towers are made by a continuous process on site, running around the clock until the tower is finished. Tendons are installed and tensioned once the tower has reached its height. The tendons are expensive and the demands on workmanship and climate control when slipforming are high.

Figure J-6: Close-up of a precast concrete tower section
Source: Jimeno [87]

Towers from prefabricated elements

Elements are prefabricated in a factory, shipped to the site and assembled. An example can be seen in Figure J-6. A big advantages is the ability to have more control over casting conditions, resulting in a more even quality throughout the tower. Being able to avoid the high costs that come with production on site makes it cheaper, but certain designs require a large number of different moulds, which in turn will raise costs [3].

Hybrid towers

Hybrid towers also exist, with a conventional welded steel tower functioning as the upper part of the tower. The bottom half is made of concrete. The upper half is chosen is such a way that the aforementioned transportation restrictions are no longer an issue. According to Lyrner et al. [3], the design of the concrete section is easier, as well as getting the eigenfrequencies right. They are also more economical than pure concrete towers.

J-2-2   Timber

Timber has been used in the wind turbine and windmill industry for centuries. The earliest wind turbines used to have wooden blades, supported by timber lattice towers. Only recently the use of timber in the tower structure has been considered again, by the Germany-based TimberTower company. This design is used throughout this thesis and formed the inspiration for this research. Benefits of timber are good resistance against buckling and fatigue [3].

J-3   General tower design objectives

This section contains a few remarks that might play a role in the design of the conventional turbine towers. The tower is perhaps the least complex of the different turbine components. Since it still accounts for more than 20% of the total costs, optimizing the tower can lead to significant cost reduction [5]. The rule of thumb has been to choose a tower height from as large as the diameter of the rotor to 1.5 times as large [3].

J-3-1   Vibration control

Preventing resonance is very important. It helps ensure a longer fatigue life, noise reduction and higher stability [88]. To do this, the natural frequencies must be kept out of the range of excitation frequencies, which are governed by blade-passing and rotational frequencies [83]. Burton et al. [29] conclude that it is not always the most economical solution to try and satisfy these frequency requirement for a given combination hub height and turbine speed. Sometimes altering hub height can result in a more economic design than sticking to a certain height.

J-3-2   Fatigue

According to Burton et al. [29], pitch regulated turbines will experience increased rotor thrust fluctuations than stall regulated ones, increasing the possible critical influence of fatigue. "Fatigue is also more likely to be critical at low wind-speed sites, because the percentage reduction in extreme loads is less than the percentage reduction in fatigue equivalent load" [29]. Standard welded connections only have a fatigue class between 36 and 71 [86], but fatigue in the section joints is often avoided by applying high-strength friction grip bolts [29]. The latter is also applied in steel lattice towers.

J-3-3   Safety, access and maintenance

Tubular towers provide safer and more comfortable circumstances for personnel to access the nacelle by providing shelter. Inside the tower a ladder is placed, often accompanied by an elevator. A fall protection system is present in alle types, for personnel while ascending or descending and working on top of the turbine. It includes a safety harness and shock absorption. Other requirements for the safety of personnel working on turbines include "protection from the machinery, fire protection and electrical insulation protection" [83].

A tubular turbine tower should also include a doorway at the base to allow access to the tower.

J-4   Economics

Swedish company Elforsk [3] has done research into the costs for the above-mentioned systems and materials. They have made global designs for different hub heights, not including
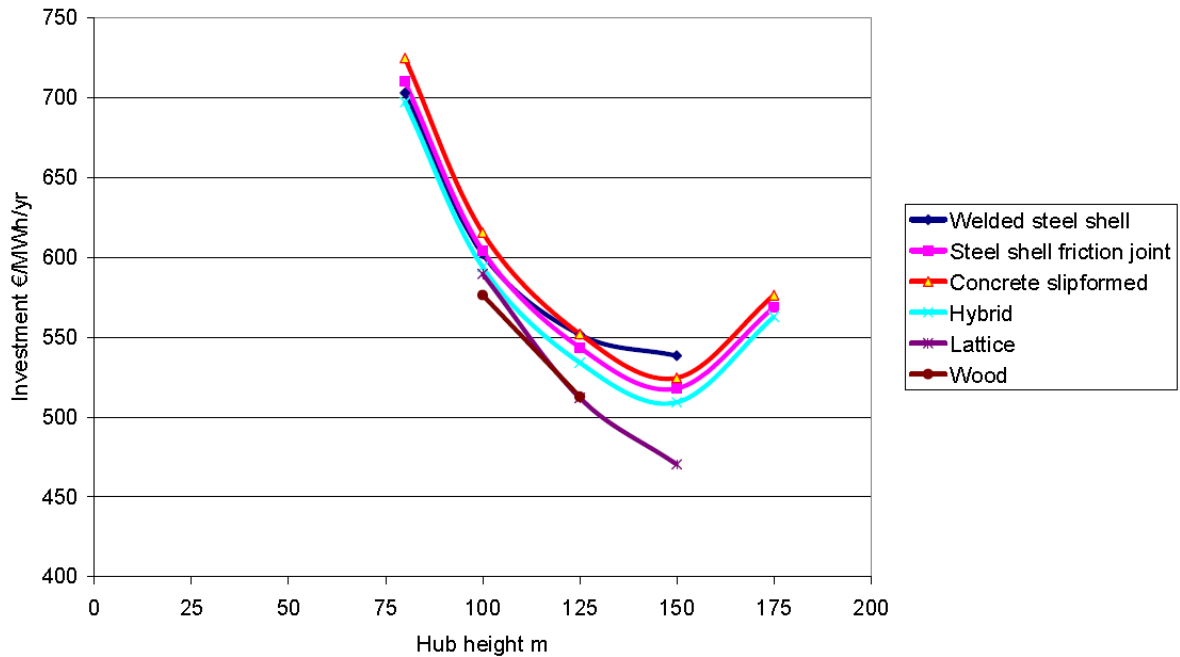
Figure J-7: Specific cost (investment costs divided by the yearly production) for various tower
materials and systems for a 3 MW turbine
Source: Lyrner et al. [3]

maintenance costs and plant/site costs such as roads and grid connections. Their results for
a 3 MW tower are shown in Figure J-7. The sudden increase in costs for hub heights of 175
m is due to the need to use lifting towers instead of conventional lifting cranes.

The costs are relatively similar for towers up to 125 m. For towers of 125 m or higher,
the relative costs start to show substantial differences. Steel welded towers become more
expensive due to the aforementioned restricted diameters and a design of 175 m turned out
to be not possible due to the same reason. The specific numbers for the 125 m tall tower
can be found in Figure J-8. Timber and steel lattice towers appear to have the lowest tower
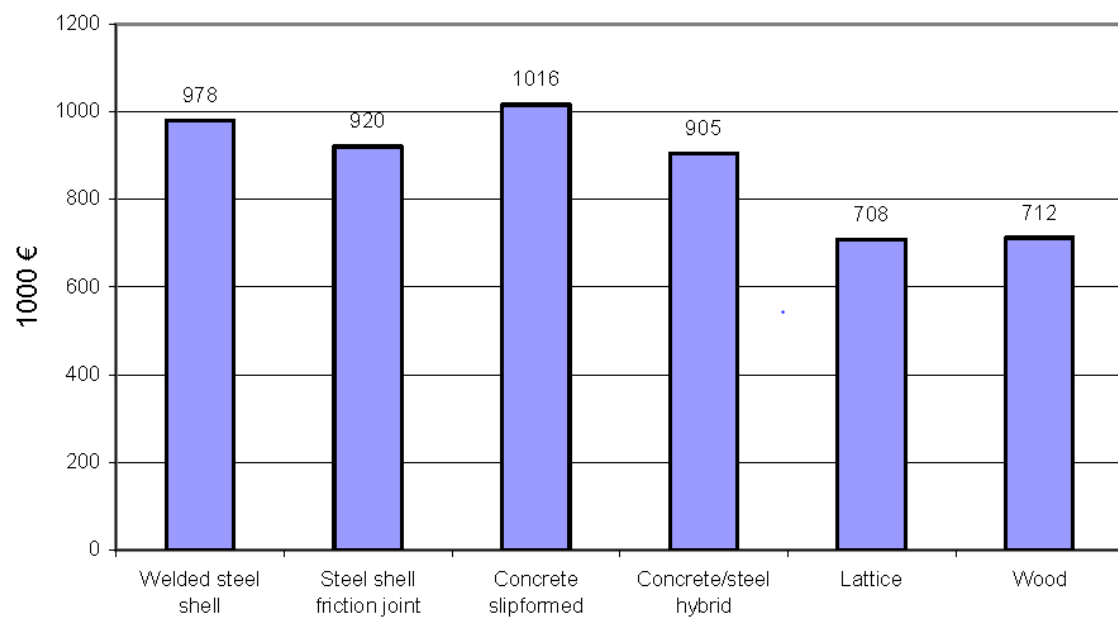costs. More information about the estimated costs can be found in the Elforsk report [3].

Figure J-8: Tower costs for a 125 m high 3 MW turbine
Source: Lyrner et al. [3]

The original TimberTower

The inspiration for this thesis came from the 100 m high TimberTower turbine in Hannover, where the tower is made of Cross Laminated Timber (CLT) panels. The project displays the structural possibilities of the material and gives the turbine a more sustainable alternative for the tower structure. The tower is shown in Figures K-1a and K-1b.

This appendix will first deal with the origin of the TimberTower, elaborating on how it came to be. A general description of the structure follows, with an overview of the advantages and disadvantages of this timber wind turbine tower. The global structural system is then explained, followed by a description of the materials that have been used. The connections are discussed in a separate section. Finally the erection process of the tower is covered.

This appendix was already written before the rest of the report, in December of 2013. In the meantime, the development of a 140 m high timber tower, carrying a 2.5 MW turbine, is well underway.

K-1 Origin of the project

The desire of the German government to increase their use of renewable energy, has led to a boost in the field of wind energy. The desire to increase the height of turbines (+1 m height $\approx$ +1% energy revenue [42]) has led to a lot of research in the field of wind energy. New concepts and materials are developed in an effort to produce the optimal wind turbine. The following part is mentioned by the company behind the TimberTower [18] as the reason for the development of their timber turbine tower.

Turbine towers, along with radio towers and electricity masts, were traditionally made of timber. Steel took over and is nowadays the most used material for the purpose of building wind turbines, reducing the use of timber in large-scale towers to zero. Other concepts, such as concrete or steel-concrete hybrid towers fail to prove their economic worth. A lot of research is conducted in the field of fibre reinforced polymers, but the knowledge is not widespread and the material remains relatively expensive. As for now, the most common design remains the tubular steel tower, despite the rising steel price.

(a) The first timber turbine tower: the TimberTower in Hannover, seen from a distance
Source: TimberTower GmbH, http://timbertower.de, accessed December 2013

(b) On the site in Hannover

Source: Hannover.de, www.hannover.de/nl/Media/01-DATA-Neu/ Bilder/Redaktion-Hannover.de/Portale /Wirtschaft/Timbertower, accessed December 2013

Figure K-1: Images of the completed TimberTower

Steel towers, however, lose their economic competitiveness for heights of 85 m or higher [19]. The traditional design is limited to a base diameter of 4.2 m, due to bridge clearances and other limitations put on the design by transportation. For towers of 100 m or more, which are becoming more common, especially for large-scale wind farms, the required diameter exceeds this 4.2 m at the base [89]. Larger turbines are therefore only feasible in areas where these restrictions are not present, or which are accessible by water.

When German engineer Gregor Prass started to work on the question on the optimal turbine tower structure in 2001, he started developing the first timber turbine tower concept. In 2008, when the theoretical phase was completed, he joined a businessman and a management consultant to form TimberTower GmbH.

Efforts made by this company resulted in the first 100 m timber turbine tower, built in Hannover, Germany. It carries a 1.5 MW nacelle, exploited by Vensys Energy Ag, also the biggest investor in the project [19, 22]. Finding investors proved to be one of the bigger hurdles. Provided that material tests turned out to be sufficient and a full-scale prototype was tested, Vensys agreed to finance and exploit the final product [89].

K-2 General information

The tower consists of CLT panels, glued together on site with a polyurethane adhesive. Together they form an octagonal hollow body. A 5 m high concrete base supports the 90 m timber structure, the latter weighing around 200 metric tonnes. The nacelle and rotor, with a

(a) The panels fit on a standard-sized truck
Source: TimberTower GmbH, http://timbertower.de,
accessed December 2013

(b) Siemens' bolted shell tower
Source: Siemens, http://www.energy.siemens
.com/hq/en/renewable-energy/wind-power/wind-
turbine-technology/tower.htm, accessed December
2013

diameter of 77 m, weigh 90 tonnes and are connected to the tower by a 5 m tall steel adapter structure, bringing the total height at 100 m. The tower is tapered, the diameter of the tower varying from 7.0 m at the base to 2.7 m at the top. The structural system will be explained in more detail later on.

Calculations predict it will produce about 3.3 million kWh during 2200 full operational hours each year, which will be enough to power more than 1000 households [89, 21]. Designers guarantee a lifespan of at least 20 years, as is common in the wind turbine field, but calculated it to last for 40 years [90].

K-2-1 Advantages

According to the company, there are a number of advantages to their concept and the use of timber in general, based on [19], [20], [21] and [22].

Ease of transportation
The individual panels fit inside a standard 40 foot shipping container, as is shown in Figure K-2a. This no longer requires so called 'abnormal loads' (e.g. large steel turbine sections) to be transported over road, reducing costs drastically. It also allows for more areas to become potential turbine sites in a cost effective way [19].

The individual elements weigh less, allowing for lighter hoisting equipment. However, it must be said that several companies such as Siemens[25] have developed steel tower concepts that offer the same advantages, shown in Figure K-2b.

The environmental benefits of timber
Compared to steel, timber requires less energy and produces less CO_2 during production. The use of timber products is also a form of CO_2-storage. It is easier to recycle than steel, or can be used to create energy through burning. After three months the tower will have produced more electricity than could have been gained from burning the material instead [21]. A hybrid tower today causes 3 times more CO_2 emissions within

its product life than the TimberTower, even if contribution from the CO_2-storage of wood and material re-use is ignored.

Timber is a renewable resource, if produced responsibly, whereas the world's steel resources are finite. As scarcity increases, so will the price. Recycling of steel is an option, but still has the same environmental disadvantages as producing new steel, although slightly smaller.

The environmental aspects of a timber turbine are considered the biggest advantage of timber over the other materials by many [22]. Especially the independence of finite resources have beneficial effects. The designers also believe that the use of timber will increase the acceptance of residents near a wind turbine site [89].

Economic benefits

In mass production the costs will be expected to be around 80% of a comparable steel tower [42], and especially for hub heights of more than 100 m timber will be the attractive alternative [21].

Where there are only a few fabricators that are able to produce the large tubular steel sections needed for a traditional steel tower, the timber elements can be produced by a large amount of timber manufacturers. This is expected to boost local economy and help keep prices compatible and stable [24].

Structural benefits of timber

Compared to steel, timber behaves quite different under the loads acting on a turbine tower and is considered to perform better overall in conducting loads to the foundation [20]. High cycle fatigue performance of timber is better than that of steel [23], allowing for a longer lifespan. The damping behaviour and fire resistance of CLT are, when compared to steel, also more favourable [24].

The specific modular concept of the TimberTower allows for large base dimensions than a traditional tower, making it possible to reach higher hub heights, which is desired by many operators.

K-2-2   Disadvantages

One of the major disadvantages of the use of timber in this particular application, is the lack of knowledge and experience. In the case of the TimberTower, the project was substantially slowed down by the building authorities [89]. General certificates for the connections are as of yet not obtained, the project was run through on a case-by-case approval.

The lack of experience also proved to make it difficult to find investors, although timber manufacturers were eager to join [22]. One might imagine that when timber turbine towers become more widespread, it will put a lot of pressure on an industry that might not be ready for this, but this is only speculation.

K-2-3   Future plans of TimberTower

A second tower is being developed. A turbine with a hub height of 140 m will be placed in Niedersachsen, becoming one of the highest in the world. The current record is set at 160 m,

shared by steel lattice towers in Prapoc, Poland and Laasow, Germany. Calculations have shown that it is technologically feasible to reach hub heights of 200 m with timber [89, 90], but there is no crane high enough for its erection (yet).

K-3 Overall structural system

K-3-1 Tower

The first design of the tower consisted of a lattice tower, but the designers soon discovered the solution would lie in the form of a closed hollow body [89]. The many connections of a lattice tower require an disproportional effort in protecting these from the elements and reduce the stiffness of the tower through slip [22].

For towers higher than 80 m, the natural frequency becomes the governing factor in the design, the extreme loads and fatigue becoming of lesser importance. Being directly related to the frequency, a sufficient stiffness could not obtained with a lattice tower [22]. The final design, with its use of CLT panels with glued connections, allows for a high stiffness. In the end the natural frequency of the tower is calculated at 0.35 Hz and will be verified by measuring in practice. At high wind speeds the top of the tower will sway about 1.2 m, which is in the same order of magnitude as a steel tower [21].

The octagonal cross section of the tower is made of 15 m long trapezoidal shaped elements, going up in a spiral-like fashion, shown in Figure K-3. The use of this helix reduces material, because it avoids places where a horizontal seam all around would weaken the structure, as is the case with traditional steel tubular towers. At any level, a maximum of two of the eight sides contain a horizontal connection. The elements are 2.9 m wide at the bottom and 1.3 m at the top, with a constant thickness of 30 cm [23].

K-3-2 Base

The tower rests on a circular concrete base plate with a diameter of about 20 m and a thickness of 60 cm. It is executed as a shallow foundation, the soil in Hannover allowing the absence of piles. On top of this plate a 4.5 m high pedestal is made to connect the foundation to the tower, containing a door opening, installations, air handling units and monitoring systems, as well as preventing vandals to be able to reach the more vulnerable tower [22]. The base is displayed in Figure K-4.

K-3-3 Other features

The nacelle is connected to the tower using a conical steel section, shown in Figure K-5a, bringing the diameter from 2.65 m to 2.37 m. This adapter also forms the transition between a octagonal shape and a circular one, making the tower suitable for every type of contemporary nacelle [24].

The scaffolding structure inside, with its primary function of easing erection (see Section K-6), houses an integrated ladder and elevator system, fire alarm and evaporation system, as is common in all turbines, [23]. It is made of regular sawn timber and has no load bearing function once the tower is completed. Part of it is shown in Figure K-5b.
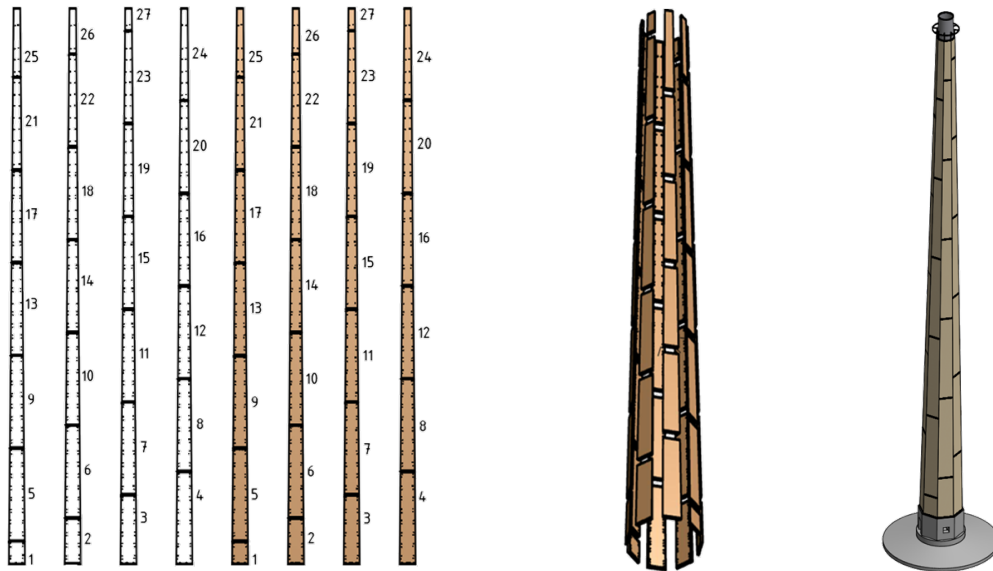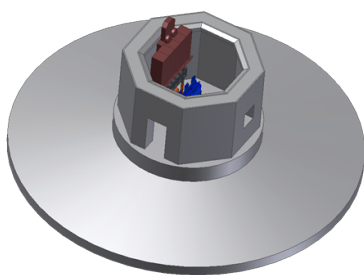
Figure K-3: The panels are arranged in a helix-shape to prevent all-around horizontal
connections
Source: TimberTower GmbH [42]

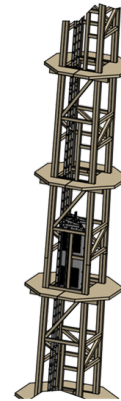**(a)**   **(b)**   **(c)**

Figure K-4: The reinforced concrete base (a) contains anchor rods that pretension the base (b)
and connect the base to the timber tower
Source: TimberTower GmbH [24]

(a) The steel adapter between tower and nacelle
Source: TimberTower GmbH [42]

(b) The scaffolding contains a ladder, lift and cables
TimberTower GmbH [42]

Figure K-5: Other components of the TimberTower design

K-4   Materials used

K-4-1   Timber

Around 400 m^3 of Cross Laminated Timber has been used in realizing the TimberTower, with a combined weight of 192 tonnes. CLT has a high strength-to-weight ratio and a high fire resistance. Its damping and fatigue behaviour are also more beneficial than that of steel [42]. Suppliers and partners are based in Germany, Austria and Switzerland and provided the PEFC-certified timber products for the project [90].

A total of 8 layers of spruce are used to form the 300 mm thick cross sections, shown in Figure K-6. Both of the outer layers and the centre layer are 80 mm thick, their grains running vertical. In-between are two layers of 30 mm with grains parallel to the ground. Besides spruce, the use of hardwood was considered. It would allow for a smaller amount of timber to be used in the design, since hardwood is more stable, but the costs would have been higher. Other than that, it would increase difficulties in obtaining certificates for the connections from the building authorities [22].

K-4-2   Adhesive

The adhesive used in the panels is a one-component polyurethane adhesive called Purbond HB-S, made by Hause Purbond in Switzerland. The moisture content in CLT usually lies between 8 and 15%. The advantages of this specific adhesive are [90]:

– No mixing necessary, short curing times;

– No solvents and formaldehyde present in the adhesive;

– Homogeneity is assured because the adhesive is not absorbed deep into the wood;

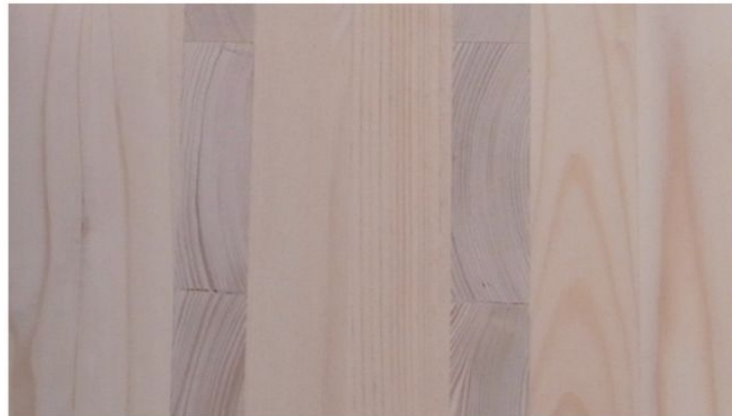– Accepted in standards (DIN 1052) as a type 1 adhesive.

Figure K-6: Cross section of the CLT panels
Source: TimberTower GmbH [42]

The same type of adhesive is used in the connection between the individual panels, albeit in a two-component form. This Purbond CR 421 is especially suited for bonding wood and steel, such as anchoring threaded bars and perforated plates in timber, exactly what it is used for in the Timber Tower [90], see also the next section. A total of 1.6 tonnes of adhesive is estimated to have been used [20].

K-4-3   Steel

Around 2000 steel plates are used in the horizontal junctures between panels, weighing 2.8 tonnes combined. The perforated plates are 2.5 mm thick and made of steel grade S235 [22]. Their function will be explained in the next section.

K-4-4   Coating

A standard PVC roof lining is used to protect the timber from the elements. It is glued to the outside of the tower, sealing off the inside and allowing for humidity control within the tower. The environmental aspects of the lining are not great and form a point that requires improvement [21].

K-5   Connections used

K-5-1   Panel connections

The connections between the individual panels were one of the biggest structural challenges [19]. The bottom and top edge of the panels are slit every 4 cm to allow a perforated steel plate to be placed inside, see Figure K-7. These plates are square, 300 mm, with a thickness of 2.5 mm. In the plate a large number of holes with a diameter of 10 mm are present. This causes the load transfer to take place through adhesion and cohesion, as well as dowel type action of the glue through the holes [22].

(a)

(b)

Figure K-7: Horizontal connections are made by steel plates inserted into slots in the bottom
and top edge of the panels
Source: TimberTower GmbH[24] [42]

Performance

Compared to other options, this connections is extremely stiff and stable. Slip, which might occur with bolted or dowelled connections, is reduced to a minimum by using adhesion [19].

Fatigue tests using a hydro-pulse machine were conducted at MPA Wiesbaden to determine the fatigue properties. Based on these results, components were chosen in such a way that failure would occur in the steel plates instead of the glue or timber. This had advantages in dimensioning the components, since the material fluctuations in steel are lower than in timber [23] and the ductility of steel is then used to be able to indicate possible failure in an early stage [19].

K-5-2   Base and top

Anchor rods were cast into the concrete base to be able to make the connection to the tower. A 85 mm thick footplate is connected to the bottom panels in the same way as the panels with each other. This footplate is carried out with holes for the anchor rods to be fastened to the footplate. A total of 196 rods were used to make this connection. The anchor rod cage pretensions the concrete walls.

At the top the same connection is made to the steel adapter. 176 steel plates welded to the adapter are glued into the top edges of the timber panels, see Figure K-9. At the other side of the adapter the nacelle is connected with pretensioned bolts [24].

K-6   Erection

First a test tower was built, comprised of the top 22 meters of the design. Designers wanted to use the experience gained from this test in optimizing the erection of the 100 m tower, the true prototype. The general erection process was as follows, based on [19, 24] and is also shown partly in Figures K-10a to K-10j:

(a)   **(b)**   **(c)**

Figure K-8: The connection between base and tower is made by gluing a footplate into the
wood (b) and connecting this with anchor bolts (c)
Source: (a)TimberTower GmbH [42], (b) Handwerk, http://handwerk.com/
timbertower-mit-holz-hart-am-wind/150/1466/38181/3, accessed December 2013, (c) Plackner [20]

Figure K-9: The connection between tower and adapter is also made with perforated steel
plates
Source: TimberTower GmbH [42]

1. Prefabrication of the CLT panels, including the outer coating.

2. Fabrication of the components for the scaffolding structure.

3. Transportation of all components to site.

4. The creation of a part of the inner scaffolding structure.
   15 m poles, 8 podium halves and some other members, all made of regular sawn structural timber, were combined on site to form 15 m high segments of the scaffolding structure. The podia, present every 3.75 m, ease erection, inspection and maintenance.

5. Mounting of the panels on this structure.
   As soon as one of the scaffolding sections was in place, CLT panels were attached in their spiral-like fasion. They were then connected to the panels already in place, using the previously mentioned connection.

6. Steps 4 and 5 were repeated until all 6 segments of the scaffolding structure and the 54 CLT panels were in place.

7. Installation of the transfer structure and turbine.

8. Use of a lift system to glue the joints of the outer coating from the outside, and also the use of special equipment to check for leakage.

The scaffolding structure houses the lift, ladder with fall protection and electronics, but has no structural function anymore when the connections between the panels have been made. For easy connection at height, boxes with the required (temporary) screws and other parts were attached to the parts before hoisting.

## K-6-1   Execution of the connections

Horizontal edges

When the panels have been placed, the steel plates are inserted into the slots in the timber and the seam is covered with a veneer panel. At each slot two drilled holes are present. One at the bottom for inserting the two-component adhesive, the second for extracting excessive glue, ensuring the entire slot is filled with glue and an airless bond is made. The holes are sealed with a non-structural dowel [20].

The connections were made from the inside, using the podia in the scaffolding structure, so the conditions in which they were made could be controlled. The connections could only be made by certified specialists and are only approved for use is service class 1 or 2 (wood is under cover, but may experience occasional wetting due to humidity) [23]. Curing of the glue took 24 hours, after which the next segment was added [90].

Vertical edges

The connections between the vertical edges of the panels are made without the addition of steel elements. At the outside, the dimensional precision makes sure the seam is very tight.
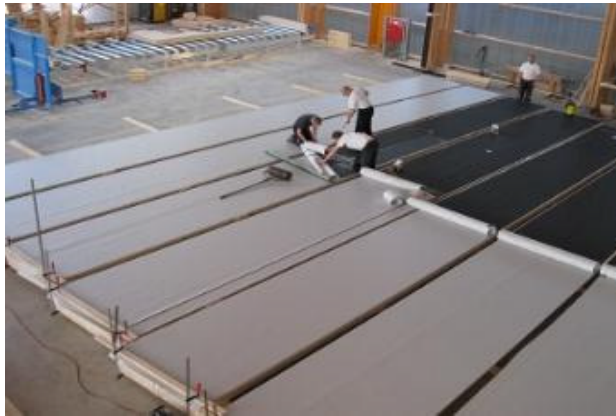
(a) Applying the coating in the shop

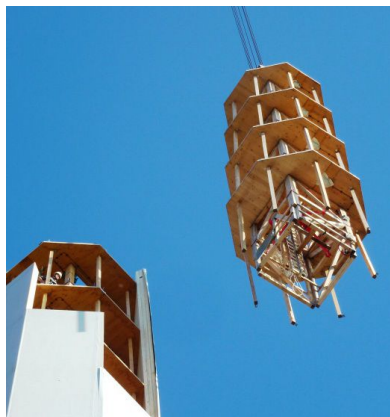

(b) Prefabricated CLT Panels

(c) Assembling a scaffolding section on site

(d) Premounting the ladder in a scaffolding section

(e) Hoisting a scaffolding section into place

(f) Panels are mounted on the scaffolding

(g) Workers align the next 15 m tall section of the scaffolding

(h) The panels are held into place by the scaffolding until the panel connections have been made

(i) Hoisting the steel adapter to the top

(j) Installing the steel adapter

Figure K-10: The erection of the first TimberTower
Source: All images courtesy of TimberTower GmbH [24] [42], except
(d) Energiezukunft, http://www.energiezukunft.eu/wind/forschung/weltweit
-erste-holz-windkraftanlage-gn10400
(f) Lignum, http://www.lignum.ch/fileadmin/_migrated/RTE/RTEmagicC_Timbertower_bild.jpg.jpg
(g) Autodesk, http://images.autodesk.com/adsk/images/timbertower_1_inline_617×300.jpg
All accessed in December 2013

On the inside, the tapering of the timber leaves the panels about 2 mm apart. As soon as the panels are in place, a strip is inserted, with holes drilled into it. They are filled with adhesive from the bottom up and again sealed with a dowel [20].

K-6-2 In practice

The goal and expectation of the designers is a to be able to erect a similar tower within 10 days, especially now that they have gained experience. In reality, the entire construction period was 4 months. The special crane used could not work under high wind conditions, resulting in many interruptions of the construction [23].

Now that the tower is completed, continuous monitoring and measuring is taking place. One of the main points of research is the vibrational behaviour of the tower, to see if it matches the calculations [21]. Strain gauges have been placed at multiple locations in the structure, to measure deformations. Other sensors monitor the moisture content in the timber, keeping it around 13%. Higher moisture contents would reduce the stiffness unacceptably [22].

K-7 Discussion

The realization of a prototype with a height of 100 m has proven that turbine towers can be made of timber. Two main aspects of the current design could perhaps be improved in further designs:

Coating
 The PVC coating used slightly undermines the environmental benefits of the timber.

Connections
 The connections use a lot of adhesive and are quite laborious.

Wind and other environmental conditions

This appendix mainly explains how wind occurs and how it is modelled according to design standards. How these wind conditions are translated into loads on turbines can be found in Appendix M.

The IEC-61400 [2] divides the environmental conditions that have to be considered in the design of a wind turbine into wind conditions and other environmental conditions. Both are subdivided into normal and extreme conditions, where the normal conditions concern common loading conditions and the extreme external conditions refer to rare design conditions. Design load cases shall consist of potentially critical combinations of these external conditions with wind turbine operational modes and other design situations.

L-1 General characteristics of wind

Understanding wind is essential for the design of wind turbines. Structurally, it is the main source of loading and needs to be modelled correctly to prevent structural failure. Economically, it is the reason the turbines produces electricity and thus revenue. Since the potential energy varies with the cube of the wind speed, it has to be understood firmly to be able to choose optimal locations for turbines.

L-1-1 Variability

Variability is perhaps the most important characteristic of wind behaviour for turbine design because it causes turbulence, as well as fluctuations in power production. Large-scale spatial variations occur because of differences in climate, where local topography plays a role on a smaller scale. Examples are the occurrence of hills, mountains and other obstacles, the presence of open water, differences in the type of vegetation and other factors described in

Burton [29]. Wind speeds are higher at larger heights above the ground and the influence of surface conditions becomes smaller at these heights.

Variations with time occur on several time-scales, described below and found in [29].

- – Yearly, or even on a scale of decades, wind speeds can change due to large-scale climatic changes. These are hard to predict and not well understood yet.

- – Seasonal variations are better understood, but other smaller variations within these still make prediction difficult.

- – Synoptic variations, as these smaller variations are called, have a time-scale of several days, associated with smaller weather systems.

- – Diurnal variations occur because of the difference in temperature between day and night. These are reasonably predictable.

- – Variations on time-scales of minutes and seconds are known as turbulence. Power output, fatigue loading and extreme loads are all influenced by turbulence.

The variation in the hourly mean wind speed over a year is well represented by a Weibull distribution. The fraction of time in which the hourly mean wind speed exceeds V is then given by:

$$F(V) = \exp(-(V/c)^k) \tag{L-1}$$

Where:
V is the wind speed;
k is a shape factor;
c is a scale parameters, given below.

When the shape factor k is set to 2, a Rayleigh distribution is obtained, which is common for many sites. The scale parameter c is then obtained by:

$$c = \frac{V_{ann}}{\sqrt{\pi}/2} \tag{L-2}$$

Where:
V_{ann} is the annual mean wind speed.

L-1-2   Turbulence

Turbulence is defined as the (random) variation of the wind speed on a small time-scale, typically 10 minutes or less, with a zero mean. Turbulence is caused by local temperature differences and friction with the surface and occurs in all directions, not just in the direction of the general wind speed, as in Figure 6-1. It is useful to think of the wind as Burton [29] does: wind consisting of a mean wind speed determined by the seasonal, synoptic and diurnal effects described earlier, which thus varies on a time-scale of one to several hours, with turbulent fluctuations superimposed. Because of its stochastic nature, turbulence is described in terms of statistical properties.

The overall turbulence is quantified by two parameters, the standard deviation of the variations σ_v and the turbulence intensity I_v. The latter is defined as the ratio between the standard deviation of the turbulence and the mean wind velocity [13]:

$$I_v = \frac{\sigma_v}{V_m} \tag{L-3}$$

Where:

V_m is the mean wind speed;
σ_v is the standard deviation of the variations;
I_v is the turbulence intensity.

Most of the variations can be described using a normal (Gaussian) distribution, for instance for fatigue calculations. The high-end tail of the distribution, however, is not very reliable, causing other methods to be required for determining extreme gusts. The way turbulence and gusts are modelled, will be discussed in section L-2-7.

L-2   Wind conditions in the standards

Wind loading on turbines is to be modelled according to the current international IEC 61400-1 standards [2]. Within this thesis, it is expanded with additional information from NEN-EN 1991 1-4 [13] regarding Dutch wind conditions and wind speeds. Other information is taken from the Wind Energy Handbook by Burton [29], which explains the background of the codes in further detail.

L-2-1   Wind turbine classes

The IEC defines several wind turbine classes with different wind speeds and turbulence parameters at hub height, instead of using parameters to describe a certain location. These classes are chosen in a way that will cover most applications, with a life span of 20 years.

The standard wind turbine classes I, II and III use the values in Table L-1. They are subdivided according to turbulence intensity (A, B, C). There is a fourth class for when special wind (or other environmental) conditions require design values to be chosen by designer and thoroughly specified. This S-class is mainly used for offshore wind turbines and tropical storm conditions, among others. When assessing a possible turbine site, the IEC specifies two ways of assuring structural integrity:

- Demonstrating that the conditions on site are less severe than those assumed for design.

- Although possibly designed for less severe conditions, still demonstrating that the structure is able to withstand the specific conditions on site.

The first one allows for a single design to be implemented at several different locations, while the latter allows for a more optimal design. Usually, the first approach is taken and the second one only when the conditions of the first approach are not satisfied [5]. With the first approach, the following conditions should be met:

Wind turbine class		I	II	III
V_{ref}	(m/s)	50	42.5	37.5
A	$I_{ref}(-)$		0.16	
B	$I_{ref}(-)$		0.14	
C	$I_{ref}(-)$		0.12	

Table L-1: Standard wind turbine classes according to the IEC 61400-1

Where:

V_{ref} is the reference wind speed average over 10 mins;

I_{ref} is the expected value of the turbulence intensity at 15 m/s (mean value);

A   is the category for higher turbulence characteristics;

B   is the category for medium turbulence characteristics;

C   is the category for lower turbulence characteristics.

– The site estimate of the extreme 10-minute average wind speed at hub height with a recurrence period of 50 years is less than V_{ref}. For V_{ref}, see table L-1. In short:

$$V_{m,50} < V_{ref}$$

– The extreme 3-second average wind speed at hub height on site with a 50 year recurrence period on site is smaller than V_{e50} (V_{e50} will be defined later). In short:

$$V_{50yrs,3secs} < V_{e,50}$$

– The site value of the probability density function of V_{hub} shall be less than the design probability density function at all values of V_{hub} between $0.2V_{ref}$ and $0.4V_{ref}$. In short:

$$p(V_{hub}) \text{ on site} < p(V_{hub}) \text{ in design}$$

for $0.2V_{ref} < V_{hub} < 0.4V_{ref}$

– The turbulence standard deviation in the design (σ_1) shall not be smaller than the estimated 90% quantile of the site turbulence standard deviation for all wind speeds at hub height between $0.2V_{ref}$ and $0.4V_{ref}$, that is:

$$\sigma_1 \geq \hat{\sigma} + 1.28\hat{\sigma}_\sigma$$

for $0.2V_{ref} < V_{hub} < 0.4V_{ref}$, with $\hat{\sigma}$ being the estimated turbulence standard variation.

L-2-2 Basic values for wind speeds

For the specific wind speeds in the Netherlands, standard NEN-EN 1991 1-4 [13] is used. In the National Annex the country is divided into wind areas I, II and III, as can be seen in Figure L-1.

The basic wind velocity is given by

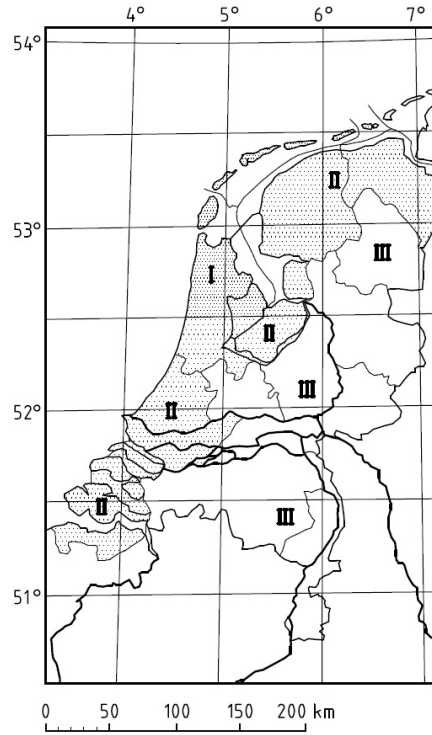$$V_b = c_{dir}c_{season}V_{b,0} \tag{L-4}$$

Figure L-1: The three different wind areas in the Netherlands
Source: NEN-EN 1991 1-4 [13]

Where:

$V_{b,0}$ is the fundamental value of the basic wind velocity
$$\begin{cases} 29.5\,m/s & \text{for area I} \\ 27.0\,m/s & \text{for area II} \\ 24.5\,m/s & \text{for area III} \end{cases}$$

c_{dir} is a directional factor; 1.0 in the Netherlands;

c_{season} is a seasonal factor; 1.0 in the Netherlands.

The 10-minute mean velocity with a probability for exceedence p is obtained by multiplying V_b with a factor c_{prob}:

$$c_{prob} = \left(\frac{1 - K\ln(-\ln(1-p))}{1 - K\ln(-\ln(0.98))} \right)^n \tag{L-5}$$

Where:

K is a shape parameter
$$\begin{cases} 0.2 & \text{for area I} \\ 0.234 & \text{for area II} \\ 0.281 & \text{for area III} \end{cases}$$

n is an exponent, set at 0.5;

p is the probability of exceedence, e.g. $p = 0.02$ represents 50 years.

L-2-3   Mean wind

The mean wind velocity with height is given by:

$$V_m(z) = c_r(z)c_o(z)V_b \tag{L-6}$$

Terrain category		$z_0\,(m)$	$z_{min}\,(m)$
0	Sea or coastal area	0.005	1
II	Area without buildings	0.2	4
III	Area with buildings	0.5	7

Table L-2: Terrain categories and parameters, taken from NEN-EN 1991-1-4 [13]

Where:

$c_r(z)$ is the roughness factor, as found below;
$c_o(z)$ is the orography factor, taken as 1.0.

The roughness factor $c_r(z)$ takes into account the variability of the mean wind velocity due to height above the ground and ground roughness upwind from the turbine. In the Eurocodes it is described as a logarithmic profile:

$$c_r(z) = \begin{cases} k_r \ln(z/z_0) & \text{for } z_{min} \leq z \leq z_{max} \\ c_r(z_{min}) & \text{for } z < z_{min} \end{cases} \tag{L-7}$$

Where:

z_0 is the roughness length, given in Table L-2;
k_r is a terrain factor, given below;
z_{max} is set at 200 m;
z_{min} is given in Table L-2.

$$k_r = 0.19 \left(\frac{z_0}{0.05} \right)^{0.07} \tag{L-8}$$

L-2-4   Turbulence

As stated before, turbulence can be seen as random variations of the wind speeds from its 10-minute average, the variations having a zero mean. It is quantified by two parameters, standard deviation σ_v and the turbulence intensity I_v. The latter is defined as the ratio between the standard deviation of the turbulence and the mean wind velocity. According to the Eurocode [13]:

$$I_v(z) = \begin{cases} \frac{\sigma_v}{V_m(z)} = \frac{k_l}{c_o(z) ln(z/z_0)} & \text{for } z_{min} \leq z \leq z_{max} \\ I_v(z_{min}) & \text{for } z \leq z_{min} \end{cases} \tag{L-9}$$

With:

$$\sigma_v = k_r V_b k_l \tag{L-10}$$

	Velocity component index (k)		
	1	2	3
Standard deviation σ_k	σ_1	$0.8\sigma_1$	$0.5\sigma_1$
Integral scale L_k	$8.1\Lambda_1$	$2.7\Lambda_1$	$0.66\Lambda_1$

Table L-3: Turbulence scale parameters according to the IEC 61400-1 for the Kaimal model

Where:

k_l is the turbulence factor, taken as 1.0.

Turbulence does not only occur in the direction of the mean wind. It consists of three orthogonal vector components: longitudinal (in the direction of the mean wind velocity), lateral (horizontal, normal to the longitudinal) and upward (normal to both others) in most turbulence models [2].

Several models have been developed to describe turbulence, including von Karman, Kaimal and Mann. The last two are described in the IEC 61400-1 in further detail. The Kaimal model is often used, because it is better suited to empirical observations of turbulence [13]. The power spectral density function for velocity component k is given by:

$$\frac{fS_k(f)}{\sigma_k^2} = \frac{4fL_k/V_{hub}}{(1 + 6fL_k/V_{hub})^{5/3}}$$ (L-11)

Where:

f is the frequency in Hz;
k is the component (1 for longitudinal, 2 for lateral and 3 for upward);
V_{hub} is the wind speed at hub height;
S_k is the single-sided velocity component spectrum;
σ_k is the velocity component standard deviation, found in Table L-3;
L is the integral scale parameter, found in Table L-3;
Λ_1 is the longitudinal turbulence scale parameter:

$$\Lambda_1 = \begin{cases} 0.7z & \text{for } z \leq 60 \text{ m} \\ 42 & \text{for } z \geq 60 \text{ m} \end{cases}$$ (L-12)

The following holds:

$$\sigma_k^2 = \int_0^\infty S_k(f)\,df$$ (L-13)

The Eurocode describes the turbulence in a similar manner, but uses some different parameters. Here

$$L(z) = \begin{cases} L_t\left(\frac{z}{z_t}\right)^\alpha & \text{for} z \geq z_{min} \\ L(z_{min}) & \text{for} z < z_{min} \end{cases}$$ (L-14)

Where:

z_t	is the reference height, 200 m;
L_t	is the reference length scale, 300 m;
α	is $0.67 + 0.05 \ln(z_0)$.

The wind distribution over frequencies is then determined by:

$$S_L(z, n) = \frac{n S_k(f)}{\sigma_v^2} = \frac{6.8 f_L(z, n)}{(1 + 10.2 f_L(z, n))^{5/3}} \tag{L-15}$$

With:

$$f_L(z, n) = \frac{n L(z)}{V_m(z)} \tag{L-16}$$

Where:

n is the natural frequency of the structure.

The main difference between the spectra derived from the two codes is that there is more energy in the lower frequency range of the Eurocode spectrum. This standard is more suited for buildings, rather than for turbines [29]. A similar spectrum is used in the load calculations in section 6-4-2.

L-2-5 Gusts

Sometimes it is useful to know the maximum gust speed that is to be expected. This is often represented by a factor G, which is the ratio of the gust speed to the mean wind speed. Empirically the t-second gust factor is determined by:

$$G(t) = 1 + 0.42 I_v \ln(3600/t) \tag{L-17}$$

L-2-6 Peak velocity pressures

According to the Eurocodes the base velocity pressure q_b can be determined using:

$$q_b = \frac{1}{2} \rho V_b^2 \tag{L-18}$$

And the peak velocity pressure by:

$$q_p(z) = [1 + 7 I_v(z)] \frac{1}{2} \rho V_m^2(z) = c_e(z) q_b \tag{L-19}$$

Where:

ρ	is the air density, $1.25 kg/m^3$;
$c_e(z)$	is the exposure factor:

$$c_e(z) = \frac{q_p(z)}{q_b} \tag{L-20}$$

This includes mean and short-term velocity fluctuations, but is mostly used for the design of buildings and not used here for turbines. For heights up to 200 m table NB5 from the National Annex can be used to determine peak wind pressure.

L-2-7   Wind models

As stated before, the wind conditions are subdivided into normal and extreme conditions. The normal conditions act frequently on the structure during its lifetime. Extreme conditions are rare, values used are defined as having a 1-year or 50-year recurrence period [2]. Extreme wind conditions can no longer be represented by standard stationary wind conditions, but require additional modelling [5].

Wind conditions are modelled by a constant mean flow , which in many cases is combined with either a varying gust profile or with a fluctuating turbulence component. The IEC-61400 standard defines a number of models which represent the conditions a wind turbine experiences during its lifetime. Combination of these models with the correct parameters and safety factors will result in the design load cases for the turbine. These will be discussed in Appendix M, showing the application of the models within different design situations.

Normal wind conditions

Here models are given for the normal wind distribution, both for mean wind speed and turbulence. These are taken directly from the IEC 61400-1, with some additional information from Burton [29].

The wind speed distribution
This determines the frequency of occurrence of individual load conditions for the normal design situations. It is common to describe the wind speed using a Weibull or Rayleigh distribution. According to the IEC, the 10-minute mean wind speed follows a Rayleigh distribution:

$$P_R(V_{hub}) = 1 - \exp\left[-\pi \left(\frac{V_{hub}}{2V_{ave}}\right)^2\right] \tag{L-21}$$

With:

$$V_{ave} = 0.2V_{ref} \tag{L-22}$$

The normal wind profile (NWP)
This denotes the average wind speed as a function of height z above the ground. For the standard classes in the IEC 61400-1 a power law is used:

$$V(z) = V(z_{hub}) \left(\frac{z}{z_{hub}}\right)^\alpha \tag{L-23}$$

Where α is to be taken as 0.2. This differs from the one used in the NEN-EN 1991 1-4, where a logarithmic profile is used.
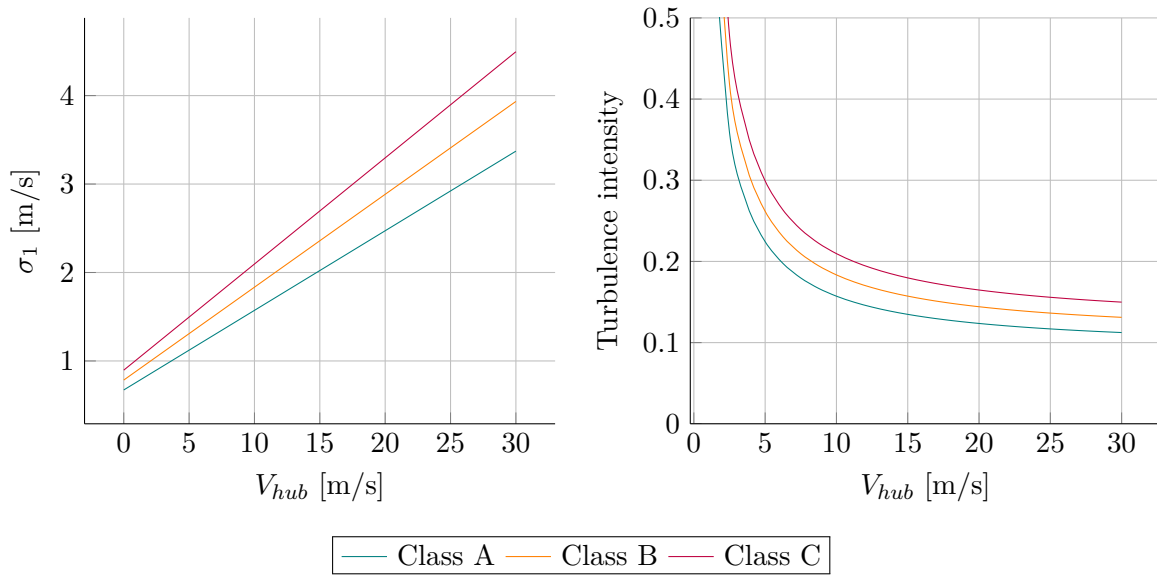
Figure L-2: Turbulence standard deviation and intensity for the normal turbine classes, based on Figure 1 of IEC 61400 [2]

The normal turbulence model (NTM)

Here a representative value of the turbulence standard variation, σ_1, is given by the 90% quantile for the given hub height wind speed:

$$\sigma_1 = I_{ref}(0.75V_{hub} + b) \tag{L-24}$$

with $b = 5.6$ m/s. The turbulence intensity is defined by:

$$I_v = \frac{\sigma_1}{V_{hub}} \tag{L-25}$$

Both formulas are displayed in Figure L-2.

Extreme wind conditions

These include wind shear events, peak wind speeds during storms and rapid changes in wind speed and direction. The models used are all part of the IEC 61400 [2].

The extreme wind speed model (EWM)

This model is to be used either as a steady or turbulent wind speed model. The steady model calculates the extreme wind speeds with a recurrence period of 50 and 1 years, respectively, with the following equations:

$$V_{e50}(z) = 1.4V_{ref}\left(\frac{z}{z_{hub}}\right)^{0.11} \tag{L-26}$$

$$V_{e1}(z) = 0.8V_{e50}(z) \tag{L-27}$$

Allowance for short-term deviations from the mean wind direction shall be made by assuming constant yaw misalignment in the range of $\pm15°$

The turbulent extreme wind model determines the 10-minute average wind speeds by:

$$V_{50}(z) = V_{ref} \left(\frac{z}{z_{hub}} \right)^{0.11} \tag{L-28}$$

$$V_1(z) = 0.8 V_{50}(z) \tag{L-29}$$

The longitudinal turbulence standard deviation is given by:

$$\sigma_1 = 0.11 V_{hub} \tag{L-30}$$

The extreme operating gust model (EOG)

This model calculates the gust magnitude at hub height by:

$$V_{gust} = \min \left\{ 1.35(V_{e1} - V_{hub}); 3.3 \left(\frac{\sigma_1}{1 + 0.1 \left(\frac{D}{\Lambda} \right)} \right) \right\} \tag{L-31}$$

Where:

Λ_1 is the turbulence scale parameter equal to $\begin{cases} 0.7z, & z \leq 60 \text{ m} \\ 42, & z \geq 60 \text{ m} \end{cases}$

D is the rotor diameter

This has been calibrated to have a recurrence period of 50 years.

The wind speed over time and height is then given by:

$$V(z,t) = \begin{cases} V(z) - 0.37 V_{gust} \sin \left(\frac{3\pi t}{T} \right) \left(1 - \cos \left(\frac{2\pi t}{T} \right) \right) & \text{for } 0 \leq t \leq T \\ V(z) & \text{otherwise} \end{cases} \tag{L-32}$$

with $V(z)$ given in Equation L-2-7 and $T = 10.5$ s. An example can be found in Figure L-3.

The extreme turbulence model (ETM)

This model uses the normal wind profile combined with turbulence defined by the following standard deviation:

$$\sigma_1 = cI_{ref} \left(0.072 \left(\frac{V_{ave}}{c} + 3 \right) \left(\frac{V_{hub}}{c} - 4 \right) + 10 \right) \tag{L-33}$$

With $c = 2$ m/s.

The extreme direction change model (EDC)

Here the magnitude of the direction change is denoted by θ_e and is limited to $\pm 180°$. It is given by:

$$\theta_e = \pm 4 \arctan \left(\frac{\sigma_1}{V_{hub} \left(1 + 0.1 \left(\frac{D}{\Lambda_1} \right) \right)} \right) \tag{L-34}$$
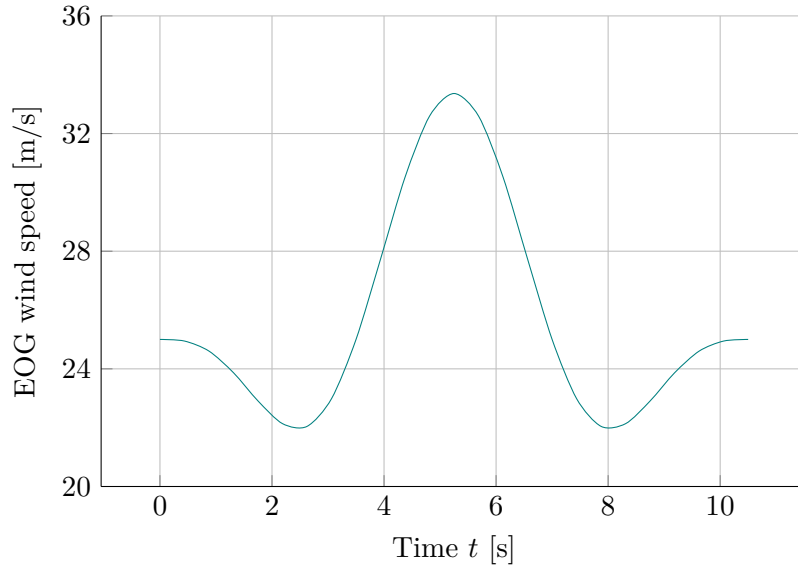
Figure L-3: Extreme operating gust for Class IA with $V_{hub} = 25$ m/s and $D = 42$ m, based on Figure 2 of IEC 61400 [2]

The NWP is used to determine the wind speeds during the direction change. The above magnitude θ_e is used in the transient function for the extreme direction change:

$$\theta(t) = \begin{cases} 0° & \text{for } t < 0 \\ \pm 0.5\theta_e(1 - \cos(\pi t/T)) & \text{for } 0 \leq t \leq T \\ \theta_e & \text{for } t > T \end{cases} \tag{L-35}$$

Where $T = 6$ s is the duration of the EDC. Signs in the formulas are to be chosen in such a way that the worst loading will occur. An example is given in Figure L-4.

The extreme coherent gust with direction change model (ECD)

This gust has a magnitude of $V_{cg} = 15$ m/s and is assumed to occur simultaneously with a certain direction change. The rise up of the wind speed is given by:

$$V(z,t) = \begin{cases} V(z) & \text{for } t \leq 0 \\ V(z) + 0.5V_{cg}(1 - \cos(\pi t/T)) & \text{for} \\ V(z) + V_{cg} & \text{for } t \geq T \end{cases} \tag{L-36}$$

The rise time T is set at 10 s and for $V(z)$ the NWP is used. This gust is modelled to occur at the same time with a direction change θ from $0°$ up to θ_{cg}. The latter is given by:

$$\theta_{cg}(V_{hub}) = \begin{cases} 180° & \text{for } V_{hub} < 4 \text{ m/s} \\ \frac{720° \, m/s}{V_{hub}} & \text{for } 4 \text{ m/s} < V_{hub} < V_{ref} \end{cases} \tag{L-37}$$

Which is then used to determine the transient function for the direction change that
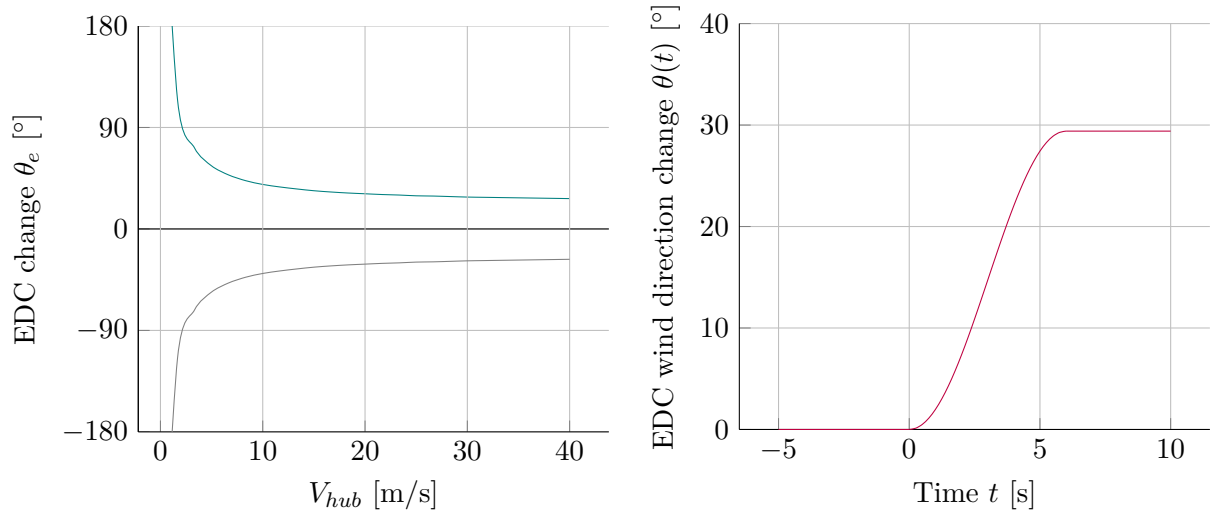
Figure L-4: Extreme direction change magnitude and transient function for class A, $V_{hub} = 25$ m/s, $D = 42$ m and $z_{hub} = 30$ m, based on Figures 3 and 4 of IEC 61400 [2]

will occur simultaneously with the gust:

$$\theta(t) = \begin{cases} 0° & \text{for } t < 0 \\ \pm 0.5\theta_{cg}(1 - \cos(\pi t/T)) & \text{for } 0 \leq t \leq T \\ \theta_{cg} & \text{for } t > T \end{cases} \tag{L-38}$$

The rise time T is again 10 s. An example can be found in Figure L-5.

The extreme wind shear model (EWS)

These conditions are modelled by two wind speed transients which will not occur at the same time. For transient vertical shear:

$$V(z,t) = \begin{cases} V_{hub}\left(\frac{z}{z_{hub}}\right)^\alpha \pm \left(\frac{z-z_{hub}}{D}\right)\left(2.5 + 0.2\beta\sigma_1\left(\frac{D}{\Lambda_1}\right)^{1/4}\right)(1 - cos(2\pi t/T)) \\ \qquad\qquad\qquad \text{for } 0 \leq t \leq T \\ V_{hub}\left(\frac{z}{z_{hub}}\right)^\alpha \\ \qquad\qquad\qquad \text{otherwise} \end{cases} \tag{L-39}$$

For transient horizontal shear:

$$V(y,z,t) = \begin{cases} V_{hub}\left(\frac{z}{z_{hub}}\right)^\alpha \pm \left(\frac{y}{D}\right)\left(2.5 + 0.2\beta\sigma_1\left(\frac{D}{\Lambda_1}\right)^{1/4}\right)(1 - cos(2\pi t/T)) \\ \qquad\qquad\qquad \text{for } 0 \leq t \leq T \\ V_{hub}\left(\frac{z}{z_{hub}}\right)^\alpha \\ \qquad\qquad\qquad \text{otherwise} \end{cases} \tag{L-40}$$
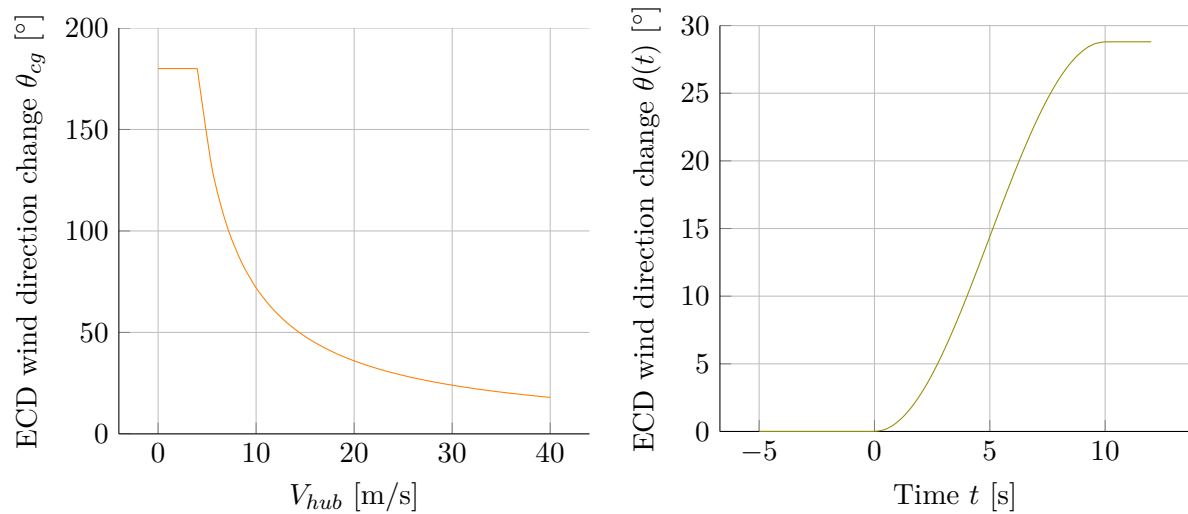
Figure L-5: Direction change magnitude and transient function of ECD conditions for class A, $V_{hub} = 25$ m/s, $D = 42$ m and $z_{hub} = 30$ m, based on Figures 6 and 7 of IEC 61400 [2]

L-2-8   Other influences on load magnitude

It should be mentioned that there are other factors that can influence the magnitude of wind loads, other than the shape of the element the wind is working on. Examples, relevant to turbine design, are:

- Tower shadow - disturbances of the wind flow due to the tower. This will mostly have effect on the blades of downwind turbines.

- Wake effects - the vicinity of other turbines, such as in a wind farm, will disrupt the regular wind flow.

Both in which $\alpha = 0.2$, $\beta = 0.6$ and $T = 12\,s$. As with the EDC, signs in the formulas should be chosen in a way that they will represent the worst loading.

For all these wind models to be used, manual calculation will no longer suffice. There are many software packages available today that are able to calculate the models and appropriate load cases for a given turbine.

L-3   Wind loading directly on the tower

Although most of the loading on the tower will come from the rotors spinning and catching wind, some of it will also occur because of the wind hitting the tower directly. NEN-EN 1991-1-4 describes methods to use the wind speed or peak velocity pressure to calculate the resulting loads on structures.

L-3-1   Wind pressure on surfaces

Wind pressures on surfaces are calculated by multiplying the peak velocity pressure (see previous chapter) by certain coefficients. The pressure on external surfaces is given by [2]:

$$w_e = q_p(z_e)c_{pe} \tag{L-41}$$

Where:
$q_p(z_e)$ is the peak velocity pressure at z_e;
z_e is the reference height for the external pressure;
c_{pe} is the pressure coefficient for external pressure.

The same method is used for pressure on internal surfaces:

$$w_i = q_p(z_i)c_{pi} \tag{L-42}$$

Where:
$q_p(z_i)$ is the peak velocity pressure at z_i;
z_i is the reference height for the internal pressure;
c_{pi} is the pressure coefficient for internal pressure.

L-3-2   Wind forces on structures

NEN-EN 1994-1-4 [13] describes two ways of calculating resulting forces on structures from direct wind loading. It must be noted that this is mostly focused on buildings, and less on towers and masts. The following section is needed, however, to understand the structural factor $c_s c_d$ used in this research.

Method 1

     The first method is the one used in this research, where the total wind force on the structure F_w is calculated using the following formula :

$$F_w = c_s c_d \sum_{\text{elements}} c_f q_p(z_e) A_{ref} \tag{L-43}$$

     Where:
$c_s c_d$ is the structural factor;
c_f force coefficient for the structure;
$q_p(z_e)$ is the peak velocity pressure at reference height z_e;
A_{ref} is the reference area of the structure.

     These parameters will be explained and defined later on.

Method 2

     The second method uses the wind pressures as described before to determine forces for external and internal pressure, and for friction. The resulting force on the structure is the appropriate summation of these forces. Although it is not used within this research, it is provided for completeness.

For external pressure:

$$F_{w,e} = c_s c_d \sum_{\text{surfaces}} w_e A_{ref} \tag{L-44}$$

Internal pressure:

$$F_{w,i} = \sum_{textsurfaces} w_i A_{ref} \tag{L-45}$$

Friction on surfaces parallel to the wind direction:

$$F_{fr} = c_{fr} q_p(z_e) A_{fr} \tag{L-46}$$

Where:

w_e is the external pressure on the surface at height z_e;
w_i is the internal pressure on the surface at height z_i;
A_{ref} is the reference area of the individual surface;
c_{fr} is the friction coefficient;
A_{fr} is the area of external surface parallel to the wind.

The pressures are given by:

$$w_e = q_p(z_e) c_{pe} \tag{L-47}$$

$$w_i = q_p(z_i) c_{pi} \tag{L-48}$$

Where:

c_{pe} is the external pressure coefficient, see the next section;
c_{pi} is the internal pressure coefficient, see the next section.

Friction may be ignored if the total friction area is smaller or equal to 4 times the total area perpendicular to the wind direction. In the Netherlands a lack of correlation between windward and leeward side for large buildings is taken into account by multiplying the forces with a factor 0.85. This is not the case for turbine towers, chimneys and masts.

Pressure and force coefficients and structural factor

The previous section contained some coefficients that will be defined here. NEN-EN 1994-1-4 is filled with expressions for the coefficients, to cover many situations. For turbine tower design, however, only a few situations are relevant.

Pressure coefficients

Pressure coefficients are to be used for buildings, circular cylinders and free-standing walls. They are different for circular cross sections than for flat surfaces. For circular cross sections the Reynolds number plays a large role. It is given by:

$$Re = \frac{b v(z_e)}{\nu} \tag{L-49}$$

Where:

b	is the diameter;
ν	is the kinematic viscosity of air, $15 \cdot 10^6$ m^2/s;
$v(z_e)$	is the peak wind velocity at height z_e.

It influences the pressure coefficient by determining the values of the two parameters on the right-hand side of the following expression:

$$c_{pe} = c_{p,0}\psi_{\lambda\alpha} \tag{L-50}$$

Where:

$c_{p,0}$	is the external pressure coefficient without free end flow conditions;
$\psi_{\lambda\alpha}$	is the end effect factor.

Both parameters can be determined using section 7.9.1 from NEN-EN 1991-1-4 [13], but this is to extensive to be included here.

Force coefficients

Force coefficients are to be used in the calculation of structural elements with various cross sections, but also for lattice structures, circular cylinders and spheres [2]. For both polygonal and circular shapes the force coefficient is given by:

$$c_f = c_{f,0}\psi_\lambda \tag{L-51}$$

Where:

ψ_λ	is the end-effect factor;
$c_{f,0}$	is the force coefficient of structural elements without free-end flow.

ψ_λ differs for many different situations and also depend on the Reynold's number. Most values can be found in section 7.13 of NEN-EN 1991-1-4, but this is too extensive to be covered here. The same holds for $c_{f,0}$, where reference is made to table 7.11 from NEN-EN 1994-1-4 [13]. Where relevant, required values and formulas have been included in the main part of this report.

The reference area to be used is given by:

$$A_{ref} = lb \tag{L-52}$$

Where:

l	is the length of the element;
b	is the diameter of circumscribed circumference.

Structural factor $c_s c_d$

This section has already been included in full in the main report For some situations, determining the vale of $c_s c_d$ is straightforward. For instance, circular chimneys with a height less than 60 m or 6.5 times the diameter will have a structural factor equal to unity. In all cases, it may be determined by the formulas below, as long as $c_s c_d$ is larger than 0.85. According to the Dutch National Annex of Eurocode 1991-1-4, the structural factor may only be split into its two separate components if the structure height is less than 50 m and the ratio h/b is smaller than 5. This will not be the case for turbine towers considered in this research, so $c_s c_d$ will be calculated as one single factor.

Under the conditions that $0.6h \geq z_{min}$ and that only the along-wind vibration plays a significant part in the fundamental mode (which is the case for turbines towers), the following formula may be used to determine $c_s c_d$:

$$c_s c_d = \frac{1 + 2k_p I_v(z_s)\sqrt{B^2 + R^2}}{1 + 7I_v(z_s)} \tag{L-53}$$

Where:

z_s is the reference height, found in 6.3.1 of Eurocode 1991-1-4 or taken as h, the height of the structure;

k_p is the peak factor;

I_v is the turbulence intensity;

B^2 is the background factor;

R^2 is the resonance response factor.

These parameters will be explained further on.

The background factor B^2 is used to account for the lack of full correlation of the surface pressure. Using $B^2 = 1$ is considered safe [13], but otherwise:

$$B^2 = \frac{1}{1 + \frac{3}{2}\sqrt{\left(\frac{b}{L(z_s)}\right)^2 + \left(\frac{h}{L(z_s)}\right)^2 + \left(\frac{b}{L(z_s)}\frac{h}{L(z_s)}\right)^2}} \tag{L-54}$$

Where:

b, h are the width and height of the structure;

$L(z_s)$ is the turbulence length scale at reference height z_s.

The peak factor k_p is defined as the ratio of the maximum of the fluctuating part of the response to its standard deviation:

$$k_p = \sqrt{2\ln(vT)} + \frac{0.6}{\sqrt{2\ln(vT)}} \tag{L-55}$$

Where:

T is the averaging time, 600s;

v is the up-crossing frequency:

$$v = n_{1,x}\sqrt{\frac{R^2}{B^2 + R^2}} \geq 0.8\text{Hz} \tag{L-56}$$

Where:

$n_{1,x}$ is the first natural frequency of the stucture.

The resonance response factor R^2 accounts for turbulence resonating with the vibration mode of the tower:

$$R^2 = \frac{\pi^2}{2\delta}S_L(z_s, n_{1,x})K_s(n_{1,x}) \tag{L-57}$$

Where:

δ is the total logarithmic decrement of damping, explained in the next chapter;

S_L is the wind power spectral density function;

K_s is the size reduction function:

$$K_s(n) = \frac{1}{1 + \sqrt{(G_y\phi_y)^2 + (G_z\phi_z)^2 + \left(\frac{2}{\pi}G_y\phi_y G_z\phi_z\right)^2}} \tag{L-58}$$

With:

$$\phi_y = \frac{c_y b n}{v_m(z_s)} \qquad \phi_z = \frac{z h n}{v_m(z_s)} \tag{L-59}$$

Where:

$c_y = c_z$ is taken as 11.5. $G_y = 1/2$, $G_z = 5/18$
              for chimneys and towers.

Annex D of Eurocode 1-1-4 [13] provides values for $c_s c_d$ for several common structures, timber structures not being amongst hem.

L-4   Other external conditions

Besides wind conditions, turbines are subjected to the following environmental/climatic conditions:

- Temperature

- Humidity

- Air density

- Solar radiation

- Rain, hail, snow and ice

- Chemically active substances

- Salinity

- Lightning

- Earthquake

The effects of these conditions should be considered during design, using a 1-year recurrence period. Normal environmental conditions have to be combined with the extreme wind conditions, while extreme environmental conditions may be combined with the normal wind conditions. The items for which the design requirements are specified in detail in the IEC 61400 can be found below.

Temperature
     The influence of temperature may play a part in:

– Components and connections where two or more materials with different thermal expansion coefficients are present;

– Materials whose mechanical properties change with temperature.

Short temperature peaks are usually neglectable for many materials, since the duration is too short for them to heat up [5]. Normal temperature conditions range from -10 to +40°, extreme temperature conditions range from -20 to +50 °. Temperature variations are not taken into account within this research.

Humidity

A relative humidity of up to 95% has to be taken into account.

Solar radition

The solar radiation intensity that is to be designed for is 1000 W/m^2.

Lightning

Section 10.6 of the IEC 61400-1 specifies the lightning conditions, but these will not be part of this thesis.

Ice

Taking ice conditions into account is not required for the standard turbine classes according to IEC 61400-1, but according to DNV Risø [5] a layer of ice with a thickness of 30 mm and a density of 700 kg/m^3 can be considered on the blades in the Netherlands. It has been decided not to include ice formation in this research.

Earthquakes

Since the research deals with turbine design in the Netherlands, no attention is paid to earthquake conditions.

Structural design of wind turbines

This appendix will shortly explain the design demands from the IEC 61400 [2], using the information on wind models and turbine classes from the previous appendix. A lot of background information concerning the codes has been provided by a elaborate report by DNV Risø [5].

M-1   Load types

To ensure the turbine will not fail during its lifetime, the loads acting on it have to be analysed. This is covered by defining load cases by combining the different external conditions from the previous appendix with the proper design situations, found below:

– Operational conditions:

  – Normal operation and power production;
  – Cut-in, cut-out, idling and standstill.

– Temporary conditions:

  – Transportation;
  – Installation and assembly;
  – Faults;
  – Maintenance and repair.
  – Testing

Wind turbines are subjected to several types of loads, each with a different load source described below.

Gravitational and inertial loads
  These can be both static and dynamic and result from gravity, vibration, rotation, but also from the site's seismic conditions.

Aerodynamic loads

Aerodynamic loads can be both static and dynamic as well. They are caused by the interaction of the airflow with the turbine, not just with the moving parts, but with the stationary parts as well. It is influenced by the wind conditions, such as average wind speed and turbulence, but also by rotor speed and the shape and surface of the turbine components. Drag will also occur on the tower.

Actuation loads

These result from the operation and control of the turbine. Braking, pitching and yawing the turbine are examples of actions that can cause these loads. The first two are of lesser significance for the tower design.

Other loads

This term includes a lot of different types of loading, not belonging to the three groups above. Examples are loads from ice formation or impact loads.

M-2 Load cases

The IEC 61400-1 specifies a number of design load cases for wind turbines, meant to represent the most significant conditions it will experience. Load cases are made by combining operational modes, standstill or erection/maintenance conditions with the external conditions described in the previous chapter. They can be subdivided into three design situations [2]:

Normal design situations have to be combined with the appropriate external conditions, which can be normal or extreme.

Fault design situations have to be combined with the appropriate external conditions. These are taken as the normal external conditions, and only taken extreme if there is a direct correlation between the fault and the extreme condition.

Transportation, installation and maintenance design situations have to be combined with the appropriate external conditions.

Each design situation consists of several load cases, given in Tables M-1 and M-2. The different cases will each be explained below. For each of these cases, the type of analysis that needs to be executed is given. Load cases denoted by U require an ultimate load analysis of material strength, blade tip deflections and stability. The letter F stands for a fatigue analysis.

A classification according to the three situations above is made by choosing the correct load factors. Normal load cases, denoted by the letter N will occur frequently during the lifetime of the turbine. They occur during normal operation of the turbine, or with minor faults. Abnormal load cases (A) occur rarely, and consist of major faults that usually require activation of the turbine's protection system. The third situation (T) relates to the transportation and erection phase. The corresponding values will be provided later.

The complete list is given, even though not all of them may relate to the tower design. The main report explains which load cases are used within this research. An explanation of all load cases in the IEC-61400 is provided below.

Design situation	DLC	Wind condition		Other conditions	Type of analysis	Partial safety factors
1. Power production	1.1	NTM	$V_{in} < V_{hub} < V_{out}$	For extrapolation of extreme events	U	N
	1.2	NTM	$V_{in} < V_{hub} < V_{out}$		F	*
	1.3	ETM	$V_{in} < V_{hub} < V_{out}$		U	N
	1.4	ECD	$V_{hub} = V_r - 2$ m/s, $V_{hub} = V_r$, $V_{hub} = V_r + 2$ m/s		U	N
	1.5	EWS	$V_{in} < V_{hub} < V_{out}$		U	N
2. Power production plus occurrence of fault	2.1	NTM	$V_{in} < V_{hub} < V_{out}$	Control system fault or loss of electrical network	U	N
	2.2	NTM	$V_{in} < V_{hub} < V_{out}$	Protection system or preceding internal electrical fault	U	A
	2.3	EOG	$V_{hub} = V_r \pm 2$ m/s and V_{out}	External or internal electrical fault including loss of electrical network	U	A
	2.4	NTM	$V_{in} < V_{hub} < V_{out}$	Control, protection or electrical system faults including loss of electrical network	F	*
3. Start up	3.1	NWP	$V_{in} < V_{hub} < V_{out}$		F	*
	3.2	EOG	$V_{hub} = V_{in}, V_r \pm 2$ m/s and V_{out}		U	N
	3.3	EDC	$V_{hub} = V_{in}, V_r \pm 2$ m/s and V_{out}		U	N
4. Normal shut down	4.1	NWP	$V_{in} < V_{hub} < V_{out}$		F	*
	4.2	EOG	$V_{hub} = V_r \pm 2$ m/s and V_{out}		U	N
5. Emergency shutdown	5.1	NTM	$V_{hub} = V_r \pm$ m/s and V_{out}		U	N
6. Parked (standing still or idling)	6.1	EWM	50 year recurrence period		U	N
	6.2	EWM	50 year recurrence period	Loss of electrical network connection	U	A
	6.3	EWM	1 year recurrence period	Extreme yaw misalignment	U	N

Table M-1: Design load cases (part 1) according to the IEC, taken directly from IEC 61400 [2].

Design situation	DLC	Wind condition		Other conditions	Type of analysis	Partial safety factors
7. Parked and fault conditions	7.1	EWM	1 year recurrence period		U	A
8. Transport, assembly, maintenance and repair	8.1	NTM	V_{maint} to be stated by manufacturer		U	T
	8.2	EWM	1 year recurrence period		U	A

Table M-2: Design load cases (part 2) according to the IEC, taken directly from IEC 61400 [2]. Legend found below.

Where:	
DLC	Design load case
ECD	Extreme coherent gust with direction change
EDC	Extreme direction change
EOG	Extreme operating gust
EWM	Extreme wind speed model
EWS	Extreme wind shear model
NTM	Normal turbulence model
ETM	Extreme turbulence model
NWP	Normale wind profile model
$V_r \pm 2\,\mathrm{m/s}$	Sensitivity to all wind speeds in the range shall be analysed
F	Fatigue
U	Ultimate strength
N	Normal
A	Abnormal
T	Transport and erection
*	Partial safety factors for fatigue

M-2-1 Power production (DLC 1.1 - 1.5)

Here the turbine is running, connected to the grid and producing power.

- DLC 1.1 and 1.2 consist of loads resulting from atmospheric turbulence that occurs during normal operation of a wind turbine throughout its lifetime.

- DLC 1.3 takes into account ultimate loading due to extreme turbulence conditions.

- DLC 1.4 and 1.5 are transient cases, containing potentially critical events in the life of the turbine.

M-2-2 Power production plus occurrence of fault or loss of electrical network connection (DLC 2.1 - 2.4)

Here the turbine is producing power, but a fault or loss of network connection triggers a transient event.

- DLC 2.1 relates to normal events, such as faults relating to control functions or loss of connection to the electrical grid.

- DLC 2.2 consist of rare events, such as faults relating to the protection system or internal electrical systems. These are to be considered as abnormal conditions.

- DLC 2.3 is another abnormal event. It consists of the combination of an internal or external fault and the potentially significant wind event, EOG. The timing is chosen in a way to achieve the worst loading.

- DLC 2.4 models the event when a fault does not cause immediate shutdown. Fatigue damage is then assessed in normal turbulence conditions (NTM).

M-2-3 Start up (DLC 3.1 - 3.3)

Start up design situations include all events resulting in loads on the turbine in the time between standstill (or idling) to normal power production.

M-2-4 Normal shut down (DLC 4.1 - 4.2)

Just like the previous, except from power production to standstill.

M-2-5 Emergency shut down (DLC 5.1)

As the name suggests, this considers the loads that occur during an emergency shutdown.

M-2-6   Parked (standstill or idling) (DLC 6.1 - 6.4)

DLC 6.1 to 6.3 use the extreme wind model (EWM) for the turbine when the rotors are not turning or idling. As can be found in the previous appendix, this consists of a steady wind model and a turbulent one. The IEC describes the use of them as follows. "If the turbulent model is used, the response shall be estimated using either a full dynamic simulation or a quasi-steady analysis with appropriate corrections for gusts and dynamic response using ISO 4354. If the steady wind model is used, the effect of resonant response shall be estimated from the quasi-steady analysis above" [2].

 – DLC 6.1 uses the steady extreme wind model with a yaw misalignment up to $\pm 15°$, or the turbulent extreme wind model with $\pm 8°$.

 – DLC 6.2 models loss of power in the early stage of a storm. Conditions to be designed for are an extreme wind situation with 180 degrees wind direction change.

 – DLC 6.3 uses an extreme wind with a 1 year recurrence period in combination with extreme yaw misalignment. The steady extreme wind model is to be used with a yaw misalignment of $\pm 30°$. For the turbulent model only 15 degrees is necessary.

 – DLC 6.4 is used with the NTM for fatigue calculations in parked mode. The number of hours in which the turbine is not standing still is estimated.

M-2-7   Parked and fault conditions (DLC 7.1)

DLC 7.1 deals with fault conditions in the parked mode. In the case of a fault in the yaw system, $180°$ misalignment is to be considered. Any other faults than yaw system or loss of power, should be modelled with the EWM and a 1 year recurrence period.

M-2-8   Transport, assembly, maintenance and repair (DLC 8.1 - 8.2)

In DLC 8.1 the manufacturer has to state all wind conditions and design situations assumed for transport, assembly, maintenance and repair, that can cause loading on the turbine. It is common to add 5 m/s to the wind speeds obtain sufficient margin for safety.

DLC 8.2 is for all transport, assembly, maintenance and repair conditions that last longer than a week. It is to be used in combination with the EWM, but no connection to the grid has to be assumed. Examples are a partially finished tower, or a tower without certain components of the nacelle and/or rotor.

M-3   Basis for structural design calculations

This section will deal with the way in which calculations are to be done on wind turbines. It is assumed the reader is familiar with the calculation principles from Eurocode 1 and 5 [13, 14], so this section will mainly focus on the additional demands made by the IEC [2] or differences found between turbine towers and regular structures.

According to the IEC, the ultimate limit state analysis of wind turbines has to consist of four types of analysis:

– Ultimate strength analysis;

– Fatigue failure analysis;

– Stability analysis;

– Critical deflection analysis.

Load calculations for these analyses are usually made by dynamic simulations. Each type uses safety factors to deal with uncertainties in loads, material properties and consequences in different ways. These factors are explained in the next subsections.

M-3-1   Partial safety factors in general

Both the Eurocodes and IEC 61400-1 use the method of partial safety factors to obtain an acceptable level of reliability. Variability and uncertainties in both materials and loads are taken into account by these factors.

For loads the characteristic value F_k is multiplied with a partial load factor γ_f to obtain the design load F_d:

$$F_d = \gamma_f F_k \tag{M-1}$$

Characteristic values of material properties f_k are divided by a partial material factor γ_m to obtain its design value f_d:

$$f_d = \frac{1}{\gamma_m} f_k \tag{M-2}$$

Component classes

The IEC introduces another partial factor by distinguishing between three component classes, by introducing a consequence of failure factor γ_n. In this way the importance of structural components and the consequences of their failure is accounted for.

– Consequence class 1 is used for components whose failure will not cause failure of a major part of the turbine, so called "fail-safe" structural components.

– Consequence class 2 are "non fail-safe" structural components whose failures may lead to the failure of a major part of the turbine.

– Consequence class 3 is used for "non fail-safe" mechanical components. This is not expected to be relevant in tower design, but is mentioned for completeness.

Turbine towers are of consequence class 2.

Unfavourable loads			Favourable loads
Normal (N)	Abnormal (A)	Transport and Erection (T)	
1.35	1.1	1.5	0.9

Table M-3: Partial safety factors for loads for ultimate strength analysis, taken from IEC 61400 [2].

M-3-2   Ultimate strength calculations

The general formula for ultimate strength calculations is provided by the IEC by adding the consequence of failure factor to the formula known from NEN-EN 1990 [26]:

$$\gamma_n S(F_d) \leq R(f_d) \tag{M-3}$$

Where:
γ_n \qquad\qquad is the partial factor for component classes;
$S(F_d)$ \qquad is the load function;
F_d \qquad\qquad is the design value for the load;
$R(f_d)$ \qquad is the resistance function;
f_d \qquad\qquad is the design value for the material strength.

Since in an ultimate strength analysis the maximum occurring load often is considered, $S(F_d) = F_d$ is usually the case. The same goes for the maximum allowable material design value, so $R(f_d) = f_d$. This gives:

$$\gamma_f F_k \leq \frac{1}{\gamma_n \gamma_m} f_k \tag{M-4}$$

Where:
γ_f \qquad\qquad is the partial safety factor for loads;
γ_m \qquad\qquad is the partial safety factor for materials;
γ_n \qquad\qquad is the partial factor for component classes.

The following values for partial factors should be used in ultimate strength design:

Partial safety factors for loads γ_f
   Table M-3 provides the appropriate partial load factors for the design situations for ultimate strength analysis of wind turbine components.

Partial safety factors for materials γ_m
   Eurocode 1995-1-1 provides partial material factors for timber and components used to connect timber elements. These can be found in Table M-4.

   When design codes are not available, the following conditions should be met according to the IEC [2]:

   – The partial safety factor shall not be less than 1.1, when multiplied with characteristics with a 95% confidence limit;

Material type	γ_m
Solid timber	1.3
Glued laminated timber	1.25
LVL, plywood, OSB	1.2
Particleboards	1.3
Fireboards	1.3
Connections	1.3
Punched metal plate fasteners	1.25

Table M-4: Partial safety factor for timber materials, taken from NEN-EN 1995 1-1 [14]

– For non fail-safe components, a factor of 1.2 should be applied for global buckling and 1.3 for rupture due to tension or compression.

Partial safety factors for consequences γ_n

According to the IEC:

$\gamma_n = 0.9$ for component class 1;
$\gamma_n = 1.0$ for component class 2;
$\gamma_n = 1.3$ for component class 3.

For timber structures, other partial factors also apply, explained in Appendix D.

M-3-3 Fatigue calculations

Fatigue calculations in the IEC 61400-1 are made using Miner's rule [2]:

$$D = \sum_{i}^{N} \frac{1}{S_i} \tag{M-5}$$

Where:

D is the total damage;
S_i is the load range for the i_{th} cycle;
N is the number of cycles to failure for a constant amplitude loading with the range given by an S-N curve.

When the sum reaches 1.0, fatigue failure is assumed to have occurred.

A sufficient number of computer simulations has to be carried out to ensure validity of the design results for the tower. A minimum of 5 simulations per load case is recommended [5], but often a higher figure is needed. These results need to be adjusted with the correct operating times at different speeds. This will result in a lifetime equivalent load, with uncertainty in the results. In some cases this uncertainty is high enough to consider increasing the partial safety factor for loads [5].

Fatigue damage increases with both wind speed and turbulence intensity. Together with this, the uncertainty in the lifetime equivalent load will also increase with these. It has been concluded that most of the fatigue damage will occur during normal operation and errors or starts and stops will contribute little [5].

The following partial safety factors should be used in fatigue design:

Partial safety factors for loads γ_f
These shall be 1.0 for both the normal and abnormal situations, according to the IEC. However, some designers [5] recommend a factor of 1.2 on the loads until a full-scale prototype has been tested.

Partial safety factors for materials γ_m
The same material factors as for ultimate strength calculations are to be used. When design codes are not available and the S-N curve is based on a 50% survival probability, γ_m has to be at least 1.5. For many materials that have a large variability in fatigue strength, the minimal partial safety factor is set to 1.7, again based on a 50% survival probability. For structural steel, γ_m may be taken as 1.1, based on a 97.7% survival probability. Other materials such as fibre composites have a γ_m of 1.2, based on a survival probability of 95%.

Partial safety factors for consequences γ_n
According to the IEC:
$\gamma_n = 1.0$ for component class 1;
$\gamma_n = 1.15$ for component class 2;
$\gamma_n = 1.3$ for component class 3.

M-3-4   Stability calculations

The same conditions apply as for the ultimate strength calculations. For steel towers, buckling often governs the shell thickness [5]. For timber structures, this information is not present, but buckling is not expected to be governing.

M-3-5   Critical deflection calculations

The most important consideration to be made in respect to the deflection calculation is the distance between tower and blade tip. This is done by calculating the elastic deflection and adding it to the undeflected position in the most unfavourable direction, checking if the tip will not hit the tower [2]. In the form of a formula [5]:

$$d_0 - \gamma u_{max} > 0 \tag{M-6}$$

Where:

d_0	is the distance between tower and blade tip in undeflected position;
γ	is the appropriate partial safety factor (IEC: $\gamma_f \gamma_m$);
u_{max}	is the maximum relative deflection.

One should be aware of the fact that the tower might deflect out of phase with the blades.

The partial factors to be used according to the IEC:

Partial safety factors for loads γ_f
  Partial safety factors for loads shall be the same as for ultimate strength calculations.

Partial safety factors for materials γ_m
  γ_m for elastic properties shall be 1.1, unless full-scale testing has been conducted. Then it has to be taken as 1.0.

Partial safety factors for consequences γ_n
  According to the IEC:
    $\gamma_n = 1.0$ for component class 1;
    $\gamma_n = 1.0$ for component class 2;
    $\gamma_n = 1.3$ for component class 3.

M-4   Load analysis

Load calculation for turbines is nowadays done using computer programs which are based on aeroelastic calculation procedures. It will solve the equations of motion for the structure under a given set of (stochastic) forces. The result is a set of loads that are used to design the various parts of the turbine, extreme loads and fatigue loads being the most important of these load results [5]. To describe the entire procedure would be beyond the scope of this thesis, so a few general remarks about the simulations are made. It is followed by several points of consideration for fatigue and extreme loads.

M-4-1   Aeroelastic simulations

The software calculates the variation in wind speed (in all three directions) at a number of points in space. Different models require different input parameters, but they all work with a certain mean wind speed and -profile with a fluctuating part (the turbulence) superimposed [5]. Two commonly applied methods for load prediction are finite element modelling (FEM) and modal analysis. The IEC requires any computer code used, to be validated with actual data.

M-4-2   Fatigue

For fatigue load distributions, the rain-flow method is often used. It is considered the best in predicting accumulated damage, compared to similar methods [5]. Many sources can be found that explain the rain-flow method, amongst which is section 4.4.1 of DNV Risø's report [5].

Stress range distributions

To select the appropriate stress range distributions, one must be aware of the various states of the turbine that can contribute to fatigue damage. This is often described in the so called 'duty cycle' of the turbine, a representative time period which defines the mode of operation for 10 minute intervals. It also contains information about the number of starts and stops during

the duty cycle, together with the associated wind conditions [5]. The different operational states are:

– Production

Calculations during production assume stationary values for the mean wind speed and turbulence intensity during 10 minutes. Stress ranges in the structural components for these stationary intervals are often well-represented by a Weibull distribution.

– Starts and stops at cut-it and cut-out;

– Idling or standstill;

– Yaw misalignment.

The last three will not contribute significantly to the fatigue damage in the tower [5].

Equivalent loads

Often it will be convenient to represent the load spectrum by a single equivalent load range S_0 and an associated equivalent number of cycles n_{eq}. They are calculated as such that they will lead to the same amount of fatigue damage as the many different load ranges that the turbine will experience:

$$S_0 = \left(\frac{\sum_i n_i S_i{}^m}{n_{eq}} \right)^{1/m} \tag{M-7}$$

Where m is the slope of the S-N curve of the material. It does however not hold for materials with bi-linear S-N curves [5].

M-4-3　Ultimate loads

Ultimate loads are calculated by a certain number n of 10-minute aeroelastic simulations, to determine the load response X. For each simulation a number of statistical quantities can be determined:

– mean value μ;

– standard deviation σ;

– skewness α_3;

– kurtosis α_4;

– rate ν of upcrossings of level μ;

– maximum x_m in 10 minutes.

Of interest for ultimate strength calculations is the overall maximum of the considered load X_m. From the probability distribution for X_m that follows from the different x_m's, a design value for X_m is often taken as a certain percentile [5].

One way to obtain this design value is through a purely statistical method using the calculated values for x_m for n simulations. Another way is through a semi-analytical method developed by Davenport [91]. It utilizes the other quantities stated above as well, not just x_m and n, thus taking into account more information about the distribution of the wind loads, such as the stochastic nature of the conditions expressed in these quantities. The latter is also considered to have more accurate results, according to experts [5]. A detailed explanation of both methods can be found in Section 4.4 of [5].

To be able to use either method, first simulations have to be run to obtain enough data to use as input. DNV/Risø[5] provides a scheme to select proper values for the characteristic extreme response and design extreme response for a turbine under operating and parked conditions. In this latter case the worst blade configuration has to be taken, that is with the blades and nacelle in a position with full drag on them.

Calculation scheme for turbine loads

1. For each load case, run at least 5 simulations of 10 minutes to calculate the extreme responses;

2. For each simulation, calculate the statistic properties as described in the above;

3. Use Davenport's method - or the purely statistical method - from the previous section to project the results for the 10-minute simulations onto the lifetime of the turbine, using the mean wind speed distribution from Appendix L;

4. From the results of the previous step, choose the appropriate characteristic value for the ultimate load in the response;

5. Apply the appropriate safety factor γ_f to obtain the design load.

M-5   Simplified load calculation methods

As stated before, most modern-day load calculations are executed by means of computer code. There are however several simplified load calculations, which pre-date the current software and are only used for preliminary calculations or quick verification nowadays [5]. The following three methods are mostly based on experience and have been used for many years.

M-5-1   Simple load basis method

This so-called simple load basis method as mentioned in section 4.5 of [5] is more suited for smaller turbines, and does not provide a good indication of the loads on larger turbines. It uses the following three parameters to calculate the loads:

Load component	Symbol	Static Load	Dynamic Load Amplitude
Horizontal force in rotor plane	F_x	0	0
Moment about horizontal axis in rotor plane	M_x	eF_0	$0.17eF_0$
Horizontal force along rotor axis	F_y	F_0	$0.17F_0$
Moment along rotor axis	M_y	$1.3M_{e,nom}$	$0.17 \cdot 1.3M_{e,nom}$
Vertical force	F_z	$-mg$	0
Moment about vertical axis	M_z	eF_0	$0.17eF_0$

Where $e = R/6$

Table M-5: Load magnitudes on tower based on the simple load basis method, taken from DNV Risø[5]

– Horizontal airflow load

$$F_0 = 300A \quad [N]$$
$$A = \pi R^2 \tag{M-8}$$

– Driving torque moment

$$M_{e,nom} = \frac{P_{nom}}{2\pi n_r \eta} \tag{M-9}$$

Where:
P_{nom} is the nominal power of the wind turbine;
n_r is the rotor frequency;
η is the efficiency, ≤ 0.9.

– The weight of the rotor mg

These are used to calculate the quantities as can be found in Table M-5.

M-5-2   Quasi-static method

This section is an exact copy of that in the main report, included for completeness The quasi-static method as found in DNV Risø's report [5] is used throughout this thesis. It uses a simplified blade load to calculate various load magnitudes. This load per unit length of the blades is:

$$p(r) = \frac{1}{2}\psi\rho V_{10}^2 D(r)C \tag{M-10}$$

Where:

$p(r)$ is the load per unit length of the blade;

ψ is the quasi-static gust factor, calculated using the formulas below;

ρ is the density of the air, 1.25 kg/m^3;

V_{10} is the extreme 10-minute mean wind speed with a recurrence period of 50 years at height h;

C is the maximum value of either the drag coefficient or the lift coefficient, ranging from 1.3-1.5;

$D(r)$ is the chord length of the blade at a distance r from the hub.

With the load per unit, the four design loads below can be calculated:

– The blade loads p are not of any interest for the tower loads directly, but are used to calculate the other forces. They are calculated as if one single blade was vertically above the hub. p can be found by summing $p(r)$ over this single blade.

– The design thrust force $F_{y,T}$ is obtained by summing the blade forces over all three blades. The orientation of the blades is arbitrary.

– The design tilt moment (part of $M_{x,T}$) is taken as the root moment of a single blade, as if it was pointed up vertically above the hub.

– The design yaw moment (leading to $M_{z,T}$) is calculated in a similar way, but with a single blade stretching horizontally from the hub.

Each of the loads described above uses different input parameters such as the threshold n^*, height h and corresponding eigenfrequency n_0 used in the formulas below. These can be found in Table M-6. The gust factor ψ in the previous equation and other required parameters are calculated as follows:

Gust factor ψ

$$\psi = \begin{cases} \left(\frac{ln(\frac{z}{z_0})+3.1}{ln(\frac{z}{z_0})} \right)^2 & \text{for } \frac{n_0 L}{U_{10}} > n^* \\ 1 + 3.9 \frac{2\sqrt{k_b + k_r}}{ln(\frac{z}{z+0})} & \text{for } \frac{n_0 L}{U_{10}} \leq n^* \end{cases} \tag{M-11}$$

Background turbulence effect k_b

$$k_b = \begin{cases} 0.9 - 2.5\frac{L}{l} & \text{for blade loads} \\ 0.75 - 3\frac{L}{l} & \text{for axial force} \end{cases} \tag{M-12}$$

L is the length of a single blade

$$l = 6.8 L_u \tag{M-13}$$

Integral length scale of the Kaimal spectrum L_u

$$L_u = 100 C z^m \tag{M-14}$$

C and m are taken from figure 3.4 from DNV Risø [5]

Load	Eigenfrequency n_0 corresponding to	Threshold n^*	Height h
Blade load	Blade flapwise bending	1.7	$z + \frac{2}{3}L$
Axial force	Tower bending	0.45	z
Tilt moment	Blade flapwise bending	1.7	$z + \frac{2}{3}L$
Yaw moment	N/A	0	z

Table M-6: The loads are calculated using different parameters, taken from table 4-6 of [5]

Resonance effect k_r

$$k_r = \frac{\frac{n_0 l}{V_{10}}}{\left(1 + 1.5\frac{n_0 l}{V_{10}}\right)^{5/3}} F(n_0) \frac{\pi^2}{2\delta} \tag{M-15}$$

Logarithmic increment of damping δ

$$\delta = 2\pi\left(\zeta_0 + \zeta_a\right) \tag{M-16}$$

ζ_0 and ζ_a are the structural and aerodynamic damping ratios

Aerodynamic admittance function $F(n)$

$$F(n) = \begin{cases} \frac{1}{1+3\frac{nL}{V_{10}}} & \text{for blade load} \\ \frac{1}{1+12\frac{nL}{V_{10}}} & \text{for axial force} \\ \frac{1}{1+4.4\frac{nL}{V_{10}}+21.8\left(\frac{nL}{V_{10}}\right)} & \text{for rotor moments} \end{cases} \tag{M-17}$$

M-5-3 Parametrised load spectra

When the entire load distribution is to be considered, and not just the extreme values, parametrised load spectra can be used. Used for instance in preliminary fatigue calculations, they are simplified load spectra, based on a relative small number of parameters. One that might be used is presented in the Danish code DS472 [92]. It is based around a characteristic aerodynamic blade load p_0, used to calculate the load distribution $p(r)$ along the blade.

$$p_0 = \frac{1}{2}\rho W^2 c C_L \tag{M-18}$$

$$W^2 = \left(\frac{4\pi}{3}n_r R\right)^2 + V_0^2 \tag{M-19}$$

$$p(r) = p_0 \frac{r}{R} \qquad \text{(M-20)}$$

Where:

c	is the characteristic chord length, taken at $r = 2/3\,R$;
C_L	is the lift coefficient at $r = 2/3\,R$;
W	is the resulting wind speed;
n_r	is the rotor frequency;
R	is the rotor radius;
r	is the distance along the blade from the hub;
V_0	is the nominal stall wind speed at hub height, can be taken as the nominal 10-minute mean wind speed V_r.

Using the above, the blade root moment becomes:

$$M_{root} = p_0 \frac{R^2}{3} \qquad \text{(M-21)}$$

These simplified formulas are then used to calculate, for instance, fatigue loads as explained below.

Parametrised load spectra and fatigue

For fatigue calculations, loads are modelled as a mean load, with a superimposed (cyclic) varying load. The load ranges of the latter are represented by a probability distribution (F_Δ) in such a way, that $F_\Delta(N)$ is the load range that is exceeded N times during the lifetime.

Deterministic part of the loads

A part of the varying load is deterministic, due to the gravitational forces arising from the cyclic movement of the blades. It will have a constant magnitude, and the number of cycles will be equal to the total number of rotations of the rotor during the lifetime of the turbine. The biggest influence on the magnitude is the mass distribution along the blades [5].

Stochastic part of the loads

The other part is due to aerodynamic loads and is stochastic of nature and is not as easily modelled. The Danish codes DS472 [92] provides a way to calculate these load ranges. A standardised distribution with load ranges F_Δ^* is multiplied by a design factor to provide F_Δ. The factor depends on the load type and direction. It is best suited for small turbines and might lead to over-conservative design of larger turbines [5].

$$F_\Delta^* = \beta(\log_{10}(N_F) - \log_{10}(N)) + 10.8 \leq 2k_\beta \qquad \text{(M-22)}$$

$$\beta = 0.11 k_\beta (I_T + 0.1)(A + 4.4) \qquad \text{(M-23)}$$

$$N_F = n_C T_L (\exp(-(V_{min}/A)^k) - \exp(-(V_{max}/A)^k)) \qquad \text{(M-24)}$$

Direction	Mean	Load range distributions		
		Deterministic		Stochastic
	$\bar{p}$	$p_{\Delta C}$	$p_{\Delta S}$	$p_{\Delta,stoch}$
Edgewise	$2M_{nom}/(3R^2)$	0	$+2mg$	$0.3F_\Delta^*(N)p_0$
Flapwise	$1.5p_0\,r/R$	0	0	$F_\Delta^*(N)p_0\,r/R$
Along blade	$(2\pi n_R)^2mr$	$-mg$	0	0
Frequency n_C		n_R	n_R	$3n_R$

Table M-7: Example of line loads on rotor blades according to the parametrised fatigue load spectrum, taken from DNV Risø[5]

Where:

I_T is the (characteristic) turbulence intensity;

k_β 1.0 for individual blade loads, 2.5 for pressure loads from all three blades;

N_F is the number of load ranges in the design lifetime (T_L);

T_L is the design lifetime corresponding to n_C;

n_C is the characteristic load frequency;

A, k are scale parameters of the Weibull distribution of the long-term; 10-minute wind speed.

Line loads on rotor blades

Line loads on rotor blades are expressed by combining the various deterministic load ranges and further combining these with the stochastic load ranges. When combining deterministic line loads, harmonically cycling loads are assumed and combined as follows:

$$p(t) = \bar{p} + \frac{1}{2}p_{\Delta C}\cos(2\pi n_C t) + \frac{1}{2}p_{\Delta S}\sin(2\pi n_C t) \qquad \text{(M-25)}$$

Where:

p is the considered load;

$\bar{p}$ is the mean;

$p_{\Delta C}, p_{\Delta S}$ are load ranges for cosinusoidal and sinusoidal load components;

n_C is the characteristic frequency to be used.

The appropriate values can be found in Table M-7.

For determining the total cyclic load ranges it is recommended to add the largest deterministic load range with the largest stochastic load range, doing the same for the second largest, third largest, and so on[5].

Rotor loads

The loads from the rotor working on the turbine are calculated by combining a deterministic mean load with a harmonically varying load with stochastic ranges [5]:

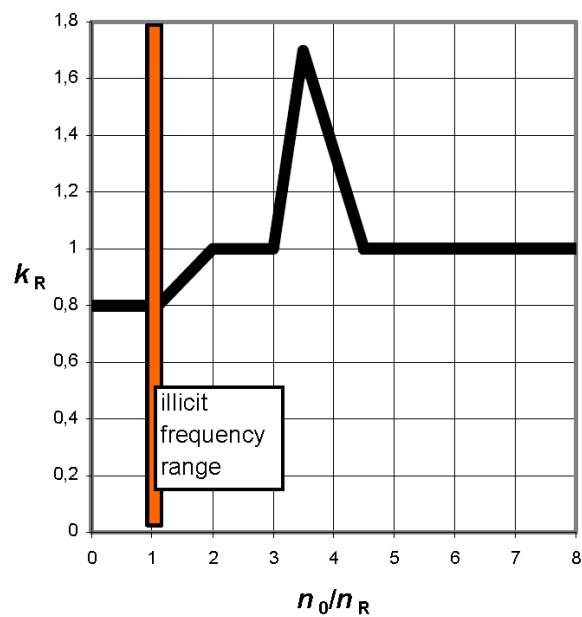$$F = \bar{F} + \frac{1}{2}F_\delta\cos(2\pi n_C t) \qquad \text{(M-26)}$$

Figure M-1: Determining k_R in Table M-8
Source: DNV Risø [5]

The appropriate values for this formula can be found in Table M-8. The correction factor k_R takes into account amplification effects by comparing the resonance frequency n_0 with the associated oscillation form. n_0 can either be equal to the tower bending frequency n_{tower} or the asymmetric rotor oscillation frequency n_{rotor}, where one blade is oscillating out of phase with the other two [5].

Load component	Symbol	Deterministic range $\bar{F}$	Stochastic load range F_Δ	Frequency n_C	Lowest resonance frequency n_0 (oscillation form)
Horizontal force in rotor plane	F_x	0	0		
Moment about horizontal axis in rotor plane	M_x	0	$0.33F_\Delta^*(N)k_Rp_0R^2$	$3n_R$	n_{rotor} (rotor, tilt, asymm.)
Horizontal force along rotor axis	F_y	$1.5p_0R$	$0.5F_\Delta^*(N)p_0R$	$3n_R$	n_{tower} (tower, bending)
Moment about rotor axis	M_y	$0.5M_{nom}$	$0.5F_\Delta^*(N)p_0R$	$3n_R$	
Vertical force	F_z	$-mg$	0		
Moment about vertical axis	M_z	0	$0.33F_\Delta^*(N)k_Rp_0R^2$	$3n_R$	n_{rotor} (rotor, yaw, asymm.)

Table M-8: Rotor load ranges according to the parametrised fatigue load spectrum, taken from DNV Risø[5]

Where:

m	is the mass of the rotor;
M_{nom}	is the nominal torque;
p_0	is the blade line load, see Equation M-19;
F_Δ^*	is the generic standardised load range distribution, see Equation M-23;
k_R	is a correction factor, see Figure M-1;
n_0	is the considered resonance frequency.

Bibliography

[1] J. Jonkman, S. Butterfield, W. Musial, and G. Scott, "Definition of a 5-MW Reference Wind Turbine for Offshore System Development Definition of a 5-MW Reference Wind Turbine for Offshore System Development," Tech. Rep. February, 2009.

[2] IEC, "NEN-EN IEC 61400-1," Tech. Rep. 015, IEC, 2005.

[3] T. Lyrner, M. Hassanzadeh, T. Stalin, and J. Johansson, "Tall towers for large wind turbines," Tech. Rep. July, Vindforsk, Stockholm, 2010.

[4] CBS, "Windenergie op land; productie en capaciteit per provincie," 2014.

[5] DNV Riso, "Guidelines for Design of Wind Turbines," tech. rep., DNV/Riso, Copenhagen, 2002.

[6] G. Schickhofer, "Characteristic Values and Test Configurations of CLT with Focus on selected Properties," in *COST Action FP1004 CLT Training Course: Structural Design of Cross Laminated Timber* (T. Harris, ed.), (Trento, Italy), pp. 35–65, 2014.

[7] Houthandel Houtex BV, "Informatieblad : Iroko," 2014.

[8] Centrum Hout, "Sterktegegevens van hout," 2007.

[9] D. W. Green, J. E. Winandy, and D. E. Kretschmann, "Mechanical Properties of Wood," in *Wood handbook*, p. Chapter 4, 1999.

[10] Grupo Losán, "Iroko," 2015.

[11] Metsä Wood, "Kerto: Engineered to perform," 2014.

[12] G. Pollmeier Massivholz, "Ingenious hardwood - Baubuche," Tech. Rep. 0, 2014.

[13] NEN, "NEN-EN 1991-1-4 + NB," Tech. Rep. april 2005, 2013.

[14] NEN, "NEN-EN 1995-1-1 + NB," Tech. Rep. april, 2011.

[15] Rijksdienst voor Ondernemend Nederland, "Windenergie op land," 2013.

[16] Global Wind Energy Council, "Global Wind Statistics 2013," 2014.

[17] VROM, "Nationaal plan van aanpak Windenergie," tech. rep., Ministerie van Volkshuisvesting, Ruimtelijke Ordening en Milieubeheer, Den Haag, 2008.

[18] TimberTower GmbH, "Holztürme für windkraft anlagen."

[19] L. Bathon, O. Bletz-Mühldorfer, F. Diehl, J. Schmidt, and M. Weil, "TimberTower für Grünen Strom," *Rheingau Regional-Magazin*, pp. 12–16, 2012.

[20] H. Plackner, "Der Wind und das Polyurethan," *Holzkurier*, pp. 22–23, 2012.

[21] B. Janzing, "Baumstarke Konstruktion," *Neue Energie*, pp. 28–33, 2013.

[22] C. G. Weelden van, "Site visit of TimberTower," 2013.

[23] W. Schäfer, "Vorzeigeprojekt in der letzten Phase," *Bauen mit Holz*, pp. 18–22, 2012.

[24] TimberTower GmbH, "Technisches datenblatt," 2012.

[25] Siemens AG, "Bolted Steel Shell Tower," 2011.

[26] NEN, "NEN-EN 1990 + A1 + A1 / C2 + NB," Tech. Rep. december 2011, 2013.

[27] Bosch & Van Rijn, "Windstats.nl," 2015.

[28] M. Koch, "Fundaties Windturbines Vlissingen," *Cement*, pp. 30–35, 2013.

[29] T. Burton, D. Sharpe, N. Jenkins, and E. Bossanyi, *Wind energy Handbook*, vol. 2. John Wiley & Sons Ltd, 2001.

[30] J. F. Mandell, D. D. Samborsky, N. K. Wahl, and H. J. Sutherland, "Testing and Analysis of Low Cost Composite Materials Under Spectrum Loading and High Cycle Fatigue Conditions," 2003.

[31] F. Ghedin, "Structural Design of a 5 MW Wind Turbine Blade Equipped with Boundary Layer Suction Technology," Tech. Rep. September, 2010.

[32] Metsä Wood, "Leno Cross Laminated Timber (CLT)," 2014.

[33] C. G. Weelden van, "CLT Training Course," 2014.

[34] Studiengemeinschaft Holzleimbau e.V., "Glued Laminated Timber - Composite Members," 2015.

[35] VENSYS, "1.5 MW Platform," 2012.

[36] D. Lungu, "Comparative study of Eurocode 1 , ISO and ASCE procedures for calculating wind loads," *IABSE Report*, vol. 74, pp. 345–354, 1996.

[37] J. De Gooijer, "Aanvraag bouwvergunning Vestas V112 94m," 2009.

[38] Rijksoverheid, "Windenergie," 2013.

[39] Rijksoverheid, "Windenergiegebieden op Land," 2013.

[40] General Electric Company, "Space Frame Tower," 2014.

[41] Techniker, "Tall Timber Buildings The Stadthaus, Hoxton, London," 2010.

[42] TimberTower GmbH, "TimberTower- Holztürme für Windkraftanlagen der Multi-megawattklasse," 2012.

[43] T. Lee, "Transverse Vibrations of a Tapered Beam Carrying a Concentrated Mass," *Journal of Applied Mechanics*, no. June 1976, pp. 366–367, 1976.

[44] P. Laura and R. Gutierrez, "Vibrations of an elastically restrained cantilever beam of varying cross section with tip mass of finite length," *Journal of Sound and Vibration*, vol. 108, pp. 123–131, 1986.

[45] TU Delft, "NF Stepped Monotower v01," 2010.

[46] S. Ilanko, "Calculation of Natural Frequencies and Modes using Energy Methods," 2005.

[47] K. Maser, M. Sanayei, L. Klimkewicz, H. Abedi, and L. Edgers, "Unknown Foundation Identification Using Stiffness Data From Field Measurements," *Tufts University*, no. 01, pp. 1–18.

[48] D. J. Dowrick, *Earthquake Risk Reduction.* Wiley, 2003.

[49] H. Svensson, *Design of Foundations for Wind Turbines.* PhD thesis, Lund University, 2010.

[50] Fugro Ingenieursbureau B.V., "Geotechnisch Grondonderzoek en Funderingsadvies Betreffende 17 Windturbines aan de Noordermeerdijk Nabij Creil in de Noordoostpolder," 2011.

[51] J. C. Nicholson, *Design of wind turbine tower and foundation systems : optimization approach.* PhD thesis, University of Iowa, 2011.

[52] Vestas, "Foundation Loads - V90 - 2.0 MW VCS," tech. rep., 2006.

[53] Vestas, "General Specification V112-3.0MW," tech. rep., 2009.

[54] L. Bathon, O. Bletz-Mühldorfer, J. Schmidt, and M. Weil, "Windenergietürme aus Holz," *Holzbau*, vol. 3, pp. 32–36, 2010.

[55] Germanischer Lloyd, "Guideline for the Certification of Offshore Wind Turbines," tech. rep., 2005.

[56] R. Harris and R. Tomasi, "CLT Training Course," in *Structural Design of Cross Laminated Timber* (R. Harris and R. Tomasi, eds.), (Trento, Italy), 2014.

[57] T. Bogensperger, T. Moosbrugger, and G. Silly, "Verification of CLT-plates under loads in plane," in *World Conference on Timber Engineering*, 2010.

[58] A. Thiel, "ULS and SLS design of CLT and its implimention in the CLTdesigner," in *Focus Solid Timber Solutions - European Conference on Cross Laminated Timber*, (Graz), pp. 77–102, 2013.

[59] A. Thiel, "ULS and SLS design of CLT in- and out-of-plane," in *COST Action FP1004 CLT Training Course: Structural Design of Cross Laminated Timber* (R. Harris, ed.), (Trento, Italy), pp. 69–97, 2014.

[60] M. Andreolli, "Design Example of a CLT Building," in *COST Action FP1004 CLT Training Course: Structural Design of Cross Laminated Timber* (R. Harris, ed.), (Trento, Italy), pp. 175–214, 2014.

[61] P. L. Gould, W. Kratzig, I. Mungan, and U. Wittek, "Natural Draught Cooling Towers," in *Proceedings of the 2. International Symposium* (P. L. Gould, W. Kratzig, I. Mungan, and U. Wittek, eds.), (Ruhr-universitat Bochum), p. Chapter 27, 2005.

[62] L. Andriamitantsoa, "STEP Lecture A19 - Creep," in *Timber Engineering STEP 1*, ch. A19, 1995.

[63] Deutsche Institut für Bautechnik, "Allgemeine bauaufsichtliche Zulassung für BS-Holz aus Buche un BS-Holz Buche-Hybridträger," 2009.

[64] Studiengemeinschaft Holzleimbau e.V., "Glued Laminated Timber - Wood Species," 2015.

[65] G. Sagot, "STEP Lecture A14 - Detailing for Durability," in *Timber Engineering STEP 1*, ch. A14, 1995.

[66] Stichting Probos, "Houtsoortenkeuze versus toepassing," in *Database 'Houtsoorten voor de Woningbouw, Utiliteitsbouw en Grond-, Weg- en Waterbouw'*, no. november, 2009.

[67] C. C. Gerhards, "Effect of moisture content and temperature on the mechanical properties of wood: an analysis of immediate effects," *Wood and Fiber*, vol. 14, no. 1, pp. 4–36, 1982.

[68] D. A. L. Silva, F. A. R. Lahr, O. B. D. Faria, and E. Chahud, "Influence of wood moisture content on the modulus of elasticity in compression parallel to the grain," *Materials Research*, vol. 15, pp. 300–304, Apr. 2012.

[69] E. Obataya, M. Norimoto, and J. Gril, "The effects of adsorbed water on dynamic mechanical properties of wood," *Polymer*, vol. 39, no. 14, pp. 3059–3064, 1998.

[70] J. Hochegger and R. Schrenk, "Declaration of Performance CLT - ERW4 - DoP 001," 2013.

[71] Impressum, "Brettsperrholz.org," 2015.

[72] R. Slavid, "Endless Stair," 2012.

[73] W. C. Young and R. G. Budynas, *Roark's Formulas for Stress and Strain.* McGraw-Hill, seventh ed ed., 1989.

[74] Duwind, "Windturbine Simulation package," 2013.

[75] E. Hau and H. von Renouard, *Wind Turbines Fundamentals, Technologies, Application, Economics.* Springer, 2013.

[76] P. Gipe, *Wind Energy Comes of Age.* John Wiley & Sons Ltd, 1995.

[77] NWEA, "De Groei van Windenergie op Land," tech. rep., NWEA, ODE, Provinciale milieufederaties, Stichting Natuur & Milieu, LTO, IPO, VNG, Ministerie van VROM, Ministerie van EZ, Ministerie van LNV, Ministerie van Defensie, 2009.

[78] Wikipedia, "Wind turbine."

[79] W. Tong, *Wind Power Generation and Wind Turbine Design.* WIT Press, 2010.

[80] Vestas, "V164-8.0 MWÂő at a Glance," 2013.

[81] Siemens AG, "Tower," 2014.

[82] P. Fairley, "Wind Turbines Shed Their Gears," 2010.

[83] G. J. van Bussel, *Wind Energy Online Reader.* Delft: TU Delft, 2008.

[84] B. Gencturk, A. Attar, and C. Tort, "Optimal Design of Lattice Wind Turbine Towers," in *15th World Conference on Earthquake Engineering*, 2012.

[85] M. Veljkovic, M. Feldmann, J. Naumes, D. Pak, C. Rebelo, and L. Simões da Silva, "Friction connection in tubular towers for a wind turbine," *Stahlbau*, vol. 79, pp. 660–668, Sept. 2010.

[86] M. Veljkovic and W. Husson, "High-strength wind turbine steel towers," tech. rep., Elforsk, 2009.

[87] J. Jimeno, "Concrete Towers for Multi-Megawatt Turbines," *Wind Systems Magazine*, no. February, 2012.

[88] K. Maalawi, "Special Issues on Design Optimization of Wind Turbine Structures," in *Wind Turbines*, pp. 3–24, Cairo: InTech, 2011.

[89] R. Sinn, "Windkraft mit hölzernem Tragwerk," *Dach+Holzbau*, pp. 54–56, 2012.

[90] B. Harreither, "Hart am Wind mit Holz: Der TimberTower," *FAPU*, pp. 17–18, 2012.

[91] A. Davenport, "The Application of Statistical Concepts to the Wind Loading of Structures," *Proc. Inst. of Civil Engineers*, vol. 19, 1961.

[92] D. Standards, "DS 472: Dansk Ingeniørforenings Code of Practice for Loads and Safety of Wind Turbine Constructions," tech. rep., 1992.